Application of Magneto-Rheological Dampers to Control Dynamic Response of Buildings

Md Ferdous Iqbal

A Thesis

in

The Department

of

Building Civil and Environmental Engineering

Presented in Partial Fulfillment of the Requirements

For the Degree of Master of Applied Science (Civil Engineering) at

Concordia University

Montreal, Quebec, Canada

June 2009

Your file Votre référence
ISBN: 978-0-494-63029-7
Our file Notre référence
ISBN: 978-0-494-63029-7

Abstract

Application of Magneto-Rheological Dampers to Control Dynamic Response of Buildings

Md Ferdous Iqbal

Earthquakes usually cause huge casualty due to the ground shaking and also due to the failure of built infrastructure such as buildings and bridges. Therefore, it is necessary to control the response of these structures to avoid collapse during earthquake. At present, various control technology is available. Among them semi-active control devices using Magneto-rheological (MR) fluid dampers are promising because of their stability and low power requirement. In this research, performance of three different models of MR dampers, namely RD-1005-3, SD-1000 and MRD-9000 is studied by integrating them into different building structures subjected to different earthquake forces. Here, the dampers and the structures are modeled numerically using the finite element method. It is found that all of the dampers are capable of controlling the response of building frames for different earthquakes. Damper performance is also investigated from the energy point of view. It is found that dampers have the capability of increasing the energy dissipation capacity of a structure without changing the structural properties such as stiffness. It is also found that this type of damper is able to provide some protection even if power supply systems fail during dynamic excitation, which is very common during earthquake. A detailed investigation is carried out to find the optimum location of dampers in simple building frames. It is observed that the performance of the dampers is highly sensitive to

the location. Therefore it is very important to investigate the performance of damper before application in a real structure.

Acknowledgements

I would like to express my sincere gratitude and appreciation to my thesis supervisors Dr. Ashutosh Bagchi and Dr. Ramin Sedaghati for providing me the unique opportunity to work in the research area of magneto-rheological damper technology and structural control through their expert guidance, encouragement and support at all levels. They generously provide their valuable time and effort to complete my thesis.

I am also grateful to Concordia University, for providing me with the computer and library facilities during my research. I also thank Concordia University library personnel to provide me assistance at all time.

I also like to thanks my wife Musammet Siddiqua and son Shadman Iqbal for their inspiration and silent prayer for my research work at the time when they needed my company most. I also thank my parents, brothers and sister for their moral support and encouragement to complete my thesis.

Finally I like to thank my colleagues and friends for their encouragement and cordial help during my research work and make my life easy in the Concordia University.

Table of Contents

List of Figures

List of Tables

List of Symbols

E - Total input energy

E_k - Kinetic energy

E_s - Elastic strain energy

E_h - Energy dissipated by inelastic deformation

E_d - Damping energy

τ - Shear stress

H - magnetic field intensity

$\dot{\gamma}$ - Shear strain rate

η - Plastic viscosity

c_0 - Damping of the MR damper

k_0 - Stiffness of the MR damper

α, β, γ - Bouc-Wen constants

z - Evolutionary variable

F - Total damper force

$I_{\max}$ - Maximum current

$I_{\min}$ - Minimum current

$[M]$ - Mass matrix

$[C]$ - Damping matrix

$[K]$ - Stiffness matrix

$[\lambda]$ - Transformation matrix

σ - Stress

ε - Strain

G - Shear modulus of the material

J - Polar moment of inertia

I_{zz} - Moment of inertia about z axis

I_{yy} - Moment of inertia about y axis

u - Displacement vector

$\dot{u}$ - Velocity vector

$\ddot{u}$ - Acceleration vector

$\ddot{u}_g$ - Ground acceleration

ζ - Damping ratio

$[\Lambda]$ - Excitation distribution vector

$T(t)$ - Kinetic energy at time t

$D(t)$ - Damping energy dissipated up to time t

$U(t)$ - Strain energy at time t

$I(t)$ - Input energy at time t

MR – Magneto-rheological

DE_T – Total damping energy

DE_{MR} – Damping energy due to MR damper

DE_S – Structural damping energy

CHAPTER 1
Introduction

Structural safety both for the structure itself, its occupants, and contents is of great importance because of the devastating consequence of earthquakes as observed in recent events. The catastrophic effects of earthquakes are due to movement of ground mass of surface motion which causes a number of severe hazardous actions such as severe damage or collapse of infrastructure and loss of human life. For example an earthquake of magnitude 6.7 that happened at Northridge, U.S.A. in 1994 was responsible for the death of 57 people, injury to 9000 people, displacement of more than 20,000 people from their homes and causing about $20 billion in losses. Another earthquake of magnitude 6.9 happened on the first anniversary of the Northridge Earthquake (1995) in the city of Kobe, Japan. In that event 5500 lives were lost, 35000 peoples were injured and the estimated loss was over $ 147 billion. In the India-Pakistan border on October 8, 2005 an earthquake of magnitude 7.6 struck. More than 75000 people were killed, 80000 injured and 2.5 million people became homeless. Peru's earthquake of magnitude 8.0 on August 15, 2007 killed at least 500 people and over 34000 houses were destroyed. Some regions in Canada are also vulnerable to earthquake. About 100 earthquakes of magnitude 5 or higher were reported during past 70 years in the vicinity of Vancouver Island (NRCAN, 2006). An Earthquake on February 28, 2001 near Seattle, which rattled the buildings and the occupants in Vancouver, could be viewed as a reminder of the seismic hazard to people living in Canada. It has also been reported that the earthquake occurred at

Saguenay in Quebec in 1988 was the strongest event (magnitude of 5.9) in the eastern North America within the last 50 years (Foo *et al.,* 2001). Canada also has a record of suffering from stronger earthquakes such as that which occurred in 1949 of magnitude 8.1 which is the largest earthquake in Canada. Every year in Canada, an average of 1500 earthquakes with magnitude varying from 2 to 5 are also reported (NRCAN, 2006). Thus the earthquake vulnerability of structures in Canada requires considerable attention from the building and bridge code authorities.

Earthquakes often causes huge casualty, which is not only due to the mechanism of earthquake but also due to the failure of constructed facilities such as collapse of buildings, bridges, and dams. Therefore, it is a great challenge for structural engineers to develop technologies to protect civil structures including their contents and occupants from hazard of strong earthquakes. Safe and performance-oriented designs of structure are key to mitigate the effects of such events. To achieve this goal, it is very important to understand the behaviour of structure subjected to vibratory motion of the ground surface during an earthquake.

To face the environmental forces like earthquake, traditionally structures have been designed through a combination of strength, deformability and energy absorption capacity. This can be achieved through a combination of structural components such as shear walls, braced frames and moment resisting frames to form lateral load resisting systems. The shape of the building is also an important consideration in this approach,

since square or rectangular buildings perform better than other shapes such as L, U or T type buildings (Wilson, 2005). Materials selection is also important, since ductile materials, such as steel are found to perform better than brittle ones, such as brick and masonry. Seismic design relies on the ability of structural elements to dissipate the seismic energy input to the structure during an earthquake. Therefore, a certain level of deformation and damage is accepted. During minor and moderate earthquakes, structures resist the seismic forces mainly by elastic deformation and hence there is no significant damage. But during strong ground motion caused by a severe earthquake, ductile structures are allowed to deform well beyond the elastic limit. In such a case, there is significant damage to the structure. It is very difficult, sometimes impossible and expensive to repair such damage and excessive deformation of the structure may lead to collapse. On the other hand, if stiffness of a structure is increased to reduce its deformation and to avoid damage of the structure due to inelastic deformation, the construction cost increases and the natural properties of structure will be changed. With the increase of stiffness, natural frequency of structure is increased and the period of structure is decreased. Figure 1.1 shows the typical design spectrum and Figure 1.2 shows design spectrum for various damping ratios. If period of structure is decreased, the structure will attract more pseudo-acceleration according to Figure 1.1. If by any means we are able to increase the damping property of structure, the structure will attract less pseudo-acceleration according to Figure 1.2 and accordingly there will be less deformation. The concept of increasing in the structural damping is effectively utilized in controlling the dynamic response of a structure and reducing its vibration. It may be

noted here that increase in damping property of a structure will not make any significant change in the natural properties of the structure (frequency and period).

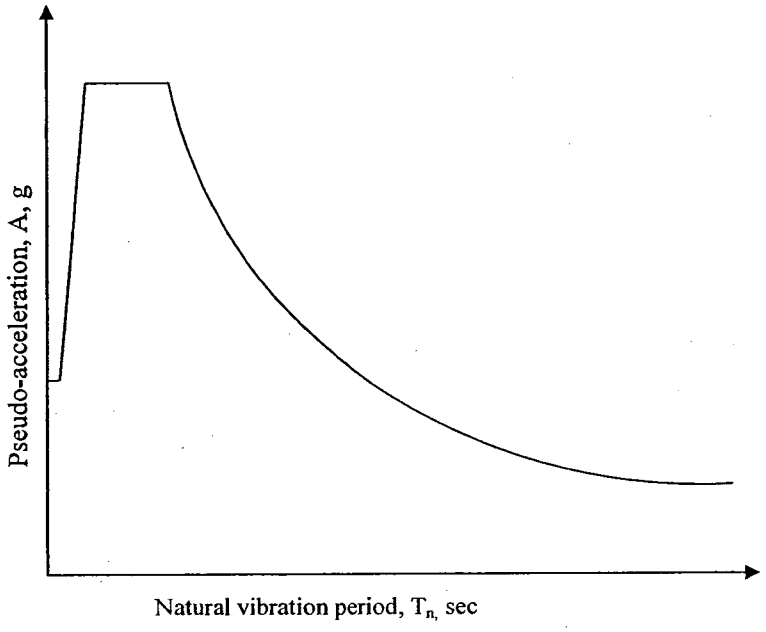

Figure 1.1: Typical design spectrum (Chopra, 2007).

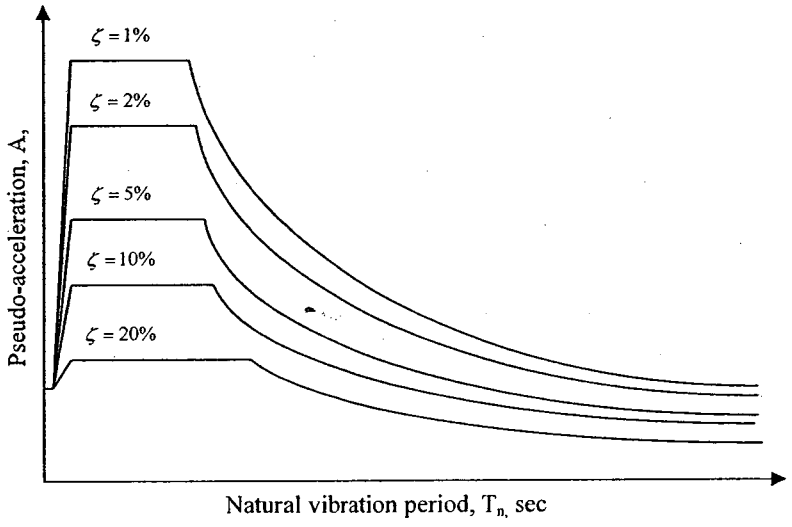

Figure 1.2: Typical deign spectrum for various damping (Chopra, 2007).

Alternatively, to mitigate the damaging effects of earthquake forces, some types of protective systems may be implemented into the structural system. If we look at the structural behaviour under seismic loading from the energy point of view, we can see that significant amount of kinetic energy is absorbed by the structure through the elastic and inelastic deformations depending on the magnitude of loading. Energy absorbed by elastic deformation is recoverable, while the energy absorbed by inelastic deformation is not, and thus inelastic deformation causes significant damage to the structure. Therefore, introducing a supplemental energy dissipative device to the structural system is one of the best ways to mitigate the damaging effects of seismic loadings. Under seismic events, the energy dissipative devices work by absorbing or reflecting a portion of the input energy that would otherwise be transmitted to the structure itself. According to the law of conservation of energy, the energy conservation relationship (Uang and Bertero 1988) can be expressed as follows:

$$E = E_k + E_s + E_h + E_d \quad \text{----------1.1}$$

Where E is the total input energy from earthquake motion; E_k is the absolute kinetic energy; E_s is the recoverable elastic strain energy; E_h is the irrecoverable energy dissipated by the structural system through inelastic deformation or other inherent forms of action and E_d is the damping energy dissipated by inherent structural damping and supplemental damping devices. The level of inherent damping of the structure is very low and therefore the amount of energy dissipated during elastic behaviour is also very low. The energy dissipation through inherent structural damping mainly arises from the thermal effect of repeated elastic straining of the material and from the internal friction

when a solid is deformed. However, many other mechanisms also contribute to the energy dissipation like friction at steel connections, opening and closing of micro cracks in concrete and friction in the structure itself and non-structural elements such as partition walls.

Therefore, integrating a supplemental energy dissipation system (supplemental damping system) into the structural system appears to be an elegant solution to reduce the demand on energy dissipation through inelastic deformation, and accordingly to control the response of a structure and minimise its vibration during earthquake event. Integration of such systems into the structure is an essential part of structural control or protective system. As it is a great challenge for engineers to protect structure as well as human life and economy, a significant amount of effort has been made to employ various control strategies in the design of engineering structures to increase their safety and reliability against strong earthquakes. As a result various control technologies has been advanced and are at various stages of development. Such control technologies offer the advantage of being able to modify dynamically the response of a structure in a desirable manner. Moreover such control system can be used in existing structure to be retrofitted or strengthened to withstand future seismic activity (Dyke *et al.,* 1996; Fujino *et al.,* 1996; Soong, 1990).

1.1 Motivation of this research

As discussed above, integrating a supplemental energy dissipating system (control system) into the structural system is a suitable alternative to control the dynamic response

of a structure and accordingly to protect the structure during earthquake. The vibration control technologies available at present can be categorized according to the nature of control as (Housner *et al.*, 1997; Spencer and Sain, 1997): (a) Passive Control System, (b) Active Control System, (c) Hybrid Control System, (d) Semi-active Control System. The control strategies will be discussed in Chapter 2.

Among the control systems mentioned above, semi-active control systems are more reliable and promising. Passive control systems are not able to deal with the change of either external loading conditions or usage patterns from those considered in its design. Active and hybrid control systems are able to deal with dynamic loading but they have high power requirement and also have potential stability problems. There are also a number of challenges associated with the active control system before getting general acceptance by the engineering and construction professions at large. These challenges include: (i) reduction of capital cost and maintenance, (ii) eliminating reliance on external power, (iii) increasing system reliability and robustness, and (iv) gaining acceptance of non-traditional technology by the profession (Spencer, 2003). Semi-active control systems become promising to address a number of these challenges (Dyke *et al.*, 1996, 1996a).

Semi-active control uses the measured structural response to determine the required control force. Therefore, they have the ability to deal with the changes in external loading condition. They can not input any energy into the system. They have properties that can be adjusted in real time and can only absorb or dissipate energy. Because of these

properties, there is no stability problem associated with this system (Yang, 2001). Another advantage of this system is that, they have an extremely low power requirement which is particularly critical during seismic events when the main power source to the structure may fail. These systems also offer the reliability of a passive system, yet maintain the versatility and adaptability of fully active system (Dyke *et al.*, 1996). Moreover, they are failsafe systems as can act as passive control system in the case of power failure (Dyke *et al.*, 1996, 1996a; Dyke and Spencer Jr. 1996; Jansen and Dyke, 2000; Yi and Dyke 2000).

There are a few varieties of semi-active devices available for civil engineering applications are: (a) Variable orifice fluid dampers, (b) Controllable friction dampers, (c) Adjustable tuned liquid dampers, (d) Controllable fluid dampers.

A magneto-rheological (MR) damper is a type of controllable fluid damper which uses magneto-rheological (MR) fluid. MR fluid consists of micron-sized, magnetically polarizable particles suspended in a liquid such as water, glycol, mineral or synthetic oil (Dyke *et al.*, 1996a). MR fluid has the properties to change reversibly from a free-flowing, linear viscous fluid to a semi-solid with controllable yield strength. Because of this property MR dampers are quite promising for civil engineering application (Carlson and Spencer Jr., 1996; Dyke *et al.*, 1996,a,b; Dyke, 1996).

1.2 Objectives of the present research

The civil engineering profession and construction industry in many countries are conservative and generally reluctant to apply new technologies. To increase the confidence of adopting new technology like application of magneto-rheological damper in civil engineering structures, more research is needed. The objectives of the present research are as follows:

1. To study different models of magneto-rheological dampers.
2. To study the performance of magneto-rheological dampers in reducing the response of building structures under earthquake excitation.
3. To evaluate effect of damper location in the structure as the optimal placement of the dampers is very important for the performance of the structure.

1.3 Organization of the thesis

This thesis has been organized into five chapters. Introduction and objective of this thesis are presented in the current chapter, i.e. Chapter 1. A thorough review of literature on different control technologies available at present, behaviour and modeling of magneto-rheological fluid, application of magneto-rheoligical dampers in building structures are presented in Chapter 2. In Chapter 3, modeling of magneto-rheological dampers used in this research is discussed. Modeling issues of structure and details of the computational issues in the context of the present research are presented in Chapter 4. A number of case studies performed in this thesis to evaluate the performance of magneto-rheological

damper are discussed in Chapter 5. Conclusions and possible future work is included in Chapter 6. The thesis ends with a list of references and appendices.

CHAPTER 2
Literature Review

2.1 Introduction

Devastating consequences of earthquakes with respect to human lives and economic losses have underscored the importance of understanding the behaviour of structures subjected to earthquakes. It is a great challenge for engineers to understand the behaviour of structures under seismic excitation and to design them to withstand strong earthquakes. In the design, a structure is provided with a combination of strength, deformability/ductility and energy absorption capacity. As the inherent capacity for energy dissipation by a structure is low, a certain level of deformation and damage must be accepted. But it is difficult or sometimes expensive or impossible to repair such damages and may lead to collapse. Supplemental damping can enhance the energy dissipation capacity of a structure substantially, and reduce or eliminate structural damage. This Chapter provides a synthesis of existing research in controlling building response using supplemental damping, particularly using MR fluid dampers.

2.2 Vibration Control Strategies

Over the past three decades, considerable attention has been given to research and development of suitable energy dissipation devices to control the response of structures under seismic loading. As a result, many new and innovative concepts of structural

protection through energy dissipation have been advanced and are of various stages of development. These concepts can be categorized according to the control strategies as follows (Housner *et al.*1997; Spencer and Sain, 1997):

A) Passive Control,

B) Active Control,

C) Hybrid Control,

D) Semi-active Control.

2.2.1 Passive Control System

A passive control system does not require external power source. Passive control devices impart forces that are developed in response to the motion of the structure. The basic function of the passive control devices when installed in a structure is to absorb or consume a part of the input energy thereby reducing energy dissipation demand on primary structural members and minimizing possible structural damage. The passive energy dissipation systems encompass a range of materials and devices for enhancing damping, stiffness and strength, and can be used both for seismic hazard mitigation and for rehabilitation of aging or deficient structures. In general, such systems are characterized by their capacity to enhance energy dissipation in the structural systems in which they are installed. These devices generally operate on principles such as frictional sliding, yielding of materials, phase transformations in metals, deformation of viscoelastic solids or liquids and fluid orificing (Housner *et al.,* 1997; Soong and Dargush 1997; Chu *et al.,* 2005).

There are some limitations of passive control systems, as they cannot deal efficiently with the change of either external loading conditions or usage patterns from those used in their design (Soong, 1990). Passive control system can be schematically shown in Figure 2.1.

The common types of passive control devices use in the structure to control earthquake response of structure are listed below.

A) Metallic Yield Dampers,

B) Friction Dampers,

C) Viscoelastic Dampers,

D) Viscous Fluid Dampers,

E) Tuned Mass Dampers,

F) Tuned Liquid Dampers.

2.2.2 Active Control System

An active control system is one in which an external source powers control actuator(s) that apply forces to the structure in a prescribed manner. These forces can be used to both add and dissipate energy in the structure. Such systems are used to control the response of structure to internal and external excitation such as machinery or traffic noise, wind or earthquakes where the safety or comfort level of the occupants is of concern. A purely active structural control system has the basic configuration as shown schematically in Figure 2.2. (Chu *et al.,* 2005)

Although active control system is adaptive to changes in external loading conditions, it has a number of serious challenges, such as high capital cost and maintenance, huge external power requirements and potential stability problems (Yuen *et al.,* 2007). Use of huge external power makes such systems vulnerable to power failure which is always a possibility during a strong earthquake.

2.2.3 Hybrid Control System

The term "hybrid control" implies the combined use of active and passive control systems. A hybrid control may use active control to supplement and improve the performance of a passive control system. This way passive control is added to an active control system to decrease its energy requirements. For example a structure equipped with distributed viscoelastic damping supplemented with an active mass damper on or near the top of the structure or a base isolated structure with actuators actively controlled to enhance performance. Hybrid control system can be schematically shown in Figure 2.3.

The only essential difference between an active and a hybrid control system in many cases is the amount of external energy used to implement control. Hybrid control system can alleviate some of the drawbacks that exist for either a passive or an active control acting alone. A benefit of hybrid control is that, in the case of a power failure the passive component of the control still offers some degree of protection which is not possible when only active control system is used. Since hybrid (active-passive) control system is

an active system care must be taken to ensure that the system is not rendered unstable by neglecting the dynamics of sensors and actuators.

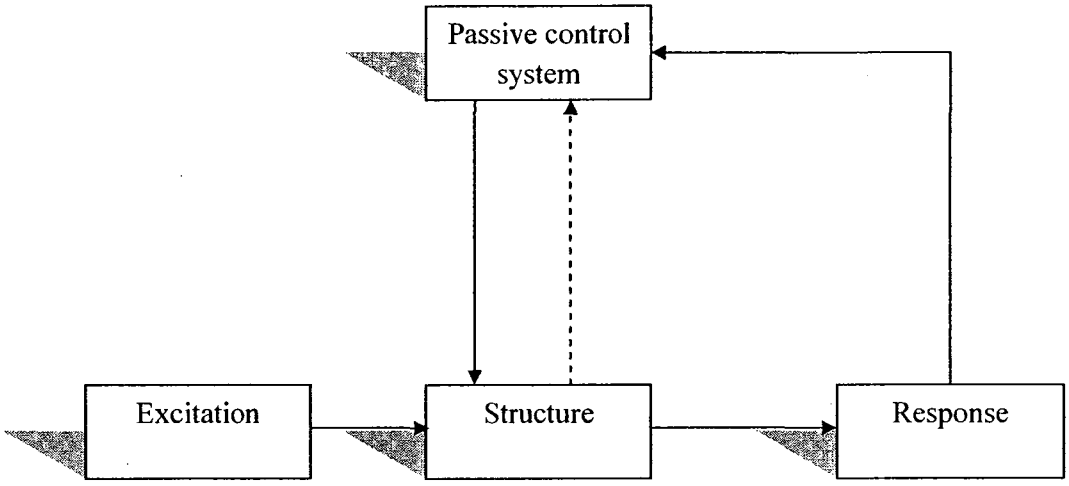

Figure 2.1: Structure with passive control (Symans and Constantinou, 1999)

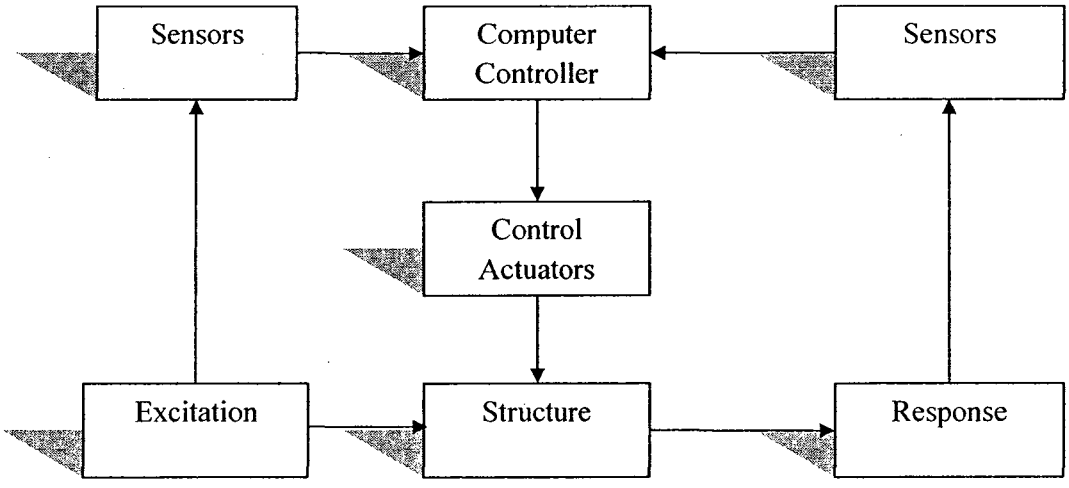

Figure 2.2: Structure with active control (Chu *et al.*, 2005)

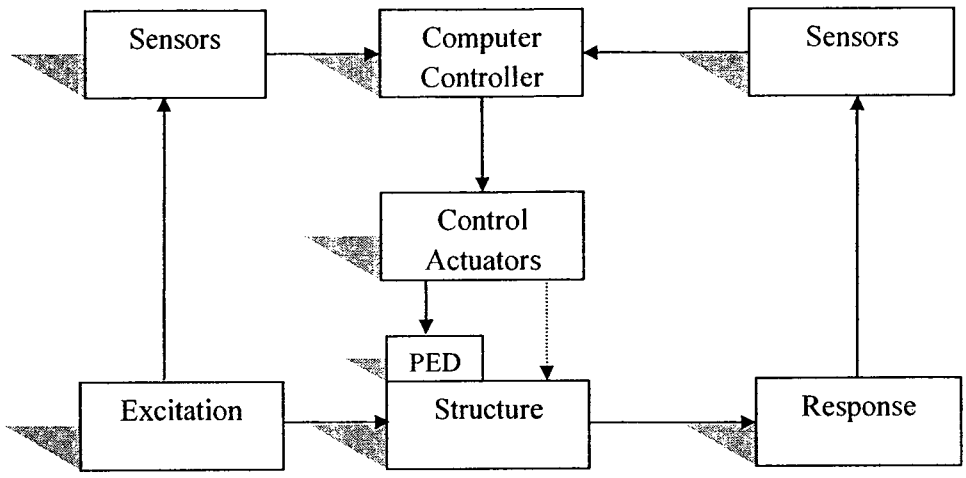

Figure 2.3: Structure with hybrid control (PED: Passive Energy Dissipation) (Chu *et al.*, 2005)

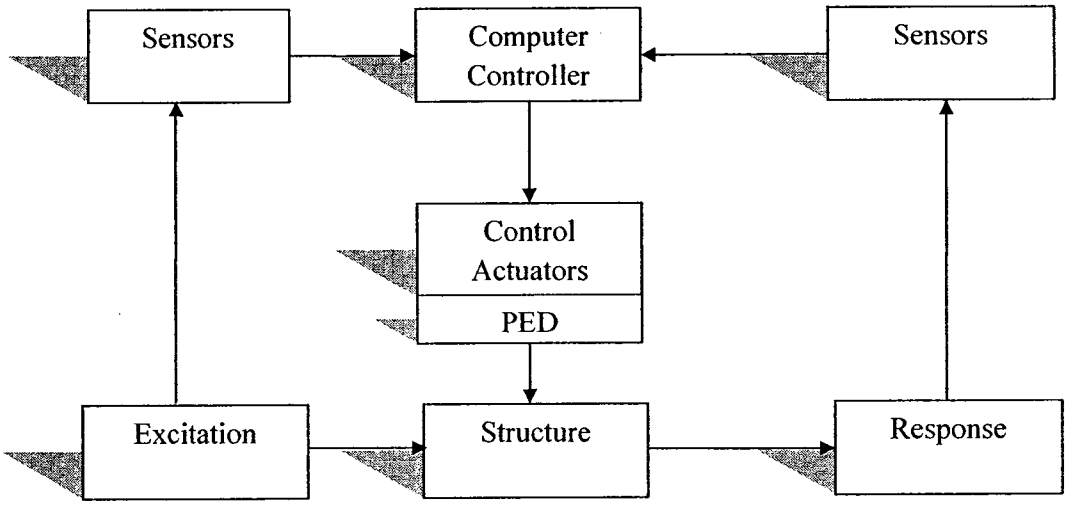

Figure 2.4: Structure with semi-active control (PED: passive energy dissipation)(Chu *et al.*, 2005)

2.2.4 Semi-active Control System

Semi-active control system is a compromise between active and passive control system which are based on semi-active devices. Semi-active devices are the combination of the best features of both passive and active control system (Housner *et al.,* 1997; Spencer and Sain 1997; Symans and Constantinou, 1999). These devices offer the adaptability of active control devices without requiring the associated large power sources. Many of these can operate on battery power alone, which is critical during seismic events when the main power source to the structure may fail.

According to presently accepted definitions, a semi-active control device is one that cannot inject mechanical energy into the controlled structural system (i.e. including the structure and control device), but has properties that can be controlled to optimally reduce the responses of the system. Therefore in contrast to active control devices, semi-active control devices do not have the potential to destabilize (in the bounded input/bounded output sense) the structural system (Housner *et al.,* 1997). Frequently such devices are referred to as controllable passive damper. Researchers found that appropriately implemented semi-active control system perform significantly better than passive control system and have the potential to achieve the majority of the performance features of fully active control system, thus allowing for the possibility of effective response reduction during a wide array of dynamic loading conditions (Dyke *et al.,* 1996a). Semi-active control system is schematically shown in Figure 2.4.

Some of the semi-active devices are:

a) Variable orifice fluid dampers,

b) Controllable friction dampers,

c) Adjustable tuned liquid dampers,

d) Controllable fluid dampers.

2.2.4.1 Controllable Fluid Damper

Controllable fluid damper is a class of semi-active devices that uses controllable fluids. The advantages of this class of semi-active devices among other semi-active devices is that they contain no moving parts other than the piston, which makes them very reliable and maintainable. Two fluids that are viable contenders for development of controllable fluid dampers are:

a) Electro-rheological (ER) fluids and

b) Magneto-rheological (MR) fluids.

These fluids are unique in their ability to reversibly change from a free-flowing, linear viscous fluid to a semi-solid with a controllable yield strength in milliseconds when exposed to an electric (for ER fluids) or magnetic (for MR fluids) field. These fluids flow freely and can be modeled as Newtonian fluid in the absence of applied electrical or magnetic field. When a field is applied, the Bingham plastic model (Shames and Cozzarelli, 1992) may be used to describe the fluid behaviour.

The discovery of ER fluids dates back to the late 1940s (Soong and Spencer, 2002), and many years of research concentrated on ER fluids. A number of ER fluid dampers have been developed, modeled and tested for civil engineering applications (Ehrgott and Masri, 1992). But still some obstacles remain in the development of commercially feasible damping devices using ER fluids. For example the best ER fluids currently can achieve a yield stress of only 3.0-3.5 kPa and common impurities (e.g. water) that might be introduced during manufacturing or usage significantly reduce the capacity of the fluid. Additionally, safety, availability and cost of the high voltage (e.g. ~ 4000 v) power supplies required to control the ER fluid are further impediments to consider (Soong and Spencer, 2002).

Recently developed MR fluids become an attractive alternative to ER fluids for use in controllable fluid dampers. MR fluid have maximum yield stress of 50 to 100 kPa and can be controlled with a low power (e.g. less than 50 watts), low voltage (e.g. ~12-24 v), and current-driven power supply outputting only ~1-2 A. It should be noted that batteries can readily supply such power levels. These fluids are not temperature sensitive and can operate at temperatures from -40 to 150° C with only modest variations in the yield stress (Carlson and Weiss, 1994). Moreover MR fluids are not sensitive to impurities like ER fluids such as those commonly encountered during manufacturing and usage. Therefore MR fluids become most promising for use in vibration control applications.

2.2.4.2 Magneto-rheological Fluid

This fluid is one kind of controllable fluids. It has characteristic to reversibly change from free-flowing, linear viscous liquids to semi-solids having controllable yield strength in milliseconds when exposed to magnetic field. The initial discovery and development of MR fluids and devices can be credited to Jacob Rabinow at the US National Bureau of Standards in the 1940s. These fluids typically consist of micron-sized magnetically polarisable particles dispersed in an appropriate carrier liquid. Normally MR fluids are free flowing liquids having a consistency similar to that of motor oil. When magnetic field is applied, the particles acquire a dipole moment aligned with the external field that causes particles forming linear chain parallel to the field (Yang *et al.,* 2002). This phenomenon as shown in Figure 2.5 can solidify the suspended particles and resist the fluid movement. Consequently, yield strength is developed within the fluid. This yield strength is controllable and depends on the magnitude of the applied magnetic field and can occur only in a few milliseconds (Yang, 2001).

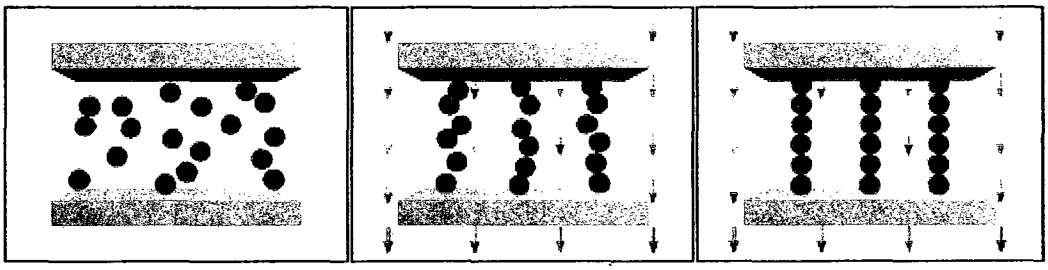

(a) No magnetic field (b) and (c) with increasing magnetic field

Figure 2.5: MR fluid behaviour (Wilson, 2005).

A typical MR fluid consists of 20-40 percent by volume of relatively pure, 3-10 micron diameter iron particles, suspended in a carrier liquid such as mineral oil, synthetic oil, water or glycol. Varieties of proprietary additives, similar to those found in commercial lubricants to discourage gravitational setting and promote particle suspension, are commonly added to MR fluid to enhance lubricity, modify viscosity and inhibit wear (Lord, 2009). The ultimate strength of the MR fluid depends on the square of the saturation magnetization of the suspended particles. Since the magnetic saturation depends on the type of the particles, selecting the particle with a large saturation magnetization is very important for obtaining a strong MR fluid (Carlson and Spencer, 1996a). The best available particle having saturation magnetization of about 2.4 tesla is made of alloys of iron and cobalt but such kinds of particles are expensive for most practical application. The most suitable and economical particles for MR fluids are simply made of pure iron and have a saturation magnetization of 2.15 tesla.

At present LORD corporation (Lord, 2009) manufactures six types of MR fluids for commercial purposes. These six types of MR fluids are:

1) MRF-122-2ED (Hydrocarbon-based)
2) MRF-122EG (Hydrocarbon-based)
3) MRF-132DG (Hydrocarbon-based)
4) MRF-140CG (Hydrocarbon-based)
5) MRF-241ES (Water-based)
6) MRF-336AG (Silicone-based).

2.2.4.3 MR Fluid Models

In the development of MR fluid devices, the MR fluid models play an important role. Performance of the MR fluid devices can be predicted with the accurate MR fluid models. In the work of Phillips (1969), modeling of ER and MR fluids has received significant attention and as such, the degree of accuracy available with existing models is quite good (Goncalves *et al.*, 2006).

In the absence of an applied magnetic field, MR fluids flow freely and can be modeled as Newtonian fluid (Chu *et al.*, 2005). When magnetic field is applied, micron-sized particles suspended in the fluid forming linear chain parallel to the field which restrict the motion of the fluid, thereby increasing the viscous characteristics of the suspension (Yang *et al.*, 2002). The mechanical energy needed to yield the microstructure increases as the applied field increases resulting in a field-dependent yield stress (Goncalves *et al.*, 2006). The field-dependent characteristics of controllable fluid may be described with the Bingham visco-plasticity model (Phillips, 1969). In this model the total shear stress is given by:

$$\tau = \tau_0(H)\mathrm{sgn}(\dot{\gamma}) + \eta(H)\dot{\gamma} \qquad |\tau| > |\tau_0| \text{ ----------2.1}$$

$$\dot{\gamma} = 0 \qquad |\tau| < |\tau_0| \text{ ----------2.2}$$

Where τ_0 is the yield stress caused by the applied magnetic field; H is the magnitude of the applied magnetic field; $\dot{\gamma}$ is the shear strain rate; and η is the field-dependent plastic viscosity, defined as the slope of the measured post-yield shear stress versus shear strain rate curve. The onset of flow does not occur until the shear stress exceeds the yield stress

(i. e. $\tau < \tau_0 \Rightarrow \dot{\gamma} = 0$). Figure 2.6 shows the Bingham plastic model, which is effective in presenting the field-dependent behaviour of yield stress.

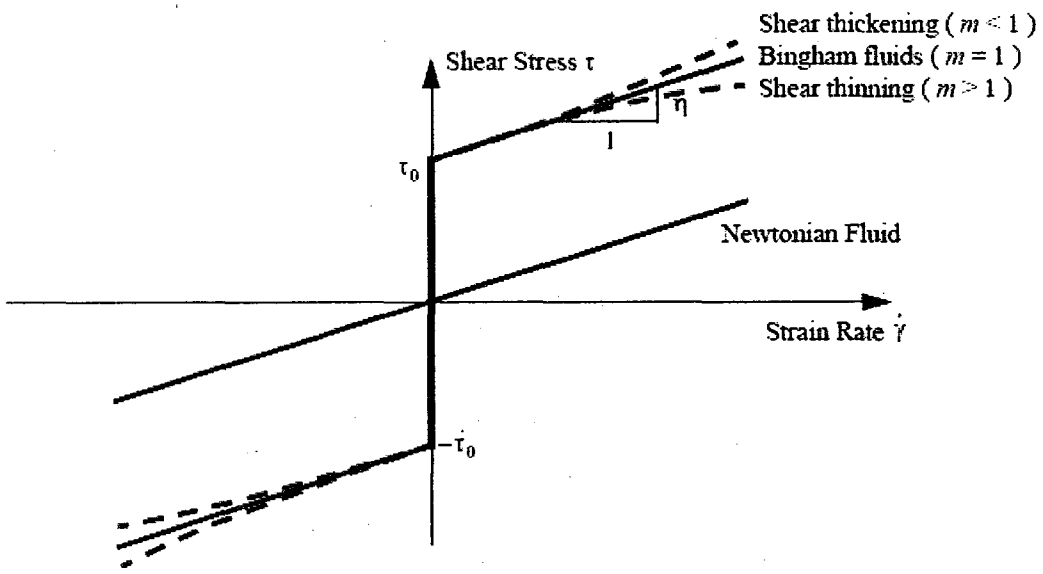

Figure 2.6: Visco-plasticity models of MR fluids (Yang, 2001).

As MR fluid typically exhibit shear thinning and thickening effect (Carlson, 2002), another model called Herschel-Bulkley visco-plasticity model (Herschel and Bulkley, 1926) may be employed to accommodate the fluid post-yield shear thinning and thickening effects. In this model, the constant post-yield plastic viscosity in the Bingham model is replaced with a power law model dependent on the shear strain rate. The model can reproduced as,

$$\tau = (\tau_0(H) + K|\dot{\gamma}|^{\frac{1}{m}})\mathrm{sgn}(\dot{\gamma}) \quad \text{----------2.3}$$

Where, m and K are the fluid parameters and m, $K>0$. Comparing Eq. 2.1 with Eq. 2.3 the equivalent plastic viscosity of Herschel-Bulkley model is

$$\eta_e = K|\dot{\gamma}|^{\frac{1}{m}-1} \quad \text{----------2.4}$$

Eq. 2.4 indicates that the equivalent plastic viscosity η_e decreases as the shear strain rate $\dot{\gamma}$ increases when $m>1$ (shear thinning). This model can also be used to describe the fluid shear thickening effect when $m<1$. The Herschel-Bulkley model reduces to the Bingham model when m=1, in which $\eta_e = K$.

2.2.4.4 Applications of MR Fluids

Interest in magneto-rheological fluids derives from their ability to provide simple, quite, rapid-response interfaces between electronic controls and mechanical systems (Jolly *et al.*, 1999). MR fluids technology has a potential for commercial success, while the commercial success of ER fluids remains elusive. A number of MR fluids and various MR fluid-based systems are now commercially available. One area of MR fluid applications is in active vibration control. They can be used as damping device to reduce vibrations by controlling the damping force needed to counteract the motion. Some of their applications are in automobile shock absorbers, engine mounts, mountain bikes, seat of tractor-trailers and off-highway vehicles (Carlson *et al.*, 1996). Rotary MR Fluid breaks are now used in exercise equipment as variable resistance elements in stair-climber and recumbent cycling machines and vibration control in domestic washing machines, (Carlson, 1999). Large capacity MR damper now is employed in seismic

response reduction of civil structure such as buildings and bridges. By using MR fluid technology, aircraft landing gear could be made more lightweight. MR fluid can also be used in lock/unlock devices. For example, the height of a bicycle seat could be adjusted by releasing the fluid and then locked into place by turning the field back on using permanent magnet. MR fluid could also be used in door closer mechanisms to dampen the door while closing and then locking the fluid to secure the door (Molyet, 2005).

All MR fluid based devices usually operates in three basic modes: (a) valve mode, (b) direct shear mode and (c) squeeze mode, or a combination of these modes (Carlson and Spencer 1996a). Figure 2.7 shows these three basic operating modes.

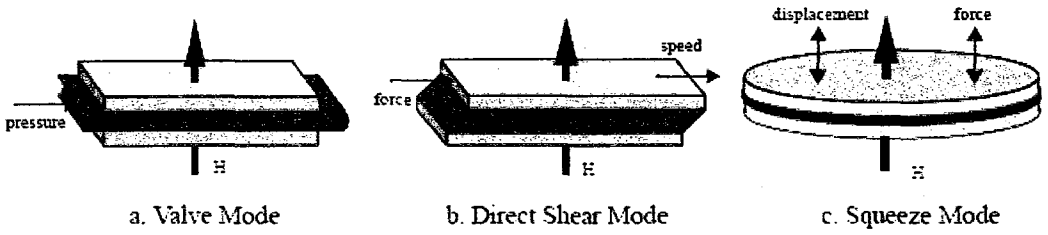

Figure 2.7: Basic operating modes for controllable fluid devices (Yang, 2001).

In the valve mode the fluid flows within a gap and resistance to flow can be controlled by changing the applied field. This can provide the force/velocity characteristics of a piston and cylinder arrangement. Examples of valve mode devices include servo-valves, dampers, shock absorbers and actuators. In the direct shear mode, the gap surfaces are free to translate or rotate with respect to each other. Such movement places the fluid in shear. In this mode continuous control of force or torque are available. Examples of direct shear mode devices are clutches, brakes, locking devices, breakaway devices and

dampers. In the squeeze mode, the gap surfaces can move away from or towards each other and the fluid is subjected to tensile and compressive loading, which results in small motions and high forces and can be used for small amplitude-vibration dampers (Stanway *et al.*, 1996, Carlson *et al.*, 1996).

MR dampers operating under direct shear mode or squeeze mode might not be suitable for civil engineering applications because in civil engineering applications, the expected damping forces and displacements are rather large in magnitude. Usually valve mode or its combination with direct shear mode is employed (Yang, 2001).

Magneto-rheological damper is a controllable fluid damper which uses MR fluid to provide controllable yield strength. Therefore it can be used as semi-active control device and expected to be applicable for a wide range of situation. There are three main types of MR damper namely mono tube, twin tube and the double ended MR damper.

2.3 Previous research on civil engineering application of MR damper

Control of civil engineering structures for earthquake hazard mitigation is a relatively new research area that is growing rapidly. Control system relying on large external power supplies may become ineffective because power supply system of the structure may fail during severe earthquake. Magneto-rheological dampers are a new class of device that can work even if the power supply systems of the structure fail during a severe seismic event as it has the low power requirements. Due to have the attractive features of

Magneto-rheological dampers described earlier, they have received the attention of many researchers in the field of Civil Engineering.

Dyke *et al.* (1996) did a research on modeling and control of magneto-rheological dampers for seismic response reduction. In their research they use the modified Bouc-Wen model (Spenser *et al.,* 1997) to model the hysteresis behaviour of MR damper and proposed a clipped-optimal acceleration feedback control strategy for controlling the MR damper. The effectiveness of their proposed algorithm and the usefulness of MR dampers for structural response reduction are demonstrated through a numerical example employing a seismically excited three-story model building shown in Figure 2.8. Two cases are studied.. In the first case, designated as passive-off, the command voltage to the MR damper is held at 0 V. In the second case the voltage to the MR damper is held at the maximum voltage level (2.25 V) and is denoted as passive-on. They found that the passive-off system reduces the maximum relative displacement of the third floor by 52.7% with respect to the uncontrolled structure and the passive-on system achieves a 68.1% reduction. Both passive systems reduce the upper story absolute accelerations and interstory displacements by approximately 50%. The clipped-optimal controller reduces the peak third-floor relative displacement by an additional 30.7% and the maximum peak interstory displacement by an additional 27.8% as compared with the best passive responses. They also compared their result with the ideal active control system. They found the peak third-floor relative displacement was 10% and the peak interstory displacements are also 15% smaller with the clipped-optimal controller than with the active control. Thus it is concluded that semi-active control system is capable of not only

approaching, but surpassing, the performance of a active control system, while only requiring a small fraction of the power that is required by the active controller.

During earthquake excitation a tall building with a large podium structure may suffer from a whipping effect due to the sudden change of lateral stiffness at the top of the podium structure. Qu and Xu (2001) worked to find the possibility of using ER/MR dampers to connect the podium structure to the tower structure to prevent this whipping effect and to reduce the seismic response of both structures. In their research they selected a 20-storey tower structure with a 5-storey podium structure shown in Figure 2.9 subjected to earthquake excitation. To evaluate the semi-active control performance on mitigation of the whipping effect and the seismic responses of both tower and podium structures they considered three cases. The first case is when the podium structure is rigidly connected to the tower structure (Case 1). The second case is when the podium structure is totally separated from the tower structure (Case 2). The last case is when the podium structure is connected to the tower structure by smart dampers (Case 3). For the case of using smart dampers to connect the podium structure to the tower structure, they used five smart dampers at each floor and a total of 25 identical smart dampers at the first five floors for both the tower and podium structures and they proposed a suboptimal displacement control strategy. They found that the maximum storey shear force of the tower structure in Case 1 jumps from 11000 kN at the 5^{th} storey to 26500 kN at the 6^{th} storey. The maximum storey shear forces of the tower structure above the 6^{th} floor in Case 1 are all much larger than those of the tower structure in Case 2. Though the maximum storey shear forces of the tower structure in the first five storeys are reduced to

some extent in Case 1, the maximum storey shear forces of the podium structures are increased in Case 1 compared with Case 2. This is because of the sudden change of lateral stiffness of the tower-podium system in Case 1, resulting in the so-called whipping effect. Thus it is clear that the whipping effect is quit unfavourable in the earthquake-resistant design of building structures. It was found that, with the installation of smart dampers, the whipping effect was totally eliminated. There was no sudden large change of the maximum storey shear force in the tower structure at the 6^{th} storey. The maximum storey shear forces of the tower structure with smart dampers at the 6^{th} storey above was much smaller than those of the tower structure in the Case 1 and almost same as in Case 2. The maximum storey shear forces of the tower structure with smart dampers in the first five storeys were much smaller than those in the Case 2. Also the maximum storey shear forces of the podium structure with smart dampers were the smallest among the three cases. Observations with respect to the maximum storey shear force were also found on the maximum floor displacement response. So, semi-active control technology may be a good solution for the problem under consideration. They also studied the "passive-off" and the "passive-on" modes. Finally they concluded that the smart dampers could not only prevent the tower structure's from whipping effect, but also, reduce the seismic responses of both the tower and podium structures at the same time. Even if the electric or magnetic field loses their functionality during earthquake, the smart dampers were still workable as passive viscous dampers. To confirm the aforementioned theoretical findings Xu *et al.* (2005) conducted an experimental study using a MR damper to connect a podium structure model to a building model. They built a slender 12-story building model and a relatively stiff three-story building model and tested under the scaled El Centro

1940 N-S ground motion for the four cases: without any Connection (Case 1), with a rigid connection (Case-2), with a MR damper connection in a passive-off mode (Case 3) and with a MR damper connection in a semi-active control mode using multilevel logic control algorithm. They found that the natural frequencies and mode shapes of the 12-story building were changed in Case 2. And shear force in the fourth floor and the acceleration and displacement responses at the top floor of the 12-story building had a considerable increase, indicating the so-called whipping effect. By using the MR damper to link the three-story building to the 12-story building and the multilevel logic control algorithm, the whipping effect of the 12-story building was totally eliminated and the seismic responses of the two buildings were significantly reduced, even compared with those of the totally two separated buildings.

Dominguez *et al.* (2007) studied the application of MR dampers in semi-adaptive structures. In their research they employed a non-linear model considering the frequency, amplitude and current excitation as dependent variables to simulate the hysteresis behaviour of the damper as discussed earlier in this thesis. They installed MR damper in a space truss structure shown in Figure 2.10 with four bays by replacing one member of the structure with the MR damper. They developed a finite element model of a bar element in which the MR damper is integrated. To validate their model, they fabricated a space truss structure with four bays embedded with MR damper and tested on a hydraulic shaker. They found good agreement between the experimental and simulation results. They observed that the amplitude and the fundamental natural frequency of the response has been well predicted by the numerical model.

Yoshida and Dyke (2005) conducted a research on the capabilities of semi-active control systems using magneto-rheological dampers when applied to numerical models of full scale asymmetric buildings. They considered one 9-story rectangular building with the asymmetry due to the distribution of shear walls and another L-shaped, 8-story building with additional vertical irregularity due to setbacks shown in Figure 2.11. In each case a device placement scheme based on genetic algorithm (GA) was used to place the control devices effectively. They evaluated the responses due to earthquake excitations, and compared the results to those of ideal active control systems and to passive control systems in which constant voltages are applied to MR dampers. They studied three separate control systems: passive-on, clipped-optimal control (Dyke *et al.*, 1996) and ideal active control. The passive-on controllers correspond to the situations in which a constant maximum voltage is applied to the MR dampers, the clipped-optimal controllers correspond to the semi-active control systems using MR dampers and the ideal active controller employs an active control system which can apply ideal control forces to the building. Results show that, the semi-active clipped-optimal control system achieves a performance similar to that of the ideal active controller. In most cases, the ideal active controller achieves a modest improvement over the clipped-optimal controller, but in some cases the clipped-optimal system performs slightly better than the ideal active control system in reducing the normed interstory drift, although it uses very little power. In comparing the performance of the clipped-optimal controller and the passive-on controller, the clipped-optimal controller is significantly better than the passive-on system in reducing the acceleration responses of both maximum and normed values.

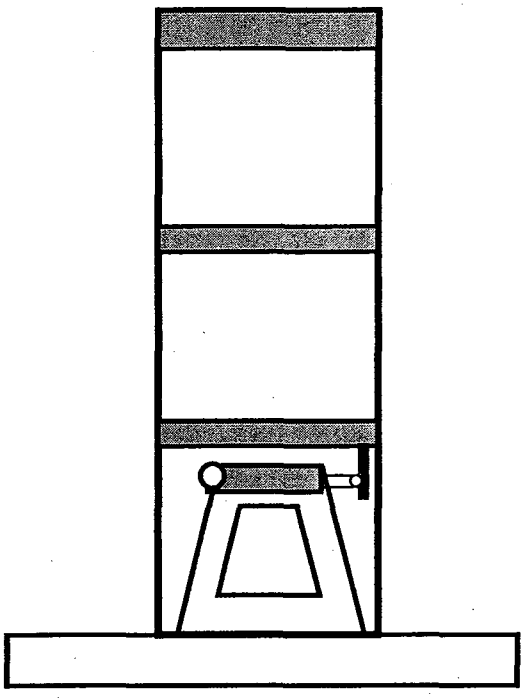

Figure 2.8: Diagram of MR damper implementation (Dyke *et al.*, 1996).

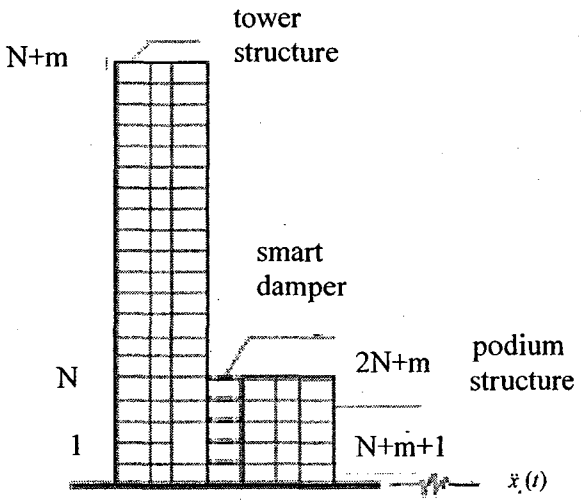

Figure 2.9: Tower structure and podium structure (Qu and Xu, 2001).

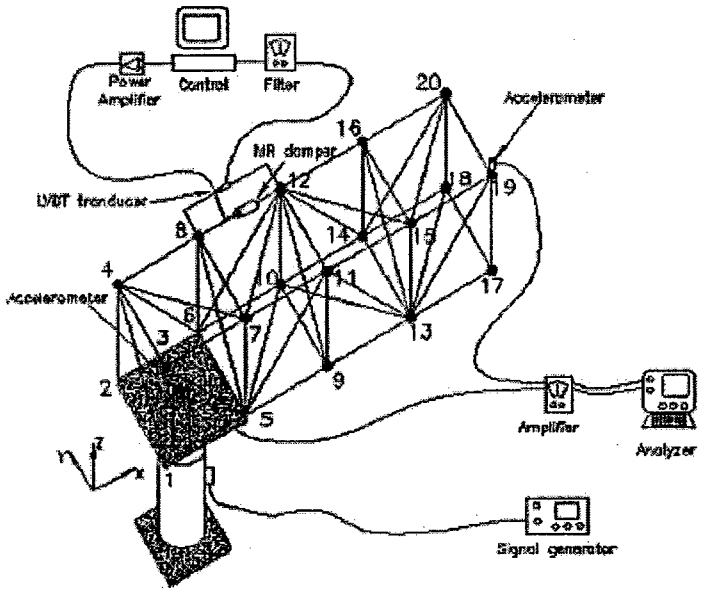

Figure 2.10: Schematic set-up of the test (Dominguez *et al.*, 2007).

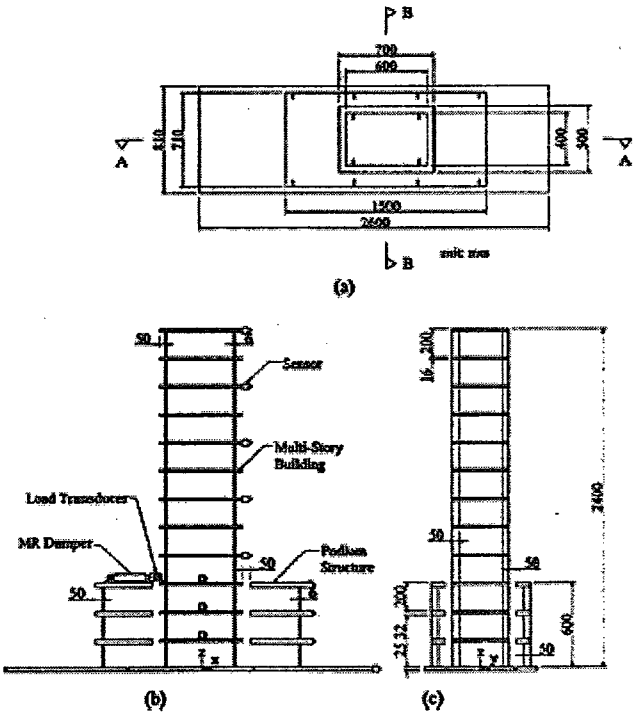

Figure 2.11: Configuration and instrumentation of building-podium structure system: (a) plan view; (b) section A-A; and (c) section B-B (Xu *et al.*, 2005).

2.4 Summary

Considerable amount of effort has been made in the research and development of suitable energy dissipation device to control the response of structure under seismic loading. As a result, many new and innovative concepts have been advanced and are of various stages of development including: passive, active, hybrid and semi-active control strategies. There are some drawbacks associated with each of the systems. Passive control is limited in the sense that it cannot deal efficiently with the change of either external loading or usage patterns from those used in its design. Although active and hybrid control system is adaptive to changes in external loading conditions, they have a number of serious challenges such as high capital cost and maintenance, huge external power requirements and potential stability problems. Semi-active control is a compromise between active and passive control systems. It combines the best features of both passive and active control systems. These devices offer the adaptability of active control devices without requiring the large power sources. Frequently such devices are referred to as controllable passive dampers. Researchers found that appropriately implemented semi-active control system perform significantly better than passive control and have the potential to achieve the majority of the performance attributes of fully active control system.

Magneto-rheological damper is a class of semi-active devices which use magneto-rheological fluid, and they are found to be more practical than other types of semi-active devices. MR fluids show controllable yield strength when exposed to magnetic field. These fluids has high yield strength with less power requirement and not sensitive to impurities. Therefore they are promising devices in vibration control area. A considerable

amount of research has been done in the area of MR damper modeling and controlling. The civil engineering profession and construction industry in many countries are conservative and generally reluctant to apply new technologies. Thus to increase the confidence of using new technology like MR damper in civil engineering structures more research is needed in this area.

CHAPTER 3

Types and Characteristics of MR Dampers

3.1 Introduction

Magneto-rheological dampers are semi-active control device that use magneto-rheological fluids to provide controllable yield strength and damping. As strength of magnetic field controls the yield stress of the fluid, it is expected to be applicable for a wide range of applications. A typical MR damper consists of a cylinder, a piston and MR fluid. MR fluid transferred from above the piston to below (and vice versa) through a valve. The MR valve is a fixed-size orifice which has the ability to apply a magnetic field using an electromagnet. This magnetic field changes the viscosity of the MR fluid and create a pressure differential for the flow of fluid in the orifice volume. The pressure differential is proportional to the force required to move the piston. Thus the damping characteristics of the MR damper is a function of current applied to the electromagnet and this relationship allows to control the damping characteristic of the MR damper in real time.

3.2 Types of MR damper

There are three main types of dampers called mono tube, twin tube and double-ended MR dampers (EL-Auoar, 2002). A mono tube MR damper shown in Figure 3.1 has only one

reservoir for the MR fluid and an accumulator mechanism to accommodate the change in volume that results from piston rod movement. The accumulator piston provides a barrier between the MR fluid and a compressed gas (usually nitrogen) that is used to accommodate the volume changes that occur when the piston rod enters the housing.

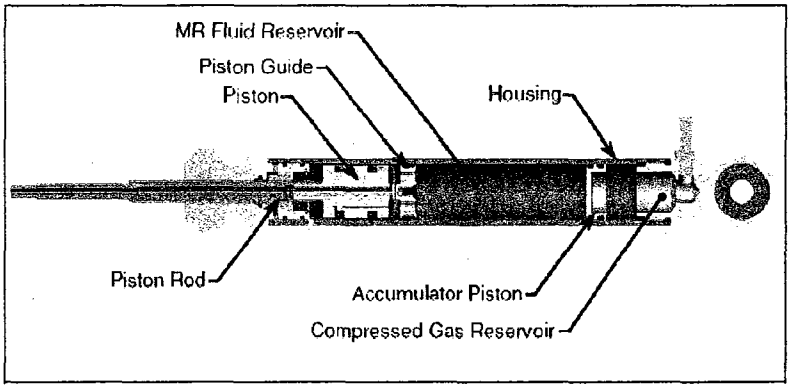

Figure 3.1: Mono tube damper (Malankar, 2001).

A twin tube MR damper is shown in Figure 3.2. It has two fluid reservoirs, one inside of the other. The damper also has an inner and outer housing, which are separated by a foot valve from each other. The inner housing guides the piston rod assembly; in exactly the same manner as in a mono tube damper. The volume enclosed by the inner housing is referred to as the inner reservoir and the space between the inner housing and the outer housing is referred to as the outer reservoir. The inner reservoir is filled with MR fluid so that no air pockets exist there. The outer reservoir, which is partially filled with MR fluids, that is used to accommodate changes in volume due to piston rod movement. Therefore, the outer tube in a twin tube damper serves the same purpose as the pneumatic accumulator mechanism in mono tube dampers. To regulate the flow of fluid between the

two reservoirs, an assembly called a "foot valve" is attached to the bottom of the inner housing.

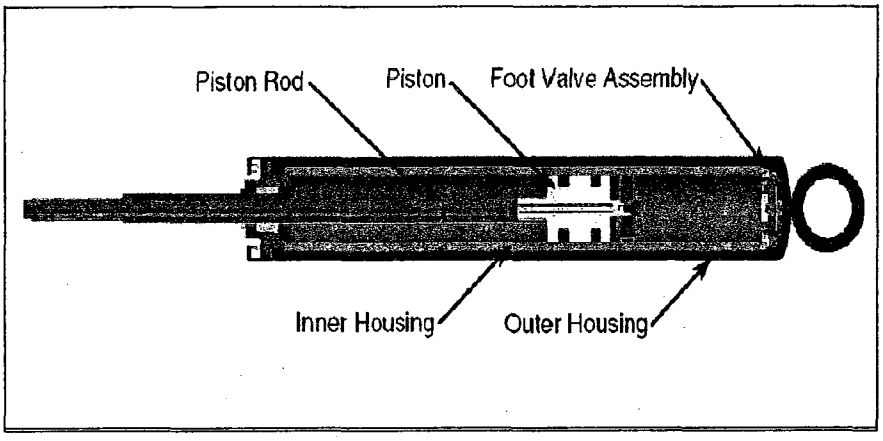

Figure 3.2: Twin tube MR damper (Malankar, 2001).

In double-ended damper as shown in Figure 3.3, a piston rod of equal diameter protrudes from both ends of the damper housing. An accumulator mechanism is not required in the double-ended damper, because, there is no volume changes as the piston rod moves relative to the damper body.

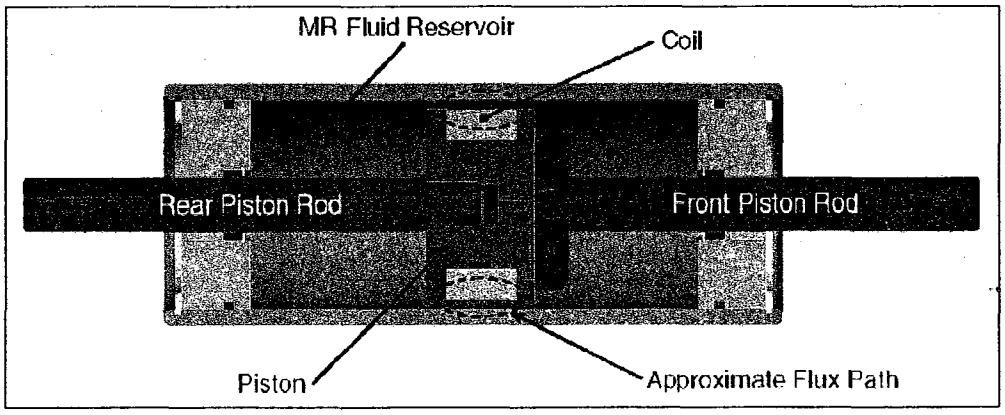

Figure 3.3: Double-ended MR damper (Malankar, 2001).

3.3 Modeling of MR fluid damper

To take the full advantage of the MR damper, it is very important to model the MR damper which can accurately reproduce the behaviour of the MR damper. Different models have been developed for describing the behaviour of MR damper. Several widely used model of MR dampers are briefly discussed here.

3.3.1 Bingham Model

The stress-strain behaviour of the Bingham viscoplastic model (Shames and Cozzarelli, 1992) is often used to describe the behaviour of MR (and ER) fluids. In this model, the plastic viscosity is defined as the slope of the measured shear stress versus shear strain rate as Eq. 2.1. Based on this model, Stanway *et al.* (1987) proposed an idealized mechanical model for the rheological behaviour of ER fluids which is applicable to MR dampers. The Bingham model consists of a Coulomb friction element placed in parallel with a viscous damper as shown in Figure 3.4.

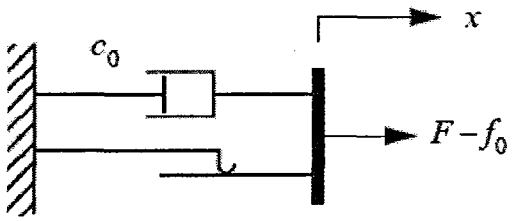

Figure 3.4: Bingham Model of a Controllable Fluid Damper (Spencer *et al.*, 1997).

In this model for nonzero piston velocities, $\dot{x}$, the force generated by the device given by

$$F = f_c \operatorname{sgn}(\dot{x}) + c_0 \dot{x} + f_0 \quad \text{----------3.2}$$

where, c_0 is the damping coefficient and f_c is the frictional force, which is related to the fluid yield stress. An offset in the force f_0 is introduced to account for the nonzero mean observed in the measured force due to the presence of the accumulator. It may be noted that at any point when the velocity of the piston is zero, the force generated in the frictional element is equal to the applied force. It was observed that the force-displacement behaviour appears to be reasonably modeled, but force-velocity behaviour of the damper is not captured well especially when the velocity is near zero (Spencer *et al.*, 1997).

3.3.2 Extended Bingham Model

Gamota and Filsko (1991) proposed a model for predicting the behaviour of ER materials, which has similar behaviour as the MR fluids. This is an extension of the Bingham model. As shown in Figure 3.5, this model consists of the Bingham model (i. e., a frictional element in parallel with a dashpot) in series with a standard model of linear visco-elastic material.

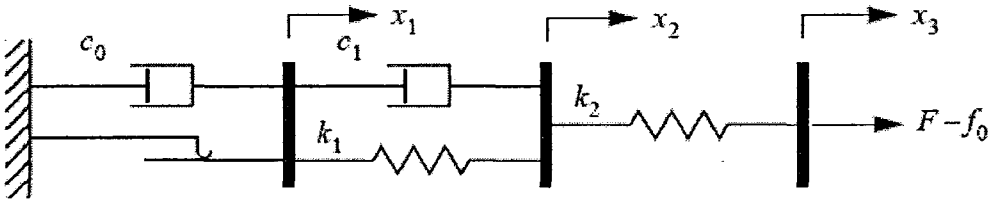

Figure 3.5: Extended Bingham Model (Gamota and Filisko, 1991).

The governing equations for this model can be represented as:

$$\left.\begin{aligned} F &= k_1(x_2 - x_1) + c_1(\dot{x}_2 - \dot{x}_1) + f_0 \\ &= c_0\dot{x}_1 + f_c \operatorname{sgn}(\dot{x}_1) + f_0 \\ &= k_2(x_3 - x_2) + f_0 \end{aligned}\right\} \qquad |F| > f_c \text{ ----------3.3}$$

$$\left.\begin{aligned} F &= k_1(x_2 - x_1) + c_1\dot{x}_2 + f_0 \\ &= k_2(x_3 - x_2) + f_0 \end{aligned}\right\} \qquad |F| \le f_c \text{ ----------3.4}$$

where, c_0 is the damping coefficient associated with the Bingham model and k_1, k_2 and c_1 are associated with the linear solid material. It may be noted that when $|F| \le f_c$, $\dot{x}_1 = 0$. It should also be noted that a decrease in the damping c_1, can produce the non-linear roll-off observed in the experimental force-velocity relationship when the velocity approaches zero but in that case it needs smaller time step to simulate the system (Spencer *et al.*, 1997).

3.3.3 Bouc-Wen Model

The Bouc-Wen (Wen, 1976) model is numerically tractable and has been used extensively to simulate the hysteresis loops presented by MR dampers since it possesses the force-displacement and force-velocity behaviour, which resembles that of real MR dampers. The Bouc-Wen model is shown in Figure 3.6.

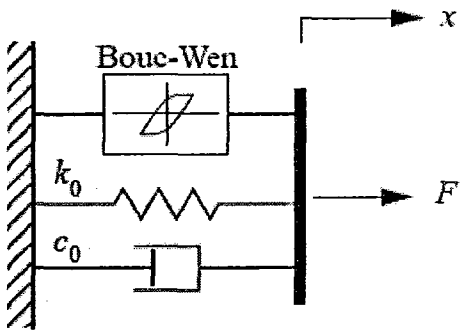

Figure 3.6: Bouc-Wen Model of the MR Damper (Spencer *et al.*, 1997).

Force in this model is governed by

$$F = c_0\dot{x} + k_0(x - x_0) + \alpha z \qquad \text{----------3.5}$$

where z is an evolutionary variable described by the first order differential equation as:

$$\dot{z} = -\gamma|\dot{x}||z|^{n-1}z - \beta\dot{x}|z|^n + A\dot{x} \qquad \text{----------3.6}$$

By tuning the parameters of the model γ, β, A, α and n one can control the linearity and smoothness of the transition from the pre-yield to the post-yield region. Due to the presence of the accumulator the force f_0 can be directly incorporated into this model as an initial deflection x_0 of the linear spring k_0. Similar to the Bingham model, the nonlinear force-velocity response of the Bouc-wen model does not roll-off in the region where the acceleration and velocity have opposite signs and the magnitude of the velocities are small (Spencer *et al.*, 1997).

3.3.4 Modified Bouc-Wen Model

To overcome the limitations associated with the above discussed model Spencer *et al.* (1997) proposed a modified Bouc-Wen model. The schematic of this model is shown in figure 3.7.

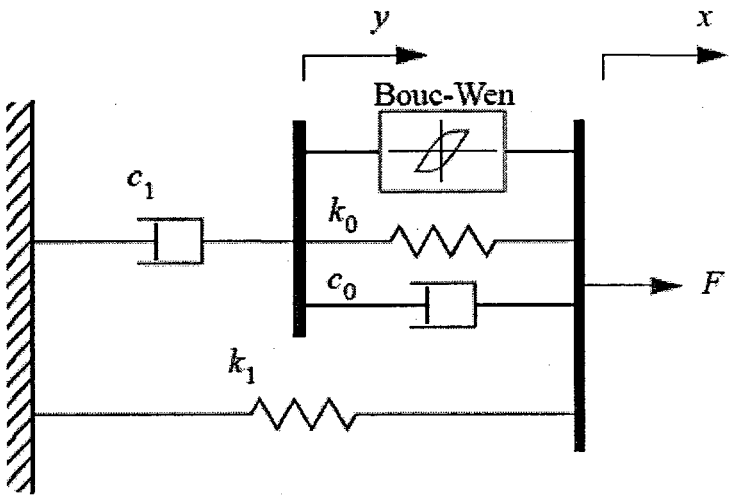

Figure 3.7: Modified Bouc-Wen Model (Spencer *et al.*, 1997)

Here the accumulator stiffness is represented by k_1 and the viscous damping observed at larger velocities by c_0. A dashpot represented by c_1, is included in the model to introduce the nonlinear roll-off in the force-velocity loops and k_0 is present to control the stiffness at large velocities. To obtain the governing equations for this model, let us consider only the upper section of the model. The forces on the either side of the rigid bar are equivalent; therefore,

$$c_1\dot{y} = \alpha z + k_0(x - y) + c_0(\dot{x} - \dot{y}) \quad \text{----------3.7}$$

where evolutionary variable z is governed by

$$\dot{z} = -\gamma|\dot{x}-\dot{y}||z|^{n-1}z - \beta(\dot{x}-\dot{y})|z|^{n} + A(\dot{x}-\dot{y}) \text{----------3.8}$$

Solving the Eq. 3.7 for $\dot{y}$ results in

$$\dot{y} = \frac{1}{(c_0 + c_1)}\{\alpha z + c_0\dot{x} + k_0(x-y)\} \text{----------3.9}$$

The total force generated by the system is then found by summing the forces in the upper and lower sections of the system giving

$$F = \alpha z + c_0(\dot{x}-\dot{y}) + k_0(x-y) + k_1(x-x_0) \text{----------3.10}$$

The total force can also be written as

$$F = c_1\dot{y} + k_1(x-x_0) \text{----------3.11}$$

Here x_0 is the initial displacement of spring k_1 associated with the nominal damper force due to the accumulator. By tuning the parameters of the model γ, β and A, one can control the shape of the hysteresis loops for the yielding element.

One of the major problems in the Bouc-wen model is the accurate determination of its characteristics parameters. Optimization or trial and error techniques are commonly used to estimate these characteristic parameters. These techniques demand high computational cost to generate the parameters. Furthermore, from the experiment, Dominguez *et al.* (2004, 2006, 2007) found that the hysteresis force for the MR damper is also sensitive to

the current, amplitude and the frequency of the excitation. To overcome the demand of high computational cost to generate the parameters and incorporate the effect of current, amplitude and frequency of the excitation, Dominguez *et al.* (2004, 2006, 2007) proposed a new non-linear model for the MR damper which includes the current, amplitude and frequency of the excitation as input variables.

Based on the rationale in the modified Bouc-Wen model incorporating the current, amplitude and frequency of the excitation as input variables may be reformulated in the following form (Dominguez *et al.*, 2006):

$$F(x(\tau),\dot{x}(\tau),I,\omega,x,0\le\tau\le t;t)=(\overline{d}_1\omega^{d_2})(d_3x_{\max}^{d_4})[c_0(I)\dot{x}+k_0(I)x+\alpha(I)z] \text{----------3.12}$$

Here ω is the frequency of the excitation, d_1 ..... d_4 are constant and z is the evolutionary variable defined by the following differential equation:

$$\dot{z}(I)=-\gamma(I)\,|\,\dot{x}\,|\,|\,z\,|^{(n-1)}\,z-\beta(I)\dot{x}\,|\,z\,|^{n}+A(I)\dot{x} \text{----------3.13}$$

Where A and β assumed to be one and zero, respectively. It was experimentally found by Dominguez *et al.* (2004, 2006, 2007) that the excellent agreement exist between the simulation and experimental results for any combinations of current, frequency and amplitude excitations, thus confirming that this model is able to predict the hysteresis force in the MR damper accurately and efficiently. As the characteristic parameters are function of the current, frequency and amplitude excitation, the hysteresis force of the MR damper can easily be evaluated for any desired combination of the frequency, amplitude and current excitations. Therefore the ability of this model to predict the

hysteresis force for any excitation condition can make it ideal for the semi-active control applications.

3.4 MR Damper used in the present research

In this research, three different MR dampers, produced by Lord Corporation (Lord, 2009) have been considered. Two of them are small scale dampers RD-1005-3, SD1000, and another is a large scale 20-ton prototype MR damper. Damper description and their behaviour details are presented in the following sections.

3.4.1 MR Damper RD-1005-3 (capacity 2.2 kN)

This MR damper is shown in Figure 3.8, is a compact magneto-rheological fluid damper offering high performance in its combination of controllability, responsiveness and energy density. As magnetic field is applied to MR fluid inside the monotube housing, the damping characteristics of the fluid increase with practically infinite precision and in under 15-millisecond response time (Lord, 2009).

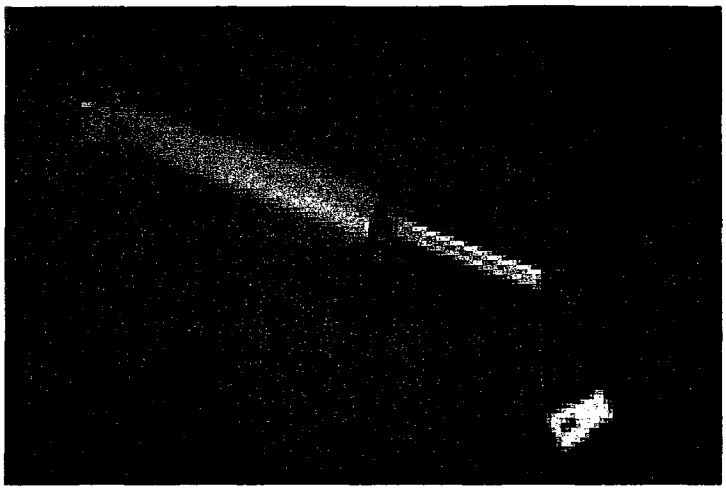

Figure 3.8: MR Damper (RD-1005-3) (Lord, 2009).

This device is a mono tube shock containing nitrogen gas at a high pressure of 300 psi (2068 kPa) in its accumulator. Summary of its typical characteristics is given in Appendix A. Behaviour of this damper is simulated using the model proposed by Dominguez *et al.* (2006) incorporating the current, amplitude and frequency of the excitation as input variables. Total damper force can be expressed by Eq. 3.12 and evolutionary variable z defined by the Eq. 3.13. Where A and β assumed to be one and zero, respectively and

$$\left.\begin{aligned} c_0(I) &= c_1 + c_2(1 - e^{-c_3(I-I_c)}) \qquad for \quad I > I_c \\ c_0(I) &= c_4 + \frac{c_4 - c_1}{I_c} I \qquad for \quad I \le I_c \end{aligned}\right\} \text{----------3.14}$$

$$k_0(I) = k_1 + k_2 I \text{----------3.15}$$

$$\left.\begin{aligned} \alpha(I) &= \alpha_1 + \alpha_2(1-e^{-\alpha_3(I-I_c)}) \qquad for \quad I > I_c \\ \alpha(I) &= \alpha_1 + \frac{\alpha_4 - \alpha_1}{I_c} I \qquad for \quad I \le I_c \end{aligned}\right\} \text{----------3.16}$$

$$\gamma(I) = \gamma_1 - \gamma_2 I \text{----------3.17}$$

$$\left.\begin{aligned} F_{z0}(I) &= F_{z01} + F_{z02}(1-e^{F_{z03}(I-I_c)}) \qquad for \quad I > I_c \\ F_{z0}(I) &= F_{z04} + \frac{F_{z04} - F_{z01}}{I_c} I \qquad for \quad I \le I_c \end{aligned}\right\} \text{----------3.18}$$

where, 16 constant $c_1, c_2, c_3, c_4, k_1, k_2, \alpha_1, \alpha_2, \alpha_3, \alpha_4, \gamma_1, \gamma_2, F_{z01}, F_{z02}, F_{z03}$ and F_{z04} relate the characteristic shape parameters to current excitation and should be specified in a way to better characterize the behaviour of MR dampers. I_c is the critical current in which the characteristic parameters change their linear behaviour in low velocity to exponential behaviour in high velocity.

Using these current dependent parameters, the solution of the evolutionary variable in Eq.-3.13 implies four different solutions which can be grouped as the following form:

$$z(I) = \frac{1}{\sqrt{\gamma(I)}} \tanh\left\{\sqrt{\gamma(I)}\left[\dot{x} + \frac{1}{\sqrt{\gamma(I)}} a \tanh \frac{F_{z0}(I)\sqrt{\gamma(I)}}{a(I)}\right]\right\} \; for \begin{cases} (z<0, x<0) \; or \\ (z \ge 0, x<0) \end{cases} \text{---3.19}$$

$$z(I) = \frac{1}{\sqrt{\gamma(I)}} \tanh\left\{\sqrt{\gamma(I)}\left[\dot{x} + \frac{1}{\sqrt{\gamma(I)}} a \tanh(-\frac{F_{z0}(I)\sqrt{\gamma(I)}}{a(I)}\right]\right\} \; for \begin{cases} (z \ge 0, x \ge 0) \; or \\ (z<0, x \ge 0) \end{cases} \text{---3.20}$$

Value of the 20 constant parameters determined experimentally by Dominguez *et al.* (2006) are given below.

$c_1 = 358$ Ns/m, $c_2 = 280$ Ns/m, $c_3 = 2.4$ A^{-1}, $c_4 = 230$ Ns/m, $k_1 = 1085$ N/m, $k_2 = 2928$ N/A-m, $\alpha_1 = 1514$ N/m, $\alpha_2 =$ 4200 N/m, $\alpha_3 = 2.2$ A^{-1}, $\alpha_4 = 82$ N/m, $\gamma_1 = 280$ m^{-2}, $\gamma_2 = 8.66$ m^{-2} A^{-1}, $d_1 = 5.08$ m, $d_2 = 0.333$, $d_3 = 0.251$ s/rad, $d_4 = 0.351$, $F_{z01} = 67$ N, $F_{z02} = 250$ N, $F_{z03} = 1.9$ A-1 and $F_{z04} = 1.32$ N.

As the characteristic parameters are function of the current, frequency and amplitude excitation, the hysteresis force of the MR damper can easily be evaluated for any desired combination of the frequency, amplitude and current excitations. Therefore the ability of this model to predict the hysteresis force for any excitation condition can make it ideal for the semi-active control applications. Typical force-displacement and force velocity behaviour of this damper under varying excitation amplitudes are shown in Figure 3.9 and 3.10, under varying current are shown in Figure 3.11 and 3.12 and under varying frequency are shown in Figure 3.13 and 3.14.

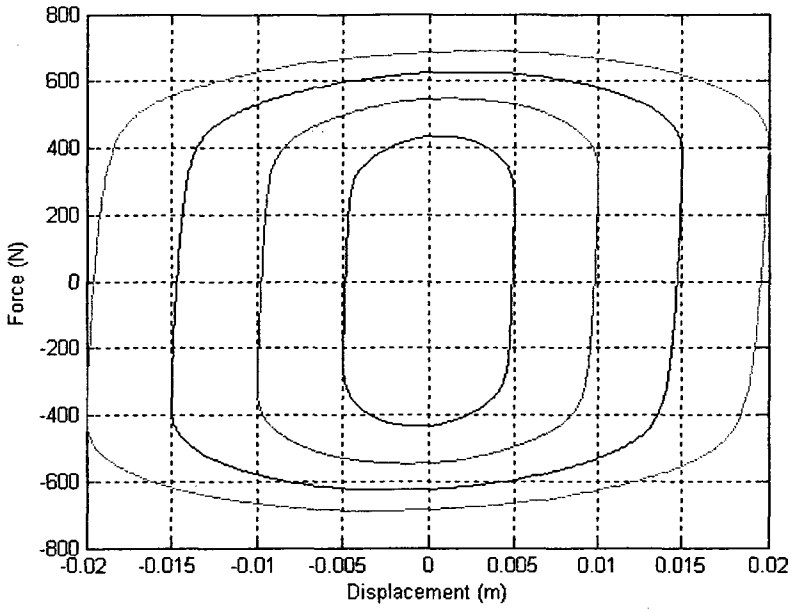

Figure 3.9: Force displacement behaviour of MR damper RD 1005-3 for amplitude of 5, 10, 15 and 20mm from inside to outside of lope.

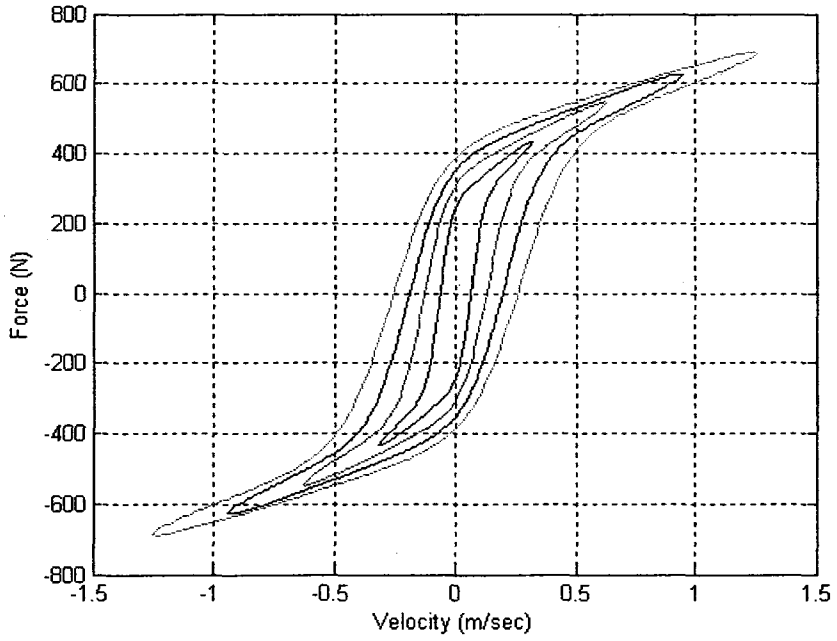

Figure 3.10: Force velocity behaviour of MR damper RD 1005-3 for amplitude of 5, 10, 15 and 20mm from inside to outside of lope.

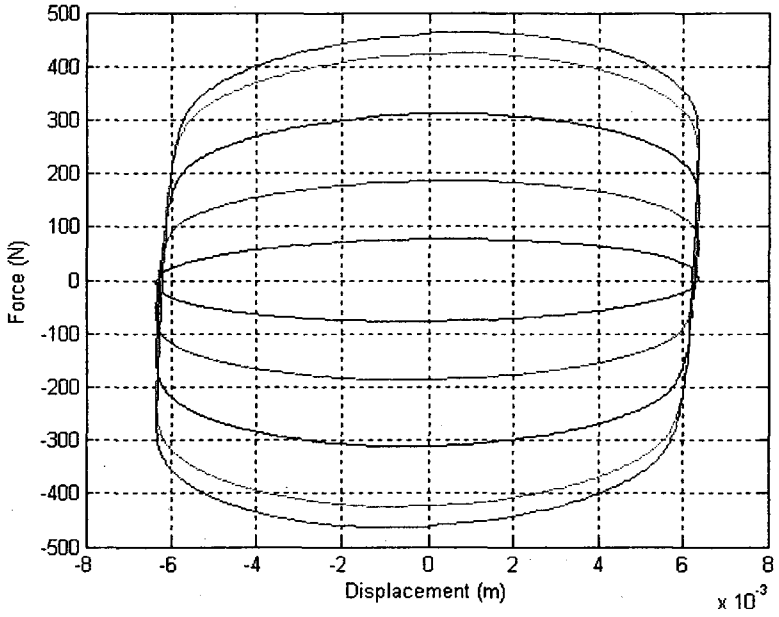

Figure 3.11: Force displacement behaviour of MR damper RD 1005-3 for current of 0, 0.25, 0.5, 1 and 1.5A from inside to outside lope.

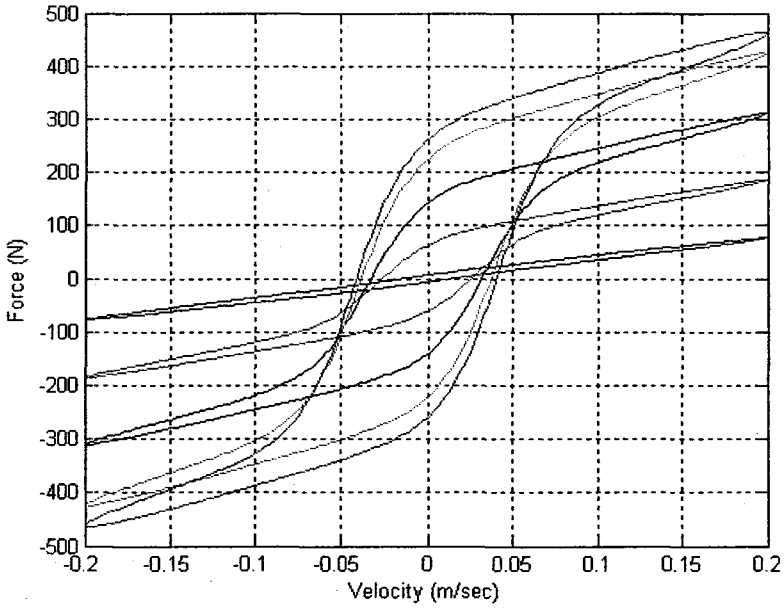

Figure 3.12: Force velocity behaviour of MR damper RD 1005-3 for current of 0, 0.25, 0.5, 1 and 1.5A from top to bottom.

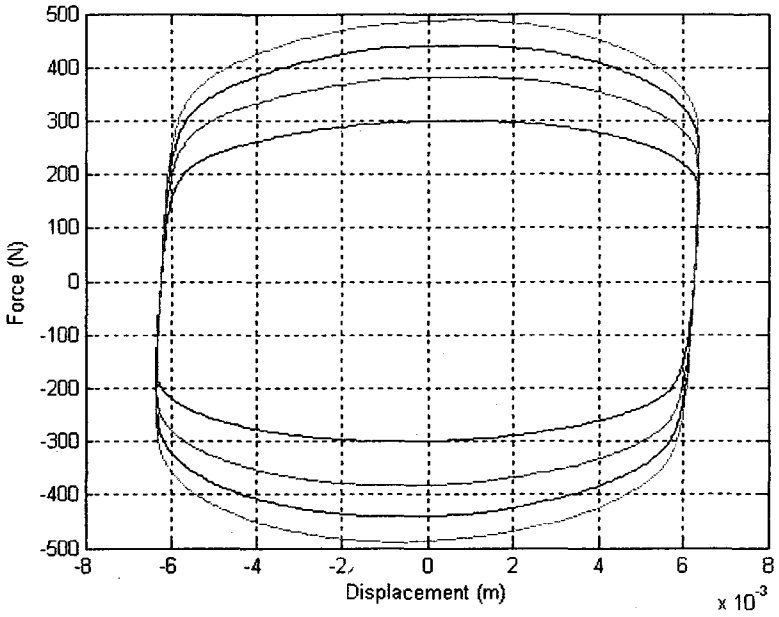

Figure 3.13: Force displacement behaviour of MR damper RD 1005-3 for frequency of 2.5, 5, 7.5 and 10 Hz from inside to outside lope.

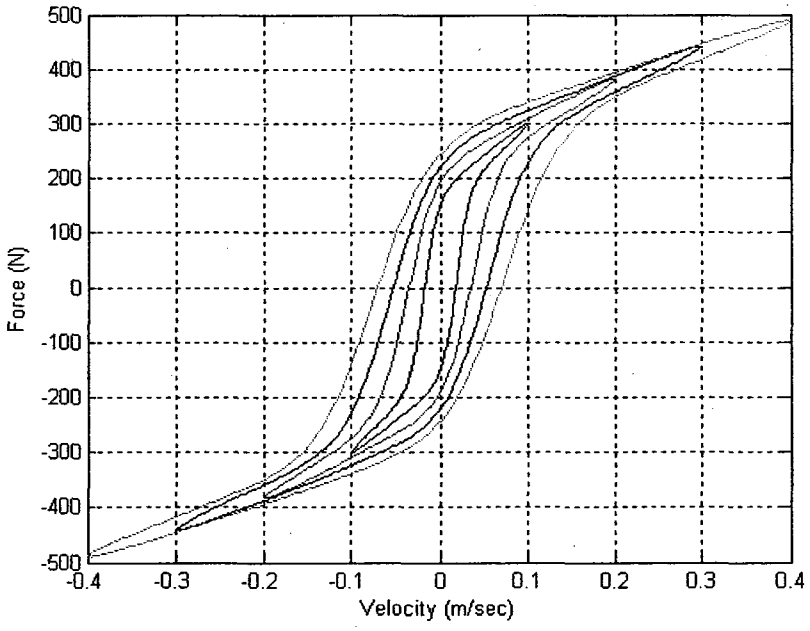

Figure 3.14: Force velocity behaviour of MR damper RD 1005-3 for frequency of 2.5, 5, 7.5 and 10 Hz from inside to outside lope.

3.4.2 MR Damper SD-1000 (capacity 3kN)

This is a fixed orifice small-scale MR fluid damper shown in Figure 3.15 manufactured by the Lord Corporation (Spencer *et al.*, 1997; Dyke *et al.*, 1996a,b; Jolly *et al.*, 1999). The main cylinder houses the piston, the magnetic circuit, an accumulator and 50 ml of MR fluid. The MR fluid valve is contained within the damper piston and consists of an annular flow channel. The magnetic field is applied radially across the resulting 0.5 mm dimension, perpendicular to the direction of fluid flow. Forces of up to 3000 N can be generated with this device. The characteristics of the damper described in Appendix A.

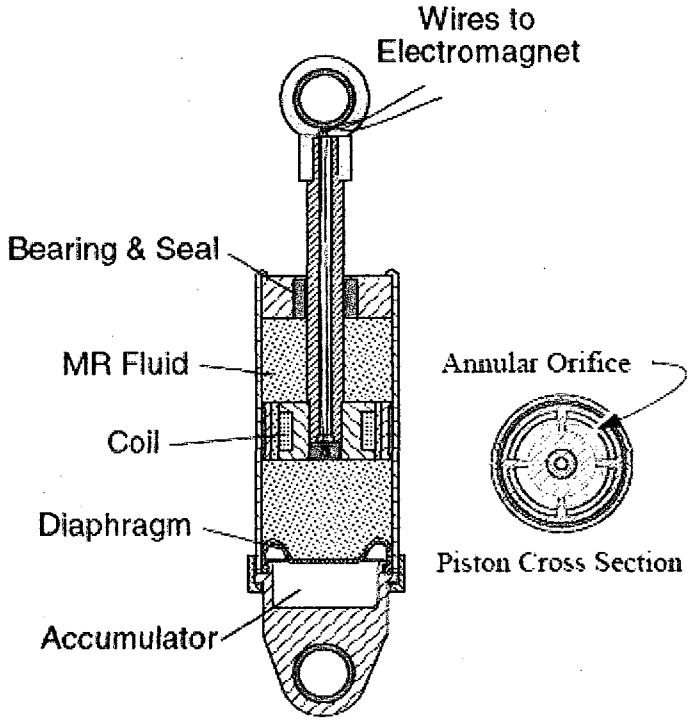

Figure 3.15: Small-scale SD-1000 MR fluid damper (Yang, 2001).

Behaviour of the MR damper is simulated using the modified Bouc-Wen model as shown in Figure 3.7 over a broad range of input (Spencer *et al.*, 1997; Dyke *et al.*, 1996a,b; Jolly *et al.*, 1999). The total damper force can be found as Eq.-3.21 or Eq.3.22.

$$F = \alpha z + c_0(\dot{x} - \dot{y}) + k_0(x - y) + k_1(x - x_0) \text{ ----------3.21}$$

Or,

$$F = c_1\dot{y} + k_1(x - x_0) \text{ ----------3.22}$$

Where the evolutionary variable z is governed by

$$\dot{z} = -\gamma|\dot{x} - \dot{y}||z|^{n-1}z - \beta(\dot{x} - \dot{y})|z|^n + A(\dot{x} - \dot{y}) \text{ ----------3.23}$$

$$\dot{y} = \frac{1}{(c_0 + c_1)}\{\alpha z + c_0\dot{x} + k_0(x - y)\} \text{ ----------3.24}$$

Here the accumulator stiffness is represented by k_1 the viscous damping observed at larger velocities by c_0. Viscous damping c_1, for force roll-off at low velocities, k_0 is represent the stiffness at large velocities, and x_0 is the initial displacement of spring k_1 associated with the nominal damper force due to the accumulator and γ, β, A are constant.

$$\alpha = \alpha(u) = \alpha_a + \alpha_b u \text{ ----------3.25}$$

$$c_1 = c_1(u) = c_{1a} + c_{1b}u \text{ ----------3.26}$$

$$c_0 = c_0(u) = c_{01} + c_{0b}u \text{ ----------3.27}$$

$$\dot{u} = -\eta(u - v) \text{ ----------3.28}$$

Where v is the applied voltage. The constants for this model are used as described by Dyke *et al.* (1996) and presented below.

c_{0a} =21.0 N s cm^{-1}, c_{0b} =3.50 N s cm^{-1}, k_0 =46.9 N cm^{-1}, c_{1a} =283 N s cm^{-1}, c_{1b} =2.95 N s cm^{-1}, k_1 =5.00 N cm^{-1}, x_0 = 14.3 cm, α_a =140 N cm^{-1}, α_b =695 N cm^{-1}V^{-1}, γ =363 cm^{-2}, β =363 cm^{-2}, A =301, n =2, η =190 s^{-1}

The damper has been implemented in a SIMULINK (MATLAB, 2007) model which is integrated to a finite element system here to study the behaviour of scaled buildings with this damper. Figure 3.16 and 3.17 shows force-displacement and force velocity behaviour respectively for different voltage input when sinusoidal displacement excitation of amplitude 1.5 cm and frequency 2.5 Hz.

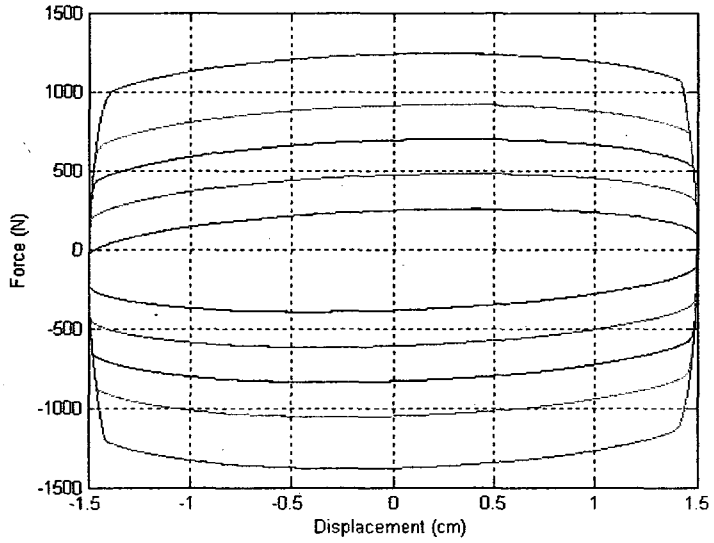

Figure 3.16: Force displacement behaviour of MR damper SD1000 for voltage 0V, 0.5V, 1V, 1.5V and 2.25V from inside to out side lope.

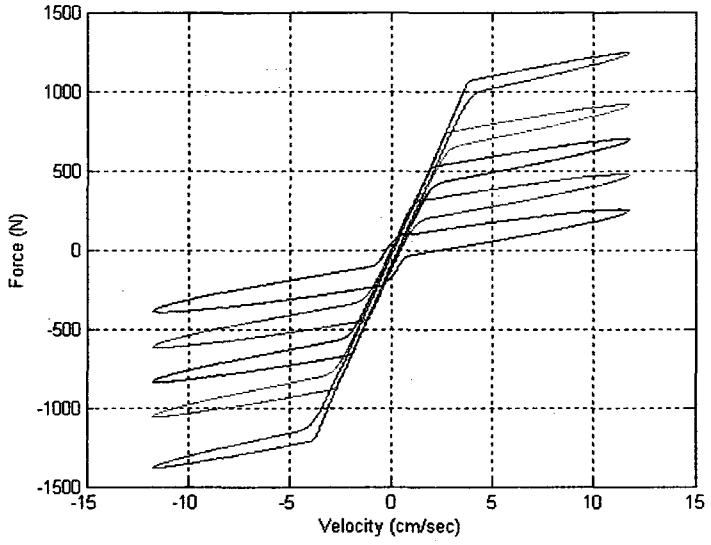

Figure 3.17: Force velocity behaviour of MR damper SD1000 for voltage 0V, 0.5V, 1V, 1.5V and 2.25V from top to bottom.

3.4.3 MR Damper MRD-9000 (capacity 200 kN)

To prove the scalability of MR fluid technology to devices of appropriate size for civil engineering applications, a full-scale, MR fluid damper has been designed and built (Spencer *et al.* 1998). For the nominal design, maximum damping force of 200000 N (20 ton) can be achieved. A schematic of the damper is shown in Figure 3.18.

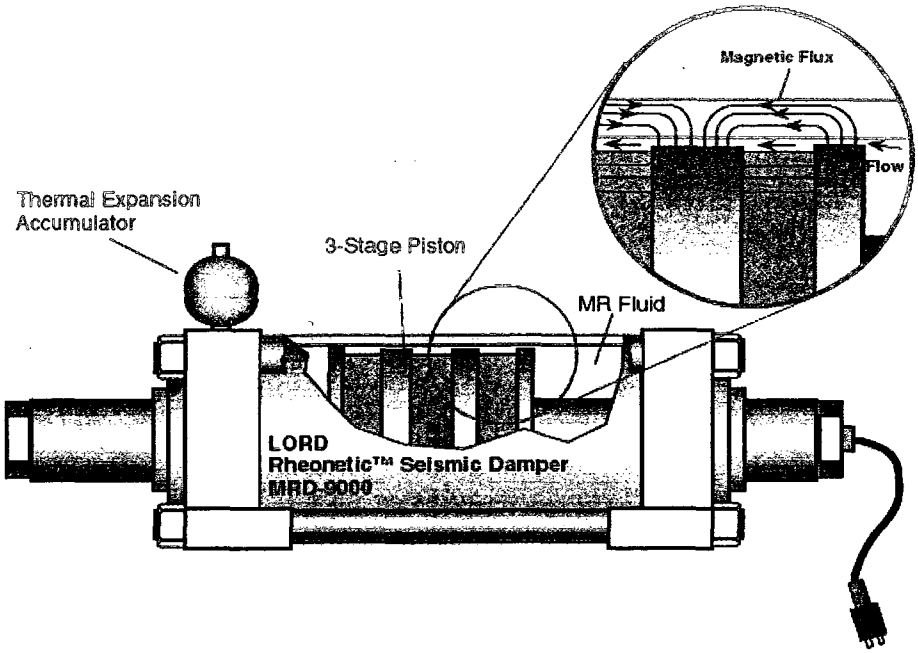

Figure 3.18: Schematic of 20-ton MR fluid damper (Yang, 2001).

It has simple geometry in shape in which the outer cylindrical housing is a part of the magnetic circuit. The effective fluid orifice is the annular space between the outside of the piston and the inside of the damper cylinder housing. The piston movement causes fluid to flow through this entire annular region. The damper is double-ended, i.e. the piston is supported by a shaft on both ends. This arrangement has the advantage that a rod-volume compensator does not need to be incorporated into the damper, although a small pressurized accumulator is provided to accommodate thermal expansion of the fluid. The damper has inside diameter of 20.3 cm and a stroke of ± 8 cm. The electromagnetic coil is wired in three sections on the piston and these results in four effective valve regions as the fluid flows pass the piston. The coils contain a total of 1.5 km of wire. The completed damper is 1 m long and with a mass of 250 kg. The damper

contains approximately 5 liters of MR fluid. The amount of fluid energized by the magnetic field at any given instant is approximately 90 cm^3. The design parameters of the 20-ton MR fluid damper are summarized in Appendix A. To predict the behaviour of the damper the mechanical model proposed by Spencer *et al.*, (1997) which is based on the modified Bouc-Wen model is used. According to this model the total force is given by Eq.3.29.

$$F = \alpha z + c_0(\dot{x} - \dot{y}) + k_0(x - y) + k_1(x - x_0) = c_1\dot{y} + k_1(x - x_0) \text{----------3.29}$$

where z and y is governed by

$$\dot{z} = -\gamma|\dot{x} - \dot{y}||z|^{n-1} - \beta(\dot{x} - \dot{y})|z|^n + A(\dot{x} - \dot{y}) \text{----------3.30}$$

$$\dot{y} = \frac{1}{(c_0 + c_1)}\{\alpha z + c_0\dot{x} + k_0(x - y)\} \text{----------3.31}$$

Here the accumulator stiffness is represented by k_1 and the viscous damping observed at larger velocities by c_0. Viscous damping is represented by c_1 for force at low velocities, k_0 represents the stiffness at large velocities, and x_0 is the initial displacement of spring k_1 associated with the nominal damping force due to the accumulator and γ, β, A are constant parameters. Yang *et al.*, (2002) proposed that α, c_0 and c_1 are function of current i and assume that the functions have the form of a third-order polynomial. For this large-scale 20-ton MR damper optimal equations for α, c_0 and c_1 are defined as (Yang et al. 2002).

$$\alpha(i) = 16566i^3 - 87071i^2 + 168326i + 15114 \text{----------3.32}$$

$$c_0(i) = 437097i^3 - 1545407i^2 + 1641376i + 457741 \text{----------} 3.33$$

$$c_1(i) = -9363108i^3 + 5334183i^2 + 48788640i - 2791630 \text{----------} 3.34$$

And the rest of the parameters are evaluated as (Yang *et al.*, 2002):

$A = 2679.0\ \text{m}^{-1}$, $\gamma = 647.46\ \text{m}^{-1}$, $\beta = 647.46\ \text{m}^{-1}$, $k_0 = 137810$ N/m, $n = 10$, $x_0 = 0.18$ m, $k_1 = 617.31$ N/m.

The damper model has been implemented in SIMULINK (MATLAB, 2007) which is integrated with a finite element system here to study the performance of full scale building frames integrated with this damper. Figure 3.19 and 3.20 shows force-displacement and force velocity behaviour respectively for different current input when sinusoidal displacement excitation of amplitude 0.0127m and frequency 1 Hz.

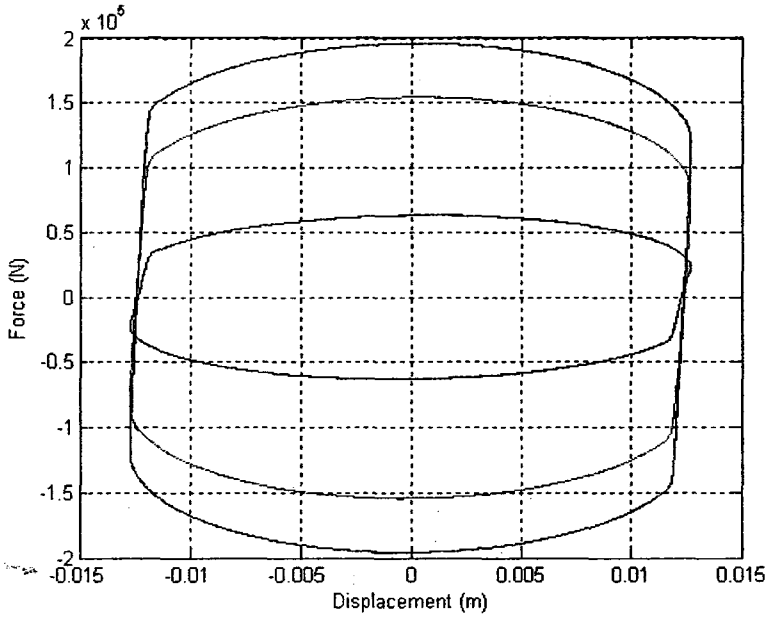

Figure 3.19: Force displacement behaviour of Mr damper MRD9000 for current 0A, 0.5A and 1A from inside to outside lope.

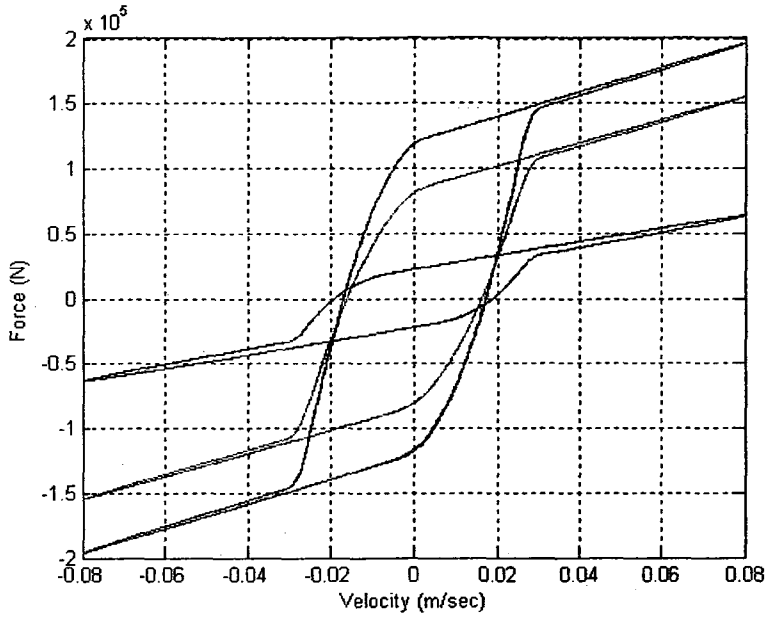

Figure 3.20: Force velocity behaviour of MR damper MRD9000 for current 0A, 0.5A and 1A from top to bottom.

3.5 Control Algorithm

Researchers have found that properly implemented semi-active control system can potentially achieve the majority of the performance criteria of fully active systems (Dyke, *et al.*, 1996; Ivers and Miller, 1989). Using semi-active approach, vibration is suppressed by enhancing damping characteristics, and therefore systems are always stable even with improper selection of control logic due to, for example, lack of exact information about the dynamic characteristics of the structure (Onoda *et al.*, 1997).

In this work on/off control strategy proposed by Dominguez, (2004) is used. In this strategy the velocity at the end of the MR damper in local coordinates and the hysteresis

force experienced by the MR damper is used. When both the velocity and hysteresis force have the same sign, it assigns maximum current and assigns zero current when the sign of both is different. The following strategies can be used for controlling an MR damper for current controlled systems.

$$\left.\begin{array}{lll} I_{\max} & when & \dot{x}_j F_z > 0 \\ I_{\min} & when & \dot{x}_j F_z \le 0 \end{array}\right\} \text{----------3.35}$$

where, $I_{\max}$ and $I_{\min}$ are the maximum and minimum currents, $\dot{x}_j$ is the damper end velocity and F_z is the damper force. If the current range is 0 to 2A, then 2A current will be needed when $\dot{x}_j F_z > 0$. For voltage controlled system the control strategy can be written as Eq. 3.36

$$\left.\begin{array}{lll} V_{\max} & when & \dot{x}_j F_z > 0 \\ V_{\min} & when & \dot{x}_j F_z \le 0 \end{array}\right\} \text{----------3.36}$$

$V_{\max}$ and $V_{\min}$ are the maximum and minimum voltages supplied to the damper.

CHAPTER 4
Computational Aspects

4.1 Introduction

Before analyzing any structure first an accurate model of the structure should be developed. Here finite element method which is powerful numerical technique has been used to model the structure. In this research two elements as space truss element and space frame elements are used to develop the building model. The system matrices are obtained by usual assembly of element matrices implemented in computer program M-FEM (Bagchi *et al.*, 2007). Once the system matrices are obtained the governing equations of motion can be established. After deriving the equations of motion in the finite element form, time integration technique can be used to solve the equations. In this work both Newmark method (Newmark, 1959) and State-space method (Lu *et al.*, 2006) are used to solve the governing differential equations. The subsequent sections describes the modeling of a structure, derivation of equations of motion, the solution process and calculation of the energy involved in the structural system during an earthquake. Finally a case is considered from previous research to validate the developed finite element program.

4.2 Finite element models of structures

To model and analyze structures in this research, Finite Element Method is used. The Finite Element Method (FEM) is a numerical method that is used frequently to find solution of complex engineering problems accurately. The basic ideas of the finite element method were presented by Turner *et al.* (1956). They presented the application of finite element for the analysis of aircraft structure and are considered as one of the key contributions in the development of the finite element method. Now this method is considered as one of the most powerful numerical techniques to efficiently solve a wide variety of practical problems.

In the finite element method, the actual continuum or body of matter like solid, liquid or gas is represented as an assemblage of subdivisions called finite elements. These elements are considered to be interconnected at specified joints called nodes or nodal points. The solution of a general structural problem using finite element method follows step-by-step procedure as (Rao, 1999):

- Discretization of the structure.
- Selection of a proper interpolation or displacement model.
- Derivation of element stiffness matrices and load vectors.
- Assemblage of element equations to obtain the overall equilibrium equations.
- Solution for the unknown nodal displacements.
- Computation of element strains and stresses.

4.2.1 Space truss element

A truss element is a bar which can resist only axial forces (compressive or tensile) and can deform only in the axial direction. Consider the pin-joint bar element as shown in Figure 4.1 where the local x-axis is taken in the axial direction of the element with origin at corner (or local node) 1. From the Figure 4.1 it can be seen that the stiffness and mass matrices of a space truss element will be of order 6x6. The stiffness and mass matrices obtained in the local axis can be transformed into global axis by using transformation matrix. The detailed formulation of element stiffness, mass and transformation matrix for space truss element can be found Appendix B.

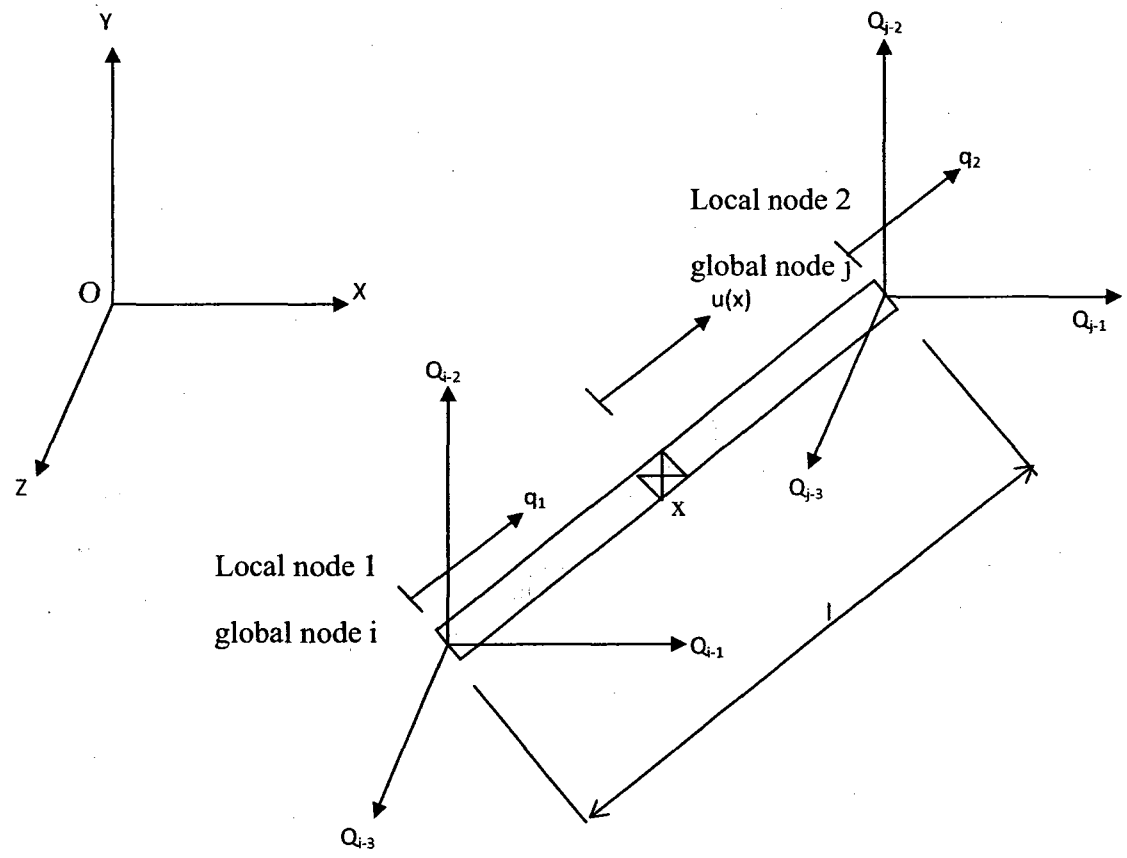

Figure 4.1: Space truss element.

4.2.2 Space frame element

A space frame element is a straight bar of uniform cross section which is capable of resisting axial forces, bending moment about the two principal axes in the plane of its cross section and twisting moment about its centroidal axis. The corresponding displacement degrees of freedom are shown in Figure 4.2. From Figure 4.2, it can be seen that the stiffness and mass matrices of a space frame element will be of order 12x12. The stiffness and mass matrices obtained in the local axis can be transformed into global axis by using transformation matrix. The detailed formulation of element stiffness, mass and transformation matrix for space frame element can also be found in Appendix B.

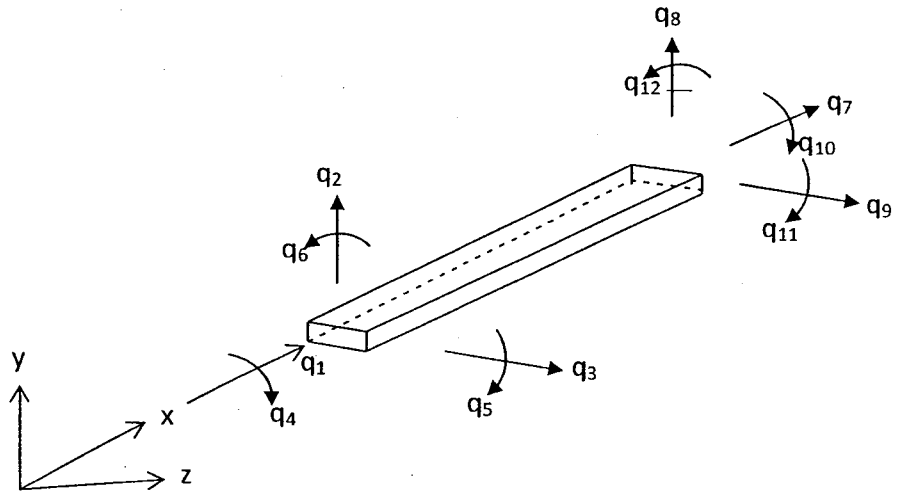

Figure 4.2: Space frame element with 12 degrees of freedom.

4.2.3 Finite element model of the bar element with MR damper

The detailed finite element model of a bar element that contains the MR damper is presented in Dominguez, *et al.* (2007) for a space truss system. A simplified model of bar element has been formulated here based on the model of Dominguez, *et al.* (2007).

Considering the mass of the MR damper is equally lumped at its both ends, the finite element model for MR damper can be obtained by applying the Second Newton's Law to the masses shown in Figure 4.3 as follows:

$$\left.\begin{aligned} c_0(\dot{x}_j - \dot{x}_i) + k_0(x_j - x_i) + \alpha z - F_0 &= \frac{m_{MR}}{2}\ddot{x}_i \\ c_0(\dot{x}_i - \dot{x}_j) + k_0(x_i - x_j) - \alpha z + F_0 &= \frac{m_{MR}}{2}\ddot{x}_j \end{aligned}\right\} \text{----------4.1}$$

where, m_{MR} is the mass of the MR damper k_0 is the time dependent stiffness mainly due to the effect of gas accumulator in the MR damper, c_0 is the time dependent viscous damping coefficient, αz is the evolutionary force and F_0 is initial force required to install the MR damper in its initial position. Eq. 4.1 can be rewritten in the matrix form as follows:

$$\begin{bmatrix} \frac{m_{MR}}{2} & 0 \\ 0 & \frac{m_{MR}}{2} \end{bmatrix}\begin{Bmatrix} \ddot{x}_i \\ \ddot{x}_j \end{Bmatrix} + \begin{bmatrix} c_0 & -c_0 \\ -c_0 & c_0 \end{bmatrix}\begin{Bmatrix} \dot{x}_i \\ \dot{x}_j \end{Bmatrix} + \begin{bmatrix} k_0 & -k_0 \\ -k_0 & k_0 \end{bmatrix}\begin{Bmatrix} x_i \\ x_j \end{Bmatrix} = \begin{bmatrix} 1 & 0 \\ 0 & 1 \end{bmatrix}\begin{Bmatrix} \alpha z \\ \alpha z \end{Bmatrix} + \begin{bmatrix} 1 & 0 \\ 0 & 1 \end{bmatrix}\begin{Bmatrix} -F_0 \\ F_0 \end{Bmatrix}$$

----------4.2

Or

$$[M_{MR}]\{\ddot{x}\} + [C_0]\{\dot{x}\} + [K_0]\{x\} = [I]\{F_z\} + [I]\{F_0\} \text{----------4.3}$$

where, $\{x\}$, $\dot{x}$ and $\ddot{x}$ are the vector of nodal displacement, velocity and acceleration for the MR damper respectively. $[M_{MR}]$ is the lumped mass matrix, $[C_0]$ is the damping matrix, K_0 is the stiffness matrix, $\{F_z\}$ is the hysteresis force vector and $\{F_0\}$ is the vector of initial force. As mentioned before, mass and stiffness matrices in the local coordinate system can be transformed to the global coordinate system using a

transformation matrix as described in Appendix B. Similarly the damping matrix can also be transformed to global coordinate system as follows:

$$[C_0]^g = [\lambda]^T [C_0][\lambda] \text{----------4.4}$$

where, $[\lambda]$ is the transformation matrix for space truss element described in Appendix B. Having FEM for the MR damper, the FEM for the bar element that contains the MR damper can be formed. The bar element can be represented as Figure 4.4 which consists of three individual members. The end element E_1 and E_3 are the bar members employed to couple the middle element representing the MR damper. Considering this, the equivalent stiffness and mass parameters may be written as follows:

$$k_{eq}^{-1} = \frac{k_0 k_2 + k_1 k_2 + k_1 k_0}{k_1 k_0 k_2} \text{----------4.5}$$

$$m_{eq} = m_1 + m_{MR} + m_2 \text{----------4.6}$$

Which can be used to formulate the following equivalent stiffness and mass matrices in the local coordinates.

$$\left.\begin{aligned} \left[K_{eq}^{(e)}\right] &= k_{eq}\begin{bmatrix} 1 & -1 \\ -1 & 1 \end{bmatrix} \\ \left[M_{eq}^{(e)}\right] &= \frac{m_{eq}}{2}\begin{bmatrix} 1 & 0 \\ 0 & 1 \end{bmatrix} \end{aligned}\right\} \text{----------4.7}$$

It should be noted here that the stiffness matrix for the MR damper bar element has time dependent coefficients due to inherent non-linearity of the controllable damper. Therefore matrix formulation of the structure can be written as

$$[M]\{\ddot{x}(t)\} + [C(t)]\{\dot{x}(t)\} + [K(t)]\{x(t)\} = \{F(t)\} \text{----------4.8}$$

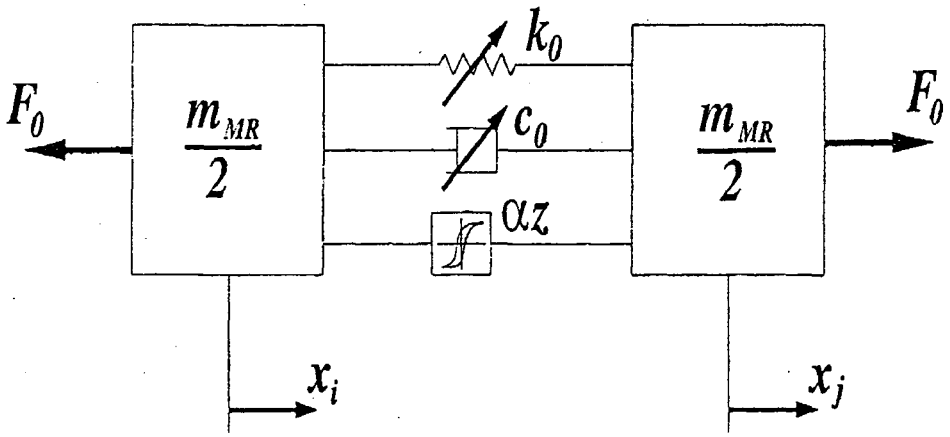

Figure 4.3: Lumped mass representation of an MR damper bar element (Dominguez *et al.*, 2007).

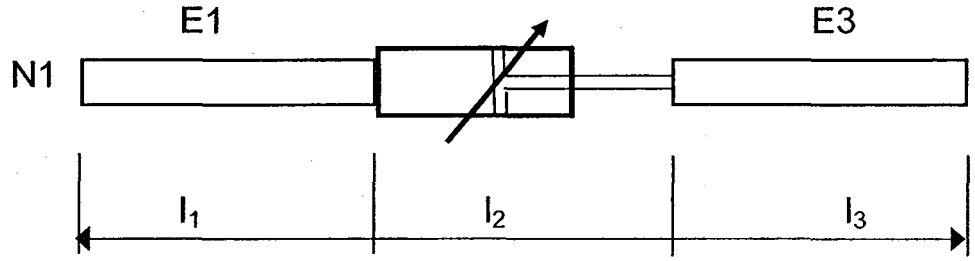

Figure 4.4: Finite element for the MR damper bar element.

4.3 Construction of damping matrix

Damping in a structural system is very important in predicting transient response, decay time or other characteristics in design and analysis. Although the damping effects in structural systems are clear, the characterization of the damping is still under development. However some approaches are available with good accuracy (Chopra, 2007; Pilkey, 1998; Hasselman, 1972; Dominguez, *et al.*, 2007). The proportional damping methodology is adopted in this work. In proportional damping, the damping matrix $[C]$ is assumed to be proportional to the mass matrix $[M]$ or to the stiffness

matrix $[K]$ or combination of both according to the Rayleigh's proportional damping. These proportional damping can be stated as;

$$[C]=\alpha[M],\ [C]=\beta[K] \text{ or } [C]=\alpha[M]+\beta[K] \quad \text{----------4.9}$$

where, α and β are constant.

The concept of proportional damping can be used to easily develop the governing differential equation. To accomplish this, one needs to obtain first the eigenvalues and eigenvectors of the undamped free vibration system. The equations of motion for undamped free vibration can be stated as:

$$[M]\{\ddot{u}\}+[K]\{u\}=\{0\} \quad \text{----------4.10}$$

The solution of Eq. 4.10 can be described by simple harmonic function as:

$$\{u\}=\{\phi\}(A\cos\omega t+B\sin\omega t) \quad \text{----------4.11}$$

where, A and B are constants of integration that can be determined from initial conditions. $\{\phi\}$ is amplitude vector, ω is the frequency of vibration of the system and t is the time variable. Substituting Eq. 4.11 into Eq. 4.10 yields:

$$[K]\{\phi\}=\omega^2[M]\{\phi\} \quad \text{----------4.12}$$

Eq. 4.12 is called the eigenvalue problem in which $\{\phi\}$ and ω are the eigenvector and eigenvalue respectively. A system having n degrees of freedom has n solutions for the eigenproblem which can be represented in matrix form as:

$$[K][\Phi]=[M][\Phi][\Omega]^2 \quad \text{----------4.13}$$

The matrix $[\Phi]$ is called modal matrix containing n column eigenvectors and $[\Omega]^2$ is known as the spectral matrix of the eigenvalue problem with the eigenvalues ω_i^2 on its diagonal as follows:

$$[\Phi]=\begin{bmatrix} \phi_{11} & \phi_{12} & \cdot & \cdot & \cdot & \phi_{1n} \\ \phi_{21} & \phi_{22} & \cdot & \cdot & \cdot & \phi_{2n} \\ \cdot & \cdot & \cdot & & & \cdot \\ \cdot & \cdot & & \cdot & & \cdot \\ \cdot & \cdot & & & \cdot & \cdot \\ \phi_{n1} & \phi_{n2} & \cdot & \cdot & \cdot & \phi_{nn} \end{bmatrix} \text{----------4.14}$$

$$[\Omega]^2=\begin{bmatrix} \omega_1^2 & & & & & \\ & \omega_2^2 & & & & \\ & & \cdot & & & \\ & & & \cdot & & \\ & & & & \cdot & \\ & & & & & \omega_n^2 \end{bmatrix} \text{----------4.15}$$

If the vector ϕ_n is a natural mode, any vector proportional to ϕ_n essentially provides the same natural mode. Natural modes have orthogonal characteristics and sometimes scale factors are applied to natural modes to standardize them associated with various DOFs. This process is called normalization. Now considering orthogonality of natural modes with respect to mass and stiffness matrices and using normalization, one may write:

$$[M_n]=[\Phi]^T[M][\Phi]=[I] \text{----------4.16}$$

where, $[I]$ is the identity matrix, which is a diagonal matrix with unit values along the main diagonal. Using Eq. 4.13 and 4.16 it can also be shown that

$$[\Phi]^T[K][\Phi]=[\Omega]^2 \text{----------4.17}$$

Now let us assume the governing differential equations of motion for damped system as:

$$[M]\{\ddot{u}\}+[C]\{\dot{u}\}+[K]\{u\}=\{F\} \text{----------4.18}$$

To decouple the Eq. 4.18, the following linear transformation can be used:

$$\{u\}=[\Phi]\{q\} \text{----------4.19}$$

where, $\{q\}$ is referred to as modal coordinates.

Now substituting Eq. 4.19 into 4.18 and multiply both sides by $[\Phi]^T$ and using Eq. 4.16 and 4.17, one can obtain:

$$[I]\{\ddot{q}\}+[\Phi]^T[C][\Phi]\{\dot{q}\}+[\Omega]^2\{q\}=[\Phi]^T\{F\} \quad \text{----------4.20}$$

It can be seen that the first and third left term of Eq. 4.20 are diagonal matrices because of orthogonality relation between the eigenvectors and mass $[M]$ and stiffness $[K]$ matrices. The second term $[\Phi]^T[C][\Phi]$ may or may not be diagonal, depending on the distribution of damping in the system. If the second term of Eq. 4.20 is diagonal then the Eq. 4.20 represents n uncoupled differential equations in modal coordinates q. Using proportional damping concept, one is able to diagonalize the second term of Eq. 4.20. It is common practice to assume the second term of Eq. 4.20 has the form:

$$[\Phi]^T[C][\Phi]=2[\Omega][\zeta] \quad \text{----------4.21}$$

Where the modal damping ratio matrix $[\zeta]$ is represented by:

$$[\zeta]=\begin{bmatrix} \zeta_1 & 0 & . & . & . & 0 \\ 0 & \zeta_2 & . & . & . & 0 \\ . & . & . & & & . \\ . & . & & . & & . \\ . & . & & & . & . \\ 0 & 0 & . & . & . & \zeta_n \end{bmatrix} \quad \text{----------4.22}$$

From the practical point of view, the damping factor ζ_i and the undamped natural frequency ω_i can be interpreted as being inherent properties of the system. Typical values of the damping ratio ζ_i for various types of structures are available from experimental studies. Knowing the modal damping factors and undamped natural frequencies, the damping matrix $[C]$ can be formed from Eq. 4.21 as:

$$[C] = 2[\Phi]^{-T}[\Omega][\zeta][\Phi]^{-1} \text{ ----------4.23}$$

4.4 Formulation of equations of motion

One of the principal problems of structural dynamics that concerns civil engineers is the behavior of structures subjected to earthquake-induced motion. Consider a one story one bay frame structure as shown in Figure 4.5(a). The mass is lumped at middle of the floor and assumed to move just horizontally (single degree of freedom). The displacement of the ground is denoted by u_g, the total displacement u^t and relative displacement between the mass and ground by u. At each instant of time these displacements are related by

$$u^t(t) = u(t) + u_g(t) \text{ ----------4.24}$$

Both u^t and u_g refer to the same frame of reference and their positive directions. The equation of motion for the structure subjected to an earthquake can be derived by using the concept of dynamic equilibrium and from the free-body diagram as shown in Figure 4.5(b).

$$f_I + f_D + f_s = 0 \text{ ----------4.25}$$

Where f_I is inertia force which can be represented as:

$$f_I = m\ddot{u}^t(t) = m(\ddot{u}(t) + \ddot{u}_g(t))$$

f_D is damping resisting force described as:

$$f_D = c\dot{u}(t)$$

where c is damping coefficient and f_s is elastic resisting force:

$$f_s = ku(t)$$

where k is lateral stiffness of the structure. Substituting the value of f_I, f_D and f_s in Eq. 4.25 yields:

$$m(\ddot{u}(t) + \ddot{u}_g(t)) + c\dot{u}(t) + ku(t) = 0$$

Or

$$m\ddot{u}(t) + c\dot{u}(t) + ku(t) = -m\ddot{u}_g(t) \text{ ----------4.26}$$

For multi degree of freedom system the equation of motion can be obtain by rewriting Eq. 4.26 in the matrix form as:

$$[M]\{\ddot{u}(t)\} + [C]\{\dot{u}(t)\} + [K]\{u(t)\} = -[M]\{1\}\ddot{u}_g(t) \text{ ----------4.27}$$

where $[M]$,$[C]$ and $[K]$ are mass, damping and stiffness matrices of the structure respectively. The derivation of stiffness and mass matrices is discussed in section 4.2 Derivation of damping matrix is discussed in section 4.3.

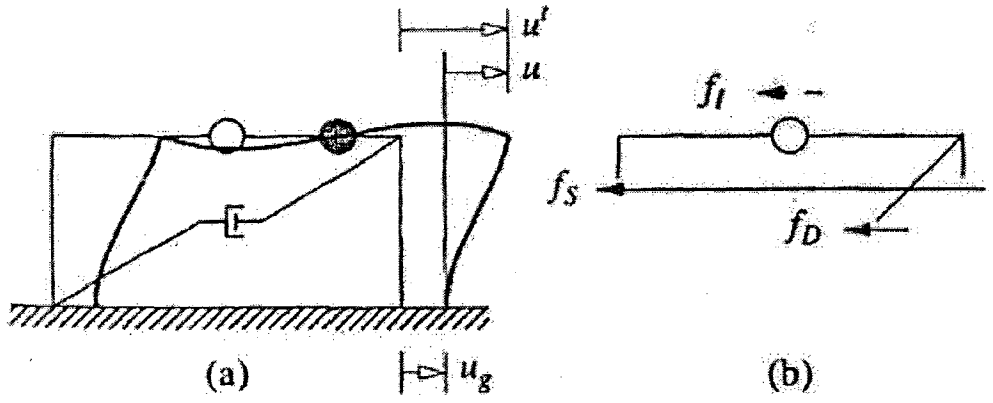

Figure 4.5: (a) System subjected to earthquake ground motion, (b) Free-body diagram (Chopra, 2007)

4.5 Solution of the equations of motion

Once the system mass, stiffness and damping matrices are identified, the governing equations of motion can be established. Various methods are available to solve the equations of motion to obtain the responses of the system. Two methods to solve the equations of motion are used in this work and described in the following sections.

4.5.1 Solution of equations of motion by Newmark's method

Let us consider the equations of motion of a system as represented by Eq.-4.8 which is repeated here for convenience.

$$[M]\{\ddot{u}(t)\}+[C]\{\dot{u}(t)\}+[K]\{u(t)\}=\{F(t)\} \quad \text{----------4.28}$$

If we consider external force $\{F(t)\}$ is due to earthquake ground excitation then

$$\{F(t)\}=-[M]\{1\}\ddot{u}_g(t) \quad \text{----------4.29}$$

If the system has n degrees of freedom (DOF), then the n coupled equations should be solved simultaneously to obtain the response of the system which can be computationally extensive especially when the number of DOFs is large. In finite element analysis, the most effective time domain method is the direct time integration method. The term "direct" meaning that prior to the numerical integration, no transformation of the equations into a different form is carried out. In direct time integration methods, the equation of motion are integrated using a numerical step-by-step procedure. Among the direct integration methods, the most popular and powerful in dynamic analysis is the Newmark's method (Newmark, 1959). It is a single step integration implicit method that satisfies the differential equation of motion at time $t+\Delta t$ after the solution at time t is found. This method can easily be extended to solve the nonlinear problem which is the

case when the MR damper is embedded in the structure. This requires an iterative process at each time step in order to balance the system equations.

Let us consider the solution of the linear dynamic equilibrium equations stated by Eq. 4.28 written in the following form:

$$[M]\{\ddot{u}\}_{t+\Delta t} + [C]\{\dot{u}\}_{t+\Delta t} + [K]\{u\}_{t+\Delta t} = \{F\}_{t+\Delta t} \text{ ----------4.30}$$

Where the mass matrix $[M]$, the damping matrix $[C]$ and the stiffness matrix $[K]$ are defined at time t. Eq. 4.30 is only satisfied if the matrices do not change during the interval Δt. The displacement and velocity vectors can be approximated in the form using Taylors Series::

$$\{u\}_{t+\Delta t} = \{u\}_t + \Delta t\{\dot{u}\}_t + \frac{\Delta t^2}{2}\{\ddot{u}\}_t + \beta \Delta t^3 \{\dddot{u}\}_t \text{ ----------4.31}$$

$$\{\dot{u}\}_{t+\Delta t} = \{\dot{u}\}_t + \Delta t\{\ddot{u}\}_t + \gamma \Delta t^2 \{\dddot{u}\}_t \text{ ----------4.32}$$

Considering that the acceleration is linear; then one may write:

$$\{\dddot{u}\} = \frac{(\{\ddot{u}\}_{t+\Delta t} - \{\ddot{u}\}_t)}{\Delta t} \text{ ----------4.33}$$

The standard form of Newmark equations are obtained by substituting the Eq. 4.33 into Eq. 4.31 and 4.32 as:

$$\{u\}_{t+\Delta t} = \{u\}_t + \Delta t\{\dot{u}\}_t + \left(\frac{1}{2} - \beta\right)\Delta t^2 \{\ddot{u}\}_t + \beta \Delta t^2 \{\ddot{u}\}_{t+\Delta t} \text{ ----------4.34}$$

$$\{\dot{u}\}_{t+\Delta t} = \{\dot{u}\}_t + (1-\gamma)\Delta t\{\ddot{u}\}_t + \gamma \Delta t\{\ddot{u}\}_{t+\Delta t} \text{ ----------4.35}$$

These Equations together with Eq. 4.30 are used iteratively, for each time step.

Wilson (1962) formulated the Newmark's method in matrix notation, adding stiffness and mass proportional damping, and eliminated the need for iteration by introducing the direct solution of equations at each time step. For this, the Eq. 4.34 and 4.35 are rewritten as:

$$\{\ddot{u}\}_{t+\Delta t} = b_1(\{u\}_{t+\Delta t} - \{u\}_t) - b_2\{\dot{u}\}_t - b_3\{\ddot{u}\}_t \text{ ----------4.36}$$

$$\{\dot{u}\}_{t+\Delta t} = b_4(\{u\}_{t+\Delta t} - \{u\}_t) - b_5\{\dot{u}\}_t - b_6\{\ddot{u}\}_t \text{ ----------4.37}$$

Where the constants b_i are defined by:

$$\left.\begin{aligned} b_1 &= \frac{1}{\beta \Delta t^2},\ b_2 = \frac{1}{\beta \Delta t},\ b_3 = \frac{1}{2\beta} - 1 \\ b_4 &= \frac{\gamma}{\beta \Delta t},\ b_5 = \frac{\gamma}{\beta} - 1,\ b_6 = \frac{\Delta t}{2}\left(\frac{\gamma}{\beta} - 2\right) \end{aligned}\right\} \text{ ----------4.38}$$

Now substituting $\{\dot{u}\}_{t+\Delta t}$ and $\{\ddot{u}\}_{t+\Delta t}$ from Eq. 4.37 and 4.36 into Eq. 4.30 yield:

$$\begin{aligned} (b_1[M] + b_4[C] + [K])\{u\}_{t+\Delta t} = \{F\}_{t+\Delta t} &+ [M](b_1\{u\}_t + b_2\{\dot{u}\}_t + b_3\{\ddot{u}\}_t) \\ &+ [C](b_4\{u\}_t + b_5\{\dot{u}\}_t + b_6\{\ddot{u}\}_t) \end{aligned} \text{ ----------4.39}$$

Eq. 4.39 can be written in the following compact form:

$$\left[\hat{K}\right]\{u\}_{t+\Delta t} = \left\{\hat{F}\right\} \text{ ----------4.40}$$

Where

$$\left[\hat{K}\right] = b_1[M] + b_4[C] + [K] \text{----------4.41}$$

$$\left[\hat{F}\right] = \{F\}_{t+\Delta t} + [M](b_1\{u\}_t + b_2\{\dot{u}\}_t + b_3\{\ddot{u}\}_t) + [C](b_4\{u\}_t + b_5\{\dot{u}\}_t + b_6\{\ddot{u}\}_t) \text{----------4.42}$$

$\left[\hat{K}\right]$ and $\left\{\hat{F}\right\}$ is called the effective stiffness matrix and the effective load vector. It may be noted here that for a linear structural problem with constant properties, the effective stiffness matrix $\left[\hat{K}\right]$ and the constants b_i are calculated only once. It is noted that Newmark's method is unconditionally stable if:

$$2\beta \geq \gamma \geq \frac{1}{2} \text{----------4.43}$$

When $\beta = \frac{1}{4}$ and $\gamma = \frac{1}{2}$, the method is called the constant-average acceleration method (Weaver and Johnston, 1987).

In nonlinear problems where $[M]$, $[C]$ or K are time variant, the dynamic equilibrium given Eq. 4.30 will generally not be achieved at time $t + \Delta t$. For these types of problems, the Newmark's method is modified (Dominguez *et al.*, 2007) to accommodate an iterative process in each step or in some of the steps. For nonlinear systems it is convenient to write the equations of motion in the incremental form. The incremental displacement, velocity and acceleration vectors at time $t + \Delta t$ and iteration $((i+1)^{th}$ required to achieve equilibrium may be written as:

$$\{\delta u\}^{i+1} = \{u\}^{i+1}_{t+\Delta t} - \{u\}^{i}_{t+\Delta t} \text{ ----------4.44}$$

$$\{\delta \dot{u}\}^{i+1} = \{\dot{u}\}^{i+1}_{t+\Delta t} - \{\dot{u}\}^{i}_{t+\Delta t} \text{ ----------4.45}$$

$$\{\delta \ddot{u}\}^{i+1} = \{\ddot{u}\}^{i+1}_{t+\Delta t} - \{\ddot{u}\}^{i}_{t+\Delta t} \text{ ----------4.46}$$

Substituting Eq. 4.36 and 4.37 into Eq.4.46 and 4.45 respectively, the incremental acceleration and velocity vector can be reduced to the following form:

$$\{\delta \ddot{u}\}^{i+1} = b_1 \{\delta u\}^{i+1} \text{ ----------4.47}$$

$$\{\delta \dot{u}\}^{i+1} = b_4 \{\delta u\}^{i+1} \text{ ----------4.48}$$

The system equations in incremental form of motion for the $(i+1)^{th}$ interval may be written as:

$$[M]\{\delta \ddot{u}\}^{i+1} + [C]^{i}_{t+\Delta t} \{\delta \dot{u}\}^{i+1} + [K]^{i}_{t+\Delta t} \{\delta u\}^{i+1} = \{\delta F\}^{i} \text{ ----------4.49}$$

Now considering Eq. 4.47 and 4.48, Eq. 4.49 can be simplified to the following form:

$$\left[\hat{K}\right]^{i+1} \{\delta u\}^{i+1} = \{\delta F\}^{i} \text{ ----------4.50}$$

Where the updated stiffness matrix is determined by

$$\left[\hat{K}\right]^{i+1} = [K]^{i}_{t+\Delta t} + b_1[M] + b_4[C]^{i}_{t+\Delta t} \text{ ----------4.51}$$

The right term in Eq. 4.50 is the unbalance force vector which is the difference between the forces at time $t+\Delta t$ before and after the matrices $[C]$ and $[K]$ are updated. It can be expressed as:

$$\{\delta F\}^i = \{F\}_{t+\Delta t} - [M]\{\ddot{u}\}^i_{t+\Delta t} - [C]^i_{t+\Delta t}\{\dot{u}\}^i_{t+\Delta t} - [K]^i_{t+\Delta t}\{u\}^i_{t+\Delta t} \quad \text{----------4.52}$$

The whole process is also described in the flowchart shown in Figure 4.6.

4.5.2 Solution of equation of motion by State-Space approach

The state-space approach is a widely used analysis tool in the modern theory of dynamics and control. The standard form of the state-space equation is a first-order differential equation. Dynamic problems, with either single DOF (degree of freedom) or multiple DOFs, can be formulated or converted into this form. The advantages of using a state-space approach in dealing with a structural dynamic problems include: (a) the theoretical basis for a standard stape-space is complete and readily obtained; (b) the discrete-time solution of a state-space equation is systematic, so it is easy for numerical implementation and modulation and (c) unlike other numerical methods for structural analysis, its discrete-time solution does not require any assumption about the variation of acceleration response within each time increment (Lu *et al.*, 2006, 2008).

Let us consider equations of motion in following form:

$$[M]\{\ddot{u}(t)\} + [C]\{\dot{u}(t)\} + [K]\{u(t)\} = -[\Lambda][M]\ddot{u}_g(t) \quad \text{----------4.53}$$

where $[\Lambda]$ is excitation distribution vector.

Multiplying both side of Eq. 4.53 by $[M]^{-1}$ yield:

$$\{\ddot{u}(t)\} = -[M]^{-1}[K]\{u(t)\} - [M]^{-1}[C]\{\dot{u}(t)\} - [\Lambda]\ddot{u}_g(t) \quad \text{----------4.54}$$

Let,

$$\left.\begin{aligned} x_1 &= u(t) \\ x_2 &= \dot{u}(t) \end{aligned}\right\} \quad \text{----------4.55}$$

Derivative of Eq. 4.55 will be

$$\left.\begin{aligned} \dot{x}_1 &= \dot{u}(t) \\ \dot{x}_2 &= \ddot{u}(t) \end{aligned}\right\} \quad \text{----------4.56}$$

Considering Eq. 4.54, 4.55 and 4.56, Eq.4.56 can be written as:

$$\left.\begin{aligned} \dot{x}_1 &= x_2 \\ \dot{x}_2 &= -[M]^{-1}[K]x_1 - [M]^{-1}[C]x_2 - [\Lambda]\ddot{u}_g(t) \end{aligned}\right\} \quad \text{----------4.57}$$

Now Eq. 4.57 can be written in matrix form as

$$\begin{Bmatrix} \dot{x}_1 \\ \dot{x}_2 \end{Bmatrix} = \begin{bmatrix} 0 & I \\ -[M]^{-1}[K] & -[M]^{-1}[C] \end{bmatrix} \begin{Bmatrix} x_1 \\ x_2 \end{Bmatrix} + \begin{bmatrix} 0 \\ -[\Lambda] \end{bmatrix} \{\ddot{u}_g(t)\} \quad \text{----------4.58}$$

Combining Eq. 4.54 and 4.55 in the matrix form

$$\begin{Bmatrix} u(t) \\ \dot{u}(t) \\ \ddot{u}(t) \end{Bmatrix} = \begin{bmatrix} I & 0 \\ 0 & I \\ -[M]^{-1}[K] & -[M]^{-1}[C] \end{bmatrix} \begin{Bmatrix} x_1 \\ x_2 \end{Bmatrix} + \begin{bmatrix} 0 \\ 0 \\ -[\Lambda] \end{bmatrix} \{\ddot{u}_g(t)\} \quad \text{----------4.59}$$

Eq. 4.58 and 4.59 can be written as standard state-space form as

$$\left.\begin{aligned}\dot{\bar{x}} &= A_s\bar{x} + B_i w \\ u &= C_o\bar{x} + D_f w\end{aligned}\right\} \text{----------4.60}$$

Where $\bar{x}$ is the state vector, u is the output vector, w is the input vector, A_s is the state matrix, B_i is the input matrix, C_o is the output matrix and D_f is the feed through (or feedforward) matrix and:

$$A_s = \begin{bmatrix} 0 & I \\ -[M]^{-1}[K] & -[M]^{-1}[C_d] \end{bmatrix} \text{----------4.61}$$

$$B_i = \begin{bmatrix} 0 \\ -[\Lambda] \end{bmatrix} \text{----------4.62}$$

$$C_o = \begin{bmatrix} I & 0 \\ 0 & I \\ -[M]^{-1}[K] & -[M]^{-1}[C_d] \end{bmatrix} \text{----------4.63}$$

$$D_f = \begin{bmatrix} 0 \\ 0 \\ -[\Lambda] \end{bmatrix} \text{----------4.64}$$

where I is the identity matrix.

Now if we consider the MR damper embedded into the structural system then the Eq. 4.53 can be rewritten as:

$$[M]\{\ddot{u}(t)\} + [C]\{\dot{u}(t)\} + [K]\{u(t)\} = -[\Gamma]f_{MR}(t) - [\Lambda][M]\ddot{u}_g(t) \text{----------4.65}$$

where $[\Gamma]$ is the MR damper placement matrix and $f_{MR}(t)$ is the force generated by MR damper. Similarly following the procedure described above, the standard form of state-space can be written as:

$$\left.\begin{aligned} \dot{\bar{x}} &= A_s \bar{x} + B_{ic} w \\ u &= C_o \bar{x} + D_{fc} w \end{aligned}\right\} \text{----------4.66}$$

Where,

$$B_{ic} = \begin{bmatrix} 0 & 0 \\ -[M]^{-1}[\Gamma] & -[\Lambda] \end{bmatrix} \text{----------4.67}$$

$$D_{fc} = \begin{bmatrix} 0 & 0 \\ 0 & 0 \\ -[M]^{-1}[\Gamma] & -[\Lambda] \end{bmatrix} \text{----------4.68}$$

The state-space method described here is implemented for MR damper and the structural system using the SIMULINK (2007) and the stiffness, mass and damping properties are calculated using M-FEM (Bagchi *et al.*, 2007). The computer implementation of this method is described in the flow chart shown in Figure 4.7.

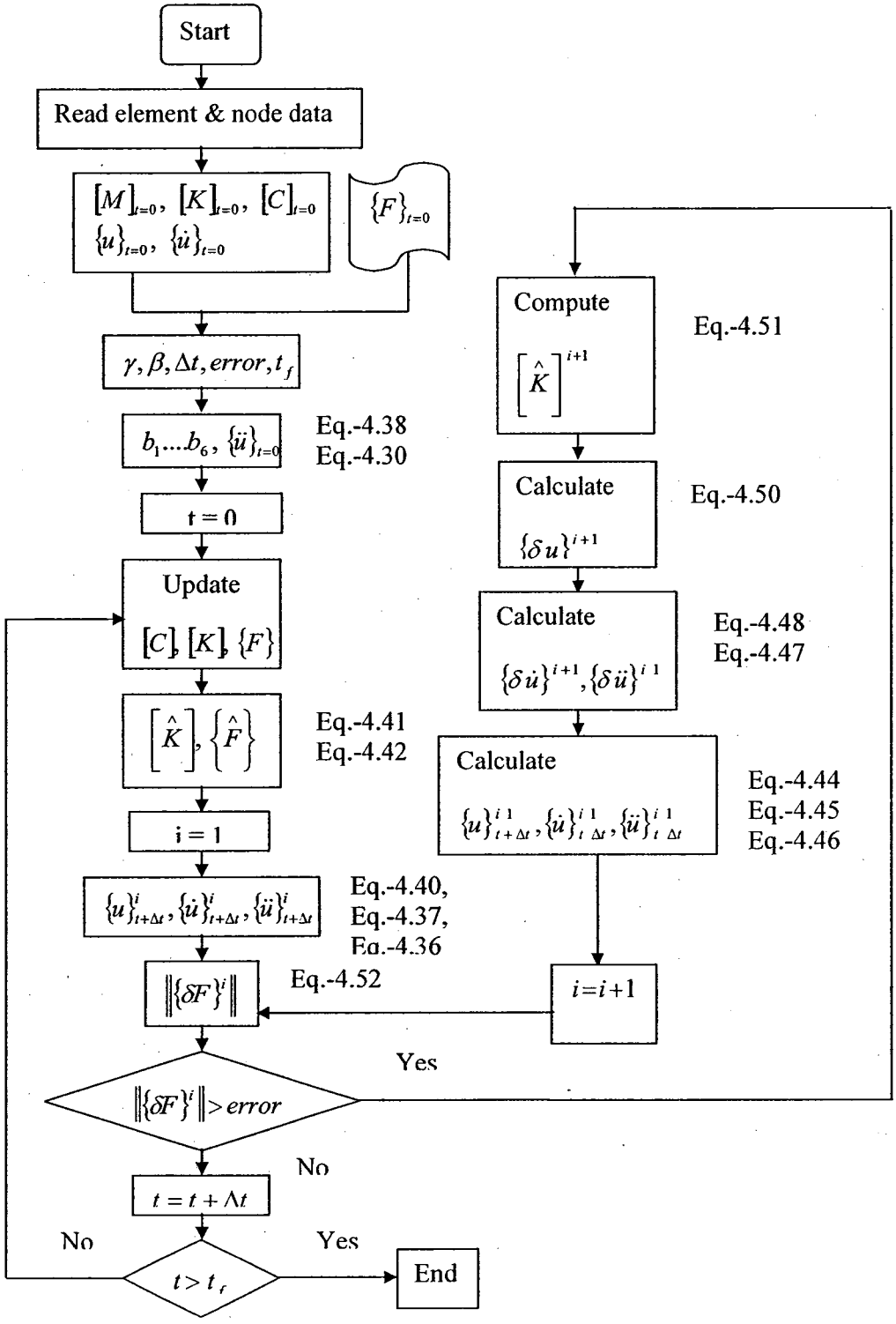

Figure 4.6: Solution process of Newmark method.

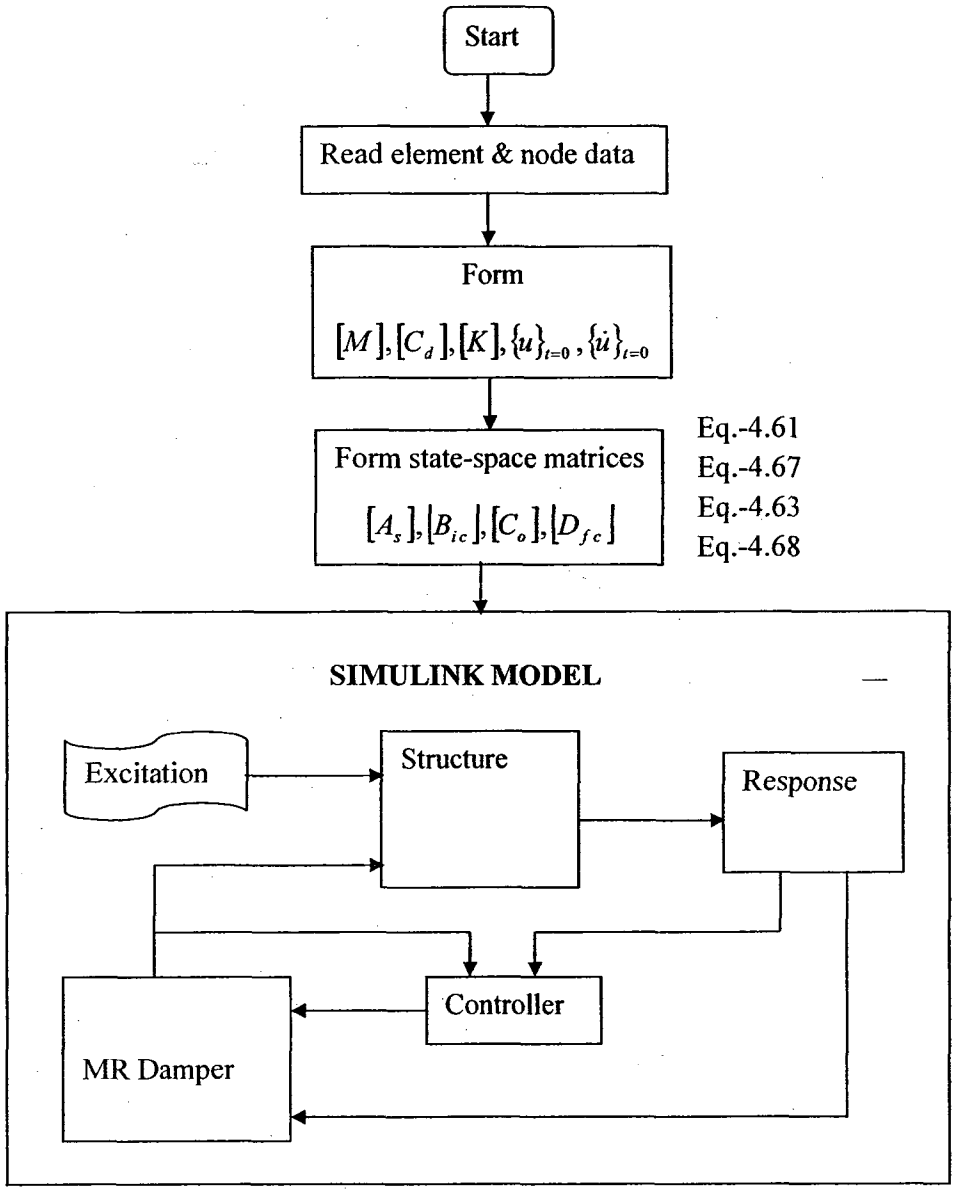

Figure 4.7: Solution process of State-space method.

4.6 Derivation of energy equation

To better understand the contribution of the energy dissipating device like damper during earthquake we also need to look at the energy balance equation. Let us consider the equation of motion for a structural system again here as:

$$[M]\{\ddot{u}(t)\}+[C]\{\dot{u}(t)\}+\{F_s(t)\}=-[M]\{\ddot{u}_g(t)\} \text{----------4.69}$$

Where $\{F_s(t)\}=[K]\{u(t)\}$

Pre-multiplying both sides of Eq. 4.69 by $\{\dot{u}(t)\}^T$ and then integrating with respect to time yields:

$$\int_0^t \{\dot{u}(t)\}^T[M]\{\ddot{u}(t)\}dt+\int_0^t \{\dot{u}(t)\}^T[C]\{\dot{u}(t)\}dt+\int_0^t \{\dot{u}(t)\}^T\{F_s(t)\}dt$$

$$=-\int_0^t \{\dot{u}(t)\}^T[M]\{\ddot{u}_g(t)\}dt \text{----------4.70}$$

Now considering that

$$\left.\begin{aligned}\{\dot{u}(t)\}&=\frac{d\{u(t)\}}{dt}\\ \{\ddot{u}(t)\}&=\frac{d\{\dot{u}(t)\}}{dt}\end{aligned}\right\} \text{----------4.71}$$

Eq. 4.70 can be rewritten in the following form

$$\int_0^{\{\dot{u}(t)\}} \{\dot{u}(t)\}^T[M]d\{\dot{u}(t)\}+\int_0^{\{u(t)\}} d\{u(t)\}^T[C]\{\dot{u}(t)\}+\int_0^{\{u(t)\}} d\{u(t)\}^T\{F_s(t)\}-$$

$$= -\int_0^{\{u(t)\}} d\{u(t)\}^T [M]\{\ddot{u}_g(t)\} \quad \text{----------4.72}$$

The first term on the left side of Eq. 4.72 can be integrated directly to yield:

$$\frac{1}{2}\{\dot{u}(t)\}^T [M]\{\dot{u}(t)\} + \int_0^{\{u(t)\}} d\{u(t)\}^T [C]\{\dot{u}(t)\} + \int_0^{\{u(t)\}} d\{u(t)\}^T \{F_s(t)\} = -\int_0^{\{u(t)\}} d\{u(t)\}^T [M]\{\ddot{u}_g(t)\}$$

$$= -\int_0^{\{u(t)\}} d\{u(t)\}^T [M]\{\ddot{u}_g(t)\} \text{----------4.73}$$

Or

$$T(t) + D(t) + U(t) = I(t) \text{----------4.74}$$

where,

$T(t)$ = kinetic energy at time t caused by the relative motion of the mass with respect to base.

$D(t)$ = energy dissipated by viscous damping up to time t.

$U(t)$ = strain energy of the system at time t.Part of this energy can be restored (elastic strain energy) when the other part is dissipated by the nonlinear behaviour of the structure (hysteretic energy)

$I(t)$ =Input energy introduced into the system.

It may be noted here that the input energy introduced into the system is equal the equivalent seismic force $-[M]\{\ddot{u}_g(t)\}$, integrated through the relative displacement of the

mass $d\{u(t)\}$. In other words, the input energy not only depends on the characteristics of the earthquake but also depend on the structure.

It is imperative to understand that for a time-step nonlinear dynamic analysis, we can calculate each energy component of Eq. 4.74 individually at the end of each time-step. The accuracy of the analysis can be quantified by comparing the sum of the energy components (left-hand-side term of Eq. 4.74) with the input energy introduced into the system (right-hand-side term of Eq. 4.74). There are many techniques available to evaluate numerically the different energy components at the end of each time increment (Filiatrault, 2002). Here the trapezoidal rule is used described as:

$$\left.\begin{aligned} T(t) &= \frac{1}{2}\{\dot{u}(t)\}^T[M]\{\dot{u}(t)\} \\ D(t) &= D(t-\Delta t) + \frac{1}{2}\left[\{u(t)\}-\{u(t-\Delta t)\}\right]^T[C]\left[\{\dot{u}(t-\Delta t)\}+\{\dot{u}(t)\}\right] \\ U(t) &= U(t-\Delta t) + \frac{1}{2}\left[\{u(t)\}-\{u(t-\Delta t)\}\right]^T\left[F_s(t-\Delta t)+F_s(t)\right] \\ I(t) &= I(t-\Delta t) - \frac{1}{2}\left[\{u(t)\}-\{u(t-\Delta t)\}\right]^T[M]\left[\{\ddot{u}_g(t-\Delta t)\}+\{\ddot{u}(t)\}\right] \end{aligned}\right\} \quad \text{----------4.75}$$

where Δt represents the time-step used in the analysis.

4.7 Software used in this work

A MATLAB (2007) based finite element program, M-FEM developed by Bagchi *et al.* (2007) is used and modified in this research work. This program was originally developed for structural heath monitoring which is capable of static and modal analysis. To serve the purpose of the present research the program is modified to (a) include finite element model of space truss element, (b) dynamic analysis algorithm of Newmark method, (c) finite element model of MR damper (RD1005-3) described by Dominguez *et al.* (2007), (d) solution algorithm of equations of motion by state-space approach which is done in combination of m-FEM and SIMULINK module of MATLAB (2007) and (e) the algorithm to calculate the different components of energy into the structural system. The modified version of M-FEM program is capable of the analysis of a structure by both Newmark method and State-Space approach and calculating the energy components.

4.8 Selected earthquake record

A total of five earthquake records are considered to conduct the time-history analysis of structure. All the data are downloaded from the website of the Pacific Earthquake Engineering Research Center (PEER, 2009) strong motion database. Figure 4.8 to 4.12 shows the time-history plots of ground motion records. Only the horizontal components of ground motion are considered. Table 4.1 shows some characteristics information of the selected earthquake.

Table 4.1: Characteristics of the selected earthquake record.

Sl. No	Earthquake Record/Component	Magnitude	PGA(g)	PGV(cm/s)	PGD(cm)
1	IMPVALL/I-ELC180	M7.0	0.313	29.8	13.32
2	MAMMOTH/I-LUL000	M6.3	0.43	23.6	7.52
3	MAMMOTH/L-LUL090	M6	0.408	33.9	6.41
4	NORTHR/SCE288	M6.7	0.493	74.6	28.69
5	IMPVALL/H-E05140	M6.5	0.519	46.9	35.35

Note: PGA- Peak ground acceleration, PGV- Peak ground velocity, PGD- Peak ground displacement.

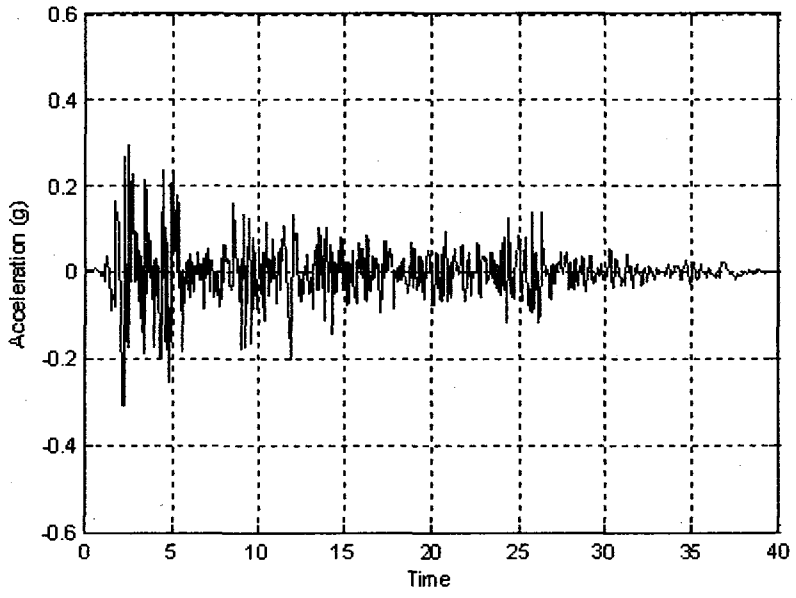

Figure 4.8: Acceleration Time-History Record of El-Centro (IMPVALL/I-ELC180) 1940/05/19

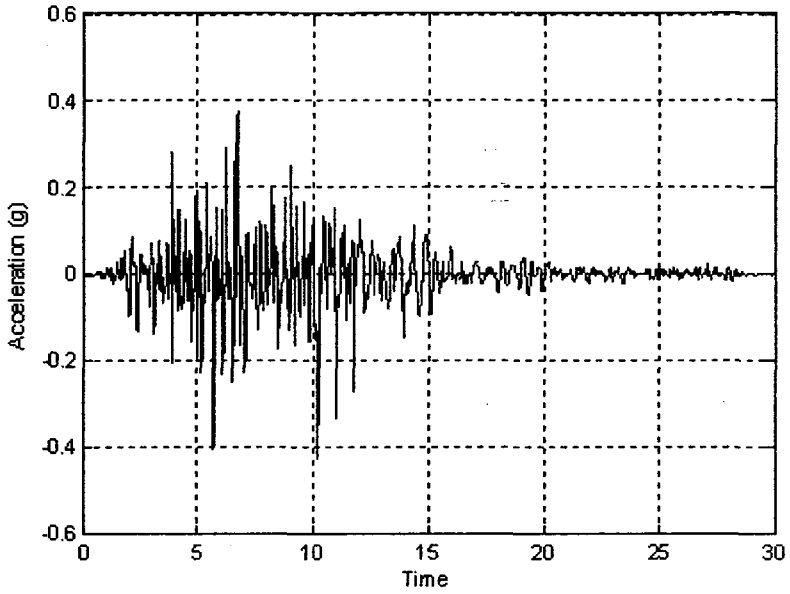

Figure 4.9: Acceleration Time-History Record of Mammoth lakes (MAMMOTH/I-LUL000) 1980/05/25

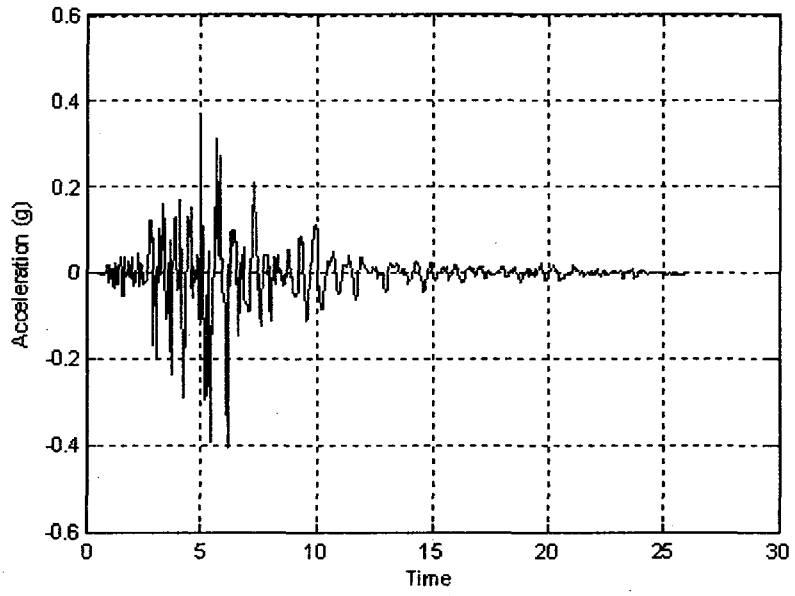

Figure 4.10: Acceleration Time-History Record of Mammoth lakes (MAMMOTH/L-LUL090) 1980/05/27.

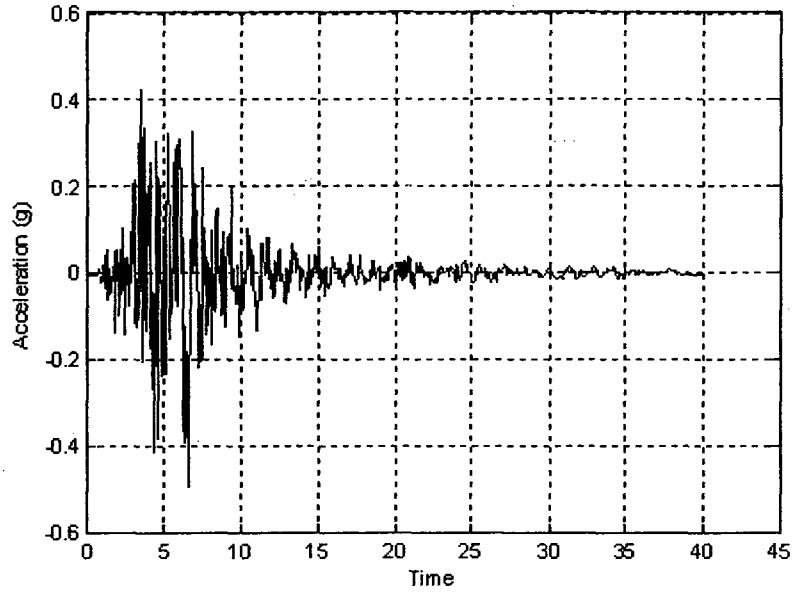

Figure 4.11: Acceleration Time-History Record of Northridge (NORTHR/SCE288) 1994/04/17.

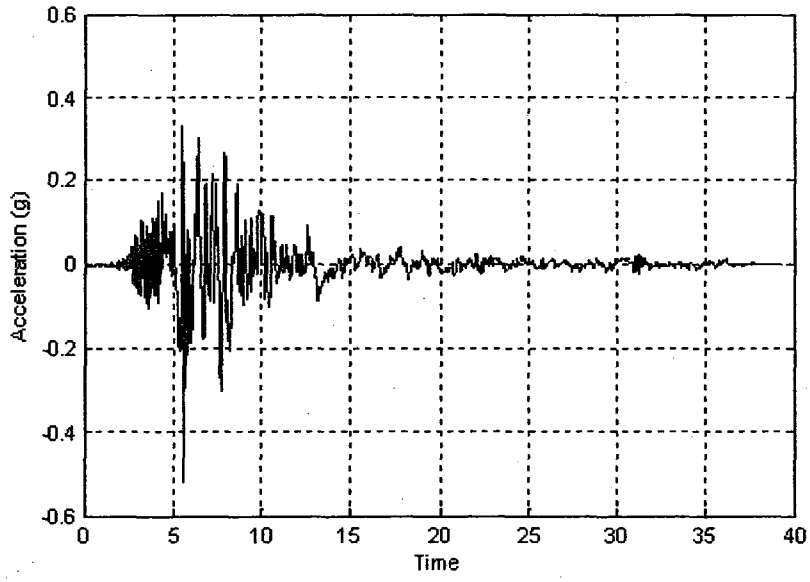

Figure 4.12: Acceleration Time-History Record of Imperial Valley (IMPVALL/H-E05140) 1979/10/15.

4.9 Validation of the finite element model

To validate the developed finite element program, a model of structure which is experimentally studied by Dyke *et al.* (1996) is investigated here. The model represents a three story structure as shown in Figure 2.8. They used MR damper model SD 1000 as semi-active device and the structure is analyzed by considering El-Centro earthquake record. As the model structure is scaled down, they reproduced the earthquake record five times the original recording speed (Figure C1). The properties of the model structure i.e. mass matrix M_s, Stiffness matrix K_s and damping matrix C_s are:

$$M_s = \begin{bmatrix} 98.3 & 0 & 0 \\ 0 & 98.3 & 0 \\ 0 & 0 & 98.3 \end{bmatrix} kg$$

$$K_s = 10^5 \begin{bmatrix} 12.0 & -6.84 & 0 \\ -6.84 & 13.7 & -6.84 \\ 0 & -6.84 & 6.84 \end{bmatrix} \frac{N}{m}$$

$$C_s = \begin{bmatrix} 175 & -50 & 0 \\ -50 & 100 & -50 \\ 0 & -50 & 50 \end{bmatrix} \frac{Ns}{m}$$

Figure 4.13a and 4.14a shows third floor displacement and acceleration responses respectively as per their analysis. Here to validate the finite element program developed in this research, the same structure is analyzed by both the Newmark method and state-space approach. For the case of Newmark method MR damper model RD1005-3 is selected and for the case of state-space approach MR damper SD1000 is used. Figure 4.13b and 4.14b shows the third floor displacement and acceleration responses

respectively when the structure is analyzed by state-space method by considering MR damper SD1000. Figure 4.13c and 4.14c shows the third floor displacement and acceleration responses respectively when the structure is analyzed by Newmark method without considering MR damper. The result shows good agreement with the Dyke's analysis results. Uncontrolled responses for both the Newmark method and state-space approach has found almost same. But control response for both the methods is not comparable as different damper is used. Controlled response for state-space approach agrees well to that of Dyke's analysis with slight variations. Table 4.2 shows the comparison of responses obtained by Dyke *et al.* (1996) and the responses obtained by using Newmark method and state-space method.

Table 4.2: Comparison of peak responses for different analysis approach.

	Uncontrolled			Controlled	
	Dyke	State-Space method	Newmark method	Dyke	State-Space method
Displacement (m) (1^{st} to 3rd floor)	0.00538	0.00522	0.00519	0.00076	0.00084
	0.00820	0.00796	0.00793	0.00196	0.00164
	0.00962	0.00926	0.00923	0.00306	0.00248
Acceleration (m/sec^2) (1^{st} to 3rd floor)	8.56	9.88	9.985	2.81	3.17
	10.30	10.43	10.38	4.94	6.25
	14.00	14.29	14.51	7.67	8.21

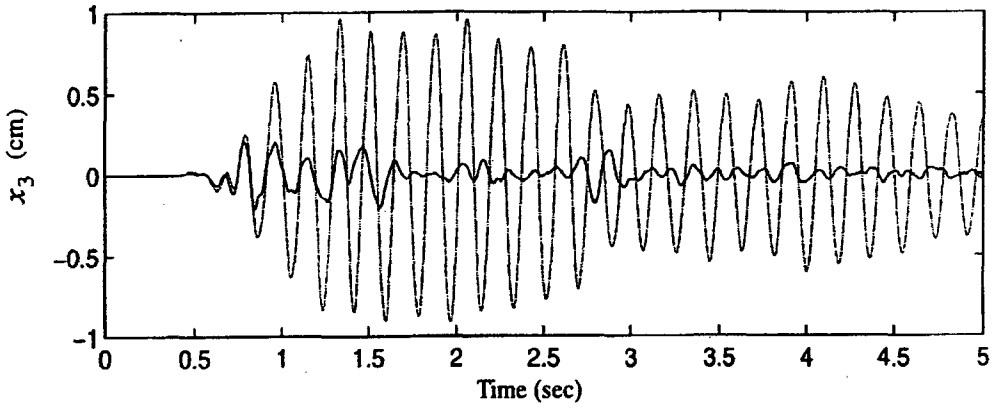

Figure 4.13a: Uncontrolled and controlled third floor displacement (Dyke *et al.*, 1996).

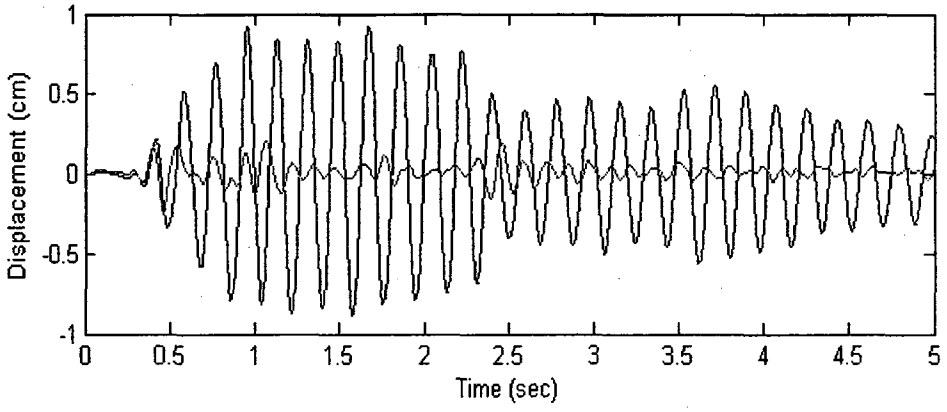

Figure 4.13b: Uncontrolled and controlled third floor displacement (State-Space method).

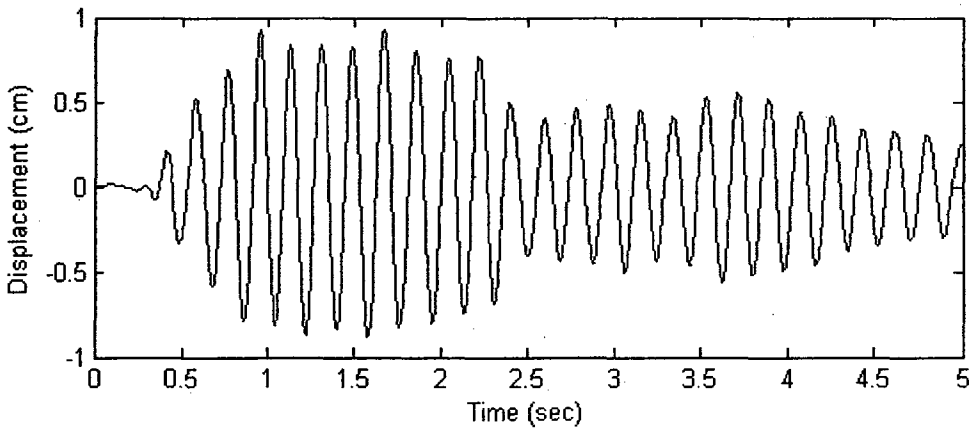

Figure 4.13c: Uncontrolled third floor displacement (Newmark method).

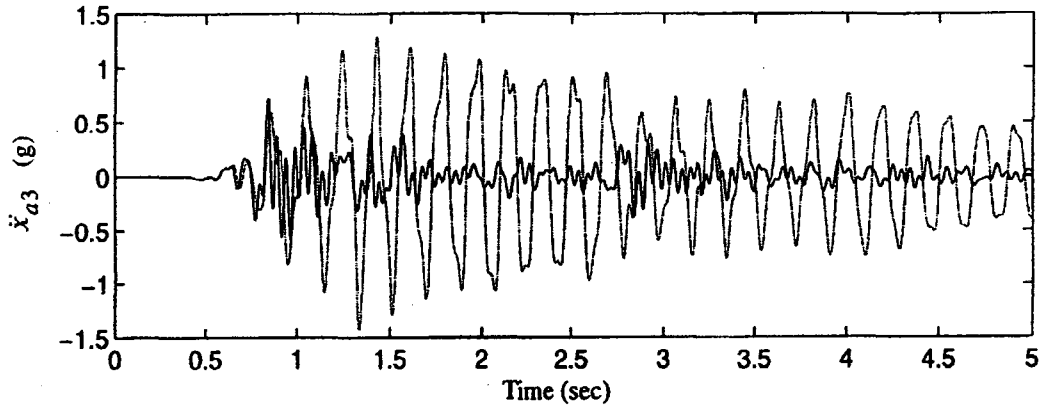

Figure 4.14a: Uncontrolled and controlled third floor acceleration (Dyke *et al.,* 1996).

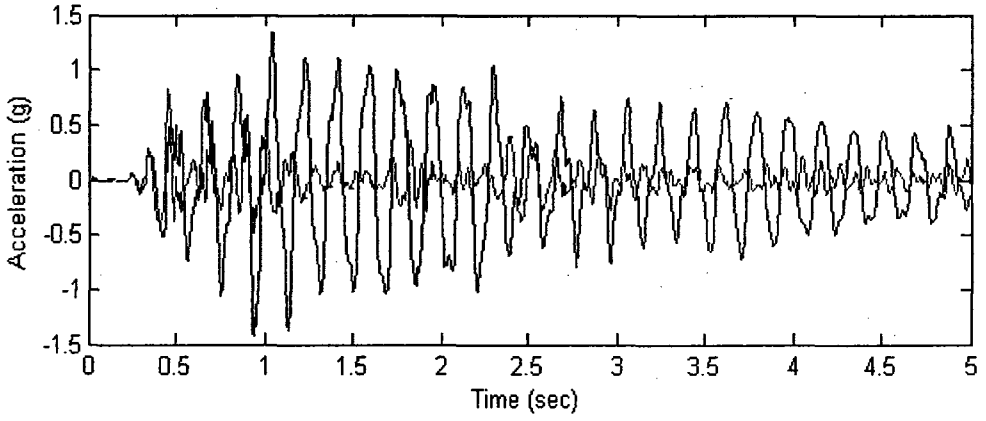

Figure 4.14b: Uncontrolled and controlled third floor acceleration (State-Space method).

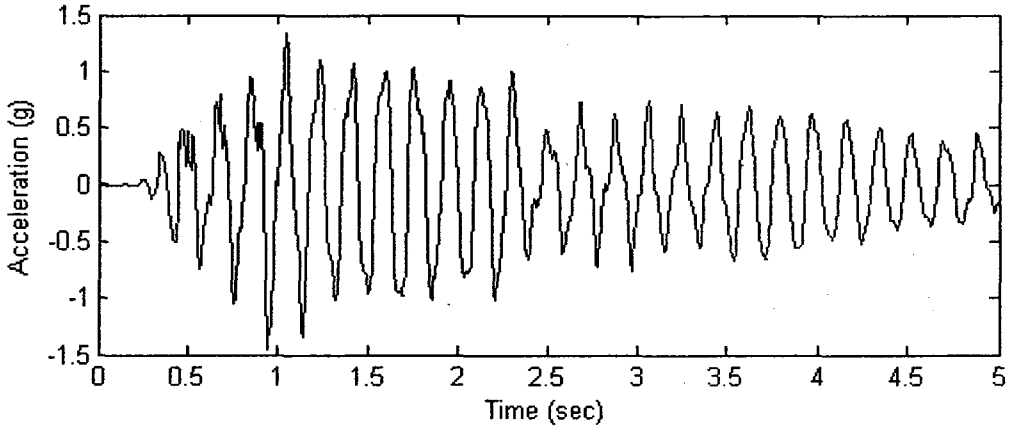

Figure 4.14c: Uncontrolled third floor acceleration (Newmark method).

CHAPTER 5
Case Studies

5.1 Introduction

Finite element model of structure as described in Chapter 4 is used to develop the numerical model of a total of six building structures. These structures are analyzed for different scenarios with respect to different MR damper configurations and earthquake excitations. A structure is first analyzed without considering MR damper and subjected to El-Centro earthquake record. To investigate the performance of MR damper, MR damper is embedded into the structures and the structure is then excited with same earthquake record and the controlled (with considering MR damper) and uncontrolled (without MR damper) responses of the structure are compared. As the power failure during earthquake which is a very common event, thus the performance of the dampers in that situation (zero current or voltage) is also studied. The suitable location for MR damper placement into the structure is also studied by placing the dampers on different locations in the structure. Suitable location of damper is evaluated based on the reduction in the response quantities, such as displacement, velocity and acceleration; increase in equivalent damping ratio; and contribution of damping energy by MR damper. Finally the structure is analyzed considering MR damper in the optimal location and subjected to different earthquake ground motions to study the damper performance with variation in ground

motion characteristics. This process is carried out for different types of MR dampers and buildings as explained in the following sections.

5.2 Description of structures considered in this research

In this work a total of six building models as shown in Figures 5.1 to 5.6 are considered. Out of six models considered, three are two dimensional (2D) and the other three are three dimensional (3D) models. Performance of MR damper RD 1005-3 (capacity 2.2 kN) is evaluated by integrating the damper into the RD2D and RD3D models; performance of MR damper SD 1000 (capacity 3 kN) is evaluated by integrating the damper into the SD2D and SD3D models; and performance of MR damper MRD 9000 (capacity 200 kN) is evaluated by integrating the damper into the MRD2D and MRD3D models. Structural configurations are summarized in Table 5.1. Figures 5.7 to 5.12 show the mode shape of the structures. From Table 5.1 it is noticed that the frequency and period for model SD2D and SD3D are not same although the sections and nodal masses are same for both. These differences are because of the fact that the cross sections of the columns are not symmetric in their local axes (I-section). Similar situation is for model MRD2D and MRD3D.

Table 5.1: Model structural configurations.

Sl. No.	Column	Beam	Nodal Mass (kg)	Frequency (Hz)			Period (Sec)		
				1st	2nd	3rd	1st	2nd	3rd
RD2D	HS38X38X3.2	HS38X38X3.2	75	5.593	15.670	22.650	0.178	0.063	0.044
RD3D	HS38X38X3.2	HS38X38X3.2	75	5.593	15.670	22.650	0.178	0.063	0.044
SD2D	SLB75X4.5	SLB75X4.3	200	5.835	18.760	31.060	0.171	0.053	0.032
SD3D	SLB75X4.5	SLB75X4.3	200	2.410	5.835	7.747	0.414	0.171	0.129
MRD2D	W310X253	W310X179	35000	1.146	3.611	6.066	0.872	0.276	0.164
MRD3D	W310X253	W310X179	35000	0.643	1.146	2.027	1.555	0.872	0.493

Modulus of elasticity of materials $E = 2x10^{11}$ N/m^2 for column and $E = 2x10^{12}$ for beam is considered for all model.

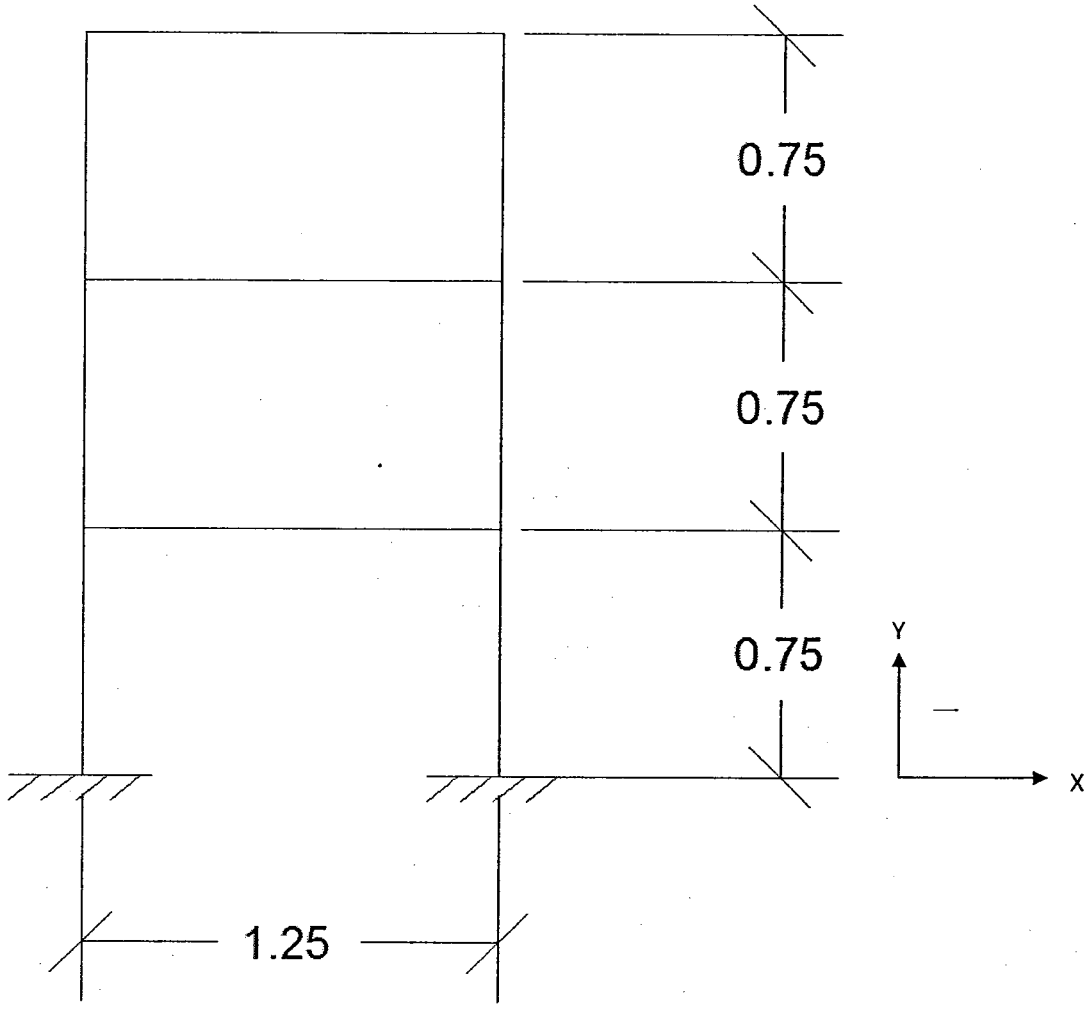

Beam & Column: HS38X38X3.2

A: 4.18 E^2 mm^2

I_{xx}= 8.22 E^4 mm^4

I_{yy}= 8.22 E^4 mm^4

J= 1.41 E^5 mm^4

Nodal mass = 75 kg

E_{beam}= 2 E^{12} N/mm^2

E_{column}= 2E^{11} N/mm^2

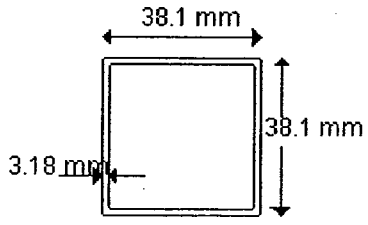

X- Section (HS38X38X3.2)

Figure 5.1: Geometry and configuration of Model RD2D.

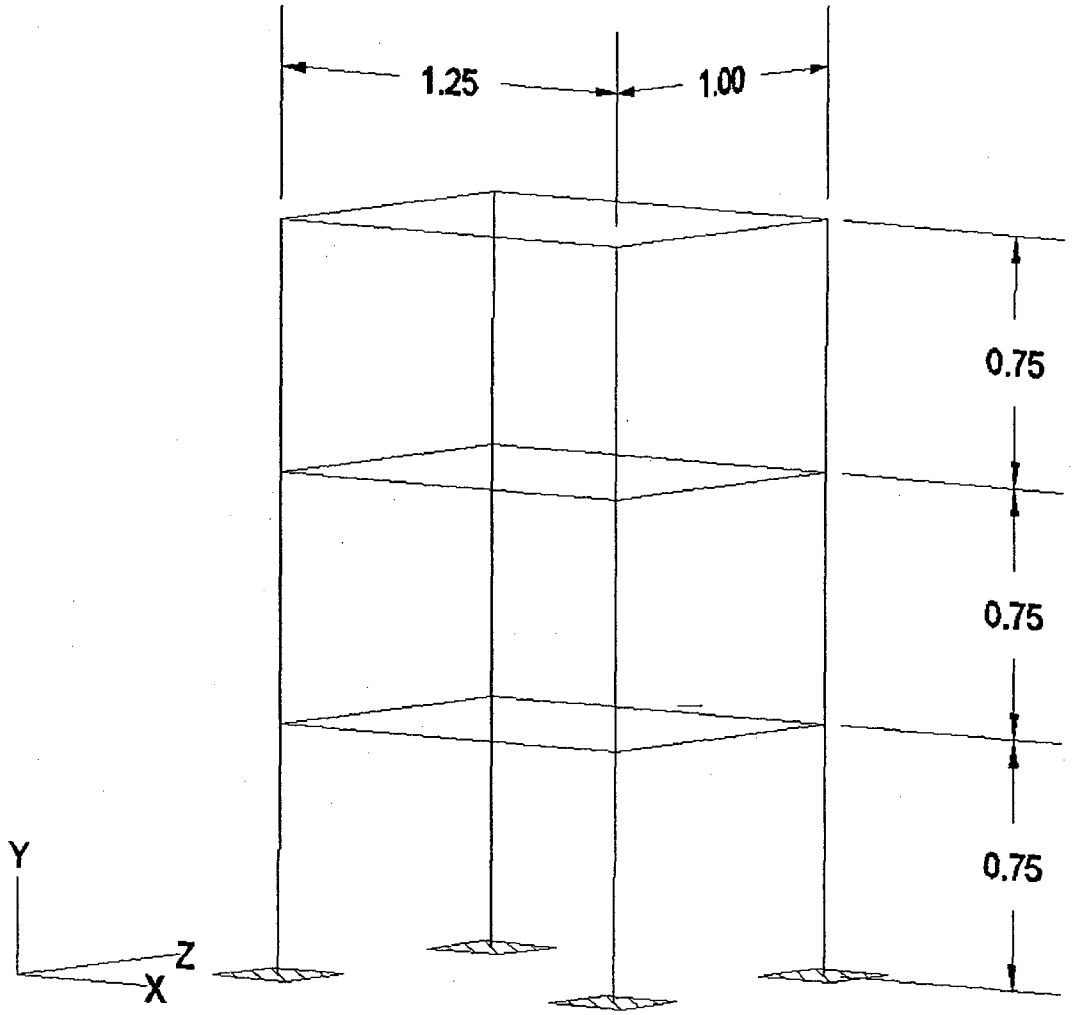

Column and Beam: HS38X38X3.2

A: 4.18 E^2 mm^2

I_{xx}= 8.22 E^4 mm^4

I_{yy}= 8.22 E^4 mm^4

J= 1.41 E^5 mm^4

Nodal mass = 75 kg

E_{beam}= 2 E^{12} N/mm^2

E_{column}= $2E^{11}$ N/mm^2

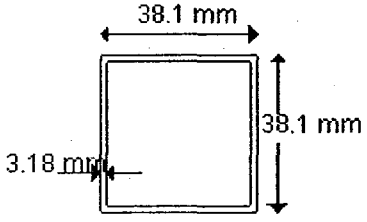

X- Section (HS38X38X3.2)

Figure 5.2: Geometry and configuration of Model RD3D.

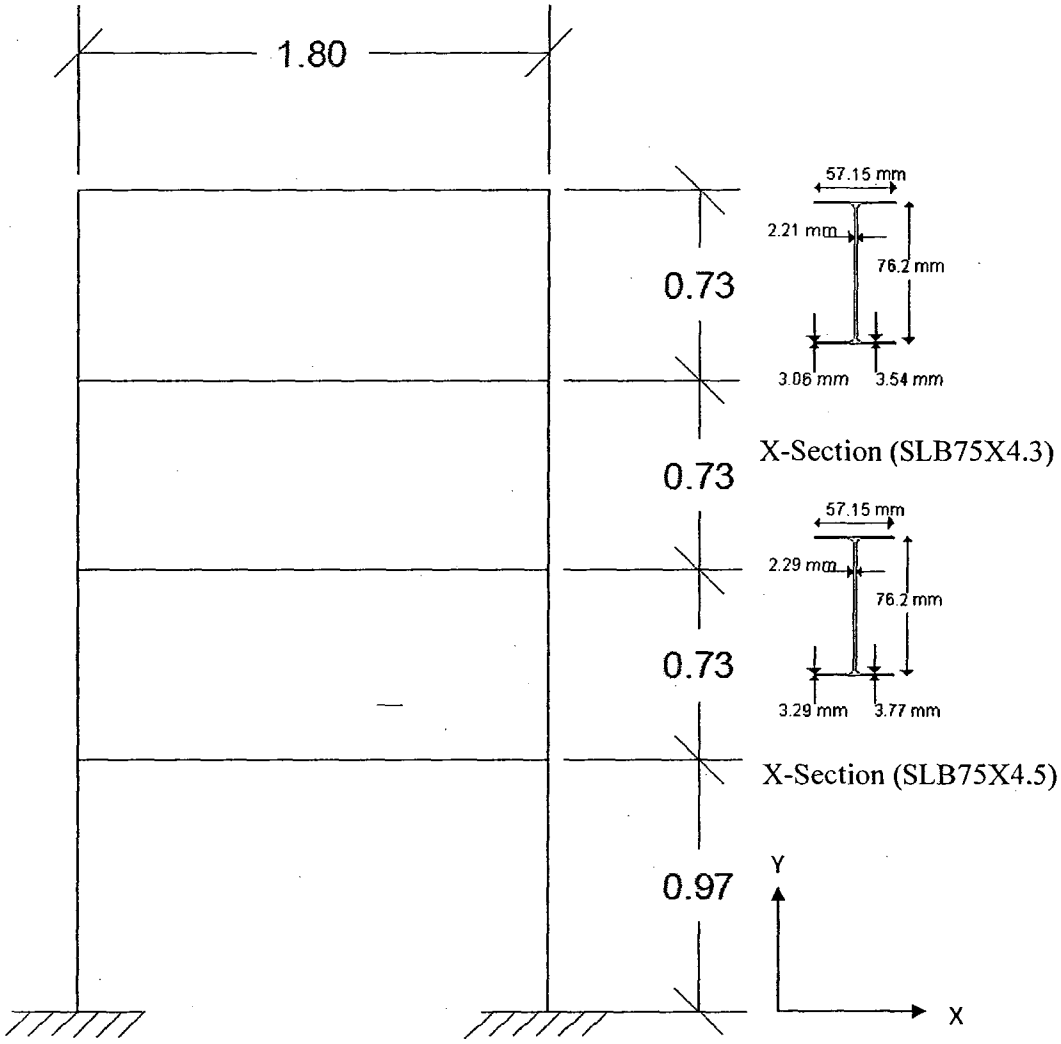

Beam: SLB75X4.3

A: 5.46 E^2 mm^2

I_{xx}= 5.81 E^5 mm^4

I_{yy}= 9.91 E^4 mm^4

J= 1.92 E^3 mm^4

Column: SLB75X4.5

A: 5.77 E^2 mm^2

I_{xx}= 6.13 E^5 mm^4

I_{yy}= 1.06 E^5 mm^4

J= 2.28 E^3 mm^4

Nodal mass = 200 kg

E_{beam}= 2 E^{12} N/mm^2

E_{column}= $2E^{11}$ N/mm^2

Figure 5.3: Geometry and configuration of Model SD2D.

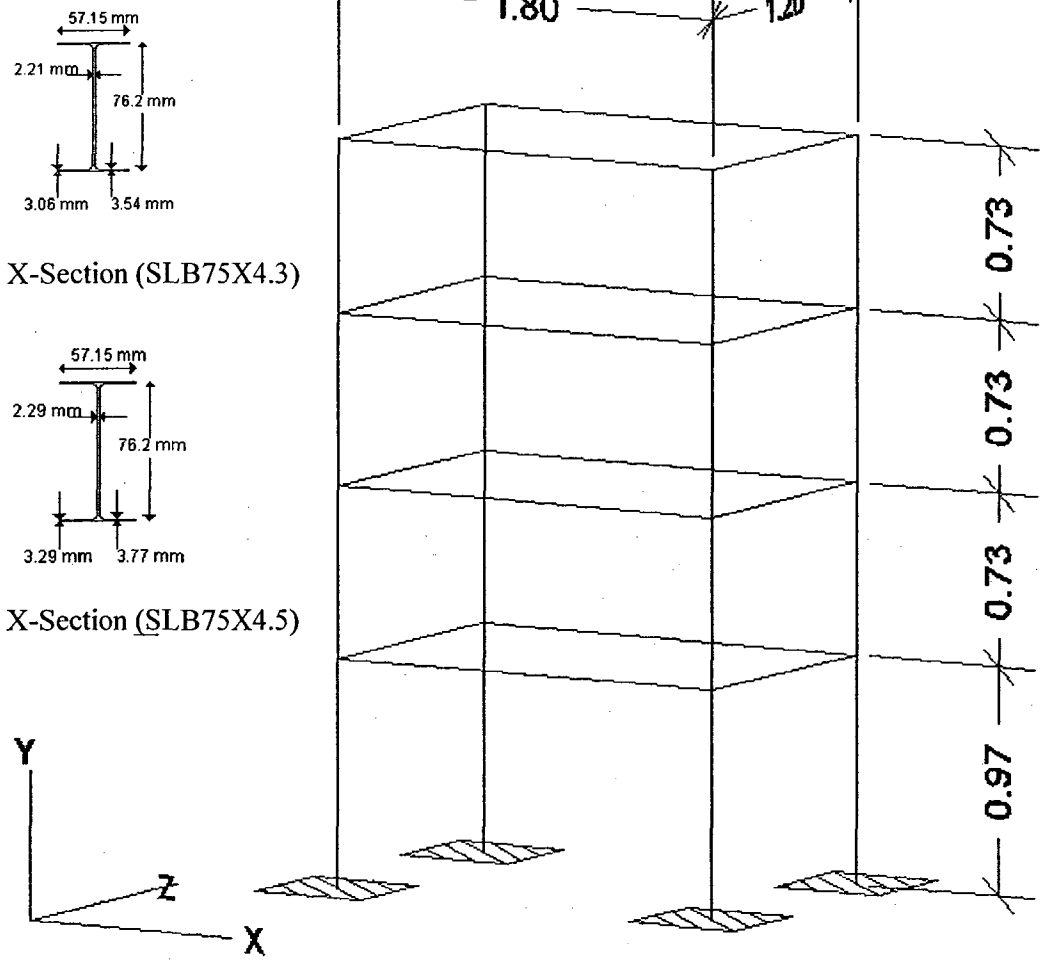

Beam: SLB75X4.3

A: 5.46 E^2 mm^2

I_{xx}= 5.81 E^5 mm^4

I_{yy}= 9.91 E^4 mm^4

J= 1.92 E^3 mm^4

Column: SLB75X4.5

A: 5.77 E^2 mm^2

I_{xx}= 6.13 E^5 mm^4

I_{yy}= 1.06 E^5 mm^4

J= 2.28 E^3 mm^4

Nodal mass = 200 kg

E_{beam}= 2 E^{12} N/mm^2

E_{column}= $2E^{11}$ N/mm^2

Figure 5.4: Geometry and configuration of Model SD3D.

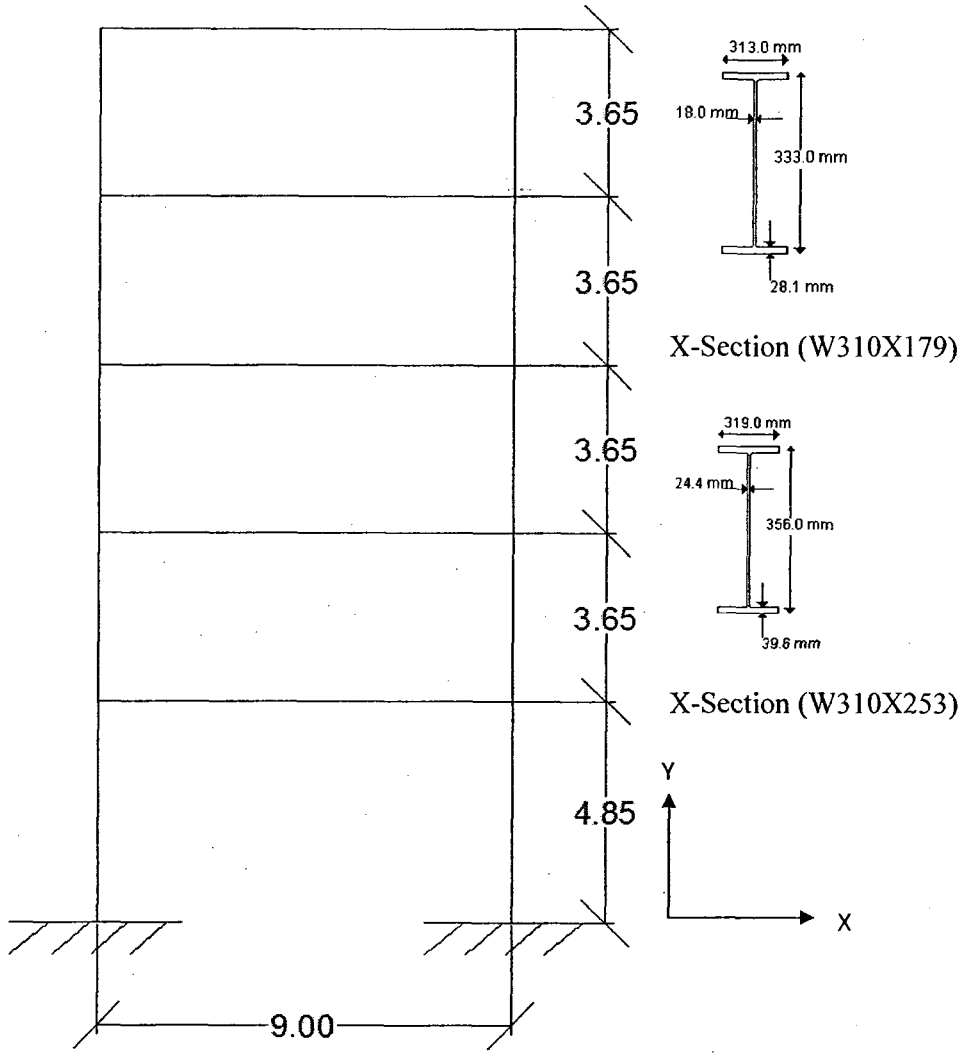

Beam: W310X179

A: 2.28 E^4 mm^2

I_{xx}= 4.45 E^8 mm^4

I_{yy}= 1.44 E^8 mm^4

J= 5.37 E^6 mm^4

Column: W310X253

A: 3.22 E^4 mm^2

I_{xx}= 6.82 E^8 mm^4

I_{yy}= 2.15 E^8 mm^4

J= 1.48 E^7 mm^4

Nodal mass = 35000 kg

E_{beam}= 2 E^{12} N/mm^2

E_{column}= 2E^{11} N/mm^2

Figure 5.5: Geometry and configuration of Model MRD2D.

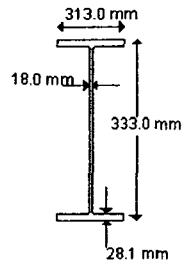

X-Section (W310X179)

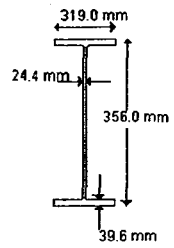

X-Section (W310X253)

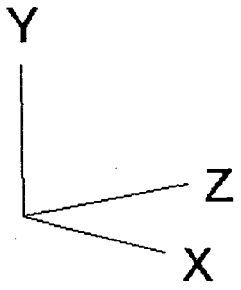

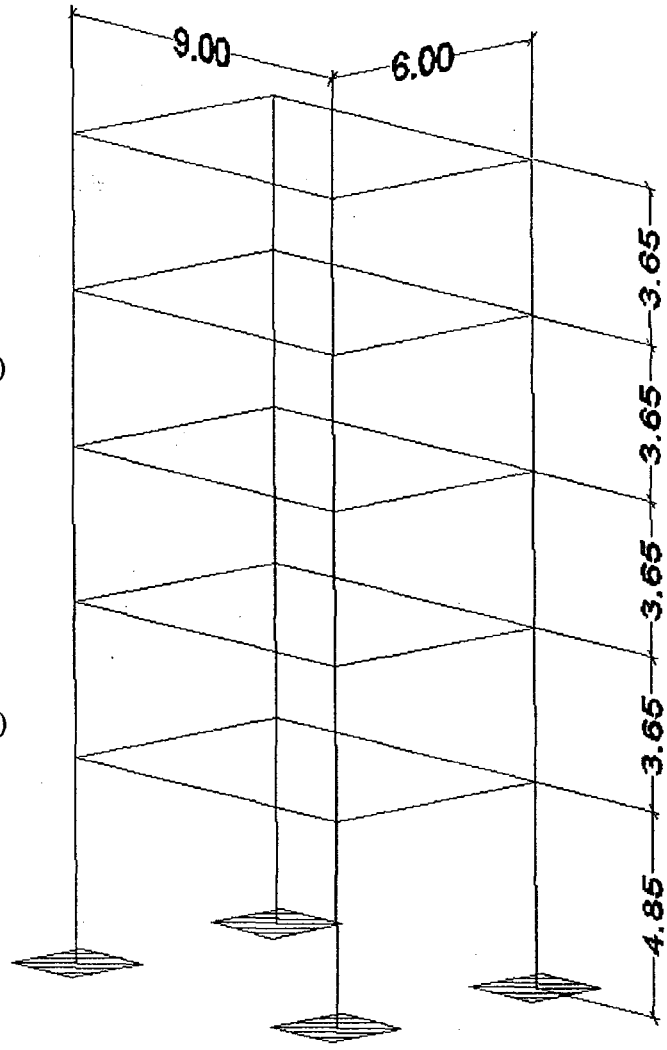

Beam: W310X179

A: 2.28 E^4 mm^2

I_{xx}= 4.45 E^8 mm^4

I_{yy}= 1.44 E^8 mm^4

J= 5.37 E^6 mm^4

Column: W310X253

A: 3.22 E^4 mm^2

I_{xx}= 6.82 E^8 mm^4

I_{yy}= 2.15 E^8 mm^4

J= 1.48 E^7 mm^4

Nodal mass = 35000 kg

E_{beam}= 2 E^{12} N/mm^2

E_{column}= 2E^{11} N/mm^2

Figure 5.6: Geometry and configuration of Model MRD3D.

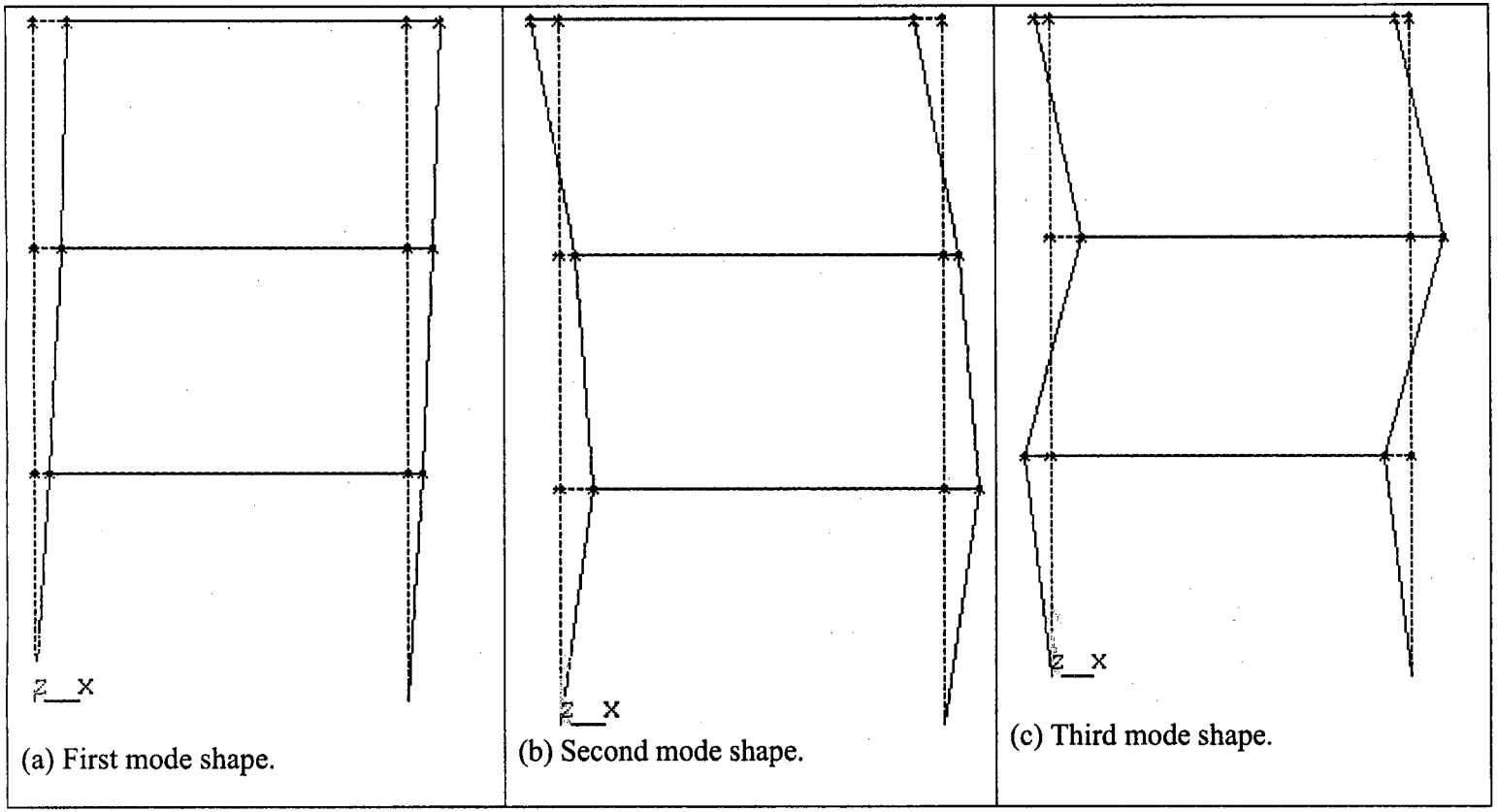

(a) First mode shape.

(b) Second mode shape.

(c) Third mode shape.

Figure 5.7: Mode shape of model RD2D.

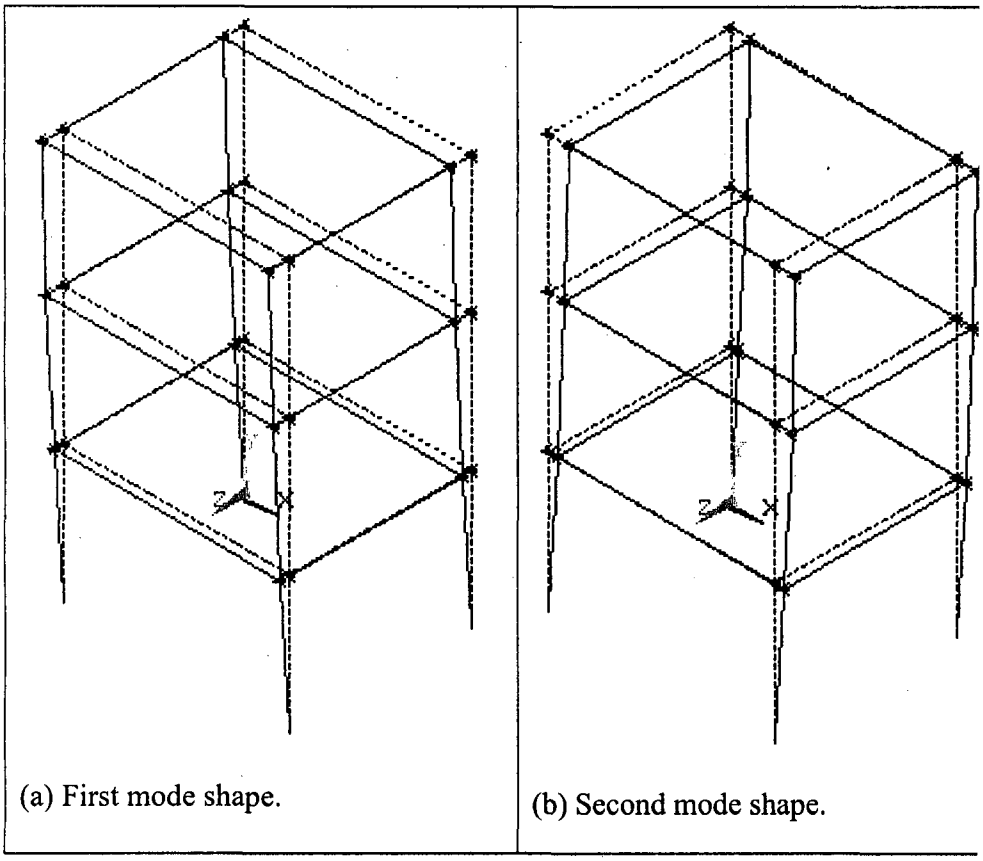

(a) First mode shape.

(b) Second mode shape.

Figure 5.8: Mode shape of model RD3D.

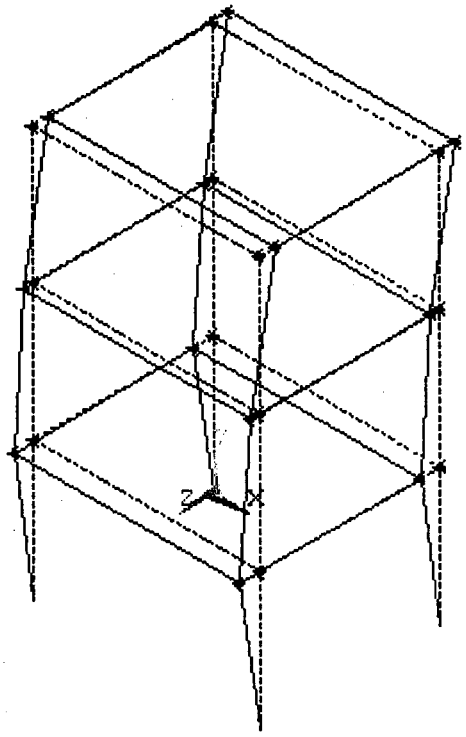

(c) Third mode shape.

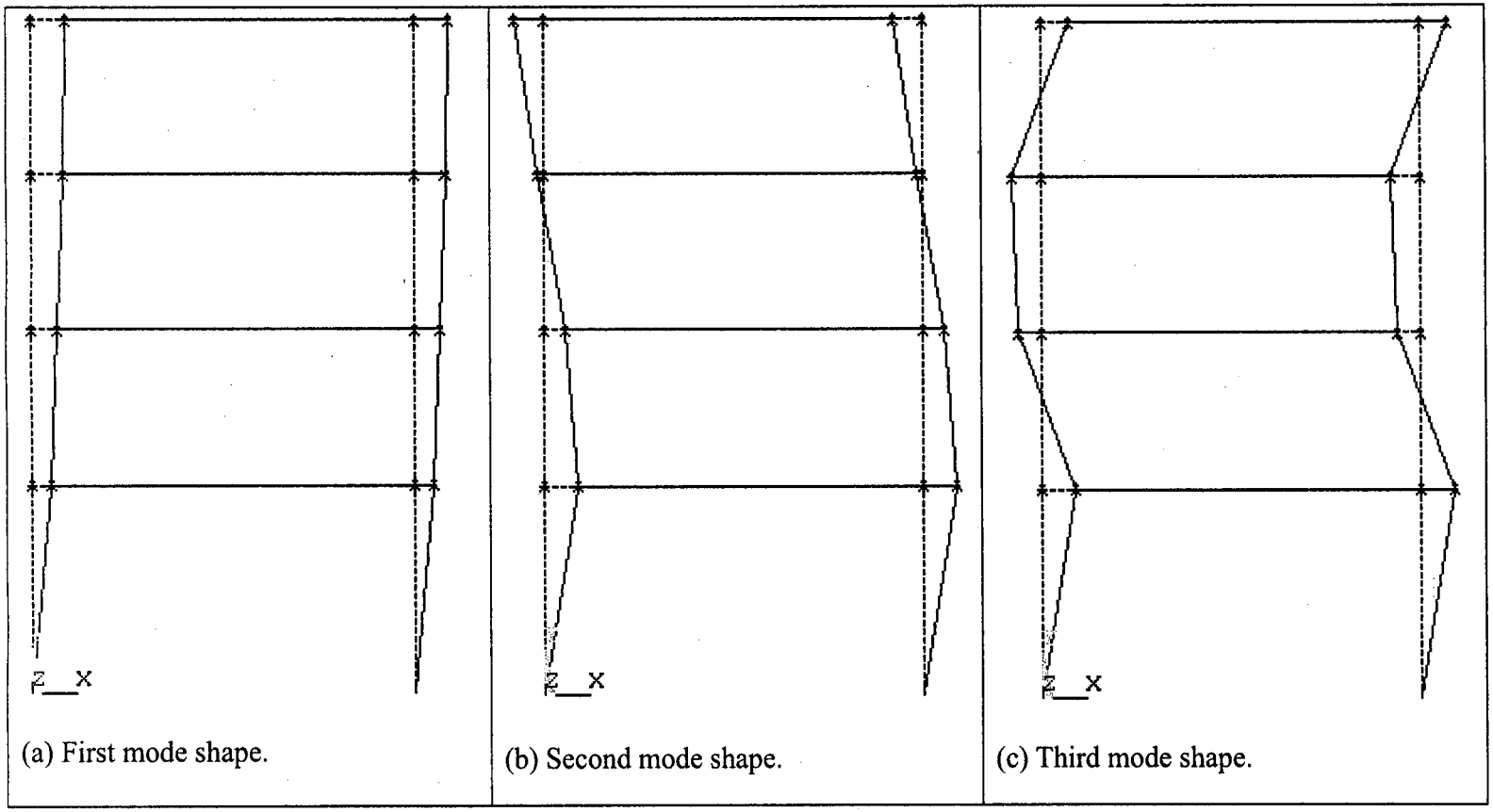

(a) First mode shape.

(b) Second mode shape.

(c) Third mode shape.

Figure 5.9: Mode shape of model SD2D.

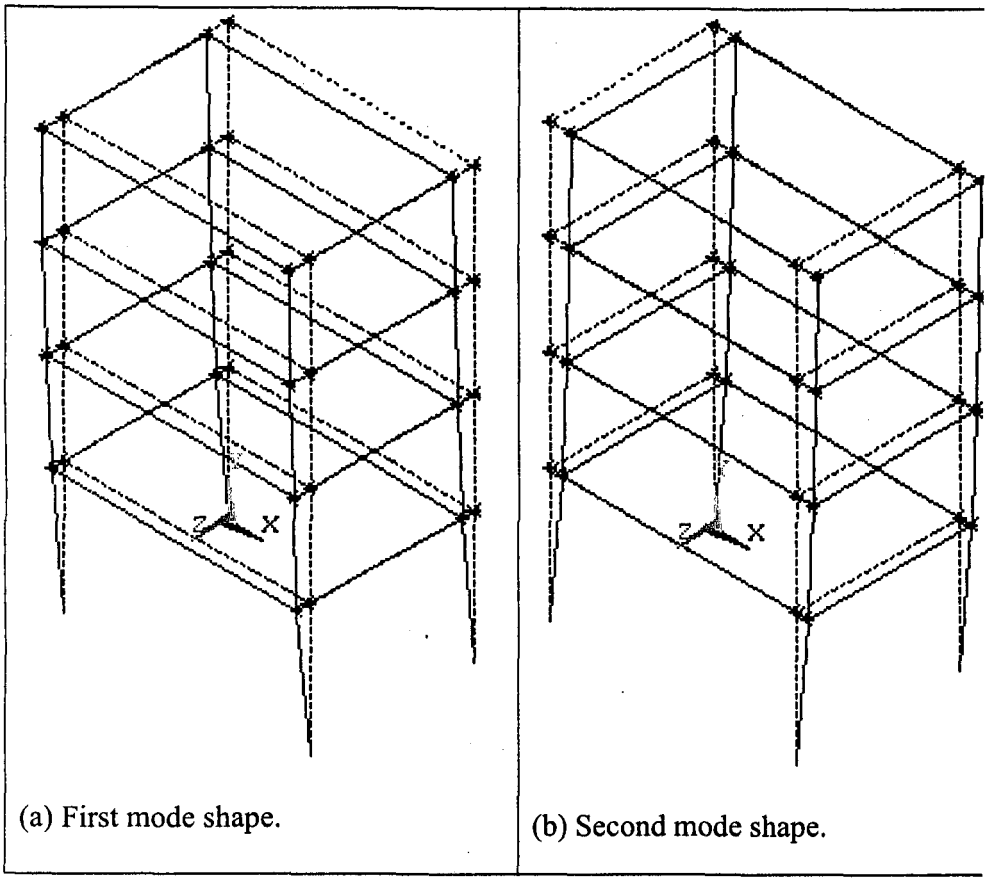

(a) First mode shape.

(b) Second mode shape.

Figure 5.10: Mode shape of model SD3D.

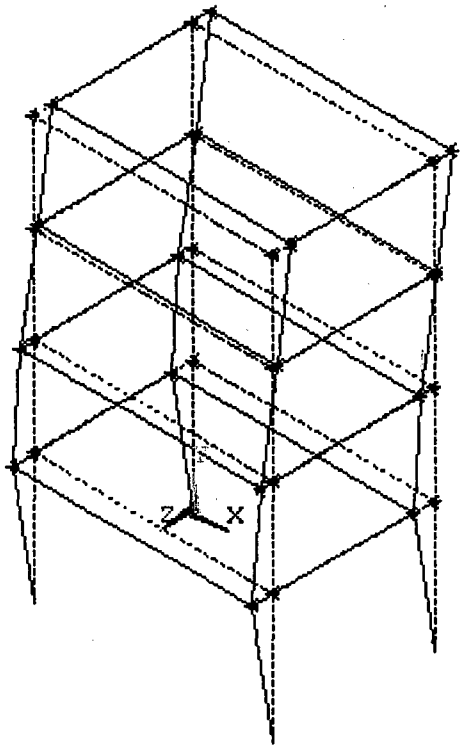

(c) Third mode shape.

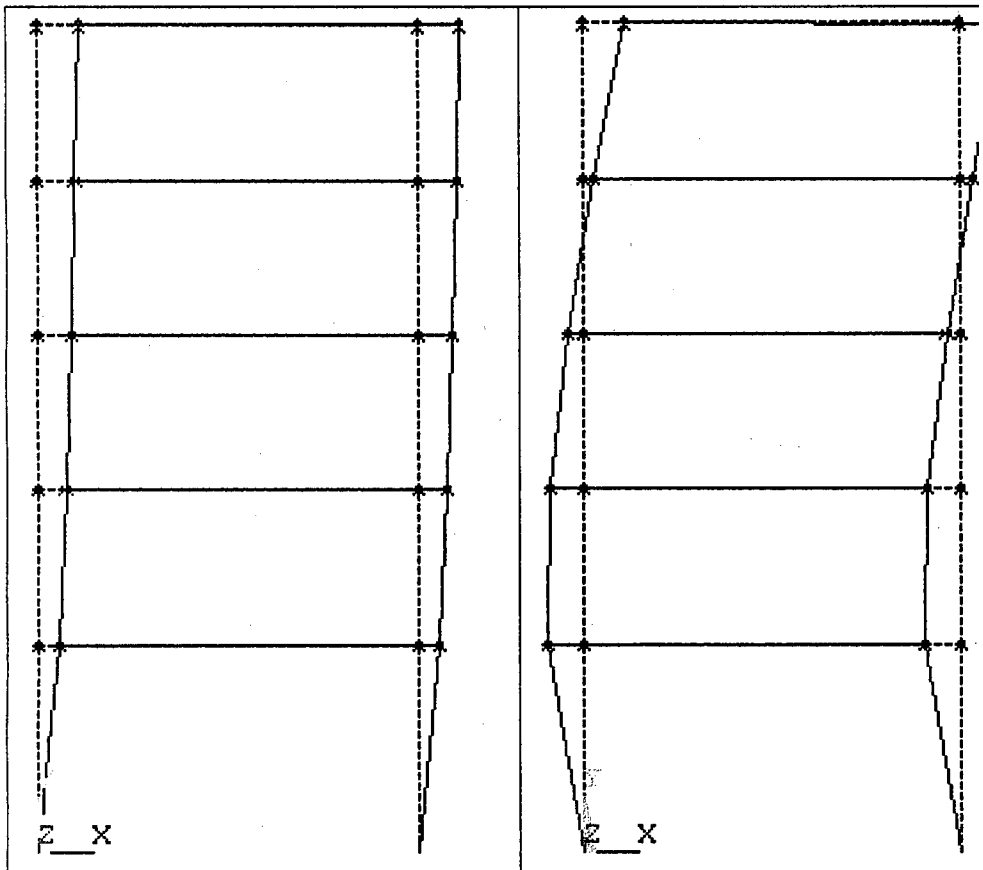

(a) First mode shape.

(b) Second mode shape.

Figure 5.11: Mode shape of model MRD2D.

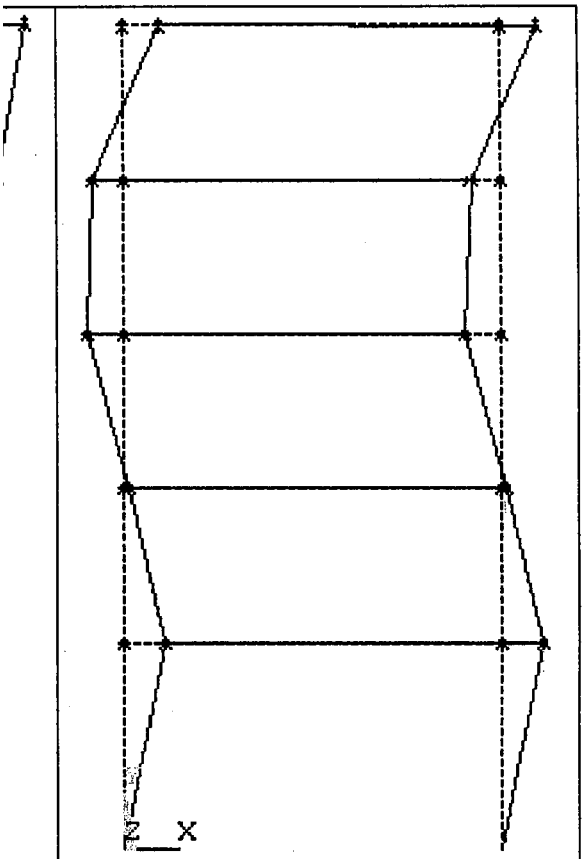

(c) Third mode shape.

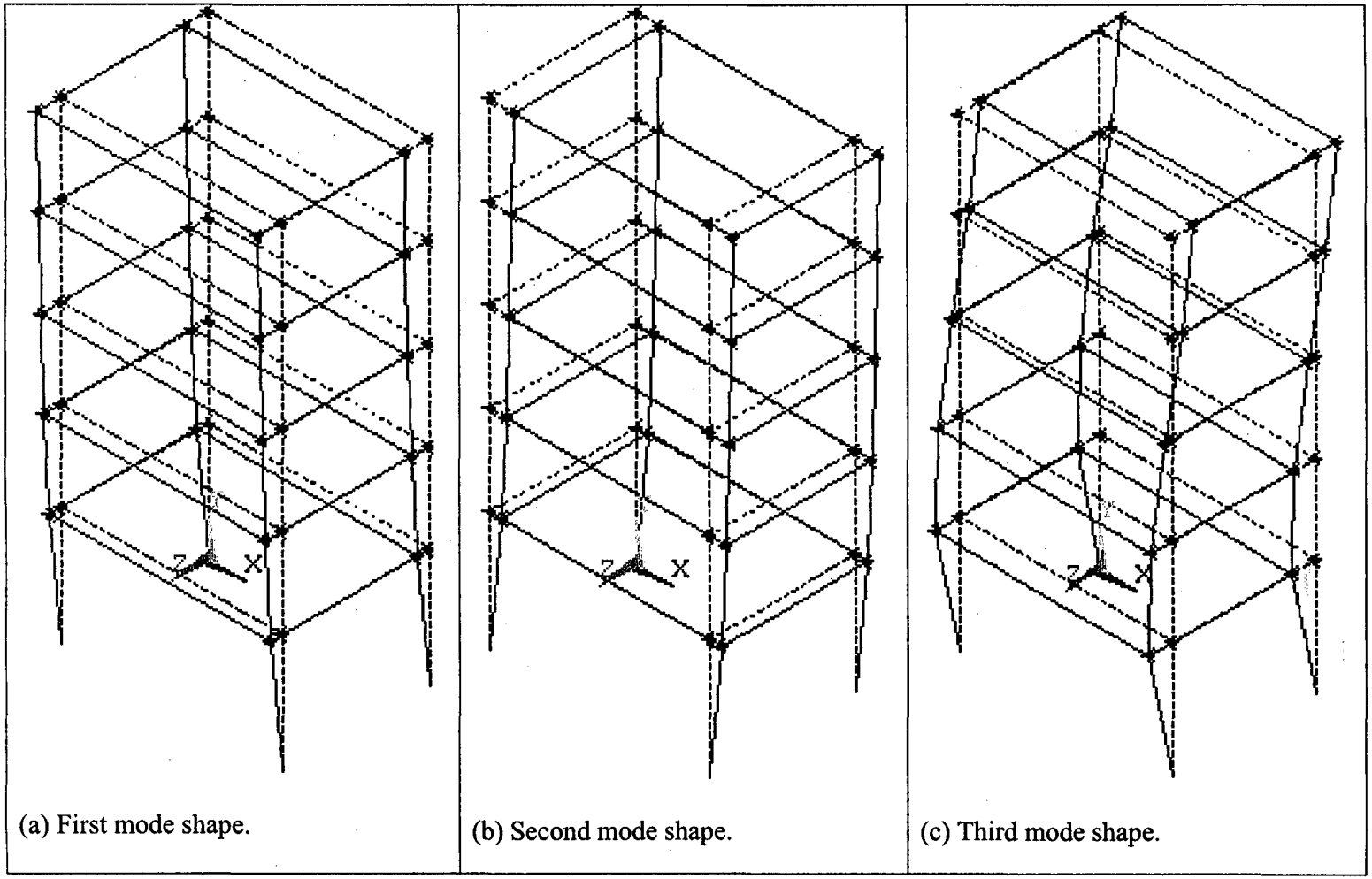

(a) First mode shape.

(b) Second mode shape.

(c) Third mode shape.

Figure 5.12: Mode shape of model MRD3D.

5.3 Performance evaluation of the 2.2 kN MR Damper (RD-1005-3)

To evaluate the performance of MR damper RD-1005-3, the damper is integrated into the model RD2D and RD3D in different cases with respect to damper location. Figure 5.13 to 5.16 shows the cases as RD2Da, RD2Db, RD2Dc for model RD2D and RD3Da for model RD3D. The damping ratio of 0.4 % is considered for all modes for both models. The dynamic time history analysis is performed using Newmark's method. The RD2D model is analyzed first without considering MR damper. The structure is excited with the El-Centro earthquake record. As the model is scaled and the fundamental frequency is higher than a full scale structure, the earthquake record is reproduced by five times the original recording speed as suggested by Dyke *et al.,* 1996. The reproduced signal is shown in Figure C1 (Appendix C). The top floor uncontrolled displacement, velocity and acceleration are found to be 0.00987 m, 0.3615 m/sec and 14.97 m/sec^2 respectively as provided in Table 5.2.

Now the 2.2 kN MR damper (RD-1005-3) is integrated into the model RD2D as case RD2Da shown in Figure 5.13. The current supplied to the damper is 0A to 2A according to the control algorithm described in the Section 3.5. The structure is excited with the same reproduced El-Centro earthquake record. The uncontrolled (without damper) and controlled (with damper) responses are summarized in Table 5.2. As it can be realized the top floor controlled displacement, velocity and acceleration has reduced to 0.0069 m, 0.2741 m/sec and 12.70 m/sec^2 respectively which is about 29%, 24% and 15% reduction with respect to displacement, velocity and acceleration of uncontrolled structure respectively. Figure 5.17 to 5.19 shown third floor uncontrolled and controlled

displacement, velocity and acceleration responses respectively. It is observed that after integrating MR damper into the model RD2D vibration of structure is damped out quickly.

Figure 5.20 shows energy time history of the uncontrolled structure. It is observed that 16.03 J of maximum strain energy experienced by structure. Figure 5.21 shows energy time history of the controlled structure. It is found that by introducing MR damper into the system, strain energy demand reduced to 8.59 J and at the same time input energy is dissipated. Figure 5.22 shows damping energy time history. It is observed that the maximum damping energy is 18.34 J. Here structural damping energy contribution is only 2.76 J where as that by MR damper is 15.58 J. Therefore it can be easily understood that MR damper could increase the damping property of structure significantly.

The power spectral density (PSD) of the top floor acceleration response history for the uncontrolled and controlled structures is shown in Figure 5.23 and 5.24, respectively. From Figure 5.23, it is observed that fundamental dominant frequency is about 5.62 Hz and PSD in this frequency is 41.31 dB. From Figure 5.24 it is observed that the dominant frequency is about 5.74 Hz and PSD at that frequency is reduced to 29.97 dB. Therefore it can be noted here that with the application of MR damper, the frequency of structure does not change but the damping property of structures changes significantly.

During the earthquake it is very common that the power supply to MR damper fails (zero current). Therefore it is necessary to study this case and find how structure react when

current to MR damper is kept zero value (Passive-off). To illustrate this, MR damper model RD-1005-3 is integrated to the model RD2D as shown in Figure 5.13. Current to the damper is kept as 0A which corresponds to the passive-off state of the damper. Table 5.3 shows the uncontrolled and controlled displacement, velocity and acceleration. The reproduced El-Centro earthquake record is used as excitation. From Table 5.3 it is observed that top floor displacement, velocity and acceleration is reduced by 3.95%, 2.39% and 6.61% respectively even there is no power supplied to the damper. Figure 5.25 also shows the uncontrolled and controlled displacement at the third floor (damper with the 0A current).

5.3.1 Effective location for MR damper placement

To find the effective location for damper, the structure considered here is a three story building frame model RD2D shown in Figure 5.1. There are three possible locations to place MR damper (on each floor). Therefore three cases are considered. In RD2Da the damper is placed at ground floor (Figure 5.13), in RD2Db damper is placed at the first floor (Figure 5.14) and in RD2Dc damper is placed at the second floor (Figure 5.15). The current to the MR damper is kept at 0A-2A according to the control algorithm as described in Section 3.5. As the structure is scaled down, the reproduced El-Centro earthquake record (five times the original recording speed) is used. The effectiveness of MR damper placement is evaluated based on the following three criteria such as, response reduction (Iqbal *et al* 2008), contribution to the damping energy and change in damping ratio (Iqbal *et al*, 2009; Karla, 2004) due to the MR damper.

Table 5.4 shows the uncontrolled and controlled floor displacement in comparison with damper location and Figure 5.26 shows the variation of the top floor displacement reduction with damper location. It is observed that the maximum displacement of the top floor is reduced by 29.28% when the damper is placed at the ground floor. Therefore it can be concluded that ground floor is the best location for this structure.

Table 5.5 shows damping energy contributed by MR damper with respect to the location of the damper and Figure 5.27 shows the variation of damping energy added by the MR damper with the damper location. It is observed that the maximum damping energy of 84.95% is added by MR damper when the damper is placed at the ground floor.

Here to find the effective damper location, variation of damping ratio with respect to damper location is also studied. The damping ratio is calculated using logarithmic decrement expression as (Chopra, 2007):

$$\zeta = \frac{1}{2\pi j} \ln \frac{u_i}{u_{i+j}} \qquad \text{----------5.1}$$

where, ζ is damping ratio, u_i is the highest peak of the free vibration response, u_{i+j} is one of the subsequent peaks, j is the number of peaks between u_i and u_{i+j} (Figure 5.28). Here the damper is placed at the ground floor level. The structure is excited with a harmonic ground excitation of amplitude 0.03 m and frequency of 4 Hz for two second, and then the structure is allowed to vibrate freely. The damping ratio is calculated using Eq. 5.1 from third floor displacement response shown in Figure 5.29. This process is repeated by changing the damper location (floor to floor). Damping ratio for the case of

without damper and with damper at different floor is summarized in Table 5.6. Variation of damping ratio added by MR damper for different location is also shown in Figure 5.30. It is observed that maximum damping ratio of 4.38% is added by MR damper when damper placed at ground floor.

Effectiveness of damper location is evaluated considering three criteria discussed above. All criteria confirm that the ground floor is the best location to place damper for the structure RD2D considered here.

5.3.2 Performance of the 2.2 kN MR damper (RD-1005-3) under different earthquakes.

From above discussion it can be concluded that MR damper has the ability to control the response of a structure and reduce the vibration of structure during an earthquake. From Section 5.3.1 it is also demonstrated that the ground floor is the best location for the damper. Here the performance of the damper will be studied under different earthquakes. Here the model RD3D (3D model of the three stories structure) is selected to integrate the MR dampers which are placed at the ground floor level (case RD3Da) as shown in Figure 5.16. Only horizontal DOFs are considered in the model. The ground excitation is applied in the X-direction. The dynamic time history analysis is performed using Newmark's method. The current supplied to the MR damper is considered to be 0A-2A according to control algorithm described in Section 3.5. Table 5.7 shows the uncontrolled and controlled floor displacement under different earthquakes. Figure 5.31 to 5.35 also show the controlled and uncontrolled displacements at the third floor level. It is observed that

with the use of dampers it is possible to reduce the displacement of structure significantly during earthquake which will subsequently reduce the demand of inelastic deformation of the structure.

Table 5.2: Uncontrolled and controlled response comparison for model RD2D under reproduced El-Centro earthquake excitation (current 0-2A).

Floor		Displacement (m)	Velocity (m/sec)	Acceleration (m/sec^2)
First floor	Uncontrolled	0.0046	0.1792	8.92
	Controlled	0.0033	0.1311	7.49
Second floor	Uncontrolled	0.0076	0.2928	11.35
	Controlled	0.0057	0.2127	9.49
Third floor	Uncontrolled	0.0098	0.3615	14.97
	Controlled	0.0069	0.2741	12.70

Table 5.3: Uncontrolled and controlled (passive-off) response under reproduced El-Centro earthquake for model RD2Da (damper RD-1005-3 with 0A current).

Floor		Displacement (m)	Velocity (m/sec)	Acceleration (m/sec^2)
First floor	Uncontrolled	0.0046	0.1792	8.92
	Controlled (passive-off)	0.0044	0.1684	8.28
Second floor	Uncontrolled	0.0077	0.2928	11.35
	Controlled (passive-off)	0.0076	0.2779	10.79
Third floor	Uncontrolled	0.0099	0.3615	14.97
	Controlled (passive-off)	0.0095	0.3529	13.98

Table 5.4: Uncontrolled and Controlled floor displacement (m) with damper location (model RD2D).

	Uncontrolled	Damper location		
		Ground Floor	First floor	Second floor
First floor	0.0046	0.0033	0.0034	0.0037
Second floor	0.0077	0.0057	0.0059	0.0068
Third floor	0.0099	0.0070	0.0074	0.0085

Table 5.5: Comparison of damping energy contribution by MR damper with damper location (model RD2D).

Location of damper	Total Damping Energy (DE) (J)	Structural DE (J)	DE by MR damper (J)	% of DE by MR damper
Ground floor	18.34	2.76	15.58	84.95
First floor	19.52	3.63	15.89	81.40
Second floor	15.29	6.05	9.24	60.46

Table 5.6: Change in damping ratio with damper location (model RD2D).

	Total Damping (% of critical damping)	Damping added by the MR damper (% of critical damping))	% Gain in damping due to MR damper
Without Damper	0.4	-	-
Damper located at Gr. Floor	4.78	4.38	1095
Damper located at 1st Floor	2.93	2.53	632.5
Damper located at 2nd Floor	1.05	0.65	162.5

Table 5.7: Uncontrolled and controlled floor displacement (m) under different earthquake (model RD3D).

		Earthquake record/component				
		IMPVALL/I-ELC180	MAMMOTH/I-LUL000	MAMMOTH/L-LUL090	NORTHR/SCE288	IMPVALL/H-E05140
First floor	Uncontrolled	0.0046	0.0019	0.0034	0.0051	0.0034
	Controlled	0.0032	0.0012	0.0030	0.0037	0.0023
Second floor	Uncontrolled	0.0077	0.0032	0.0061	0.0092	0.0063
	Controlled	0.0056	0.0023	0.0054	0.0071	0.0048
Third floor	Uncontrolled	0.0099	0.0043	0.0079	0.0116	0.0079
	Controlled	0.0068	0.0031	0.0068	0.0091	0.0063

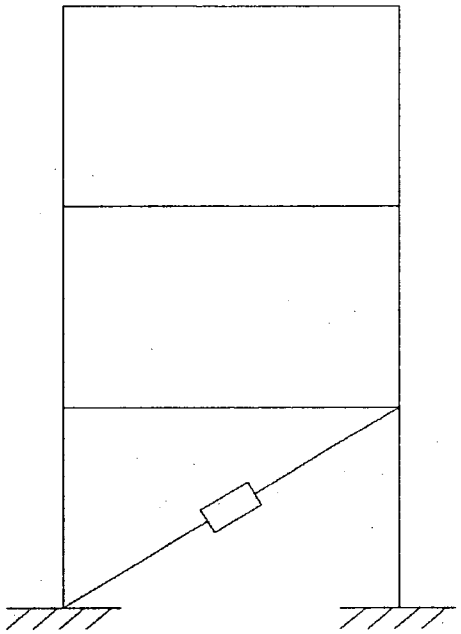

Figure 5.13: Case RD2Da (Model RD2D, MR damper RD-1005-3).

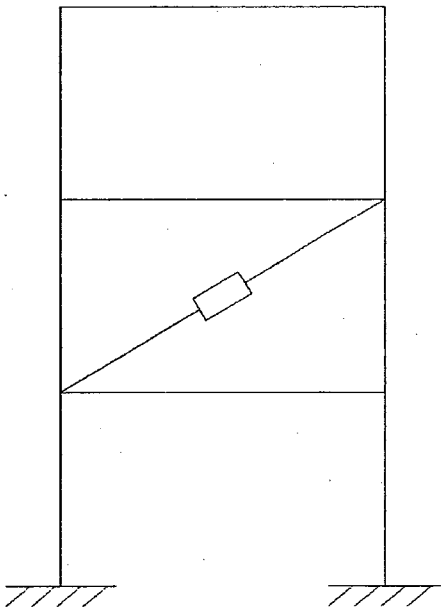

Figure 5.14: Case RD2Db (Model RD2D, MR damper RD-1005-3).

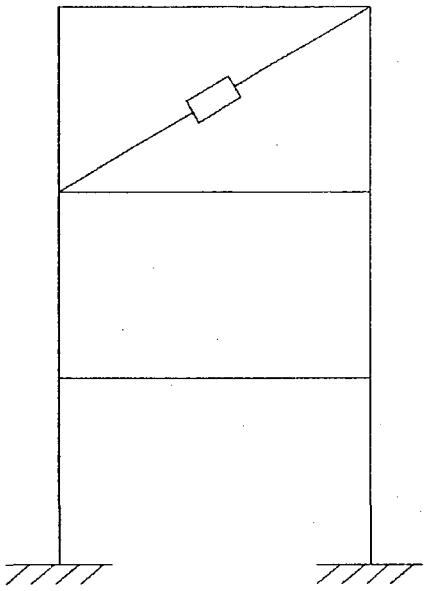

Figure 5.15: Case RD2Dc (Model RD2D, MR damper RD-1005-3).

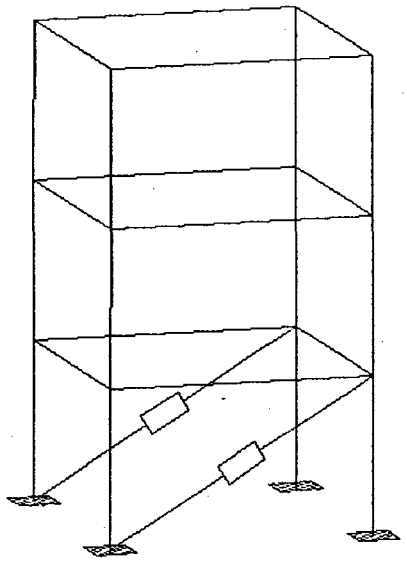

Figure 5.16: Case RD3Da (Model RD3D, MR damper RD-1005-3).

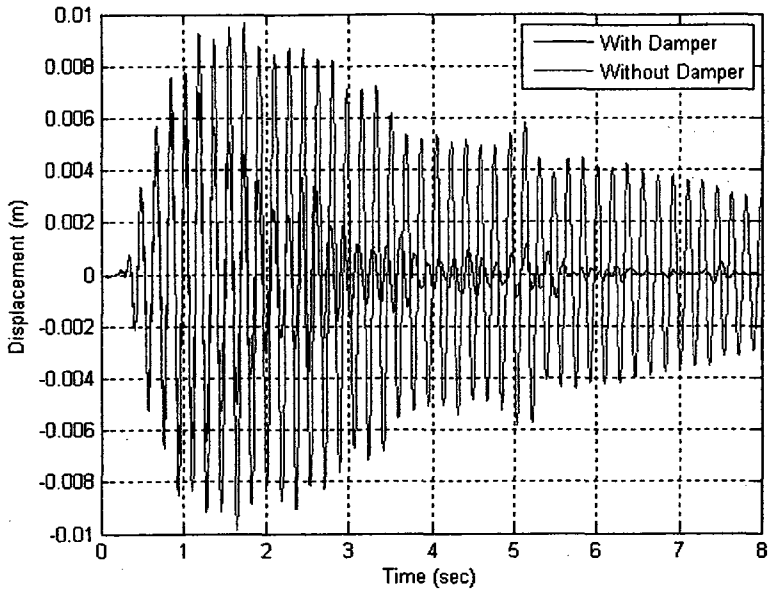

Figure 5.17: Uncontrolled and controlled third floor displacement of the structure (RD2Da) under reproduced El-Centro earthquake record.

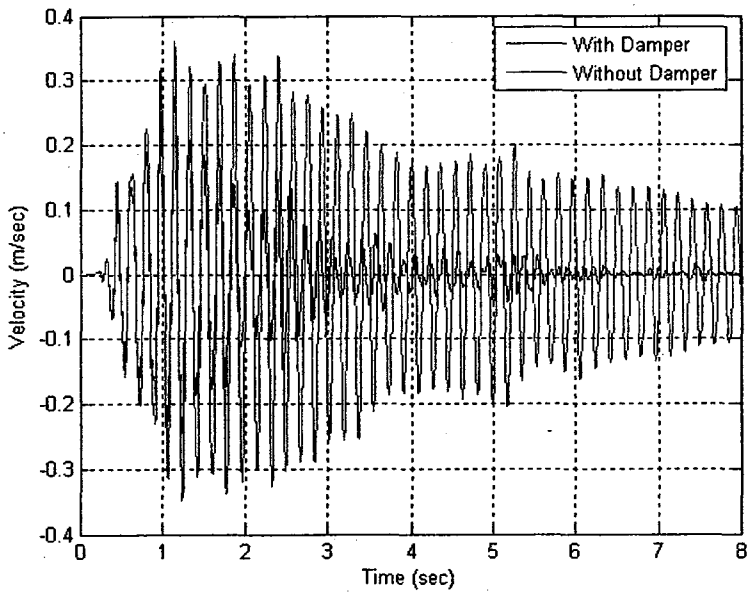

Figure 5.18: Uncontrolled and controlled third floor velocity of the structure (RD2Da) under reproduced El-Centro earthquake record.

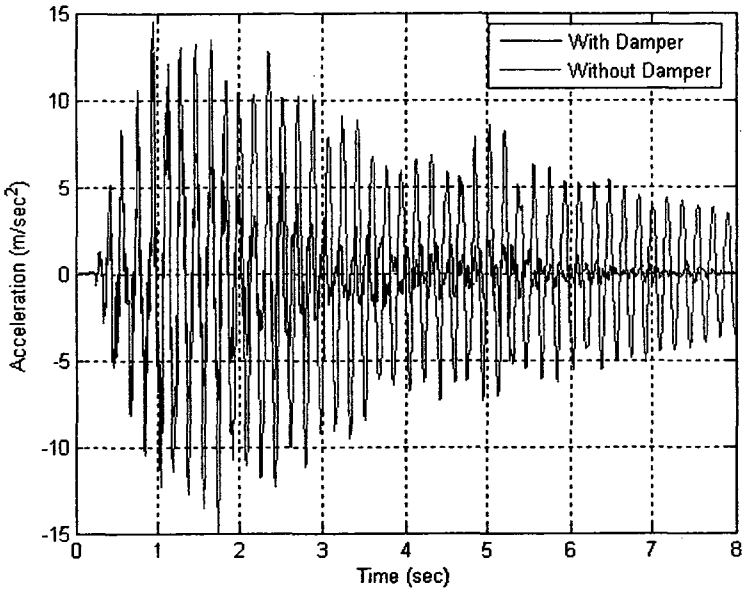

Figure 5.19: Uncontrolled and controlled third floor acceleration (model RD2Da) under reproduced El-Centro earthquake record.

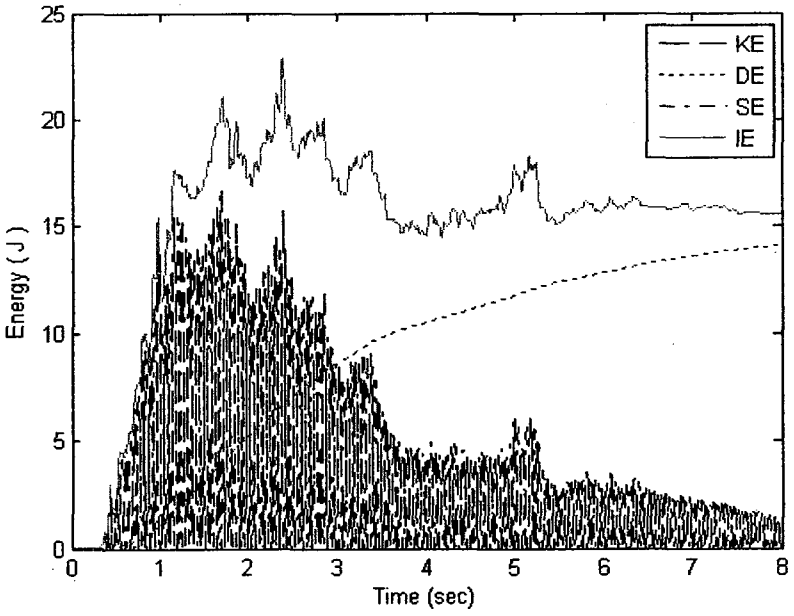

Figure 5.20: Energy history of the uncontrolled structure (RD2D) under reproduced El-Centro earthquake record.

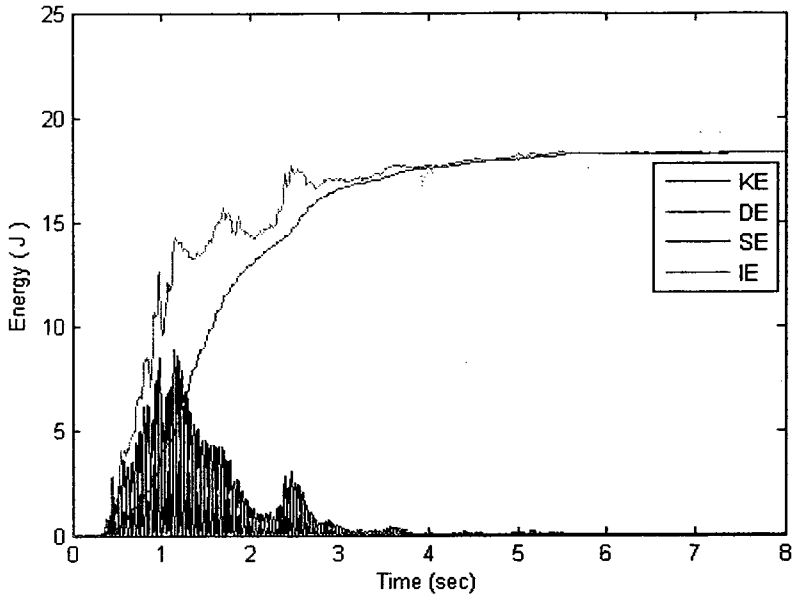

Figure 5.21: Energy history of the controlled structure (RD2Da) under reproduced El-Centro earthquake record.

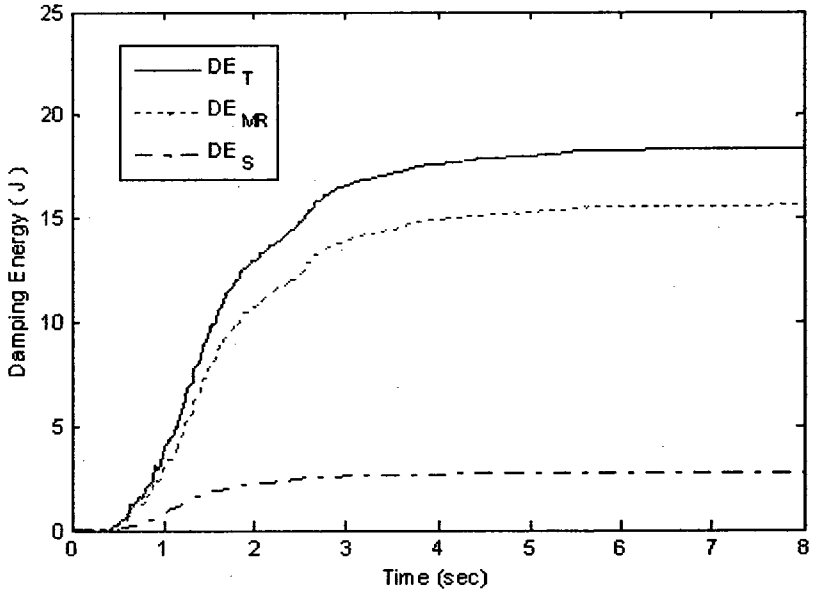

Figure 5.22: Damping energy history of the controlled structure (RD2Da) under reproduced El-Centro earthquake record.

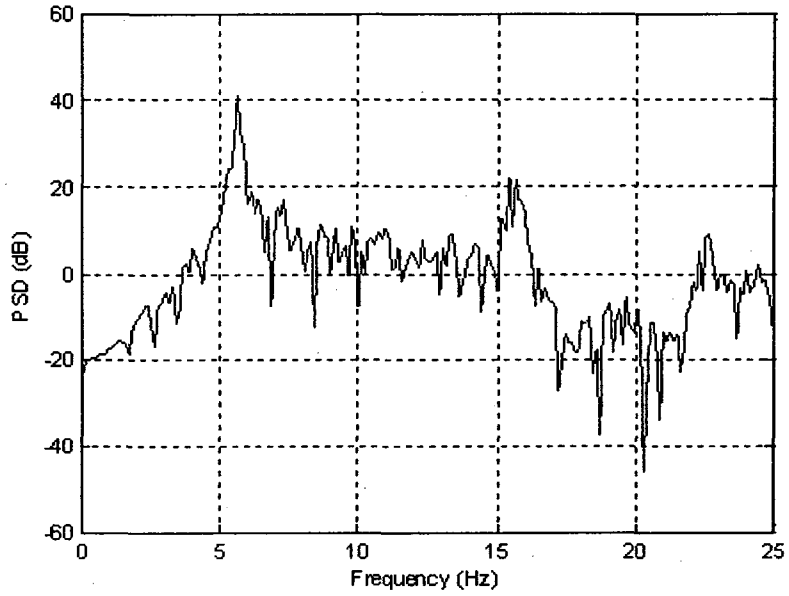

Figure 5.23: Power spectral density of the top floor accelerations of the uncontrolled structure (RD2D) under reproduced El-Centro earthquake record.

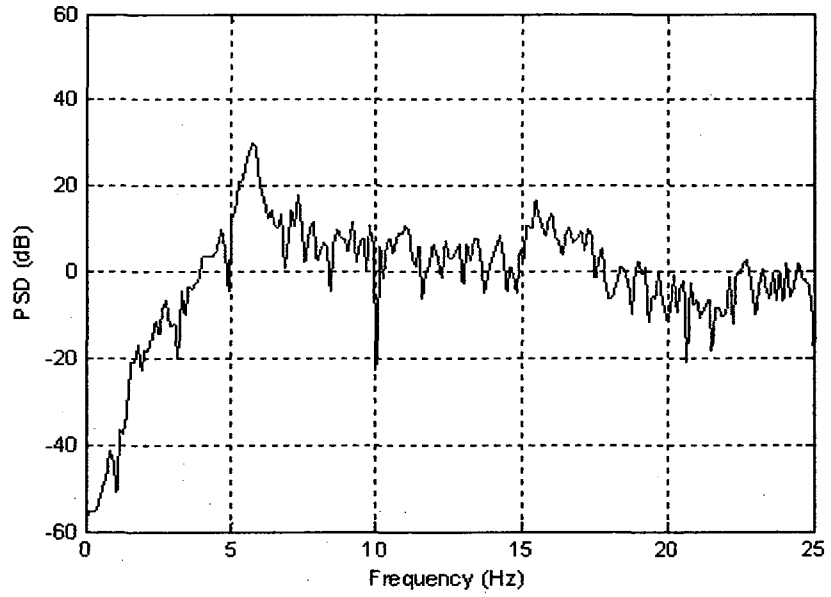

Figure 5.24: Power spectral density of the top floor accelerations of the controlled structure (RD2Da) under reproduced El-Centro earthquake record.

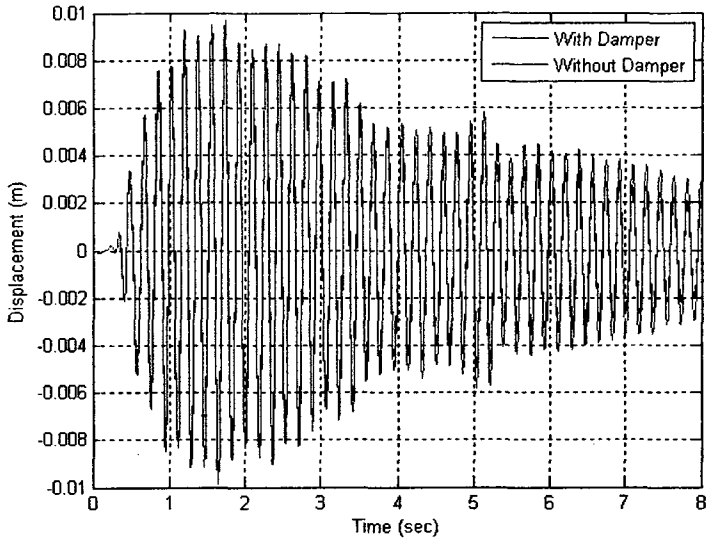

Figure 5.25: Uncontrolled and controlled (passive-off) third floor displacement under reproduced El-Centro earthquake (RD2Da).

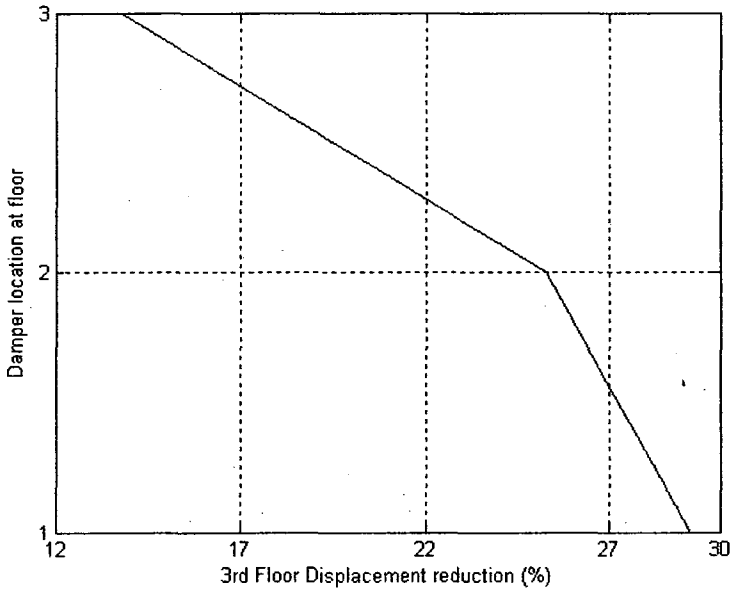

Figure 5.26: Third floor displacement reduction for different damper locations for model RD2D under reproduced El-Centro earthquake.

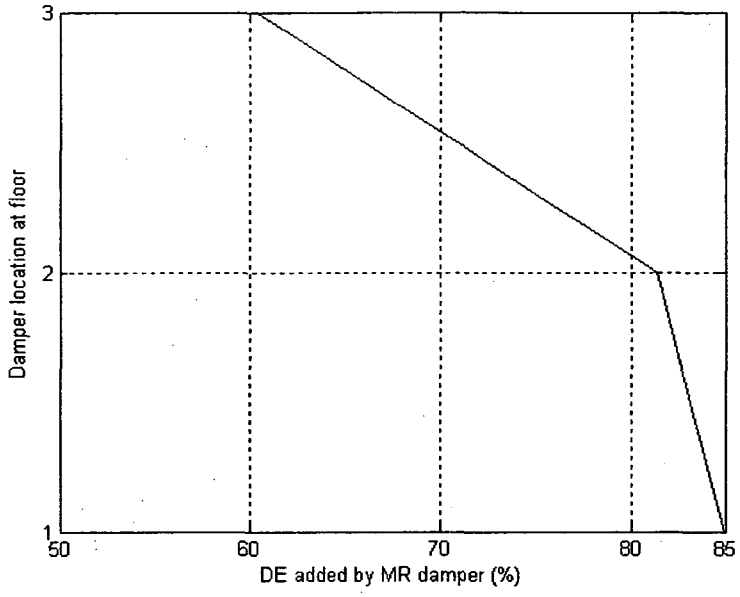

Figure 5.27: Contribution of damping energy (DE) by MR damper with damper location in RD2D model under reproduced El-Centro earthquake.

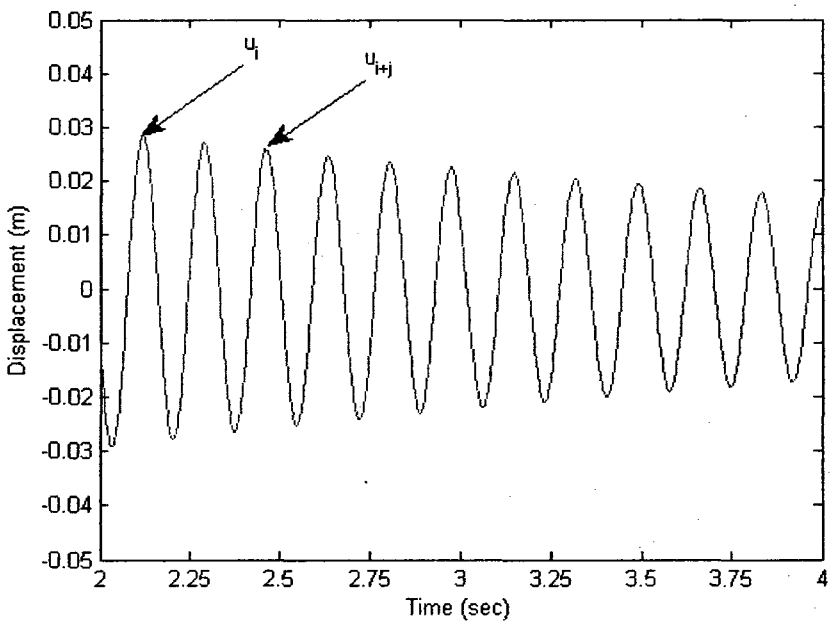

Figure 5.28: Typical free vibration response of RD2D model.

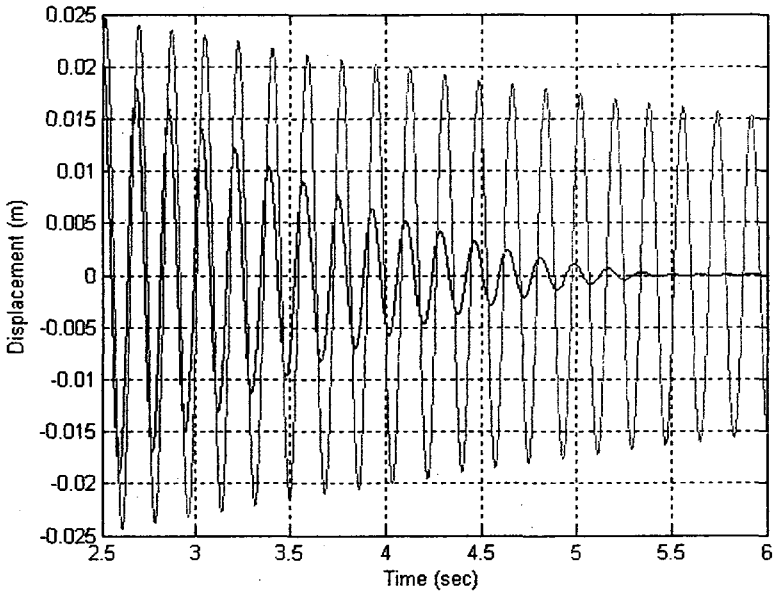

Figure 5.29: Top floor displacement (free vibration) of the uncontrolled and controlled structure (RD2D) when damper is located at ground floor.

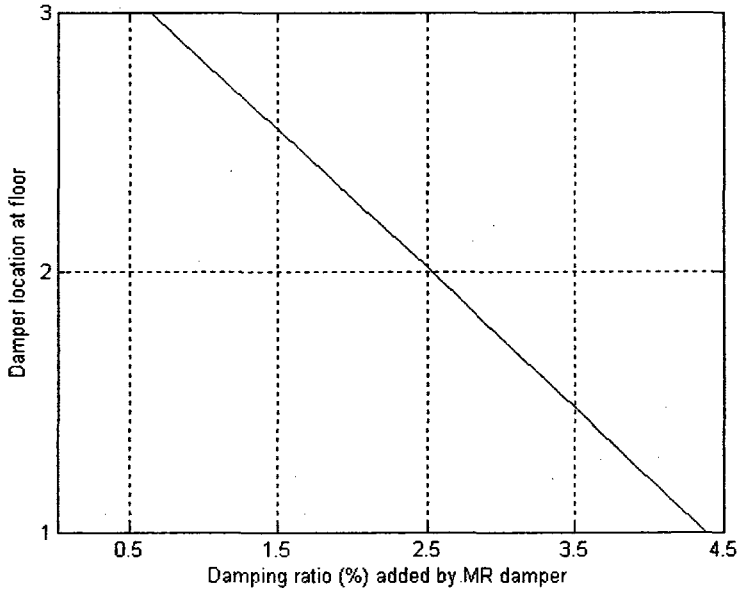

Figure 5.30: Contribution of damping ratio by MR damper with damper location (model RD2D) under reproduced El-Centro earthquake record.

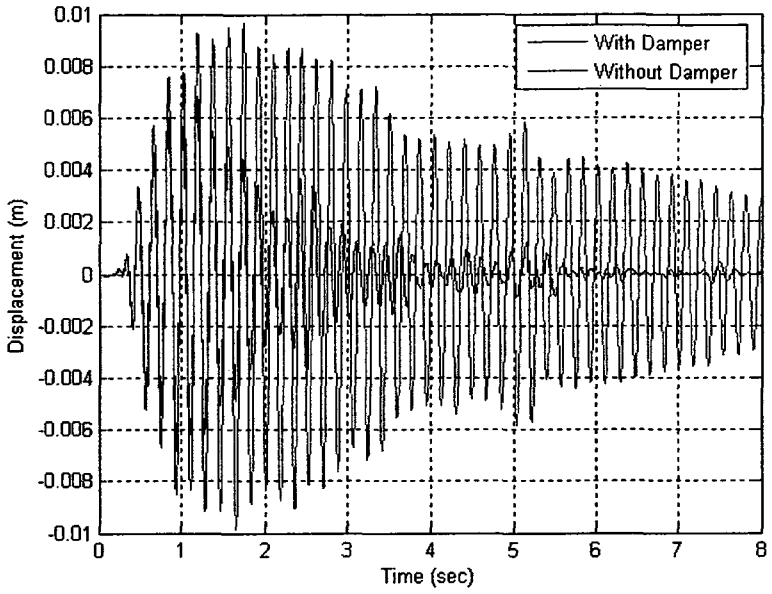

Figure 5.31: Third floor displacement of the uncontrolled and controlled structure (RD3D) under reproduced El-Centro (IMPVALL/I-ELC180) earthquake.

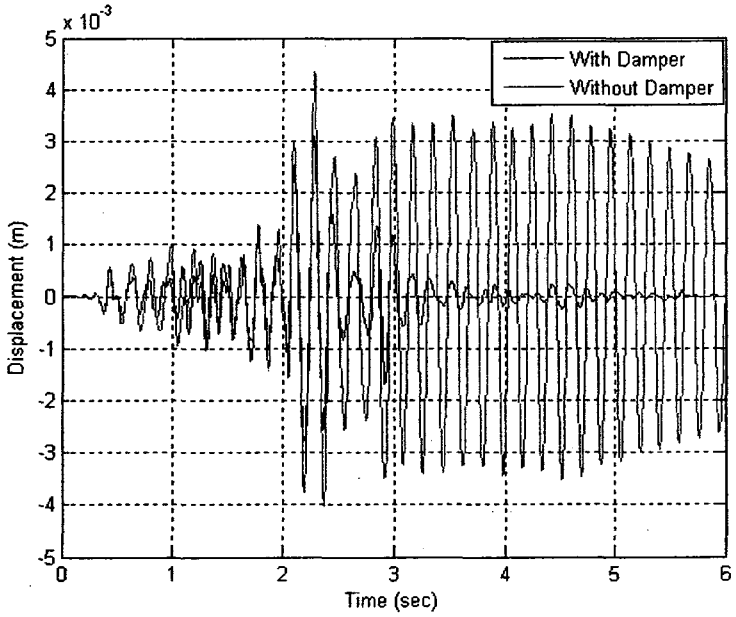

Figure 5.32: Third floor displacement of the uncontrolled and controlled structure (RD3D) under reproduced Mammoth Lake (MAMMOTH/I-LUL000) earthquake.

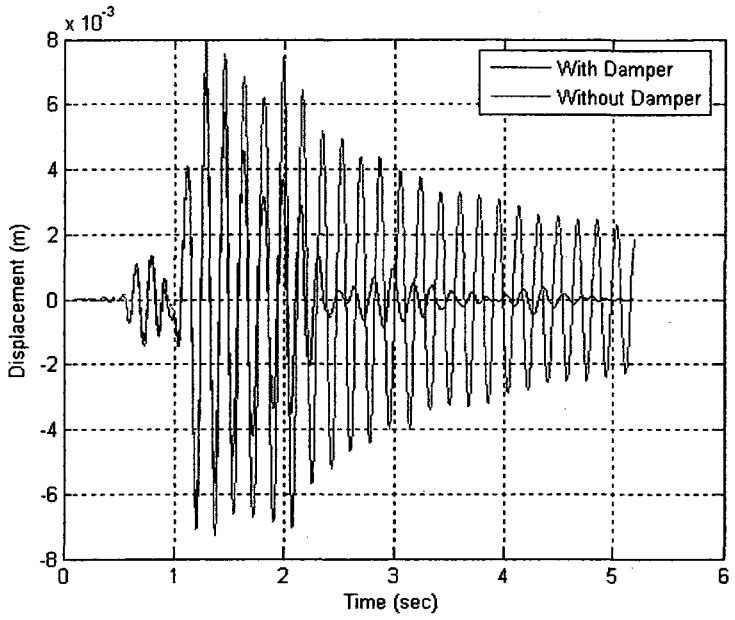

Figure 5.33: Third floor displacement of the uncontrolled and controlled structure (RD3D) under reproduced Mammoth Lake (MAMMOTH/L-LUL090) earthquake.

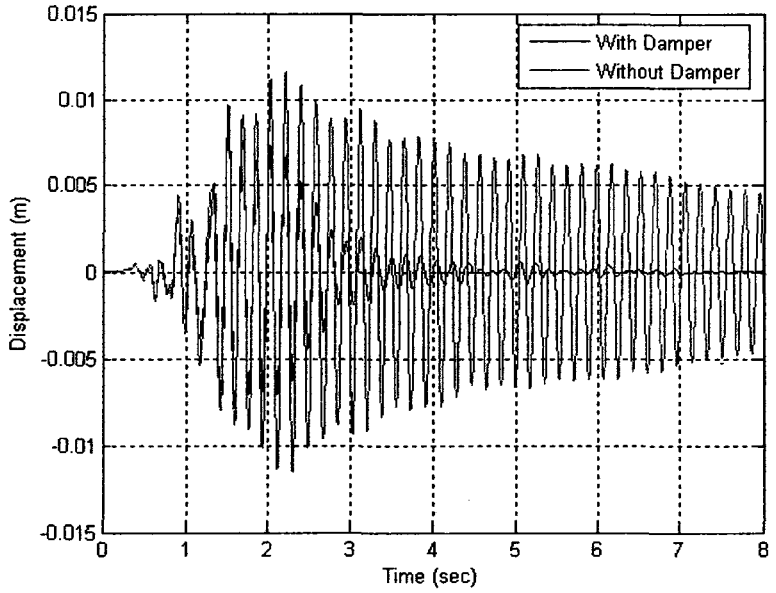

Figure 5.34: Third floor displacement of the uncontrolled and controlled structure (RD3D) under reproduced Northridge (NORTHR/SCE288) earthquake.

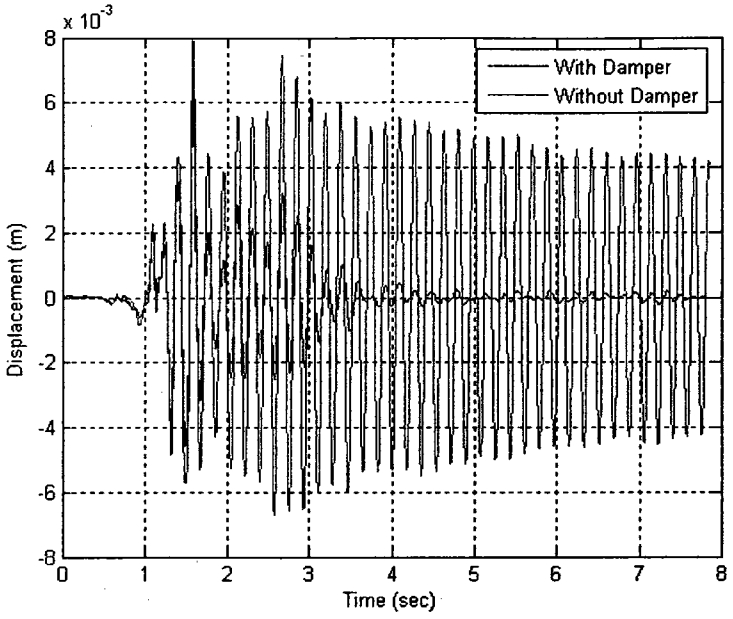

Figure 5.35: Third floor displacement of the uncontrolled and controlled structure (RD3D) under reproduced Imperial valley (IMPVALL/H-E05140) earthquake.

5.4 Performance evaluation of the 3 kN MR damper (SD-1000)

To evaluate the performance of MR damper SD-1000, the damper is integrated into the SD2D and SD3D models, and different cases with respect to damper location have been considered. Figure 5.36 to 5.40 show the cases designated as SD2Da, SD2Db, SD2Dc, SD2Dd for model SD2D and SD3Da for model SD3D. The damping ratio of 0.75 % of critical damping is considered for all modes for model SD2D and SD3D. The analysis is performed by State-Space method as discussed earlier. Model SD2D is analyzed first without considering the damper. The structure is excited with the El-Centro earthquake record. As the model is scaled and the fundamental frequency is high (5.835 Hz), the earthquake record is reproduced by five times the original recording speed (Figure C1).

The top floor uncontrolled displacement, velocity and acceleration are found to be 0.0095 m, 0.3561 m/sec and 13.49 m/sec^2 as provided in Table 5.8.

Now MR damper SD-1000 is integrated into the model SD2D as case SD2Da shown in Figure 5.36. The voltage supplied to the damper is 0 to 2.25V according to the control algorithm described in the Section 3.5. The structure is excited with the same reproduced El-Centro earthquake record. The uncontrolled (without damper) and controlled (with damper) responses are summarized in Table 5.8. The fourth floor uncontrolled and controlled displacements, velocities and accelerations are shown in Figure 5.41 to 5.43 respectively. It is observed that after integrating MR damper into the model SD2D model, the top floor displacement, velocity and acceleration are reduced by 59.54%, 64.70% and 47.72% respectively with respect to uncontrolled structure. It is also observed that because of the damper, vibration of structure is damped out rapidly.

Figure 5.44 shows the uncontrolled energy time history. It is observed that 68.33 J of maximum strain energy experienced by structure. Figure 5.45 shows the energy time history of the controlled structure. It is found that with the application of the damper, the strain energy demand reduced to 10.43 J and at the same time the input energy is dissipated by damping. Figure 5.46 shows the damping energy time history. It is observed that the maximum damping energy is 54.91 J. Here the structural damping energy contribution is only 5.05 J while the damping energy contribution due to the MR damper is 49.86 J. Therefore, it can be easily understood that the MR damper could increase the damping property of structure significantly.

The power spectral density of the top floor acceleration response for the uncontrolled and controlled structures are shown in Figures 5.47 and 5.48, respectively. From Figure 5.47 it can be realized that the dominant frequency is 5.86 Hz in which the PSD of acceleration has the value of 42.86 dB. From Figure 5.48 it is observed that the dominant frequency has not changed and is 5.869 Hz however the PSD of acceleration is reduced to 23.68 dB. Therefore it can be noted that with the application of MR damper, the frequency of structure has not been changed but the damping property of the structure is increased significantly.

A case is considered to simulate the situation when power supply to the MR damper fails, which is a common scenarios during an earthquake. In this case, MR damper SD-1000 is integrated to the model SD2D as shown in Figure 5.36 and the voltage to the damper is kept as 0V (passive-off). Table 5.9 shows the displacement, velocity and acceleration of the uncontrolled and controlled structure. The reproduced El-Centro earthquake record is used as excitation. From Table 5.9 it is interesting to note that top floor displacement, velocity and acceleration are reduced by 19.1%, 27.16% and 14.08% respectively even when there is no power supplied to the damper (i.e. passive-off). Figure 5.49 shows fourth floor displacement of the uncontrolled and controlled structure (passive-off).

5.4.1 Effective location for MR damper placement

To find the effective location for a MR damper, the structure considered here is a four story building frame shown in Figure 5.3 (model SD2D). Four cases are considered as there are four possible locations to place the MR damper on each floor. For Case SD2Da

damper is placed at ground floor, for Case SD2Db damper is placed at first floor, for Case SD2Dc damper is placed at second floor and for Case SD2Dd damper is placed at third floor. The arrangements of damper placement for four cases are shown in Figure 5.36, 5.37, 5.38 and 5.39. The voltage to the MR damper is used 0 - 2.25V according to the control algorithm as described in Section 3.5. Again the structure is scaled down, the reproduced El-Centro earthquake record is used. The effectiveness of MR damper placement is evaluated based on three criteria discussed before which are response reduction, contribution to the damping energy and change in damping ratio due to MR damper.

Table 5.10 shows the comparison of the floor displacements for the uncontrolled and controlled structure with the damper location and Figure 5.50 shows the reduction in the top floor displacement with the damper location. It can be realized that the maximum floor displacement is reduced by 59.54% when damper is placed at ground floor. Therefore it can be concluded that ground floor is the best location for this structure.

Table 5.11 shows damping energy contributed by MR damper with respect to the location of the damper and Figure 5.51 shows the variation of damping energy added by the MR damper with the damper location. It is observed that the maximum damping energy of 90% is added by MR damper when the damper placed at the ground floor level.

To evaluate the effect of damper location on damping ratio, the structure is excited with harmonic ground excitation of amplitude 0.03 m and frequency 4 Hz for the duration of

two seconds, and then the structure is allowed to vibrate freely. With a MR damper placed at the ground floor, the fourth floor displacement response is shown in Figure 5.52. Damping ratio is calculated by using Eq. 5.1 from the fourth floor displacement response as shown in Figure 5.52. This process is repeated by changing the damper location to different floors. The damping ratio calculated for the structure without damper and with damper at different floor is summarized in Table 5.12. Variation of damping ratio added by MR damper with different locations is also shown in Figure 5.53. As it can be seen the maximum damping ratio of 2.6% (approximately 4 times the structural damping ratio) is added by MR damper when damper placed at ground floor.

Effectiveness of damper location is evaluated here considering response reduction, damping energy contribution and change in damping ratio as discussed above. It can be concluded that the ground floor is the best location to place damper for the structure SD2D considering different evaluation criteria.

5.4.2 Performance of 3 kN MR damper (SD-1000) under different earthquakes.

As demonstrated before it can be concluded that MR dampers have the ability to control the response of structure and reduce the vibration of structure during earthquake. From the Section 5.4.1, it is also established that the ground floor is the best location to install an MR damper. Here the performance of MR damper will be studied under different earthquakes. The SD3D model is selected to integrate MR damper and the damper is placed at ground floor level (case SD3Da) as shown in Figure 5.40. Only the horizontal

DOFs are considered here. Ground excitation is applied in Z-direction as indicated in Figure 5.40. The dynamic time history analysis is done by State-Space method. The control voltage to the MR damper is used in the range of 0-2.25V, according to control algorithm described in Section 3.5. As this structure is also scaled down, the earthquake record is reproduced five times the recording speed (Figure C1 to C5). Table 5.13 shows the floor displacements of the uncontrolled and controlled structure under different earthquake excitations. Figure 5.54 to 5.58 shows fourth floor displacement of the controlled and uncontrolled structure respectively under different earthquake excitations. It is observed that with the use of damper it is possible to reduce the displacement of structure during earthquake which will reduce the demand of inelastic deformation of structure.

Table 5.8: Uncontrolled and controlled response comparison under reproduced El-Centro earthquake excitation (model SD2D).

Floor		Displacement (m)	Velocity (m/sec)	Acceleration (m/sec^2)
First floor	Uncontrolled	0.0056	0.1963	8.68
	Controlled	0.0020	0.0865	5.08
Second floor	Uncontrolled	0.0075	0.2694	11.17
	Controlled	0.0028	0.1077	5.22
Third floor	Uncontrolled	0.0088	0.3267	12.29
	Controlled	0.0034	0.1178	5.549
Fourth floor	Uncontrolled	0.0095	0.3561	13.49
	Controlled	0.0038	0.1257	7.05

Table 5.9: Uncontrolled and controlled (passive-off) response under reproduced El-Centro earthquake for model SD2D.

Floor		Displacement (m)	Velocity (m/sec)	Acceleration (m/sec^2)
First floor	Uncontrolled	0.0056	0.1963	8.68
	Controlled (passive-off)	0.0043	0.162	6.59
Second floor	Uncontrolled	0.0075	0.2694	11.17
	Controlled (passive-off)	0.0059	0.2194	8.26
Third floor	Uncontrolled	0.0088	0.3267	12.29
	Controlled (passive-off)	0.0071	0.2487	10.64
Fourth floor	Uncontrolled	0.0095	0.3561	13.49
	Controlled (passive-off)	0.0077	0.2594	11.59

Table 5.10: Uncontrolled and Controlled floor displacement (m) with damper location (model SD2D).

Floor	Uncontrolled	Damper location			
		Ground floor	First floor	Second floor	Third floor
First floor	0.0056	0.0020	0.0042	0.0046	0.0051
Second floor	0.0075	0.0028	0.0057	0.0062	0.0069
Third floor	0.0088	0.0034	0.0068	0.0074	0.0082
Fourth floor	0.0095	0.0038	0.0074	0.0080	0.0089

Table 5.11: Comparison of damping energy contribution by MR damper with damper (model SD2D).

Location of damper	Total DE (J)	Structural DE (J)	DE by MR damper (J)	% of DE by MR damper
Ground floor	54.91	5.051	49.86	90.8
First floor	106.8	41.13	65.71	61.53
Second floor	123.9	67.78	56.09	45.27
Third floor	140.4	114.4	25.93	18.47

Table 5.12: Change in damping ratio with damper location (model SD2D).

	Total Damping (% of critical damping)	Damping added by the MR damper (% of critical damping))	% Gain in damping due to MR damper
Without Damper	0.75	-	
Damper at ground floor	3.35	2.60	346.67
Damper at first floor	1.24	0.49	65.33
Damper at second floor	1.06	0.31	41.33
Damper at third floor	0.88	0.12	16

Table 5.13: Uncontrolled and controlled floor displacement (m) (Z-direction) under different earthquake (model SD3D).

Floor		Earthquake record/component				
		IMPVALL/I-ELC180	MAMMOTH/I-LUL000	MAMMOTH/L-LUL090	NORTHR/SCE288	IMPVALL/H-E05140
First floor	Uncontrolled	0.0075	0.0024	0.0029	0.0173	0.0105
	Controlled	0.0028	0.0012	0.0020	0.0102	0.0046
Second floor	Uncontrolled	0.0100	0.0028	0.0040	0.0230	0.0140
	Controlled	0.0042	0.0018	0.0032	0.0144	0.0064
Third floor	Uncontrolled	0.0113	0.0028	0.0051	0.0272	0.0164
	Controlled	0.0053	0.0023	0.0047	0.0178	0.0078
Fourth floor	Uncontrolled	0.0125	0.0032	0.0058	0.0295	0.0175
	Controlled	0.0058	0.0029	0.0053	0.0198	0.0083

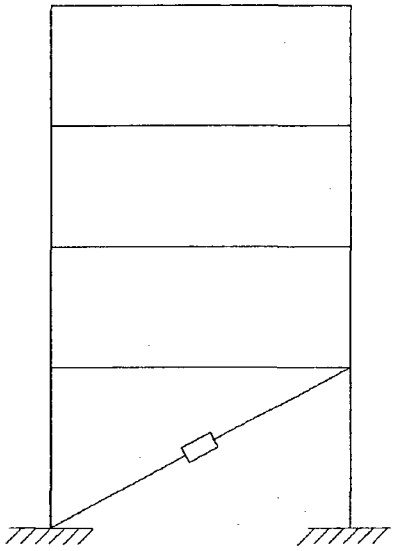

Figure 5.36: Case SD2Da (Model SD2D, MR damper SD-1000).

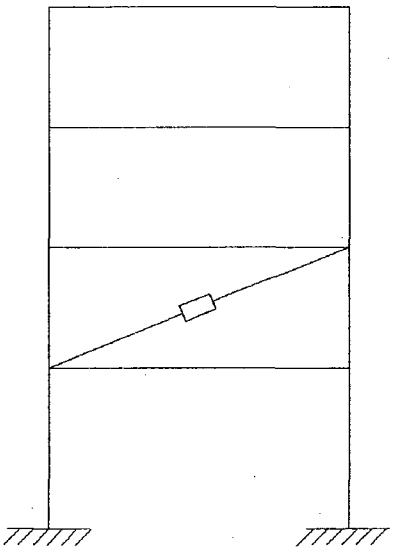

Figure 5.37: Case SD2Db (Model SD2D, MR damper SD-1000).

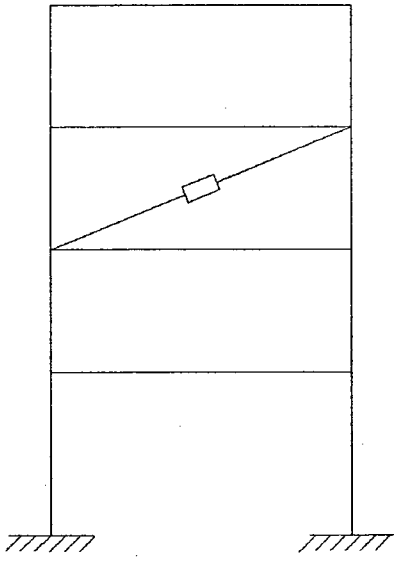

Figure 5.38: Case SD2Dc (Model SD2D, MR damper SD-1000).

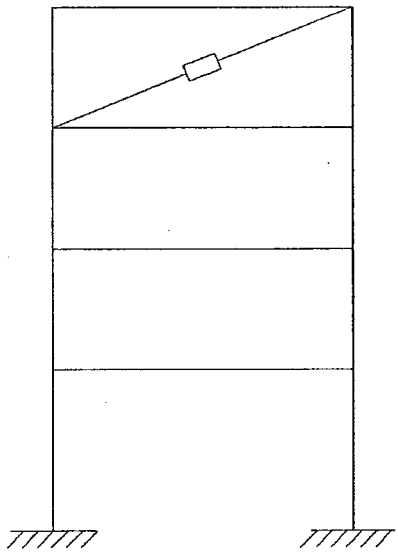

Figure 5.39: Case SD2Dd (Model SD2D, MR damper SD-1000).

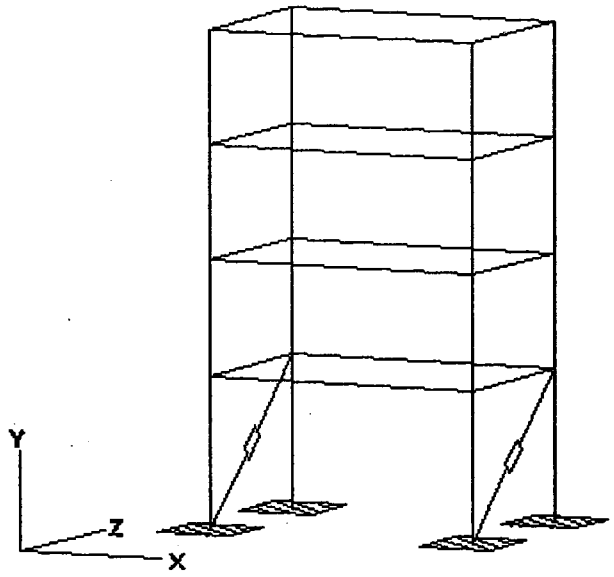

Figure 5.40: Case SD3Da (Model SD3D, MR damper SD-1000).

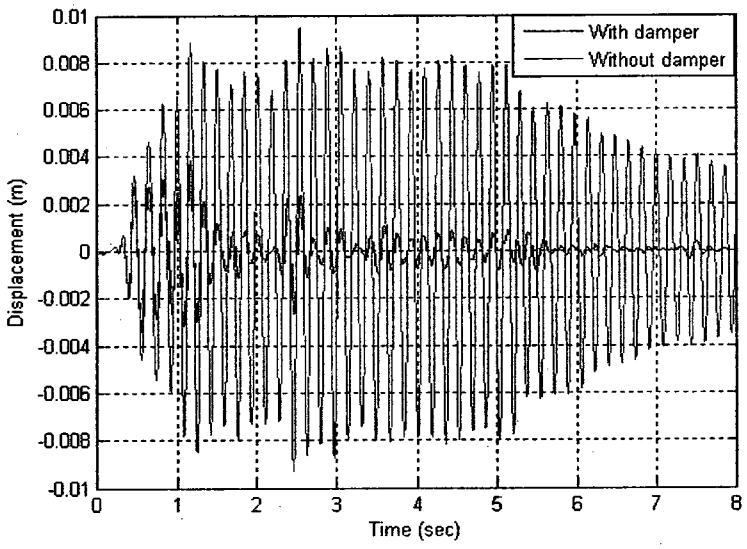

Figure 5.41: Uncontrolled and controlled fourth floor displacement (model SD2Da) under reproduced El-Centro earthquake record.

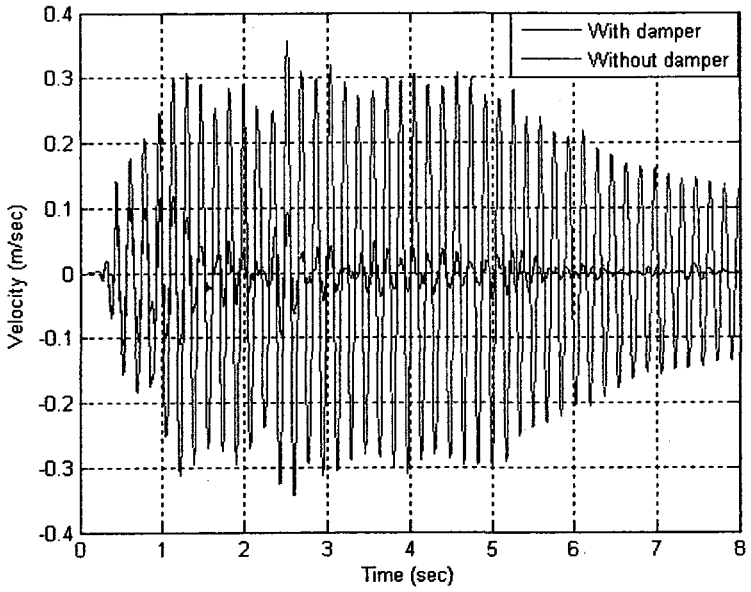

Figure 5.42: Uncontrolled and controlled fourth floor velocity (model SD2Da) under reproduced El-Centro earthquake record.

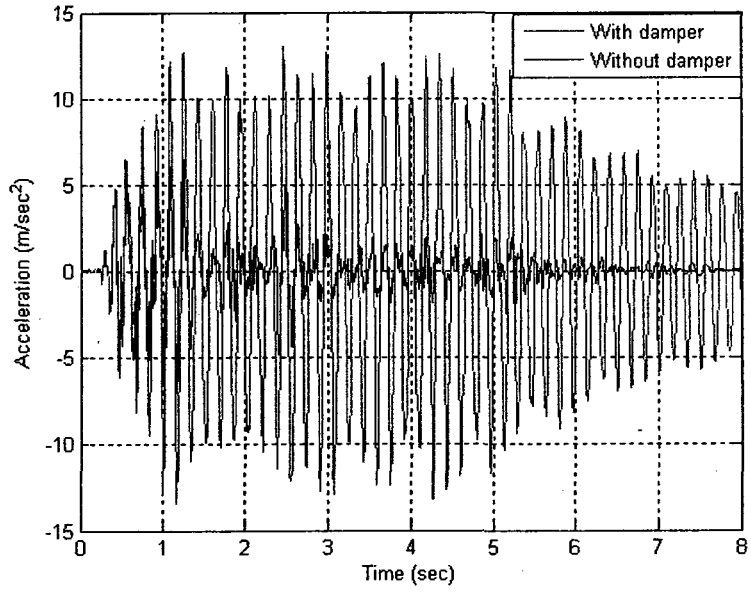

Figure 5.43: Uncontrolled and controlled fourth floor acceleration (model SD2Da) under reproduced El-Centro earthquake record.

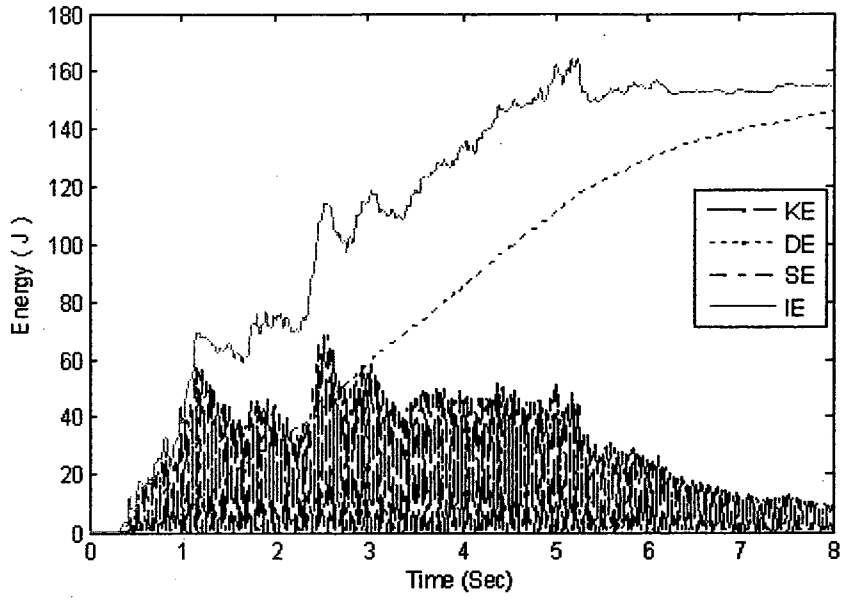

Figure 5.44: Energy time history of the uncontrolled structure (SD2D) under reproduced El-Centro earthquake record.

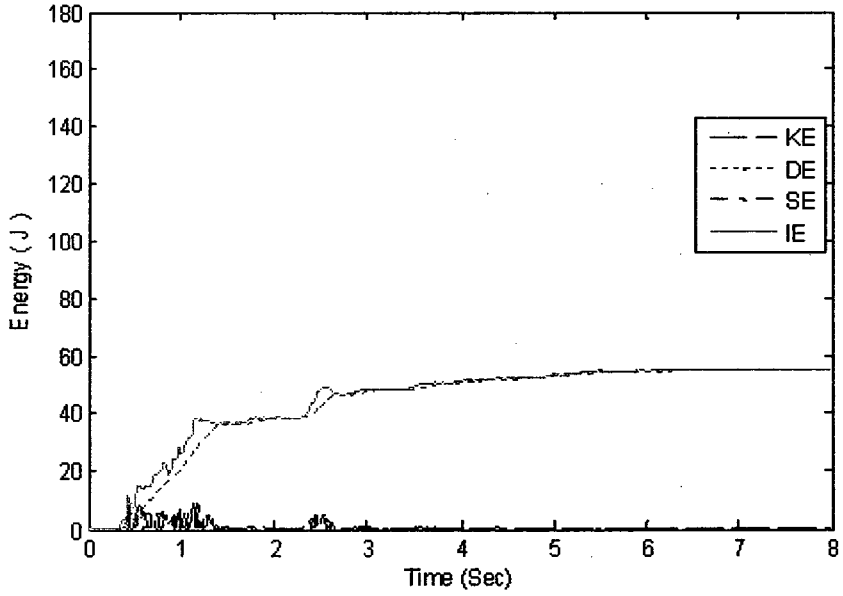

Figure 5.45: Energy history of the controlled structure (SD2Da) under reproduced El-Centro earthquake record.

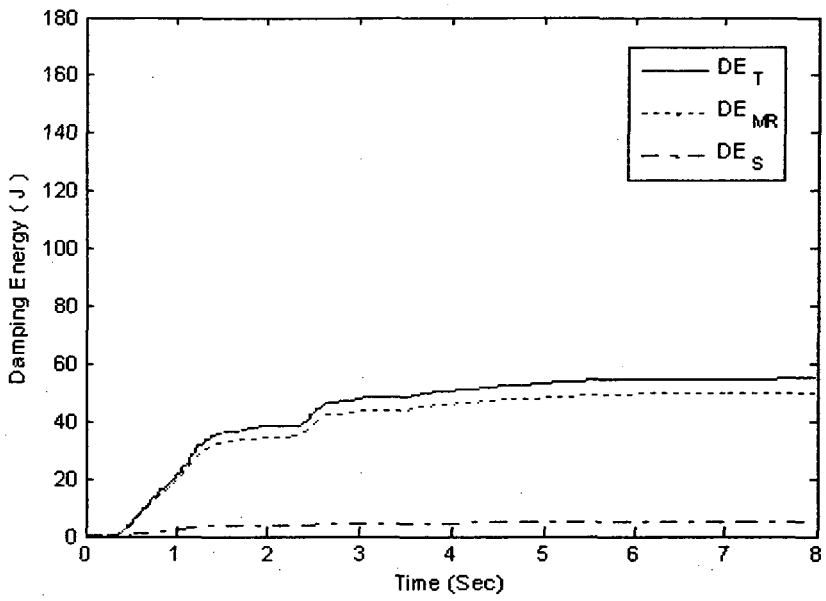

Figure 5.46: Damping energy history of the controlled structure (SD2Da) under reproduced El-Centro earthquake record.

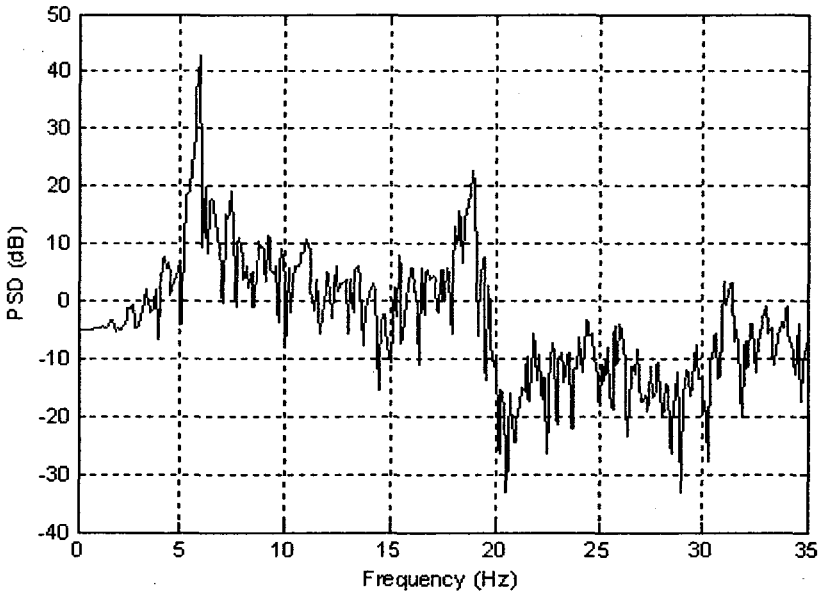

Figure 5.47: Power spectral density of the top floor accelerations of the uncontrolled structure (SD2D) under reproduced El-Centro earthquake record.

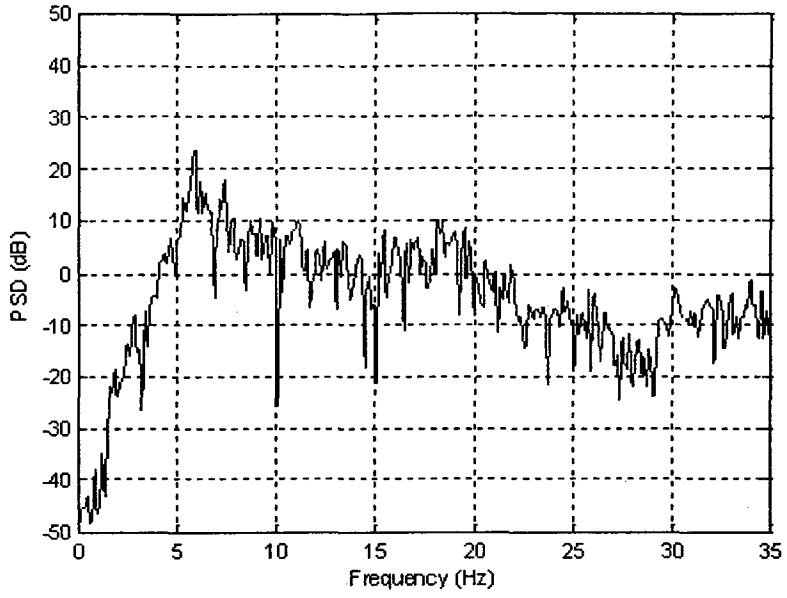

Figure 5.48: Power spectral density of the top floor accelerations of the controlled structure (SD2Da) under reproduced El-Centro earthquake record.

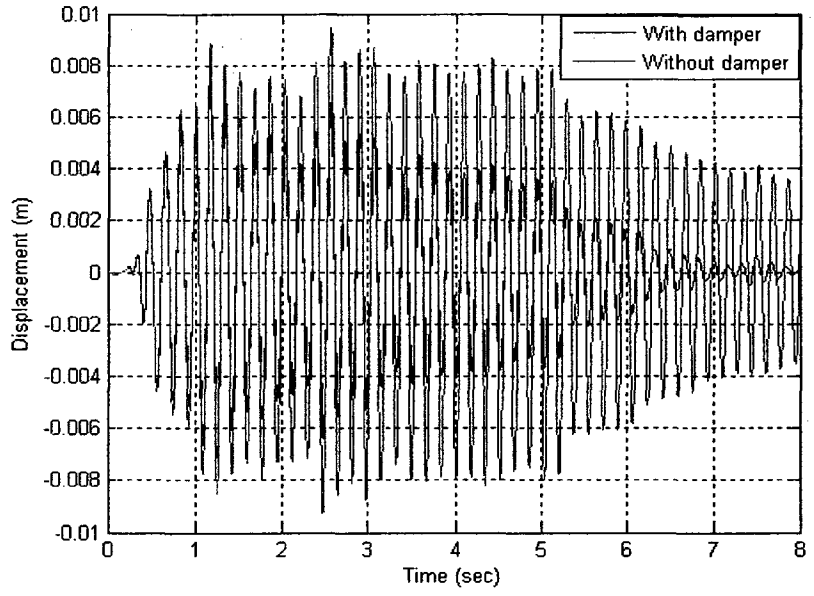

Figure 5.49: Uncontrolled and controlled (passive-off) fourth floor displacement under reproduced El-Centro earthquake (model SD2Da).

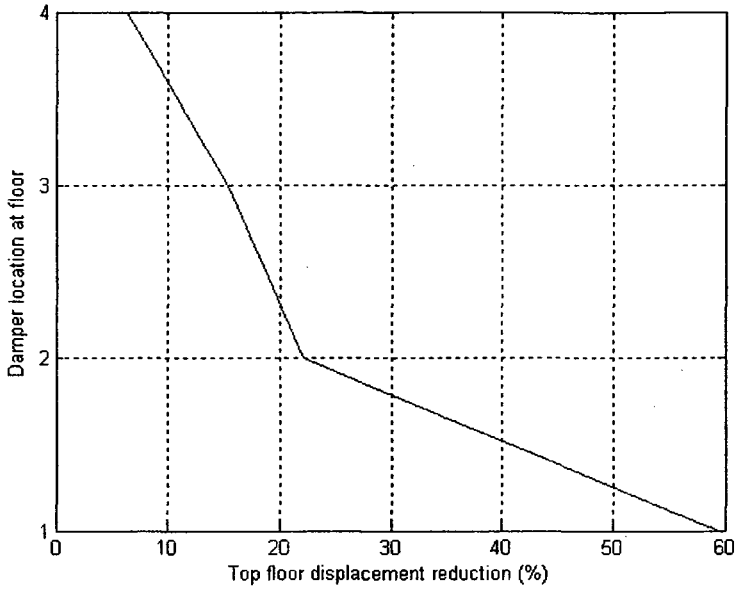

Figure 5.50: Fourth floor displacement reduction variation with damper location (model SD2D) under reproduced El-Centro earthquake record.

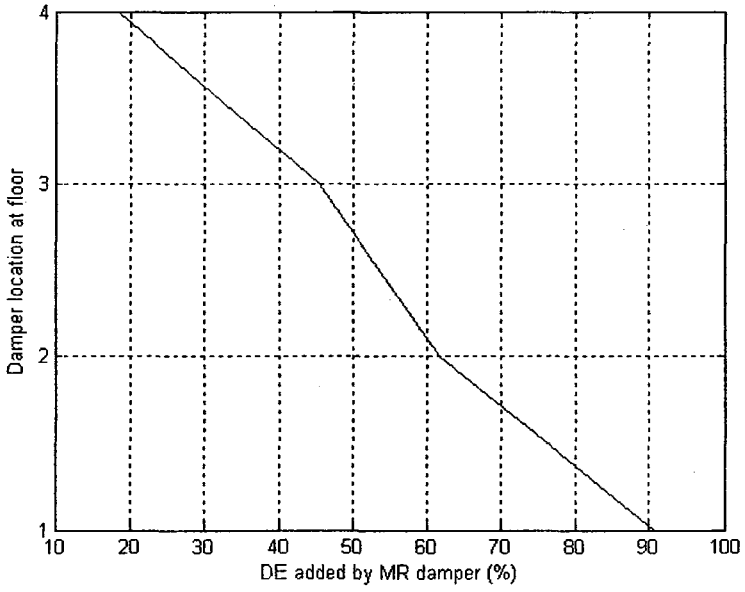

Figure 5.51: Contribution of damping energy by MR damper with damper location (model SD2D) under reproduced El-Centro earthquake record.

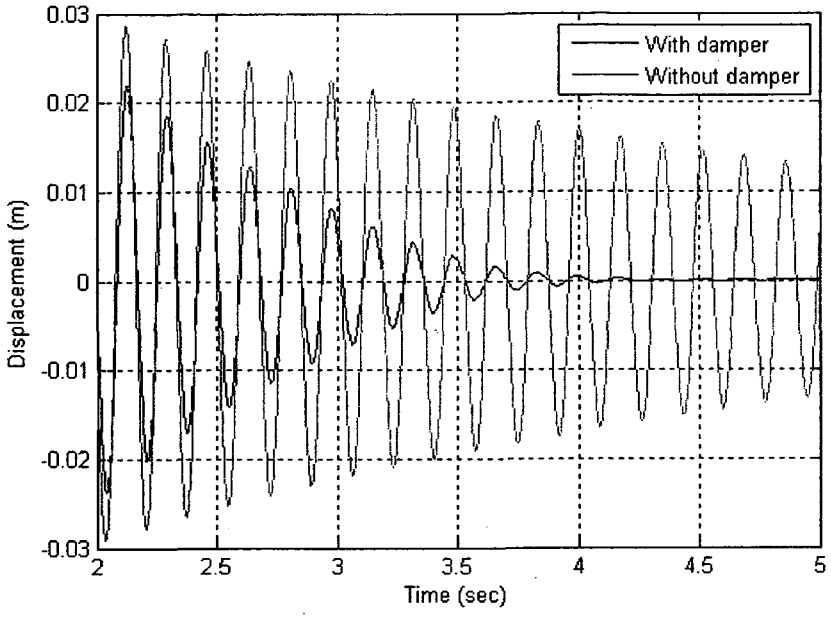

Figure 5.52: Fourth floor displacement (free vibration) of the uncontrolled and controlled structures (SD2D) when damper at ground floor.

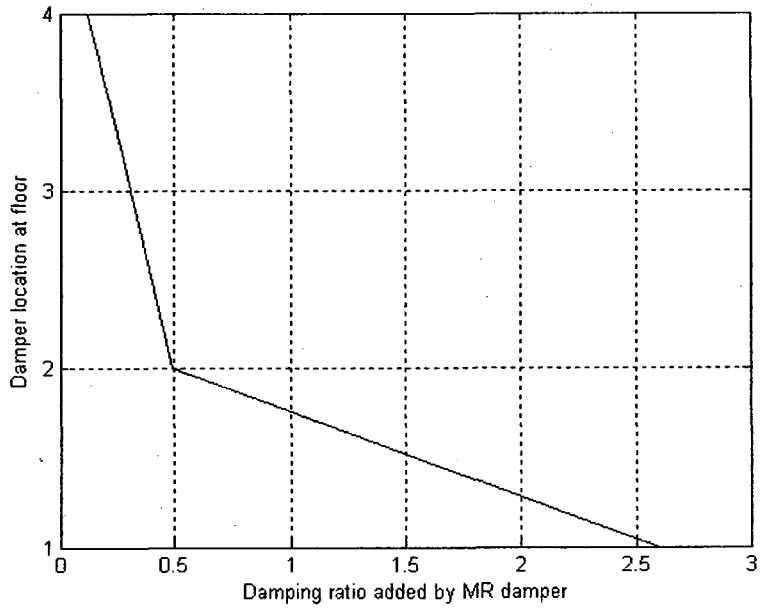

Figure 5.53: Contribution of damping ratio by MR damper with damper location (model SD2D) under reproduced El-Centro earthquake record.

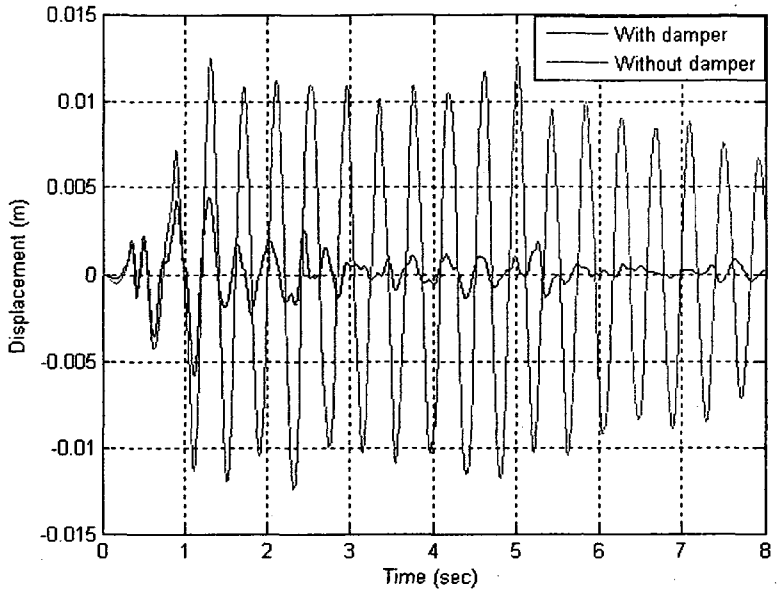

Figure 5.54: Fourth floor uncontrolled and controlled displacement of the structure (SD3D) under reproduced El-Centro (IMPVALL/I-ELC180) earthquake.

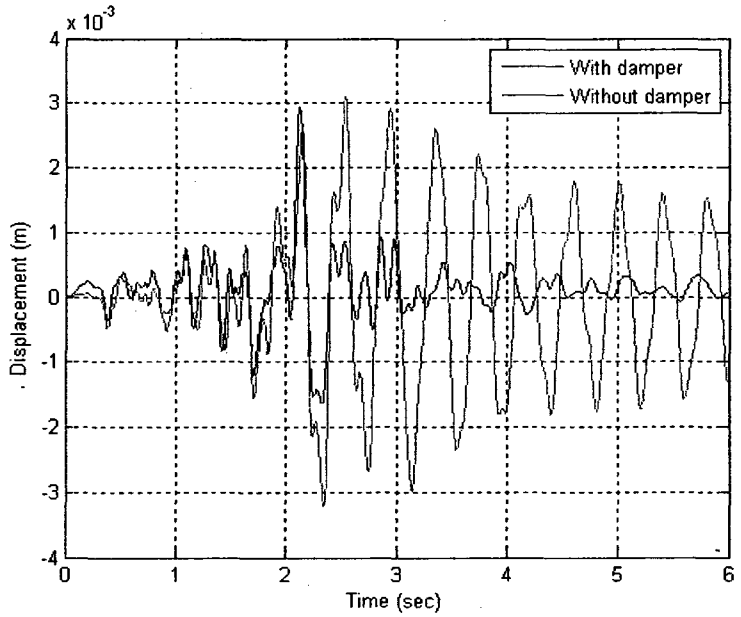

Figure 5.55: Fourth floor uncontrolled and controlled displacement of the structure (SD3D) under reproduced Mammoth Lake (MAMMOTH/I-LUL000) earthquake.

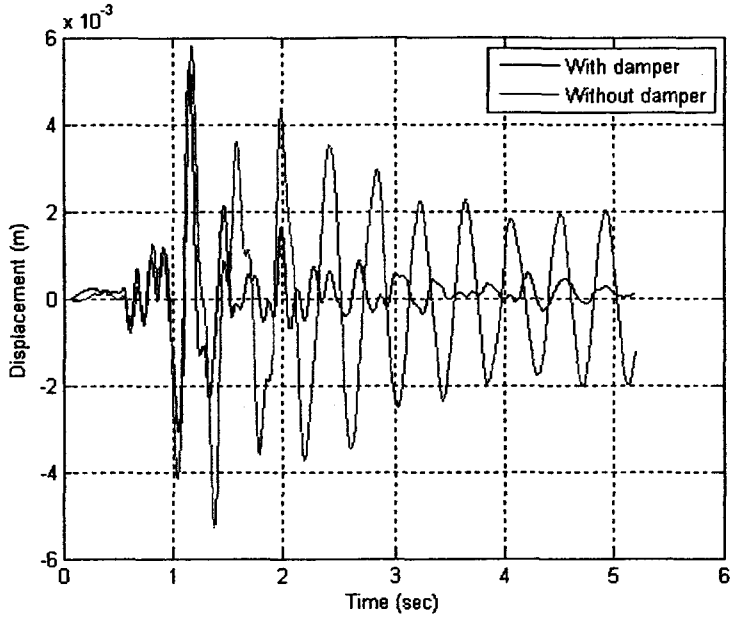

Figure 5.56: Fourth floor displacement under reproduced Mammoth Lake (MAMMOTH/L-LUL090) earthquake (model SD3D).

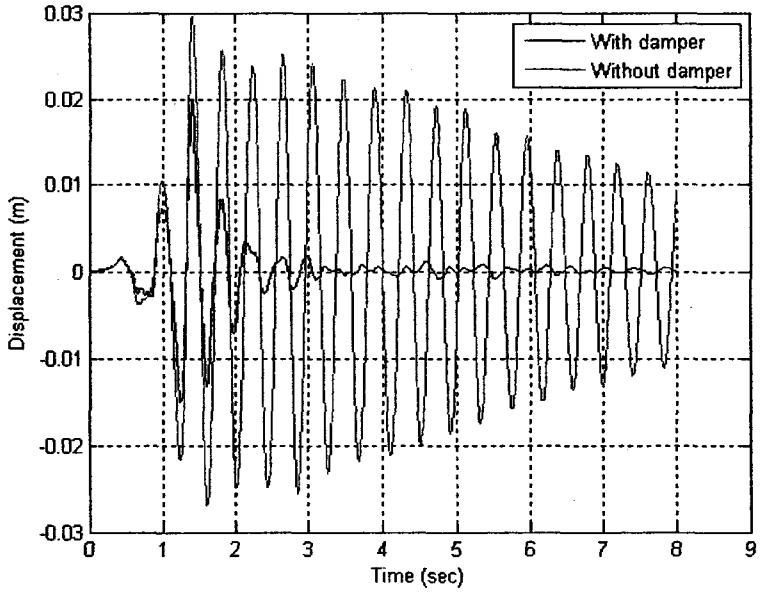

Figure 5.57: Fourth floor displacement under reproduced Northridge (NORTHR/SCE288) earthquake (model SD3D).

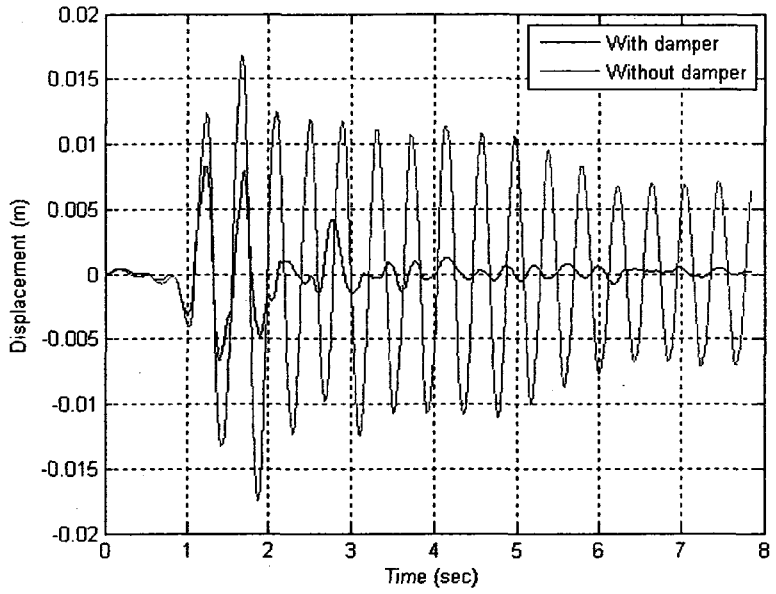

Figure 5.58: Fourth floor displacement under reproduced Imperial valley (IMPVALL/H-E05140) earthquake (model SD3D).

5.5 Performance evaluation of 200 kN MR damper (MRD-9000)

To evaluate the performance of MR damper MRD-9000 the damper is integrated into the model MRD2D and MRD3D in different cases with respect to damper location. Figure 5.59 to 5.63 shows the cases as MRD2Da, MRD2Db, MRD2Dc, MRD2Dd, MRD2De for model MRD2D and MRD3Da for model MRD3D. The damping ratio of 1 % is considered for all modes for model MRD2D and MRD3D. The structure is excited with the El-Centro earthquake record. The analysis is done using the State-Space method. The model MRD2D is analyzed first without considering MR damper and the top floor displacement, velocity and acceleration are found to be 0.2325 m, 1.679 m/sec and 13.73 m/sec^2 as given in Table 5.14.

Now MR damper MRD-9000 is integrated into the model MRD2D as case MRD2Da shown in Figure 5.59. The current supplied to the damper varies between 0 and 2A according to the control algorithm described in the Section 3.5. The structure is again excited with the same El-Centro earthquake record. The uncontrolled (without damper) and controlled (with damper) responses are summarized in Table 5.14. The fifth floor uncontrolled and controlled displacement, velocity and acceleration are also shown in Figures 5.65 to 5.67, respectively. It is observed that after integrating MR damper into the model MRD2D, the top floor displacement, velocity and acceleration reduced by 47.91%, 58.43% and 25.49%, respectively. It is also observed that because of damper, vibration of structure is damped out rapidly.

Figure 5.68 shows energy time history of the uncontrolled structures. It is observed that 322.4 kJ of maximum strain energy experienced by structure. Figure 5.69 shows the energy time history of the controlled structure. As it can be seen, the application of MR damper causes the strain energy demand to be reduced to 81.2 kJ and at the same time input energy is dissipated. Figure 5.70 shows damping energy time history. It is observed that the maximum damping energy is 315 kJ. Here structural damping energy contribution is only 49.89 kJ where as damping energy contribution by the MR damper is 265.1 kJ. Therefore it can be easily understand that MR damper could increase the damping property of structure significantly.

The power spectral density is of the top floor acceleration response of the uncontrolled and controlled structures are shown in Figures 5.71 and 5.72, respectively. From Figure

5.71, it is observed that the dominant frequency is 1.147 Hz in which PSD is 40.53 dB. From Figure 5.72, it is observed that with the application of MR damper the dominant frequency become 1.172 Hz and power is reduced to 23.54 dB. Therefore it can be noted here that with the application of MR damper, the frequency of the structure is not changed but the damping property of structure is increased significantly.

As a common event in a severe earthquake, a case of power failure to MR damper is considered by setting the damper in the passive mode (i.e. current set to zero). In this case MR damper MRD-9000 is integrated to the model MRD2D as shown in Figure 5.59, and the current to the damper is kept as 0A. Table 5.15 shows uncontrolled and controlled displacement, velocity and acceleration. The El-Centro earthquake record is used as excitation. From Table 5.15 it is observed that top floor displacement, velocity and acceleration is reduced by 40.77%, 46.27% and 35.18% respectively even when there is no power supplied to the damper. Figure 5.73 shows fifth floor uncontrolled and controlled displacement (passive-off).

5.5.1 Effective location for MR damper placement

To find the effective location for a MR damper, the structure considered here is a five story building frame as shown in Figure 5.5. There are five possible locations to place MR damper (on each floor). Therefore five cases are considered. For Case MRD2Da, the damper is placed at the ground floor level, for Case MRD2Db damper is placed at first floor, for Case MRD2Dc damper is placed at second floor, for Case MRD2Dd damper is placed at third floor and for Case MRD2De damper is placed at fourth floor. The

arrangements of damper placement for five cases are shown in Figure 5.59, 5.60, 5.61, 5.62 and 5.63. The current to the MR damper is used 0-2A according to the control algorithm as described in Section 3.5. El-Centro earthquake record is also used. Similarly, the effectiveness of MR damper placement is evaluated based on the following three criteria: response reduction, contribution to the damping energy and change in damping ratio due to MR damper.

Table 5.16 shows the floor displacement of the uncontrolled and controlled structures in comparison with the damper location. Figure 5.74 shows top floor displacement reduction variation with damper location. It is observed that the top floor maximum displacement is reduced by 47.91% when the damper is placed at the ground floor level. Therefore it can be concluded that ground floor is the best location for this structure.

Table 5.17 shows the damping energy contributed by MR damper with respect to the location of damper. Figure 5.70 shows damping energy time history when damper is located at ground floor. And Figure 5.75 shows the variation of damping energy added by MR damper with the damper location. It is observed that the maximum damping energy of 84.16% is added by MR damper when the damper is placed at the ground floor.

To evaluate the effect of the damper location on the damping ratio, the structure is excited with harmonic ground excitation of amplitude 0.05 m and frequency 1 Hz for five seconds, and then the structure is allowed to vibrate freely. MR damper is placed at ground floor. Fifth floor displacement response is shown in Figure 5.76. Damping ratio

is calculated by using Eq. 5.1 from fifth floor displacement response shown in Figure 5.76. This process is repeated by changing the damper location (floor to floor). Damping ratio without damper and with damper at different floor is summarized in Table 5.18. Variation of damping ratio added by MR damper with different location is also shown in Figure 5.77. It is observed that maximum damping ratio of 3.98% of critical damping is added by MR damper when damper placed at ground floor.

Effectiveness of damper location is evaluated considering above mentioned three criteria. It is clearly understood that the ground floor is the best location to place damper for the structure considered here.

5.5.2 Performance of MR damper (MRD-9000) under different earthquakes.

Here the performance of MR damper will be studied under different earthquakes. The model MRD3D is selected to integrate MR damper and the damper is placed at the ground floor (case MRD3Da) as shown in Figure 5.64. Only horizontal DOF is considered here. Ground excitation is applied in Z-direction. Analysis is performed by the State-Space method. Current to the MR damper is used 0-2A according to the control algorithm described in Section 3.5. Table 5.19 shows uncontrolled and controlled floor displacement under different earthquakes. Figure 5.78 to 5.82 shows controlled and uncontrolled fifth floor displacement. It is observed that with the use of damper it is possible to reduce the displacement of structure during earthquake which will subsequently reduce the demand of inelastic deformation of structure.

Table 5.14: Uncontrolled and controlled response comparison under El-Centro earthquake excitation (model MRD2D).

Floor		Displacement (m)	Velocity (m/sec)	Acceleration (m/sec^2)
First floor	Uncontrolled	0.1150	0.8803	7.57
	Controlled	0.0485	0.5700	7.31
Second floor	Uncontrolled	0.1581	1.1850	9.67
	Controlled	0.0710	0.7006	6.95
Third floor	Uncontrolled	0.1935	1.4150	10.66
	Controlled	0.0927	0.7309	6.72
Fourth floor	Uncontrolled	0.2190	1.5780	12.46
	Controlled	0.1107	0.6913	7.84
Fifth floor	Uncontrolled	0.2325	1.6790	13.73
	Controlled	0.1211	0.6979	10.23

Table 5.15: Uncontrolled and controlled (passive-off) response under El-Centro earthquake (damper MRD-9000, model MRD2D).

Floor		Displacement (m)	Velocity (m/sec)	Acceleration (m/sec^2)
First floor	Uncontrolled	0.1150	0.8803	7.57
	Controlled (passive-off)	0.0641	0.5547	5.70
Second floor	Uncontrolled	0.1581	1.1850	9.67
	Controlled (passive-off)	0.0900	0.7270	6.17
Third floor	Uncontrolled	0.1935	1.4150	10.66
	Controlled (passive-off)	0.1122	0.8448	6.59
Fourth floor	Uncontrolled	0.2190	1.5780	12.46
	Controlled (passive-off)	0.1287	0.9009	7.46
Fifth floor	Uncontrolled	0.2325	1.6790	13.73
	Controlled (passive-off)	0.1377	0.9021	8.90

Table 5.16: Uncontrolled and controlled floor displacement (m) with damper location (model MRD2D).

Floor	Uncontrolled	Damper location				
		Ground Floor	First floor	Second floor	Third floor	Fourth floor
First floor	0.115	0.0485	0.0880	0.0969	0.1009	0.1074
Second floor	0.1581	0.0710	0.1207	0.1319	0.1387	0.1470
Third floor	0.1935	0.0927	0.1491	0.1586	0.1690	0.1793
Fourth floor	0.219	0.1107	0.1707	0.1790	0.1881	0.2025
Fifth floor	0.2325	0.1211	0.1836	0.1891	0.1977	0.2120

Table 5.17: Comparison of damping energy contribution by MR damper with damper (model MRD2D).

Location of damper	Total DE (kJ)	Structural DE (kJ)	DE by MR damper (kJ)	% of DE by MR damper
Ground floor	315.00	49.89	265.10	84.16
First floor	542.90	223.40	319.50	58.85
Second floor	581.80	294.50	287.30	49.38
Third floor	608.90	384.10	224.80	36.92
Fourth floor	632.50	531.60	118.90	18.80

Table 5.18: Change in damping ratio with damper location (model MRD2D).

	Total Damping (% of critical damping)	Damping added by the MR damper (% of critical damping))	% Gain in damping due to MR damper
Without Damper	1.00	-	
Damper at ground floor	4.98	3.98	398
Damper at first floor	2.20	1.20	120
Damper at second floor	1.91	0.91	91
Damper at third floor	1.53	0.53	53
Damper at fourth floor	1.25	0.25	25

Table 5.19: Uncontrolled and controlled floor displacement (m) (Z-direction) under different earthquake (model MRD3D).

Floor		Earthquake record/component				
		IMPVALL/I-ELC180	MAMMOTH/I-LUL000	MAMMOTH/L-LUL090	NORTHR/SCE288	IMPVALL/H-E05140
First floor	Uncontrolled	0.0823	0.0471	0.1032	0.2552	0.1020
	Controlled	0.0445	0.0294	0.0613	0.1930	0.0548
Second floor	Uncontrolled	0.1094	0.0622	0.1378	0.3466	0.1408
	Controlled	0.0666	0.0465	0.0926	0.2629	0.0862
Third floor	Uncontrolled	0.1293	0.0710	0.1606	0.4186	0.1752
	Controlled	0.0811	0.0599	0.1155	0.3271	0.1098
Fourth floor	Uncontrolled	0.1461	0.0813	0.1731	0.4664	0.2052
	Controlled	0.0960	0.0681	0.1273	0.3731	0.1303
Fifth floor	Uncontrolled	0.1547	0.0869	0.1794	0.4893	0.2250
	Controlled	0.1250	0.0695	0.1355	0.3938	0.1461

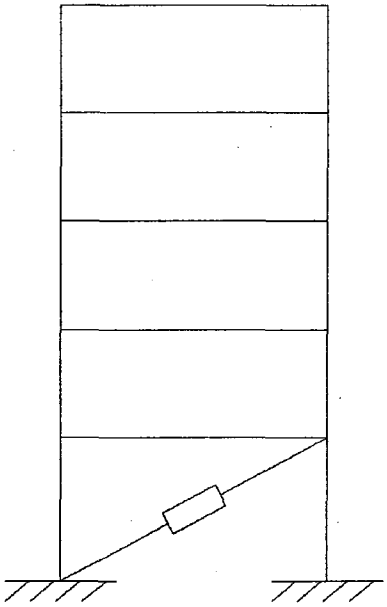

Figure 5.59: Case MRD2Da (Model MRD2D, MR damper MRD-9000).

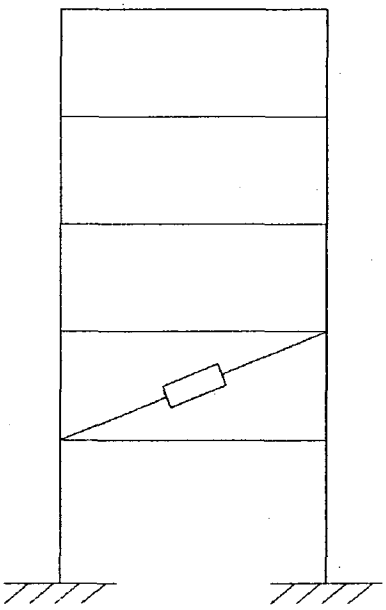

Figure 5.60: Case MRD2Db (Model MRD2D, MR damper MRD-9000).

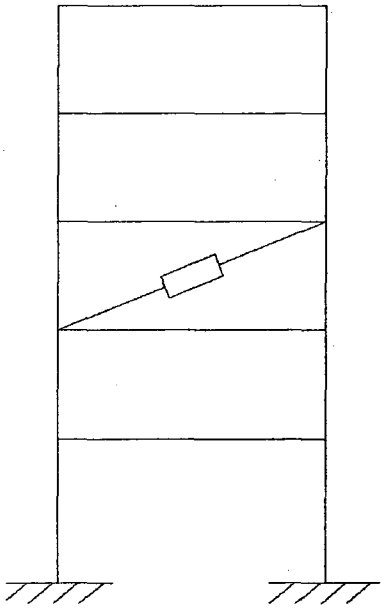

Figure 5.61: Case MRD2Dc (Model MRD2D, MR damper MRD-9000).

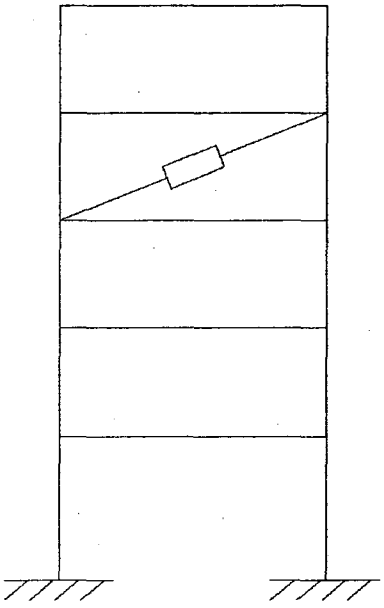

Figure 5.62: Case MRD2Dd (Model MRD2D, MR damper MRD-9000).

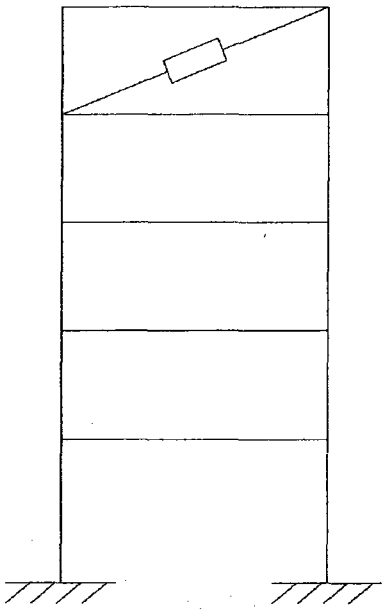

Figure 5.63: Case MRD2De (Model MRD2D, MR damper MRD-9000).

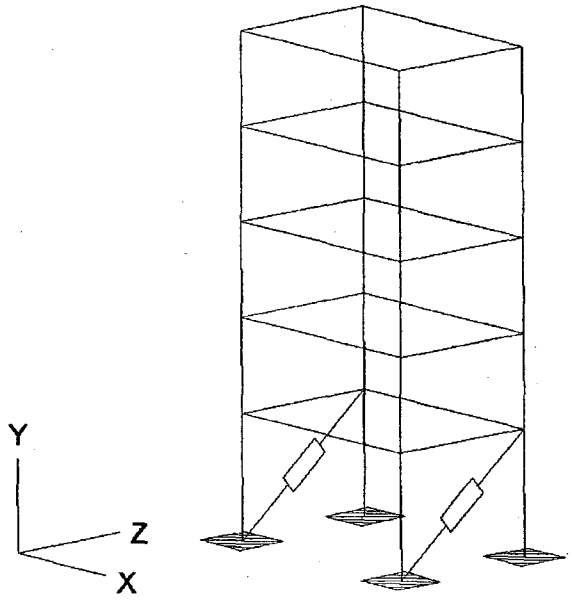

Figure 5.64: Case MRD3Da (Model MRD3D, MR damper MRD-9000).

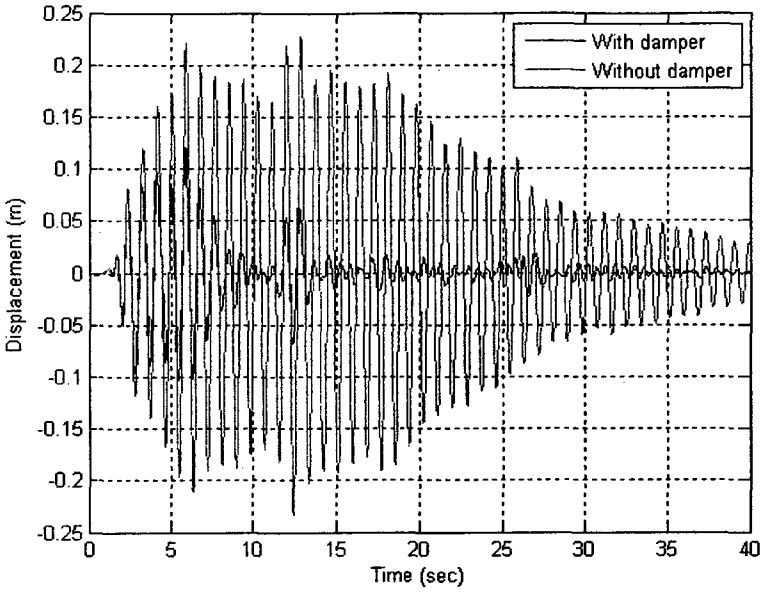

Figure 5.65: Uncontrolled and controlled fifth floor displacement of the structure (MRD2Da) under El-Centro earthquake.

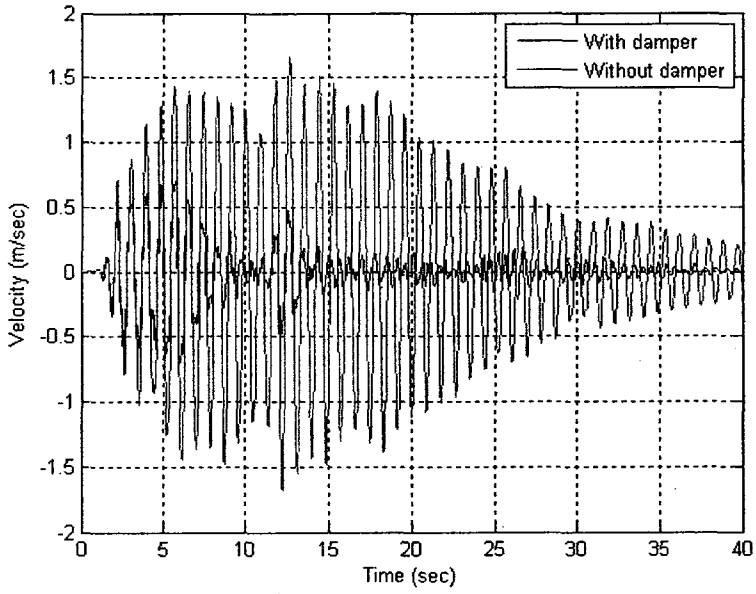

Figure 5.66: Uncontrolled and controlled fifth floor velocity of the structure (MRD2Da) under El-Centro earthquake.

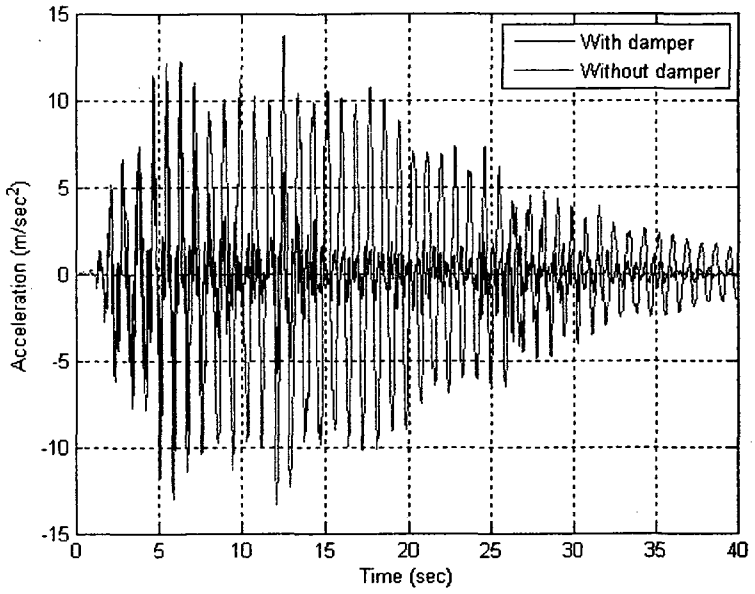

Figure 5.67: Uncontrolled and controlled fifth floor acceleration of the structure (MRD2Da) under El-Centro earthquake.

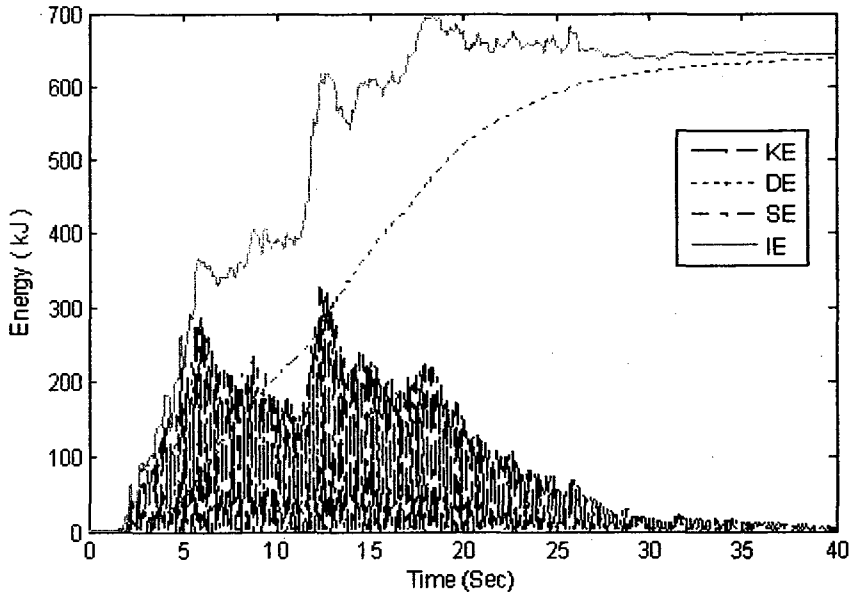

Figure 5.68: Energy history of the uncontrolled structure (MRD2D) under El-Centro earthquake record.

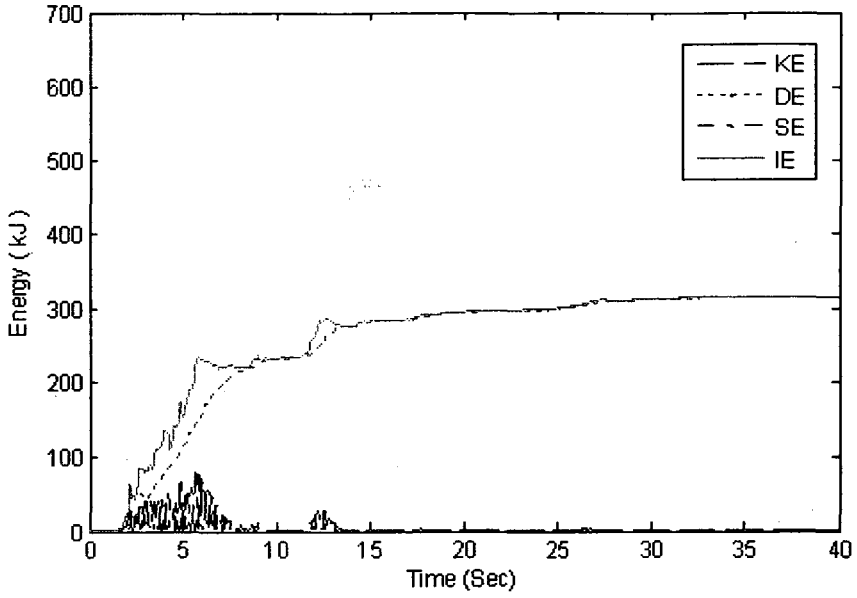

Figure 5.69: Energy history of the controlled structure (MRD2Da) under El-Centro earthquake record.

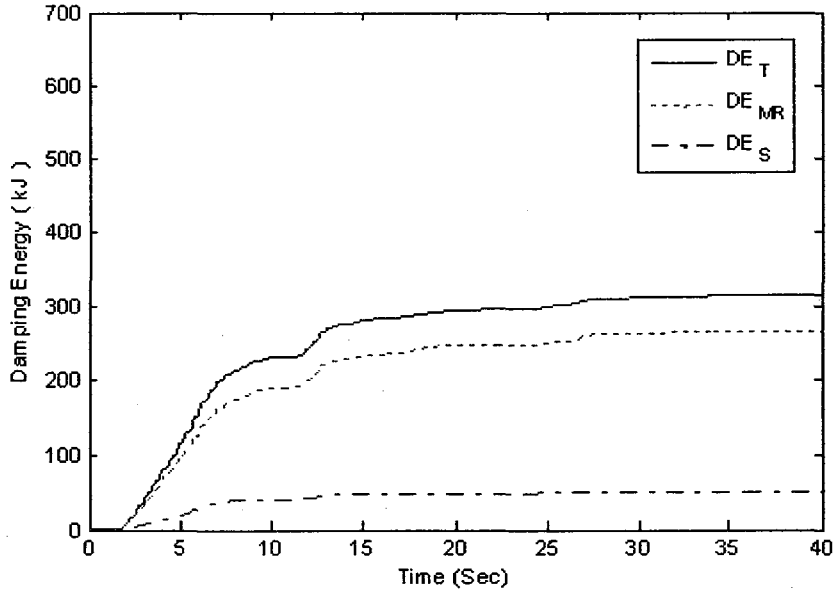

Figure 5.70: Damping energy history of the controlled structure (MRD2Da) under El-Centro earthquake record.

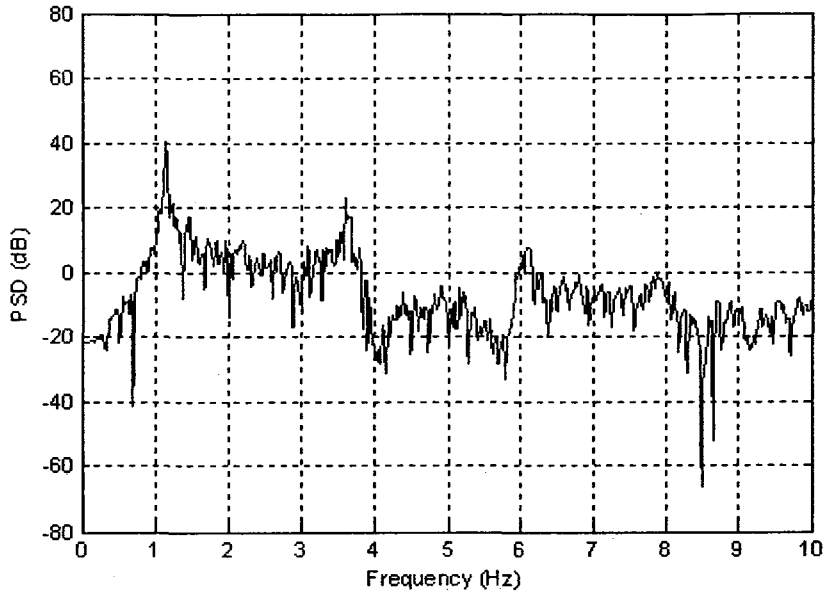

Figure 5.71: Power spectral density of the top floor acceleration of the uncontrolled structure (MRD2D) under El-Centro earthquake record.

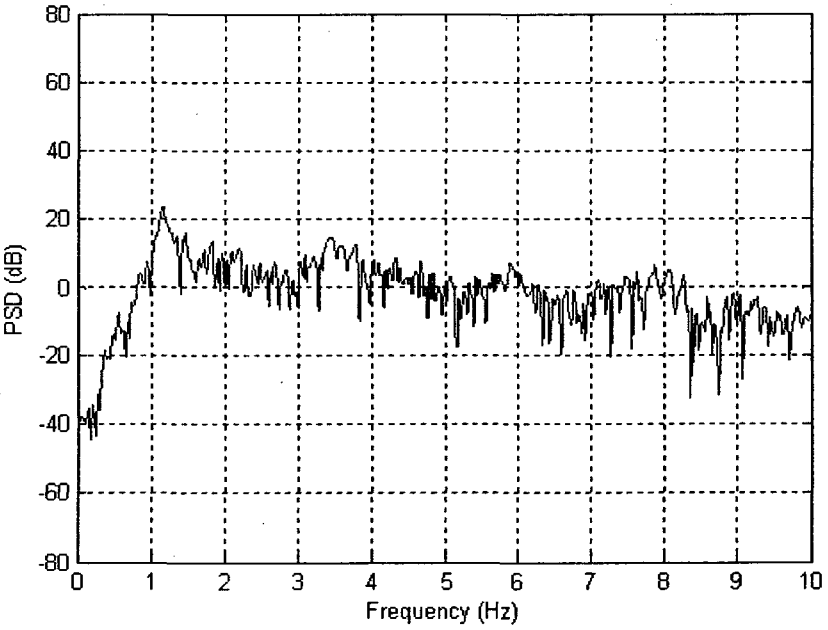

Figure 5.72: Power spectral density of the top floor acceleration of the controlled structure (MRD2Da) under El-Centro earthquake record.

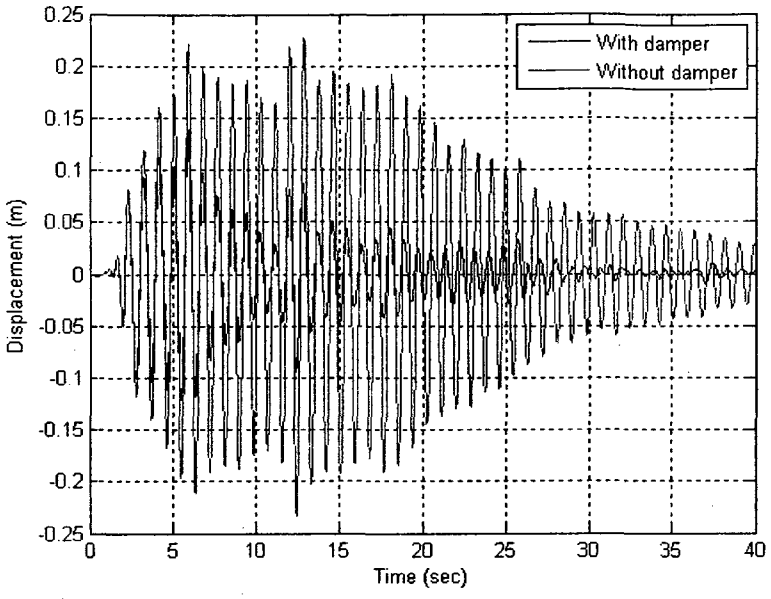

Figure 5.73: Uncontrolled and controlled fifth floor displacement under El-Centro earthquake (damper MRD-9000 with current 0A, case MRD2Da).

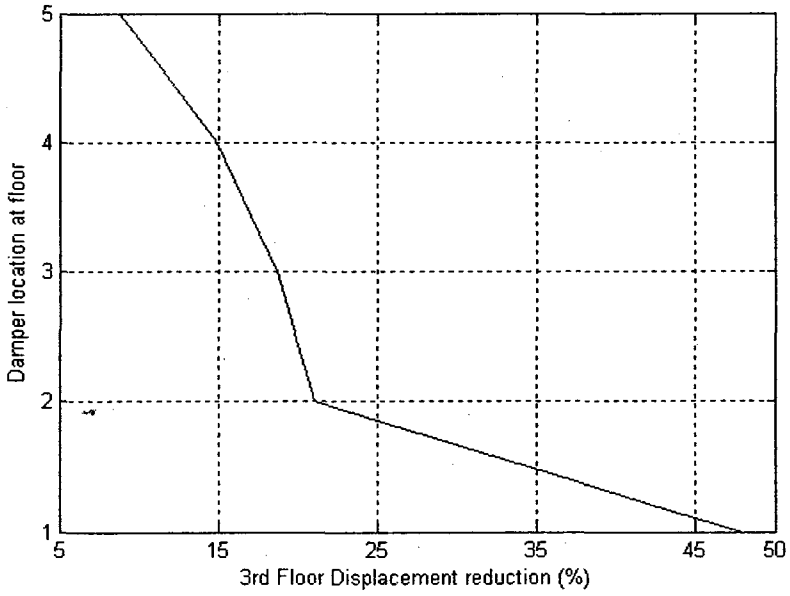

Figure 5.74: Fifth floor displacement reduction variation with damper location (model MRD2D).

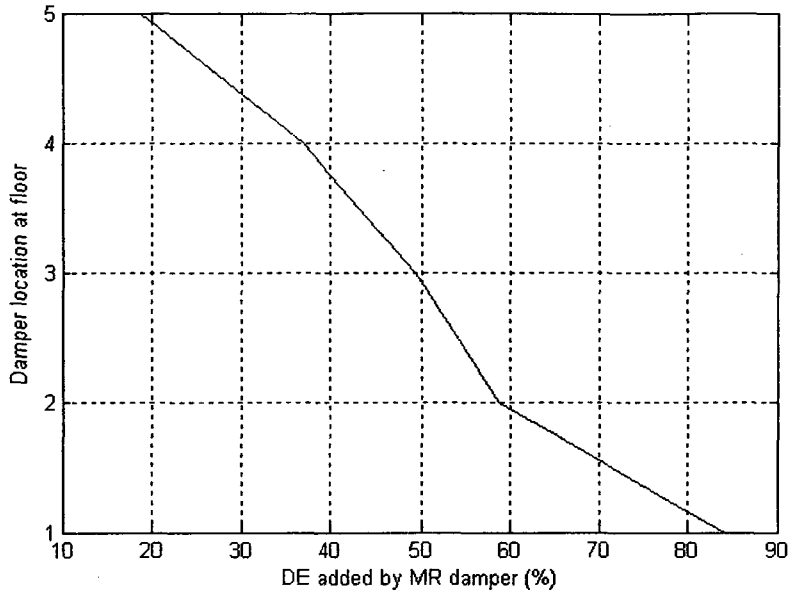

Figure 5.75: Contribution of damping energy by MR damper with damper location (model MRD2D).

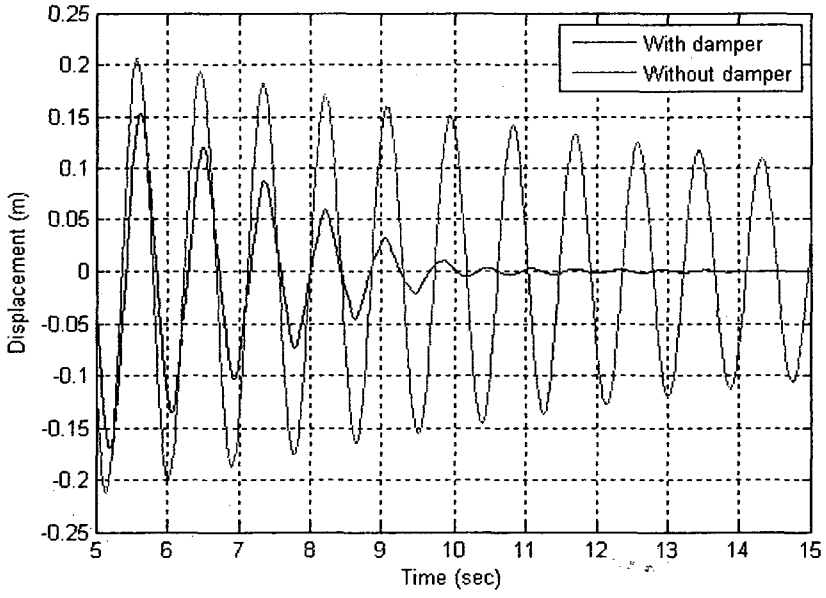

Figure 5.76: Uncontrolled and controlled fifth floor displacement (free vibration) when damper at ground floor (model MRD2Da).

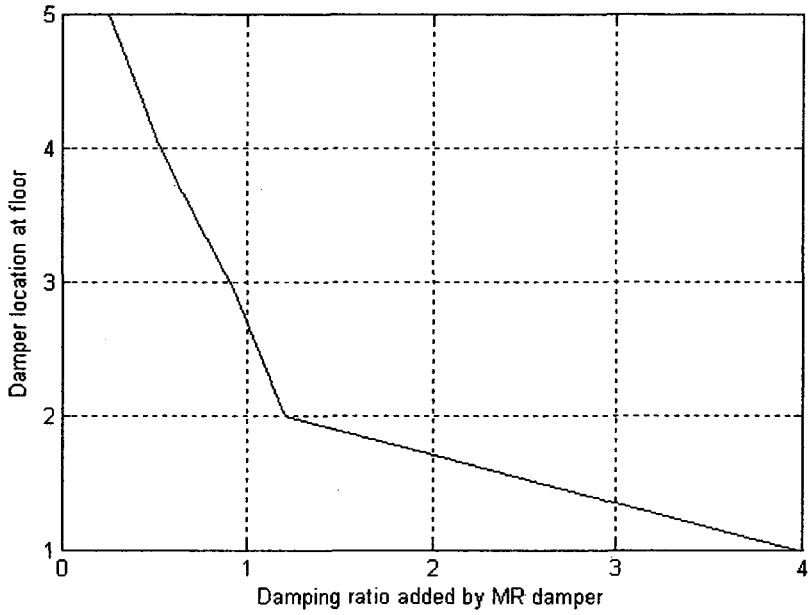

Figure 5.77: Contribution of damping ratio by MR damper with damper location (model MRD2Da).

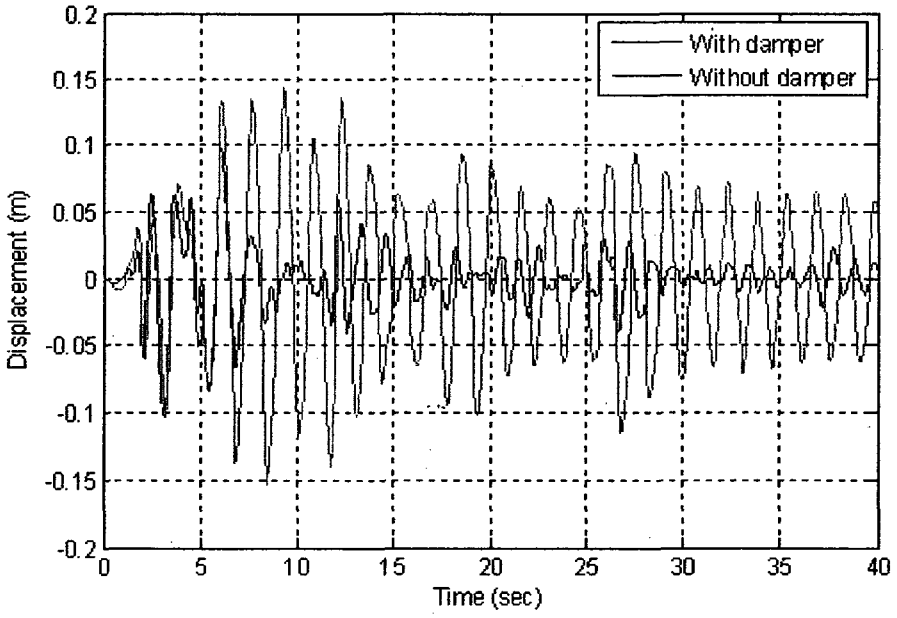

Figure 5.78: Fifth floor displacement of the uncontrolled and controlled structure (MRD3D) under El-Centro (IMPVALL/I-ELC180) earthquake.

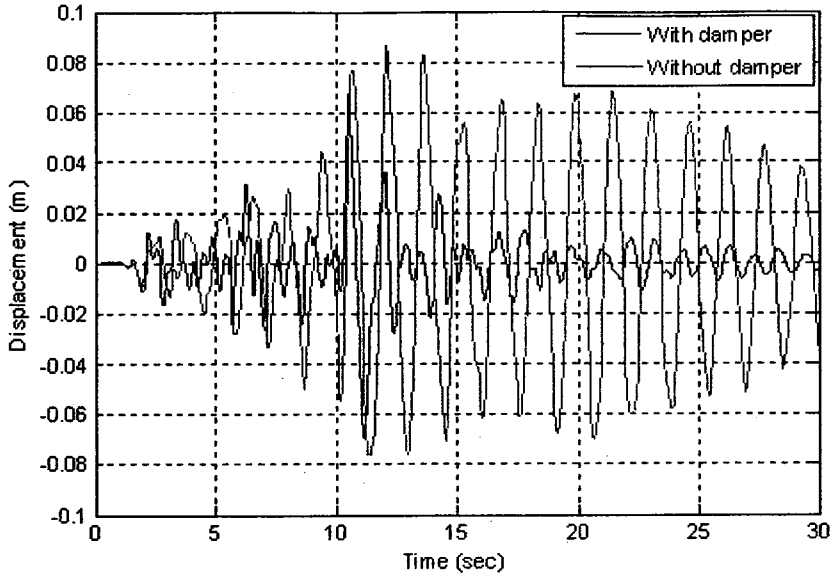

Figure 5.79: Fifth floor displacement of the uncontrolled and controlled structure (MRD3D) under Mammoth Lake (MAMMOTH/I-LUL000) earthquake.

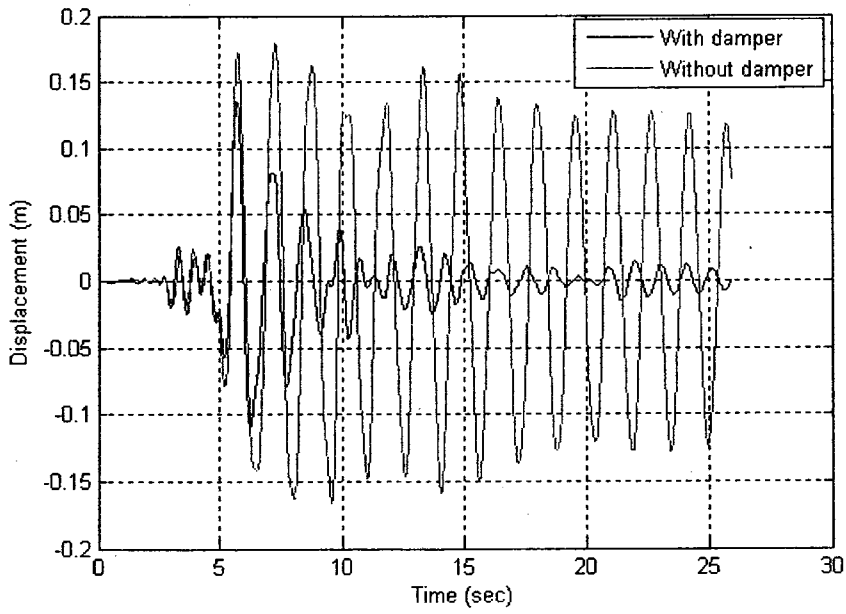

Figure 5.80: Fifth floor displacement of the uncontrolled and controlled structure (MRD3D) under Mammoth Lake (MAMMOTH/L-LUL090) earthquake.

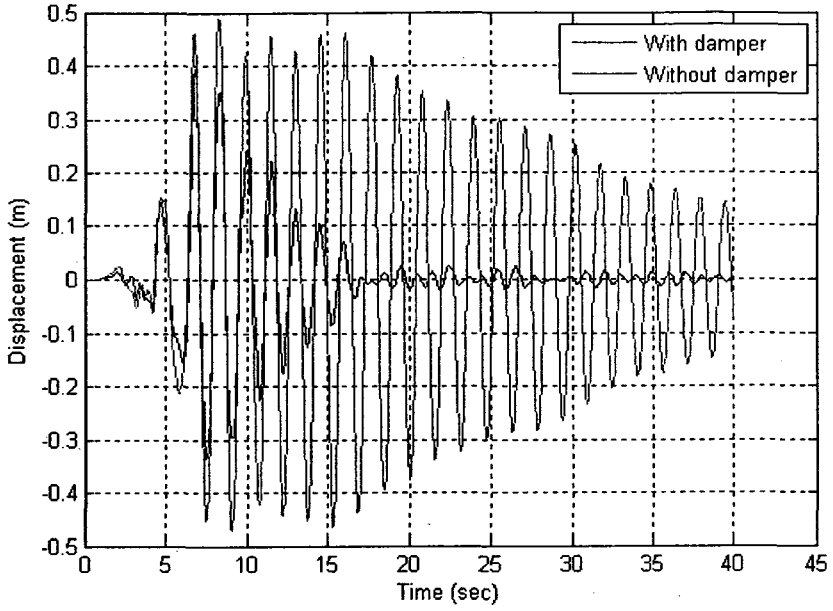

Figure 5.81: Fifth floor displacement of the uncontrolled and controlled structure (MRD3D) under Northridge (NORTHR/SCE288) earthquake.

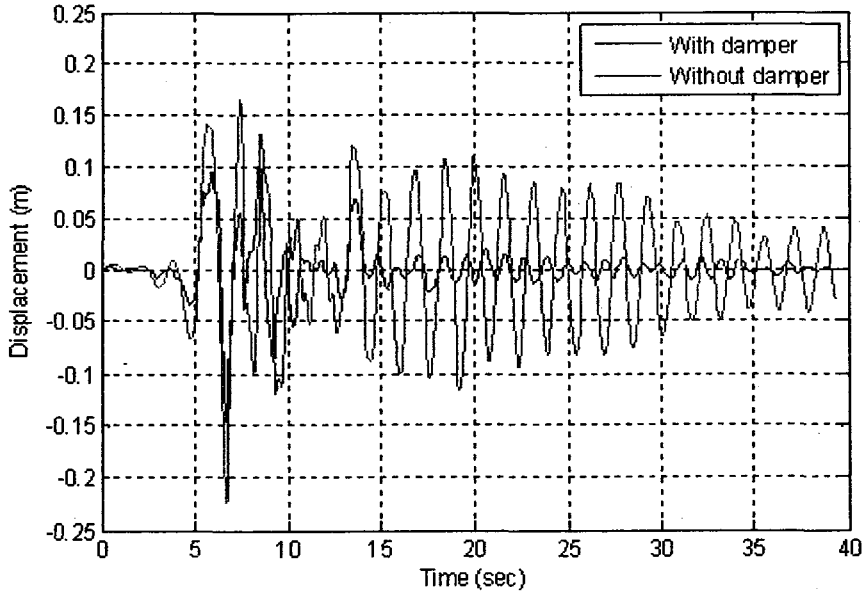

Figure 5.82: Fifth floor displacement of the uncontrolled and controlled structure (MRD3D) under Imperial valley (IMPVALL/H-E05140) earthquake.

CHAPTER 6
Summary and Conclusions

6.1 Summary

A semi-active control devices based on magneto-rheological fluids are currently being developed for a number of applications particularly for controlling the dynamic responses of structures. Because of its mechanical simplicity, low operating power requirements, robustness and failsafe characteristics it has becomes a promising device for wide ranges of applications ranges from automotive, aerospace structures to transportation infrastructures. Although, their use in automotive and aerospace structures is well known, but in Civil Engineering structures such as buildings and bridges is still in exploratory stages. In this research performance of three different MR damper RD-1005-3, SD-1000 and MRD-9000 to control vibration response of building structures under different earthquake excitations have been investigated.

MR damper RD1005-3 is modeled using finite element method and integrated into the structure as MR damper bar element and the governing differential equations of whole systems in finite element form is solved using Newmark's method. For MR damper SD1000 and MRD9000, the modeling has been accomplished by SIMULINK and integrated into the finite element model of structures. The system governing equations are then solved using State-Space method. Although SIMULINK model of dampers are

easier to construct than programming them into finite element system in MATLAB, they are computationally less efficient and more cumbersome as compared to the finite element systems.

At first MR damper RD-1005-3 is investigated in both 2D and 3D building structures (models RD2D and RD3D). To simulate the behaviour of this damper, a model bases on Bouc-Wen model is used which incorporates the current, frequency and amplitude of excitation. Performance of this damper is investigated through numerical simulations in which the MR damper is employed to control the dynamic response of a model of a two dimensional three-story building structure subjected to El Centro earthquake. The damper is connected between ground and first floor diagonally. It is observed that by application of MR damper, the peak displacement, velocity and acceleration of the third floor are reduced by 29.19%, 24.18% and 15.16%, respectively. It is also observed that the vibration of the structure is damped out rapidly, and the demand of strain energy absorbed by structure is reduced by 46.41%. The passive-off mode of the damper is also investigated in which no current is supplied to MR damper. This is important as during earthquake power supply may fail. In this case the peak displacement, velocity and acceleration of the third floor are reduced by 3.95%, 2.39% and 6.61%, respectively. This shows that MR damper behaves as a regular passive damper in the case of power failure thus demonstrate its fail safe features. A study is conducted to find the optimum location of damper placement. In this case, the performance of a damper is studied by connecting the damper in different possible locations. Different performance criteria such as response reduction, increase in damping ratio, and contribution to the damping energy by

MR damper are considered. It is found that the performance of the damper is highly sensitive to the location of damper placement and the ground floor is generally the best location to place MR damper. Finally the performance of damper is studied by employing the damper into the model of a three dimensional, three-story structure subjected to different earthquakes. It is found that the damper performed very well capable of reducing structural responses under different earthquake excitation.

Next performance of MR damper SD-1000 is evaluated by integrating it into the model of two dimensional four-story building structure (Model SD2D). The behaviour of the damper is characterized using Bouc-Wen model. The structure is analyzed under El Centro earthquake. It is found that by integrating MR damper SD-1000 to a building frame, it is possible to reduce the peak displacement, velocity and acceleration of the top floor by 59.54%, 64.7% and 47.72%, respectively. It is also found that the demand on strain energy absorbed by structure is reduced by 84.73%. It is interesting to note that the peak displacement, velocity and acceleration of the top floor are also reduced by 19.1%, 27.16% and 14.08%, respectively when there is no power supplied to the damper (passive-off mode). Optimum damper location is also found at the ground floor in this case. The damper performance is also investigated when it is integrated into the 3D building model (SD3D) under different earthquake excitations. It is shown that this damper was also able to reduce the vibration caused by different earthquake excitations effectively.

Finally the performance of a large scale MR damper, MRD-9000 of 200 kN capacity is evaluated by integrating the damper in a full scale model of two dimensional five story building frame (model MRD2D). The hysteresis behaviour of the damper is investigated using the modified Bouc-Wen model. The structure is analyzed under El Centro earthquake. It is found that the damper is capable to reduce the peak displacement, velocity and acceleration at the top floor by 47.91%, 58.43% and 25.49%, respectively. The demand on strain energy absorbed by structure is reduced by 74.81%. It is also found that the peak displacement, velocity and acceleration top floor are reduced by 40.77%, 46.27% and 35.18%, respectively even when there is no power supplied to the damper. Optimum damper location is also found to be at the ground floor in this case. The damper performance is also investigated under different earthquakes using the 3D model of the structure, MRD3D. It is demonstrated that this damper can also control the response under different earthquake excitations effectively.

6.2 Conclusions

It can be concluded that magneto-rheological damper have the ability to control the dynamic response of building structures during earthquake. Damper can be used as semi-active control device to protect and mitigate damaging effect during severe earthquake. MR damper increases the damping property of a structure adaptively without changing the natural frequencies of the structures, increases the energy dissipation capacity of the structure and reduces the demand of energy dissipation through the inelastic deformation during severe earthquake. It is shown that magneto-rheological damper is capable to provide some protection even if power system fails, which is a common case during an

earthquake event. Also it is found that the performance of damper is highly sensitive to the location of damper placement and optimum location is found at ground floor in all cases. It should be noted that the optimum location of damper before application of damper because, optimum location of damper in real structure depends on the type of structure such as asymmetry due to shape, stiffness etc.

6.3 Future work

1. In this work it is assumed that structure is in elastic state in all situations while the damper shows non-linearity. But in real cases structure may undergo inelastic state if the damping energy is not adequate. Therefore inelastic analysis is needed to evaluate the performance of magneto-rheological damper.

2. As observed, the behaviour of MR damper depends on the current, frequency and amplitude of excitation, therefore to model the MR damper SD-1000 and MRD-9000, these parameters should be included as input variables. Also modeling of the MR dampers are primarily based on tests conducted with harmonic excitations. Further experimental and analytical studies are needed for refining the existing models to account for random excitations.

3. Only a set of simple structure with respect to geometry is considered here, but in reality a structure may have asymmetry due to geometry or stiffness and mass distributions. Therefore to find the optimum location, asymmetry structure need to be considered in future studies.

4. Here some of the dampers are modelled using SIMULINK and integrated with a finite element system. To enhance the computational efficiency and flexibility, they should be directly modelled in a finite element system. However, further numerical and experimental studies are needed to construct such models.

5. In this research On/Off control strategy is considered which uses maximum or minimum current/voltage according to the control algorithm (depending on velocity and force of MR damper). Further study is needed to explore the control strategies, which able to use current/voltage between the maximum and minimum. Also the effect of power supply disturbance during earthquakes needs to be studied.

REFERENCES

1. Armenakas, A. E. (1991), "*Modern Structural Analysis*". McGraw-Hill Inc.

2. Bagchi, A; Humar, J and Noman, A. (2007), "Development of a finite element system for vibration based damage identification in structures", *Journal of Applied Sciences*, vol. 7, n.17, p. 2404-2416.

3. Carlson, J. D., and Spencer Jr., B. F. (1996). "Magneto-Rheological Fluid Dampers for Semi-Active Seismic Control." *3rd International Conference on Motion and Vibration Control*, Chiba, Japan, p. 35-40.

4. Carlson, J. D. and Weiss, K. D. (1994). "A Growing Attraction to Magnetic Fluids," *Machine Design*, vol. 66. no. 15. p. 61-64.

5. Carlson, J. D. and Spencer Jr., B. F. (1996a). " Magneto-rheological fluid dampers: scalability and design issues for application to dynamic hazard mitigation." *Proc. 2nd Workshop on Structural Control: Next Generation of Intelligent Structures.* Hong Kong, China, p. 99-109.

6. Carlson, J. D. (2002). "What Makes a Good MR Fluid?" *Journal of Intelligent Material Systems and Structures*, vol. 13, p. 431-435.

7. Carlson, J. D. (1999). "Low-Cost MR Fluid Sponge Devices." *Journal of Intelligent Material Systems and Structures*, vol. 10, p. 589-594.

8. Chopra, A. K., (2007), *Dynamics of Structures: Theory and Applications to Earthquake Engineering*. Third Edition, Prentice Hall, Upper Saddle River, NJ, 07458.

9. Chu, S. Y., Soong, T. T., and Reinhorn, A. M. (2005). "*Active, Hybrid and Semi-active Structural Control.*" John Wiley & Sons Ltd.

10. Dominguez, A., Sedaghati, R. and Stiharu, I. (2007), "Modeling and application of MR dampers in semi-adaptive structures." *Journal of Computers and Structures*, (Atricle in press).

11. Dominguez, A., Sedaghati, R. and Stiharu, I. (2006), "A new dynamic hysteresis model for the magnetorheological dampers." *Smart Mater Struct*, 15(5): 1179-118.

12. Dominguez, A., Sedaghati, R. and Stiharu, I. (2004), "Modeling the hysteresis phenomenon of magnetorheological dampers." *Smart Mater Struct*, 13: 1351-1361.

13. Dominguez, A. (2004), "Design Optimization and Vibration Control of Adaptive Structures". *Ph. D Thesis*, Concordia University, Montreal, Canada.

14. Dyke, S. J.; Spencer Jr., B. F.; Sain, M. K. and Carlson, J. D. (1996). "Modeling and control of Magnetorheological dampers for seismic response reduction." *Smart Mat. and Struct.*, 5: 565-575.

15. Dyke, S. J., Spencer Jr., B. F., Sain, M. K., and Carlson, J. D. (1996a). "Seismic response reduction using magnetorheological dampers." *Proc., IFAC World Cong.*, Vol. L, Int. Fed. Of Automatic Control, 145-150.

16. Dyke, S. J., and Spencer Jr., B. F. (1996). "Seismic Response Control Using Multiple MR Dampers." *2nd International Workshop on Structural Control*, Hong Kong, Japan, 163-173.

17. Dyke S. J. (1996). "Acceleration feedback control strategies for active and semi-active systems: modeling, algorithm development and experimental verification". *Ph. D Dissertation* Department of Civil Engineering and Geological Sciences, University of Notre Dame, Notre Dame, IN.

18. Dyke, S. J., Spencer Jr, B. F., Sain, M. K., and Carlson, J. D. (1996b)."Experimental Verification of Semi-Active Structural Control Strategies Using Acceleration Feedback." *Third International Conference on Motion and Vibration Control*, Chiba, Japan, 291-296.

19. Ehrgott, R. and Masri, S. F. (1992). "Modeling the oscillatory dynamic behaviour of electrorheological materials in shear." *Smart materials and Structures*, 1:275-285.

20. El-Aouar, W. H., (2002). "Finite Element Analysis Based Modeling of Magneto Rheological Dampers, *M. S. Thesis*, Virginia Polytechnic Institute and State University, Virginia.

21. Filiatrault, A. (2002). "*Elements of Earthquake Engineering and Structural Dynamics*". Ecole Polytechnique, Montreal, Canada.

22. Foo S., Naumoski N., Saatcioglu M., (2001), "*Seismic Hazard, Building Codes and Mitigation Options for Canadian Buildings*", Office of Critical Infrastructure Protection and Emergency Preparedness, 2nd Floor, Jackson Bldg. Ottawa, ON K1A 0W6, Canada.

23. Fujino, Y., Soong, T. T. and Spencer Jr., B. F. (1996). Structural Control: Basic Concepts and Applications. *Proc., ASCE Struct. Cong.* XIV, p. 1277-1287.

24. Gamota, D. R. and Filisko, F. E. (1991). "Dynamic Mechanical Studies of Electrorheological Materials: Moderate Frequencies." *Journal of Rheology*, vol. 35, p. 399-425.

25. Goncalves, F. D., Koo, J, and Ahmadian, M. (2006). "A review of the state of the art in Magnetorheological Fluid Technologies – Part I: MR fluid and MR fluid models." *The Shock and Vibration Digest*, vol. 38, No. 3, 203-219.

26. Hasselman, T. K. (1972). " Amethod of constructing a full modal damping matrix from experimental measurement.". *AIAA Journal*, 10:552-557.

27. Herschel, W. H., and Bulkley, R. (1926). "Model for time dependent behavior of fluids." *Proc. American Society of testing Materials*, 26, 621.

28. Housner, G. W.; Bergman, L. A.; Caughey, T. K.; Chassiakos, A. G.; Claus, R. O.; Masri, S. F.; Skelton, R. E.; Soong, T. T.,; Spencer, B. F.; and Yao, J. T. P. (1997). "Structural Control: Past, Present, and Future." *Journal of Engineering Mechanics*, vol. 123, no. 9, pp. 897-971.

29. Ivers, D. E. and Miller, L. R., (1989), "Experimental comparison of passive, semi-active on/off, and semi-active continuous suspensions", *SAE technical Paper Series No 892484.*

30. Iqbal, F.; Bagchi, A.; and Sedaghati, R. (2008). "Application of Magneto-Rheological dampers to control the dynamic response of buildings". *Cansmart 2008, International Workshop, Smart materials and Structures*, October 23-24, 2008, Montreal, Quebec, Canada. p. 69-78.

31. Iqbal, F.; Bagchi, A.; and Sedaghati, R. (2009). "Dynamic Response Control of Building Using Magneto-Rheological Damper". *CSCE Annual Conference, Canadian Society for Civil Engineering*, May 27-30, 2009, Paper ID - GC - 159.

32. Jansen, L. M., and Dyke, S. J. (2000). "Semi-active control strategies for MR Dampers: A comparative Study." *Journal of Engineering Mechanics*, 126(8), 795-803.

33. Jolly, M. R., Bender, J. W. and Carlson, J. D., (1999). "Properties and Application of Commercial Magnetorheological Fluids." *J. of Intelligent Material Systems and Structures*, vol. 10, No. 1, p. 5-13.

34. Karla, A. V. (2004). "Effects of MR Damper Placement on Structure Vibration Parameters". http://mase.wustl.edu/wusceel/reujat/2004/villarreal.pdf

35. Lord Corporation (2009), www.lord.com.

36. Lu, L. Y., Chung, L. L., Wu, L. Y. and Lin, G. L. (2006). "Dynamic analysis of structures with friction devices using discrete-time state-space formulation". *Computer and Structures*, 84: 1049-1071.

37. Lu, L. Y., Lin, G. L. and Lin, C. H. (2006). "A Unified Analysis Model for Energy Dissipation Devices Used in Seismic Structures". *Computer-Aided Civil and Infrastructure Engineering*, 24: 41-61.

38. Malankar, K. (2001). "Finite Element Based Modeling of Magnetorheological Dampers." *M. S. Thesis*, Shivaji University, Kolhapur, India.

39. MATLAB (2007). The Math Works, Inc. Natic, Massachusetts.

40. Molyet, K. E. (2005), "Smart Rheological Fluids in Motion Control Applications." *Ph. D thesis*, The University of Toledo.

41. Natural Resources Canada (NRCAN), "Earthquakes Canada – East", http://seismo.nrcan.gc.ca/major_eq/majoreq_e.php (Updated on August 2006).

42. Newmark, N. M. (1959). "A method of computation for structural dunamics." *Proc. A.S.C.E.*, 8:67-94.

43. Onoda, J., Ung, H. O. and Minesugi, K. (1997). "Semi-active vibration suppression of truss structures by electro-rheological fluid." *46th International Astronautical Congress*, October 2-6, Oslo, 40(11);771-779.

44. PEER, (2009). Pacific Earthquake Engineering Research Center: NGA Database, http://peer.berkeley.edu/smcat/

45. Phillips, R. W. (1969). "Engineering applications of fluids with a variable yield stress." *Ph. D Thesis*, University of California, Berkeley, California.

46. Pilkey, D. F. (1998). "Computation of Damping Matrix for Finite Element Model *Updating*". *Ph. D Tesis*, Virginia Polytechnic Institute and State University, U.S.A.

47. Qu, W. L. and Xu, Y. L. (2001). "Semi-active control of seismic response of tall buildings with podium structure using ER/MR dampers" *Struct. Design Tall Build.*, 10(3), 179-192.

48. Rao, S. S. (1999). *The Finite Element Method in Engineering*, Butterworth-Heinemann.

49. Shames, I. H., and Cozzarelli, F. A. (1992). "*Elastic and Inelastic Stress Analysis*." Prentice-Hall, Englewood Cliffs, New Jersey.

50. SIMULINK (2007). The Math Works, Inc. Natic, Massachusetts.

51. Soong, T. T., (1990). "*Active Structural Control: Theory and Practice*" (Harlow: Longman Scientific and Technical).

52. Soong, T. T., and Dargush, G. F. (1997). "*Passive Energy Dissipation Systems in Structural Engineering.*" John Wiley & Sons Ltd.

53. Soong, T. T., and Spencer, B. F. (2002). "Supplemental energy dissipation: state-of-the-art and state-of-the-practice". *Journal of Engineering Structures*, vol. 24, p. 243-259.

54. Spencer, B. F., (2003). "State of the Art of Structural Control". *Journal of Structural Engineering (ASCE)*, vol. 129(7), p. 845-856.

55. Spencer, B. F. and Sain M. K. (1997). "Controlling buildings: a new frontier in feedback." *Special Issue of the IEEE Control Systems Magazine on Emerging Technology*, vol. 17, no. 6, p. 19-35.

56. Spencer Jr., B. F., Yang, G., Carlson, J. D., and Sain, M. K. (1998). "Smart Dampers for Seismic Protection of Structures: A Full-Scale Study", *Pro. of Second World Conference on Structural Control*, Kyoto, Japan, vol. 1, p. 417-426.

57. Spencer, B. F., Dyke, S. J., Sain, M. K., and Carlson, J. D. (1997). "Phenomenological model for magnetorheological dampers". *J. of Engineering mechanics*, vol. 123, n. 3, p. 230-238.

58. Stanway, R., Sproston, J. L. and El-Eahed, A. K. (1996). "Applications of electrorehological fluids in vibration control: A Survey", *Smart Materials and Structures*, vol. 5, no. 4, p 464-482.

59. Stanway, R., Sproston, J. L. and Stevens, N. G. (1987). "Non-linear Modeling of an Electro-rheological Vibration Damper." *J. Electrostatics*, vol. 20, p. 167-184.

60. Suhardjo, J. Et al. (1990), " Feedback-feed forward control of structures under seismic excitation." *Structural Safety*, v 8, n 1-4, Jul, p 69-89.

61. Symans, M. D. and Constantinou, M. C. (1999). "Semi-active control systems for seismic protection of structures: a state-of-the-art review." *Engineering Structures*, 21(6), p. 469-487.

62. Turner, M. J., Clough, R. W., Martin, H. C. and Topp, L. J. (1956). "Stiffness and deflection analysis of complex structures." *Journal of Aeronautical Science*, 23, 805-824.

63. Uang, C-M., and Bertero, V. V. (1988). "Use of energy as a design criterion in earthquake-resistant design." Report No. UCB/EERC-88/18, University of California, Berkeley.

64. Weaver, W. Jr. and Johnston, P. R. (19870. *Structural Dynamics by Finite Elements*, Prentice Hall.

65. Wen, Y. K. (1976). "Method of Random Vibration of Hysteretic Systems." *Journal of Engineering Mechanics Division*, ASCE, vol. 102, no. EM2, p. 249-263.

66. Wilson, C. M. D., (2005). "Fuzzy Control of Magnetorheological Dampers For Vibration Reduction Of Seismically Excited Structures." *Ph. D. Thesis*, The Florida State University.

67. Wilson. E. L. (1962). "Dynamic response by Step-By-Step Matrix Analysis." *Proceedings of Symposium on the Use of Computers in Civil Engineering,* October 1-5, Lisbon, Portugal.

68. Xu, Y. L.; Chen, J.; Ng, C. L. and Qu, W. L. (2005). "Semi-active seismic response control of buildings with podium structure" *Journal of Structural Engineering*, ASCE, 131(6), p. 890-899.

69. Yang, G. (2001). "Large-scale magnetorheological fluid damper for vibration mitigation: Modeling, Testing and Control." *Ph. D Thesis*, University of Notre Dame.

70. Yang, G., Spencer B. F. Jr., Carlson, J. D., and Sain M. K. (2002). "Large-scale MR fluid dampers: Modeling and dynamic performance considerations." *Eng. Struct.*, 24(3), 309-323.

71. Yi, F., and Dyke, S. J. (2000). "Performance of Smart Structures." *Proceedings of SPIE* – The International Society for Optical Engineering, Newport Beach, CA, vol. 3988, pp. 94-104.

72. Yoshida, O. and Dyke, S. J. (2005). "Response control in full scale irregular buildings using MR dampers." *ASCE Journal of Structural Engineering*, 131(5), p. 734-742.

73. Yuen, K-V., Shi, Y., Deck, J. L. and Lam, H-F. (2007). "Structural protection using MR dampers with clipped robust reliability-based control." *Journal of Structural and Multidisciplinary Optimization*, vol. 34, no. 5, p. 431-443.

Appendix A

Characteristics of MR Damper

Table A.1: Characteristics of MR damper RD-1005-3 (Lord, 2009).

Description	**Values**
Compressed length mm (in)	155 (6.1)
Extended length mm (in)	208 (8.2)
Body diameter mm (in)	41.1 (1.63)
Shaft diameter mm (in)	10 (0.39)
Weight g (lb)	800 (1.8)
For installation on pin mm (in)	12 (0.47)
Electrical characteristics: Input current Input voltage Resistance	 2 Amp maximum 12 V DC 5 ohms at ambient temperature 7 ohms at 160^0 F (70^0 C)

Damper forces (peak to peak) N (lb) 5 cm/sec at 1 Amp 20 cm/sec at 0 Amp	 > 2224 (500) < 667 (150)
Minimum tensile strength N (lb)	4448 (1000)
Maximum operating temperature C (F)	70^0 (160^0)
Storage temperature C (F)	-40^0 to 100^0 (-40^0 to 212^0)
Response time (millisecond)	< 15
Durability	2 million cycles

Table A.2: Characteristics of MR damper SD-1000.

Extended length	21.5 cm
Cylinder diameter	3.8 cm
Stroke length	± 2.5 cm
Maximum input power	< 10 watts
Magnetic field (current 0 to 1 Amp)	0 to 200 kA/m
Coil Resistance (R)	4 Ω
Maximum force	3000 N

Table A.3: Design parameters of the 20-ton large-scale MR fluid damper.

Stroke	±8 cm
Maximum velocity	10 cm/s
Nominal Cylinder Bore (ID)	20.32 cm
Maximum input power	< 50 watts
Nominal Maximum Force	200000 N
Effective Axial Pole Length	~5.5-8.5 cm
Coils	~3x1000 turns
Fluid Maximum Yield Stress τ_0	~70 kPa
Apparent Fluid Plastic Viscosity η	1.5 Pa-s
Fluid η/τ_0^2	$2x10^{-10}$ s/Pa
Gap	~1.5-2 mm
Active Fluid Volume	~90 cm^3
Wire	16 gauge
Inductance (L)	~6 henries
Coil Resistance (R)	~3x7 ohms

Appendix B

Modeling of Structure

Modeling of structure is done in the present research by finite element method. In finite element method mainly two element is used here one space frame element and other is MR damper bar element which is modified form of space truss element. In the subsequent sections the process of forming different element matrices are discussed.

B.1 Typical element Stiffness matrix

If we consider a typical element, then the force displacement relationship will be as Eq.B.1

$$\left[k^{(e)}\right]\vec{\phi}^{(e)} = \vec{p}^{(e)} \quad \text{----------B.1}$$

where $\left[k^{(e)}\right]$ is element stiffness matrix, $\vec{\phi}^{(e)}$ and $\vec{p}^{(e)}$ are vector of nodal displacement and nodal force of element e. Let a transformation matrix $\left[\lambda^{(e)}\right]$ exist between the local and the global coordination system such that

$$\vec{\phi}^{(e)} = \left[\lambda^{(e)}\right]\vec{\Phi}^{(e)} \quad \text{----------B.2}$$

And

$$\vec{p}^{(e)} = \left[\lambda^{(e)}\right]\vec{P}^{(e)} \quad \text{----------B.3}$$

here, lower case and capital letters is used to denote the characteristics pertaining to the local and the global coordinate systems. By substituting Eq B.2 and Eq. B.3 into Eq. B.1, we obtain

$$[k^{(e)}][\lambda^{(e)}]\vec{\Phi}^{(e)} = [\lambda^{(e)}]\vec{P}^{(e)} \quad \text{----------B.4}$$

Pre-multiplying the Eq. B.4 throughout by $[\lambda^{(e)}]^{-1}$, we get

$$[\lambda^{(e)}]^{-1}[k^{(e)}][\lambda^{(e)}]\vec{\Phi}^{(e)} = \vec{P}^{(e)} \quad \text{----------B.5}$$

Nor considering $[\lambda^{(e)}]^{T} = [\lambda^{(e)}]^{-1}$

$$[\lambda^{(e)}]^{T}[k^{(e)}][\lambda^{(e)}]\vec{\Phi}^{(e)} = \vec{P}^{(e)} \quad \text{----------B.6}$$

Or,

$$[K^{(e)}]\vec{\Phi}^{(e)} = \vec{P}^{(e)} \quad \text{----------B.7}$$

Where,

$$[K^{(e)}] = [\lambda^{(e)}]^{T}[k^{(e)}][\lambda^{(e)}] \quad \text{----------B.8}$$

$[K^{(e)}]$ is the element stiffness matrix corresponding to the global coordinate system.

B.2 Stiffness and mass matrix for the space truss element

A truss element is a bar which can resist only axial forces (compressive or tensile) and can deform only in the axial direction. Consider the pin-joint bar element as shown in Figure B.1 where the local x-axis is taken in the axial direction of the element with origin at corner (or local node) 1. A linear displacement model is assumed as Eq. B.9.

$$u(x) = q_1 + (q_2 - q_1)\frac{x}{l} \quad \text{----------B.9}$$

Or

$$\{u(x)\} = [N]\vec{q}^{(e)} \text{ ----------B.10}$$

Where

$$[N] = \left[(1-\frac{x}{l}) \quad \frac{x}{l}\right] \text{ ----------B.11}$$

$$\vec{q}^{(e)} = \begin{Bmatrix} q_1 \\ q_2 \end{Bmatrix} \text{ ----------B.12}$$

Where q_1 and q_2 represent the nodal degrees of freedom in the local coordinate system, l denotes the length of the element, and the superscript e denotes the element number. The axial strain can be expressed as

$$\varepsilon_{xx} = \frac{\partial u(x)}{\partial x} = \frac{q_2 - q_1}{l} \text{ ----------B.13}$$

Or

$$\{\varepsilon_{xx}\} = [B]\vec{q}^{(e)} \text{ ----------B.14}$$

Where

$$[B] = \left[-\frac{1}{l} \quad \frac{1}{l}\right] \text{ ----------B.15}$$

From the stress-strain relation

$$\sigma_{xx} = E\varepsilon_{xx} \text{ ----------B.16}$$

$$\{\sigma_{xx}\} = [D]\{\varepsilon_{xx}\} \text{ ----------B.17}$$

Where $[D] = [E]$ and E is the Young's modulus of the material. From the principal of minimum potential energy, the stiffness matrix of the element (in the local coordinate system) can be express by Eq. B.18 (Rao, 1999).

$$\left[k^{(e)}\right]=\iiint_{V^{(e)}}[B]^T[D][B]dV = A\int_{x=0}^{l}\begin{Bmatrix}-\frac{1}{l}\\ \frac{1}{l}\end{Bmatrix}E\begin{Bmatrix}-\frac{1}{l} & \frac{1}{l}\end{Bmatrix}dx \quad \text{----------B.18}$$

$$\left[k^{(e)}\right]=\frac{AE}{l}\begin{bmatrix}1 & -1\\ -1 & 1\end{bmatrix} \quad \text{----------B.19}$$

Mass matrix $\left[m^{(e)}\right]$ for space truss element can be express as Eq. B.20 in the local coordinate system and if we consider mass lumped at node.

$$\left[m^{(e)}\right]=\frac{m}{2}\begin{bmatrix}1 & 0\\ 0 & 1\end{bmatrix} \quad \text{----------B.20}$$

Where m is the total mass of the element.

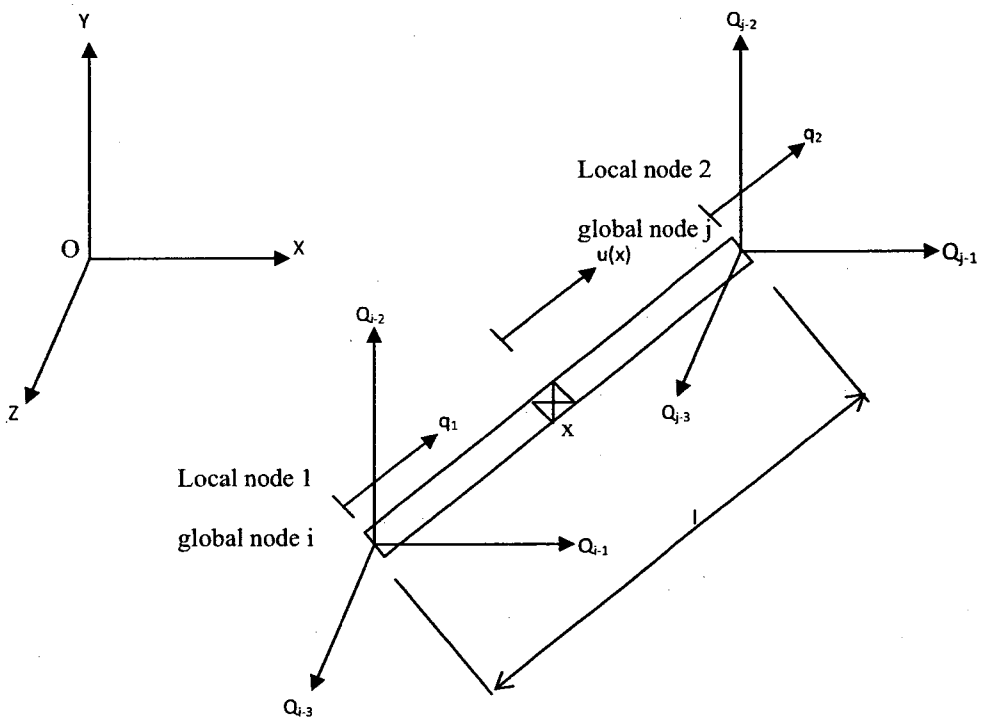

Figure B.1: Space truss element.

B.3 Transformation matrix for space truss element

For assembling process in order to get system stiffness and mass matrices, it is necessary to transform first these matrices from local to global coordinates. To transform these matrices from local coordinate to global coordinate system we need to appropriate transformation matrix. Transformation matrix is also necessary when the field variable is a vector quantity like displacement and velocity.

In Figure B.1 let the local nodes 1 and 2 of the element correspond to nodes i and j respectively of the global system. The local displacements q_1 and q_2 can be resolved into components Q_{i-1}, Q_{i-2}, Q_{i-3} and Q_{j-1}, Q_{j-2}, Q_{j-3} parallel to the global X, Y, Z axes, respectively. Then the two sets of displacements are related as Eq. B.21.

$$\vec{q}^{(e)} = [\lambda]\vec{Q}^{(e)} \quad \text{----------B.21}$$

where the transformation matrix $[\lambda]$ and the vector of nodal displacements of element e in the global coordinate system, $\vec{Q}^{(e)}$, are given by Eq. B.22.

$$[\lambda] = \begin{bmatrix} l_{ij} & m_{ij} & n_{ij} & 0 & 0 & 0 \\ 0 & 0 & 0 & l_{ij} & m_{ij} & n_{ij} \end{bmatrix} \quad \text{----------B.22}$$

$$\vec{Q}^{(e)} = \begin{Bmatrix} Q_{i-1} \\ Q_{i-2} \\ Q_{i-3} \\ Q_{j-1} \\ Q_{j-2} \\ Q_{j-3} \end{Bmatrix} Q_{i-1} \quad \text{----------B.23}$$

$$l_{ij} = \frac{X_j - X_i}{l},\ m_{ij} = \frac{Y_j - Y_i}{l},\ n_{ij} = \frac{Z_j - Z_i}{l} \quad \text{----------B.24}$$

$$l = \left\{(X_j - X_i)^2 + (Y_j - Y_i)^2 + (Z_j - Z_i)^2\right\}^{1/2} \text{----------B.25}$$

Now the stiffness and mass matrix of the element in the global coordinate system can be obtain as

$$\left[K^{(e)}\right] = [\lambda]^T \left[k^{(e)}\right] [\lambda] \text{----------B.26}$$

$$\left[M^{(e)}\right] = [\lambda]^T \left[m^{(e)}\right] [\lambda] \text{----------B.27}$$

Now the stiffness and mass matrix is in global coordinate system and can be assembled to get system stiffness and mass matrix.

B.4 Stiffness and mass matrix for space frame element

A space frame element is a straight bar of uniform cross section which is capable of resisting axial forces, bending moment about the two principal axes in the place of its cross section and twisting moment about its centroidal axis. The corresponding displacement degrees of freedom are shown in Figure B.2. From the Figure B.21 it can be seen that the stiffness matrix of a space frame element will be of order 12X12. If we choose the local x y z coordinate system coincide with the principle axes of the cross section with x-axis representing the centroidal axis of the frame element, then the displacement can be separated into four groups each of which can be considered independently of others and then obtain the total stiffness matrix of the element by superposition.

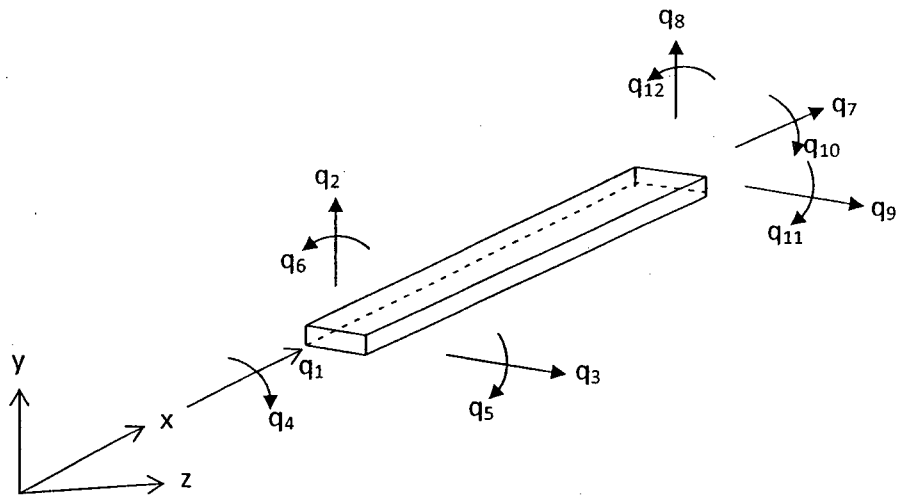

Figure B.2: Space frame element with 12 degrees of freedom.

(A) Axial Displacements

Considering the nodal displacement q_1 and q_7 as Figure B.2 and B.3a and linear displacement model, the stiffness matrix (corresponding to the axial displacement same as truss element) will be as Eq. B.28.

$$\left[k_a^{(e)}\right] = \iiint_{V^{(e)}} [B]^T [D][B] dV = \frac{AE}{l}\begin{bmatrix} 1 & -1 \\ -1 & 1 \end{bmatrix} \text{----------B.28}$$

where A, E and l are the area of cross section, Young's modulus and length of the element respectively. $\left[k_a^{(e)}\right]$ is the element stiffness matrix for axial displacement.

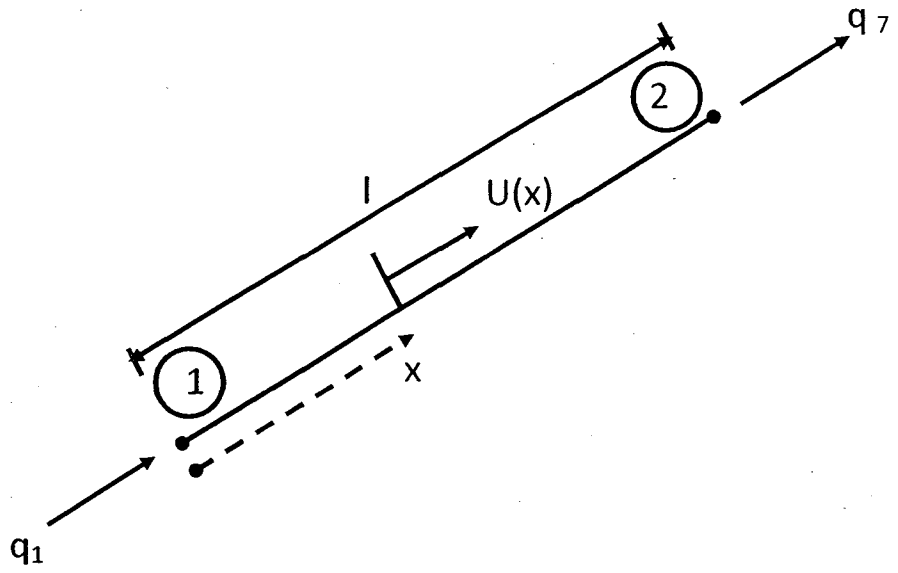

Figure B.3a: Axial degrees of freedom.

(B) Torsional Displacements

Here the degrees of freedom (torsional displacements) are given by q_4 and q_{10} as shown in Figure B.2 and B.3b. By assuming a linear variation of the torsional displacement or twist angle, the displacement model can be expressed as Eq. B.29

$$\theta(x) = [N]\vec{q}_t \text{ ----------B.29}$$

Where

$$[N] = \left[(1 - \frac{x}{l}) \quad (\frac{x}{l}) \right] \text{ ----------B.30}$$

And

$$\vec{q}_t = \begin{Bmatrix} q_4 \\ q_{10} \end{Bmatrix} \text{ ----------B.31}$$

If we assume the cross section of the frame element is circular, the shear strain induced in the element can be expressed by Eq. B.32.

$$\varepsilon_{\theta x} = r\frac{d\theta}{dx} \text{ ----------B.32}$$

where r is the distance of the fiber from the centroidal axis of the element. Thus the strain-displacement relation can be as

$$\vec{\varepsilon} = [B]\vec{q_t} \text{ ----------B.33}$$

Where

$$\vec{\varepsilon} = \{\varepsilon_{\theta x}\} \text{ and } [B] = \left[-\frac{r}{l} \quad \frac{r}{l}\right] \text{ ----------B.34}$$

From Hooke's law, the stress-strain relation

$$\vec{\sigma} = [D]\vec{\varepsilon} \text{ ----------B.35}$$

Where

$$\vec{\sigma} = \{\sigma_{\theta x}\}, \qquad [D] = [G]$$

And G is the shear modulus of the material. The stiffness matrix of the element corresponding to torsional degrees of freedom,

$$[k_t^{(e)}] = \iiint_{V^{(e)}} [B]^T [D][B] dV$$

$$[k_t^{(e)}] = G\int_{x=0}^{l} dx \iint_A r^2\, dA \begin{Bmatrix} -\frac{1}{l} \\ \frac{1}{l} \end{Bmatrix} \begin{Bmatrix} -\frac{1}{l} & \frac{1}{l} \end{Bmatrix} \text{ ----------B.36}$$

Since $\iint_A r^2\, dA = J =$ polar moment of inertia of the cross section, so

$$\left[k_t^{(e)}\right] = \frac{GJ}{l}\begin{bmatrix} 1 & -1 \\ -1 & 1 \end{bmatrix} \text{----------B.37}$$

The quantity $\frac{GJ}{l}$ is called the torsional stiffness of the frame element and depend on the cross section.

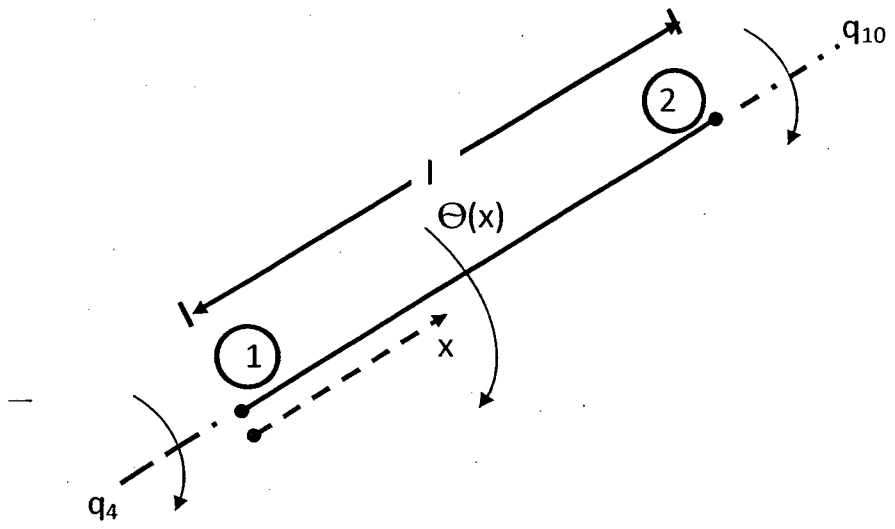

Figure B.3b: Torsional degrees of freedom.

(C) Bending Displacements in the Plane xy

Here the four bending degrees of freedom are q_2, q_6, q_8 and q_{12} as shown in Figure B.2 and B.3c. As we consider bending displacements in the xy plane, the element can be considered as beam element. The deformed shape of the element can be described by the transverse displacements q_2, q_6 and rotation q_8, q_{12}. As there are four nodal displacements, we assume a cubic displacement model for $\upsilon(x)$

$$\upsilon(x) = \alpha_1 + \alpha_2 x + \alpha_3 x^2 + \alpha_4 x^3 \text{----------B.38}$$

where the constants α_1 to α_4 can be found by using the conditions

$\upsilon(x) = q_2$ and $\frac{d\upsilon}{dx}(x) = q_6$ at $x = 0$,

And

$\upsilon(x) = q_8$ and $\frac{d\upsilon}{dx}(x) = q_{12}$ at $x = l$

Thus Eq. B.38 can be expressed as

$$\upsilon(x) = [N]\vec{q} \text{ ----------B.39}$$

Where $[N]$ is given by

$$[N] = [N_1 \quad N_2 \quad N_3 \quad N_4] \text{ ----------B.40}$$

With

$$\left.\begin{aligned} N_1(x) &= (2x^3 - 3lx^2 + l^3)/l^3 \\ N_2(x) &= (x^3 - 2lx^2 + l^2x)/l^2 \\ N_3(x) &= -(2x^3 - 3lx^2)/l^3 \\ N_4(x) &= (x^3 - lx^2)/l^2 \end{aligned}\right\} \text{ ----------B.41}$$

And $\vec{q} = \begin{Bmatrix} q_2 \\ q_6 \\ q_8 \\ q_{12} \end{Bmatrix}$ ----------B.42

According to simple beam theory, plane sections of the beam remain plane after deformation and hence the axial displacement u due to the transverse displacement υ can be expressed as (from Figure-B.4).

$$u = -y\frac{\partial \upsilon}{\partial x}$$

where y is the distance from the neutral axis. The axial strain is given by

$$\varepsilon_{xx} = \frac{\partial u}{\partial x} = -y\frac{\partial^2 \upsilon}{\partial x^2} = [B]\vec{q} \text{ ----------B.43}$$

where

$$[B] = -\frac{y}{l^3}\left[(12x-6l) \quad l(6x-4l) \quad -(12x-6l) \quad l(6x-2l)\right] \text{----------B.44}$$

Now assuming $[D]=[E]$ the stiffness matrix can be found by

$$[k_{xy}^{(e)}] = \iiint_{V^{(e)}} [B]^T [D][B] dV = E \int_{x=0}^{l} dx \iint_{A} [B]^T [B] dA$$

$$[k_{xy}^{(e)}] = \frac{E I_{zz}}{l^3}\begin{bmatrix} 12 & 6l & -12 & 6l \\ 6l & 4l^2 & -6l & 2l^2 \\ -12 & -6l & 12 & -6l \\ 6l & 2l^2 & -6l & 4l^2 \end{bmatrix} \text{----------B.45}$$

where $I_{zz} = \iint_A y^2 \, dA$ is the area moment of inertia of the cross section about z-axis.

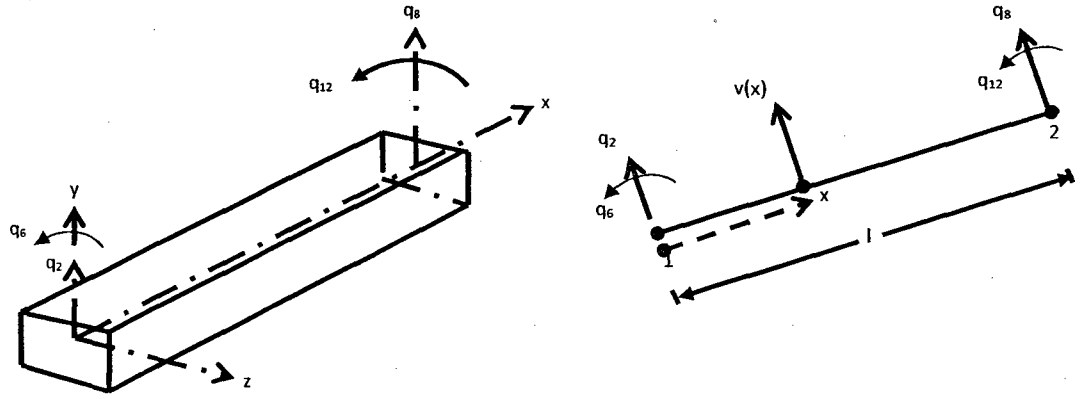

Figure B.3c: Bending degrees of freedom in xy plane.

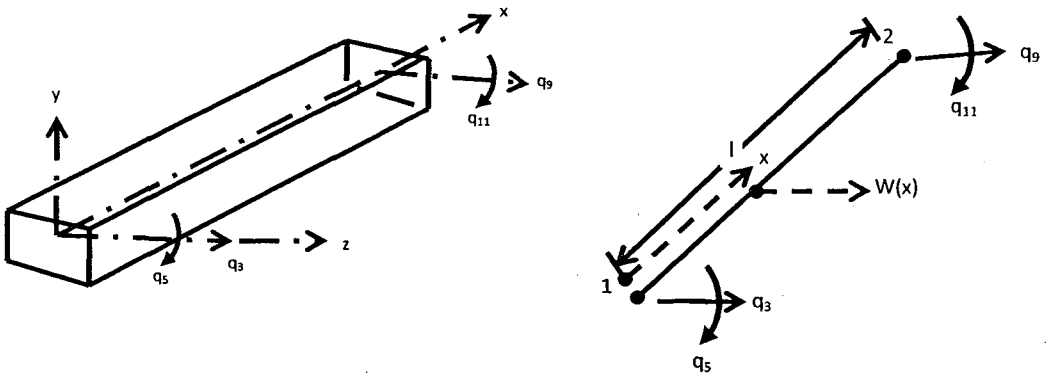

Figure B.3d: Bending degrees of freedom in xz plane.

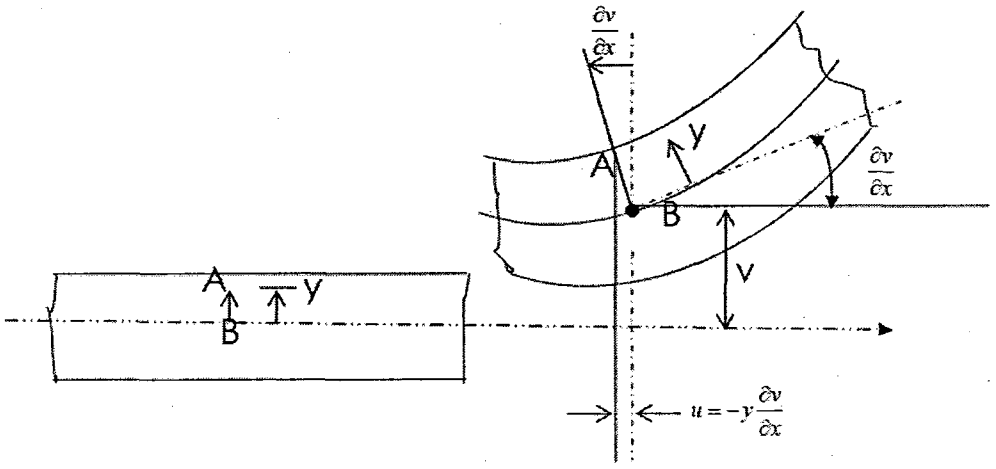

Figure B.4: Deformation of an element of frame in xy plane.

(D) Bending Displacements in the Plane xz

Here bending of the element takes place in the xz plane instead of xy plane. Thus we have the degrees of freedom q_3, q_5, q_9 and q_{11} in place of q_2, q_6, q_8 and q_{12} as shown in Figure B.2 and B.3d respectively. By proceeding as in the case of bending in the plane xy, it can easily be derived the stiffness matrix as

$$\left[k_{xz}^{(e)}\right]=\frac{E\,I_{yy}}{l^3}\begin{bmatrix}12 & 6l & -12 & 6l\\ 6l & 4l^2 & -6l & 2l^2\\ -12 & -6l & 12 & -6l\\ 6l & 2l^2 & -6l & 4l^2\end{bmatrix}$$ ----------B.46

where I_{yy} denotes the area moment of inertia of the cross section of the element about y-axis.

(E) Total Element Stiffness Matrix

The stiffness matrices derived for different sets of displacements can now be superposed to obtain the overall stiffness matrix of the frame element as

$$\left[k^{(e)}\right]=\begin{bmatrix}
\frac{EA}{l} & 0 & 0 & 0 & 0 & 0 & -\frac{EA}{l} & 0 & 0 & 0 & 0 & 0\\
0 & \frac{12EI_{zz}}{l^3} & 0 & 0 & 0 & \frac{6EI_{zz}}{l^2} & 0 & -\frac{12EI_{zz}}{l^3} & 0 & 0 & 0 & \frac{6EI_{zz}}{l^2}\\
0 & 0 & \frac{12EI_{yy}}{l^3} & 0 & -\frac{6EI_{yy}}{l^2} & 0 & 0 & 0 & -\frac{12EI_{yy}}{l^3} & 0 & -\frac{6EI_{yy}}{l^2} & 0\\
0 & 0 & 0 & \frac{GJ}{l} & 0 & 0 & 0 & 0 & 0 & -\frac{GJ}{l} & 0 & 0\\
0 & 0 & -\frac{6EI_{yy}}{l^2} & 0 & \frac{4EI_{yy}}{l} & 0 & 0 & 0 & \frac{6EI_{yy}}{l^2} & 0 & \frac{2EI_{yy}}{l} & 0\\
0 & \frac{6EI_{zz}}{l^2} & 0 & 0 & 0 & \frac{4EI_{zz}}{l} & 0 & -\frac{6EI_{zz}}{l^2} & 0 & 0 & 0 & \frac{2EI_{zz}}{l}\\
-\frac{EA}{l} & 0 & 0 & 0 & 0 & 0 & \frac{EA}{l} & 0 & 0 & 0 & 0 & 0\\
0 & -\frac{12EI_{zz}}{l^3} & 0 & 0 & 0 & -\frac{6EI_{zz}}{l^2} & 0 & \frac{12EI_{zz}}{l^3} & 0 & 0 & 0 & -\frac{6EI_{zz}}{l^2}\\
0 & 0 & -\frac{12EI_{yy}}{l^3} & 0 & \frac{6EI_{yy}}{l^2} & 0 & 0 & 0 & \frac{12EI_{yy}}{l^3} & 0 & \frac{6EI_{yy}}{l^2} & 0\\
0 & 0 & 0 & -\frac{GJ}{l} & 0 & 0 & 0 & 0 & 0 & \frac{GJ}{l} & 0 & 0\\
0 & 0 & -\frac{6EI_{yy}}{l^2} & 0 & \frac{2EI_{yy}}{l} & 0 & 0 & 0 & \frac{6EI_{yy}}{l^2} & 0 & \frac{4EI_{yy}}{l} & 0\\
0 & \frac{6EI_{zz}}{l^2} & 0 & 0 & 0 & \frac{2EI_{zz}}{l} & 0 & -\frac{6EI_{zz}}{l^2} & 0 & 0 & 0 & \frac{4EI_{zz}}{l}
\end{bmatrix}$$

----------B.47

(F) Mass Matrix for Space Frame Element

By considering mass lumped at node, the mass matrix $[m^{(e)}]$ for space frame element can be express as Eq. B.48 in the local coordinate system.

$$[m^{(e)}]=\frac{m}{2}\begin{bmatrix}1&0&0&0&0&0&0&0&0&0&0&0\\0&1&0&0&0&0&0&0&0&0&0&0\\0&0&1&0&0&0&0&0&0&0&0&0\\0&0&0&m_r&0&0&0&0&0&0&0&0\\0&0&0&0&m_r&0&0&0&0&0&0&0\\0&0&0&0&0&m_r&0&0&0&0&0&0\\0&0&0&0&0&0&1&0&0&0&0&0\\0&0&0&0&0&0&0&1&0&0&0&0\\0&0&0&0&0&0&0&0&1&0&0&0\\0&0&0&0&0&0&0&0&0&m_r&0&0\\0&0&0&0&0&0&0&0&0&0&m&0\\0&0&0&0&0&0&0&0&0&0&0&m_r\end{bmatrix} \quad \text{----------B.48}$$

where m is total mass of the element. m_r is a factor to avoid 0 mass for rotational mass if rotational mass ignored.

Now according to Eq. B.8 the stiffness and mass matrix in the global coordinate system can be obtained as:

$$\left.\begin{aligned}[K^{(e)}]&=[\lambda^{(e)}]^T[k^{(e)}][\lambda^{(e)}]\\[M^{(e)}]&=[\lambda^{(e)}]^T[m^{(e)}][\lambda^{(e)}]\end{aligned}\right\} \quad \text{----------B.49}$$

B.5 Transformation matrix for space frame element

The 12X12 transformation matrix for space frame element $\lambda^{(e)}$ can be derived as

$$\left[\lambda^{(e)}\right]=\begin{bmatrix}
\lambda_{11} & \lambda_{12} & \lambda_{13} & 0 & 0 & 0 & 0 & 0 & 0 & 0 & 0 & 0 \\
\lambda_{21} & \lambda_{22} & \lambda_{23} & 0 & 0 & 0 & 0 & 0 & 0 & 0 & 0 & 0 \\
\lambda_{31} & \lambda_{32} & \lambda_{33} & 0 & 0 & 0 & 0 & 0 & 0 & 0 & 0 & 0 \\
0 & 0 & 0 & \lambda_{11} & \lambda_{12} & \lambda_{13} & 0 & 0 & 0 & 0 & 0 & 0 \\
0 & 0 & 0 & \lambda_{21} & \lambda_{22} & \lambda_{23} & 0 & 0 & 0 & 0 & 0 & 0 \\
0 & 0 & 0 & \lambda_{31} & \lambda_{32} & \lambda_{33} & 0 & 0 & 0 & 0 & 0 & 0 \\
0 & 0 & 0 & 0 & 0 & 0 & \lambda_{11} & \lambda_{12} & \lambda_{13} & 0 & 0 & 0 \\
0 & 0 & 0 & 0 & 0 & 0 & \lambda_{21} & \lambda_{22} & \lambda_{23} & 0 & 0 & 0 \\
0 & 0 & 0 & 0 & 0 & 0 & \lambda_{31} & \lambda_{32} & \lambda_{33} & 0 & 0 & 0 \\
0 & 0 & 0 & 0 & 0 & 0 & 0 & 0 & 0 & \lambda_{11} & \lambda_{12} & \lambda_{13} \\
0 & 0 & 0 & 0 & 0 & 0 & 0 & 0 & 0 & \lambda_{21} & \lambda_{22} & \lambda_{23} \\
0 & 0 & 0 & 0 & 0 & 0 & 0 & 0 & 0 & \lambda_{31} & \lambda_{32} & \lambda_{33}
\end{bmatrix}$$

Or

$$\left[\lambda^{(e)}\right]=\begin{bmatrix}
[\underline{\lambda}] & [0] & [0] & [0] \\
[0] & [\underline{\lambda}] & [0] & [0] \\
[0] & [0] & [\underline{\lambda}] & [0] \\
[0] & [0] & [0] & [\underline{\lambda}]
\end{bmatrix} \text{----------B.50}$$

Where,

$$[\underline{\lambda}]=\begin{bmatrix}
\lambda_{11} & \lambda_{12} & \lambda_{13} \\
\lambda_{21} & \lambda_{22} & \lambda_{23} \\
\lambda_{31} & \lambda_{32} & \lambda_{33}
\end{bmatrix} \text{----------B.51}$$

$$[0]=\begin{bmatrix}
0 & 0 & 0 \\
0 & 0 & 0 \\
0 & 0 & 0
\end{bmatrix} \text{----------B.52}$$

λ_{11}, λ_{12} and λ_{13} of the Eq. B.51 can be found by referring to the Figure B.5 where

$$\left.\begin{aligned}\lambda_{11} &= \cos\phi_{11} = \frac{X1(K) - X1(J)}{L} \\ \lambda_{12} &= \cos\phi_{12} = \frac{X2(k) - X2(J)}{L} \\ \lambda_{13} &= \cos\phi_{13} = \frac{X3(K) - X3(J)}{L}\end{aligned}\right\} \text{----------B.53}$$

It is apparent that the three direction cosines λ_{11}, λ_{12} and λ_{13} of the axis of an element of a space structure do not specify the orientation of its local x_2 and x_3 (Figure B.6) axes with respect to the global $\bar{x}_1$, $\bar{x}_2$ and $\bar{x}_3$ axes of the structure. To accomplish this, additional information is required. The direction cosines of the local axes of an element of a space structure with respect to the global axes of the structure can be established if in addition to the three direction cosines of the axis of the element one direction cosine of its x_2 or x_3 axis is known. The direction cosines of the local axes of an element of a space structure relative to the global axes of the structure can be establish from the global coordinates of the nodes to which the element is connected and the global coordinates of a point in the x_1x_2 or x_1x_3 plane which is not located on the x_1 axis and the point is denoted node i. Referring to the Figure B.5, B.6 and B.7 the element λ_{21}, λ_{22}, λ_{23}, λ_{31}, λ_{32} and λ_{33} of matrix $[\underline{\lambda}]$ can be found as follows (Armenakas, 1991):

$$\left.\begin{aligned}\lambda_{21} &= -\frac{\lambda_{11}\lambda_{12}\cos\psi + \lambda_{13}\sin\psi}{\sqrt{\lambda_{11}^2 + \lambda_{13}^2}} \\ \lambda_{22} &= \sqrt{\lambda_{11}^2 + \lambda_{13}^2}\cos\psi \\ \lambda_{23} &= -\frac{\lambda_{12}\lambda_{13}\cos\psi - \lambda_{11}\sin\psi}{\sqrt{\lambda_{11}^2 + \lambda_{13}^2}}\end{aligned}\right\} \text{----------B.54}$$

$$\left.\begin{aligned}\lambda_{31} &= \frac{\lambda_{11}\lambda_{12}\sin\psi - \lambda_{13}\cos\psi}{\sqrt{\lambda_{11}^2 + \lambda_{13}^2}} \\ \lambda_{32} &= -\sqrt{\lambda_{11}^2 + \lambda_{13}^2}\sin\psi \\ \lambda_{33} &= \frac{\lambda_{12}\lambda_{13}\sin\psi + \lambda_{11}\cos\psi}{\sqrt{\lambda_{11}^2 + \lambda_{13}^2}}\end{aligned}\right\} \text{----------B.55}$$

Where

$$\left.\begin{aligned}\sin\psi &= \frac{x_3^{i\beta}}{\sqrt{(x_2^{i\beta})^2 + (x_3^{i\beta})^2}} \\ \cos\psi &= \frac{x_2^{i\beta}}{\sqrt{(x_2^{i\beta})^2 + (x_3^{i\beta})^2}}\end{aligned}\right\} \text{----------B.56}$$

And

$$\begin{aligned}x_2^{i\beta} &= -\frac{\lambda_{11}\lambda_{12}[X1(I) - X1(J)]}{\sqrt{\lambda_{11}^2 + \lambda_{13}^2}} + (\sqrt{\lambda_{11}^2 + \lambda_{13}^2})[X2(I) - X2(J)] - \frac{\lambda_{12}\lambda_{13}[X3(I) - X3(J)]}{\sqrt{\lambda_{11}^2 + \lambda_{13}^2}} \\ x_3^{i\beta} &= -\frac{\lambda_{13}[X1(I) - X1(J)]}{\sqrt{\lambda_{11}^2 + \lambda_{13}^2}} + \frac{\lambda_{11}[X3(I) - X3(J)]}{\sqrt{\lambda_{11}^2 + \lambda_{13}^2}}\end{aligned}$$

----------B.57

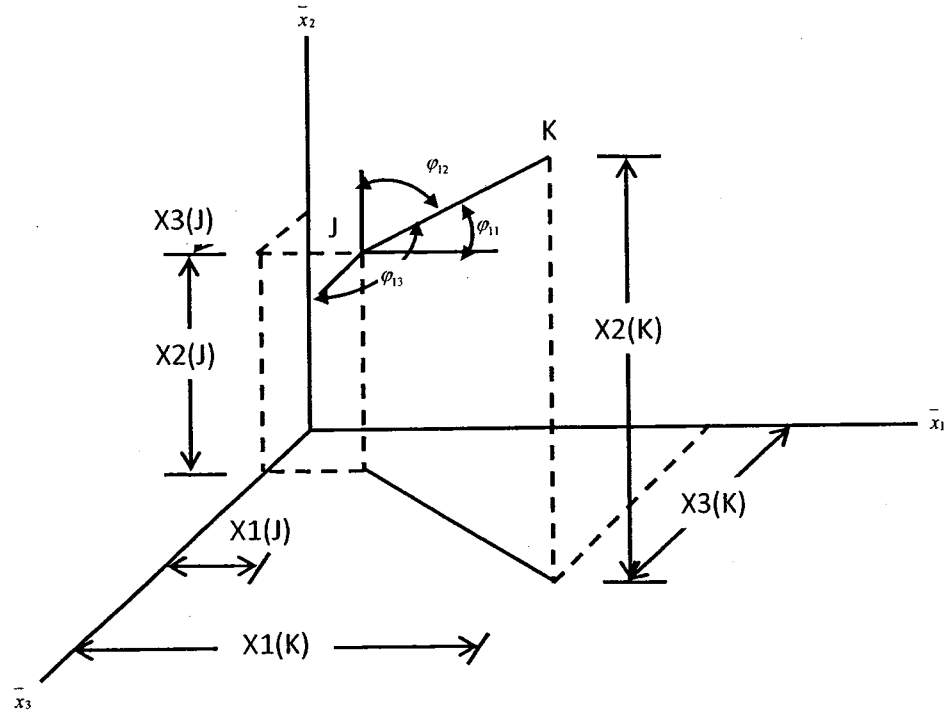

Figure B.5: Element of a space structure.

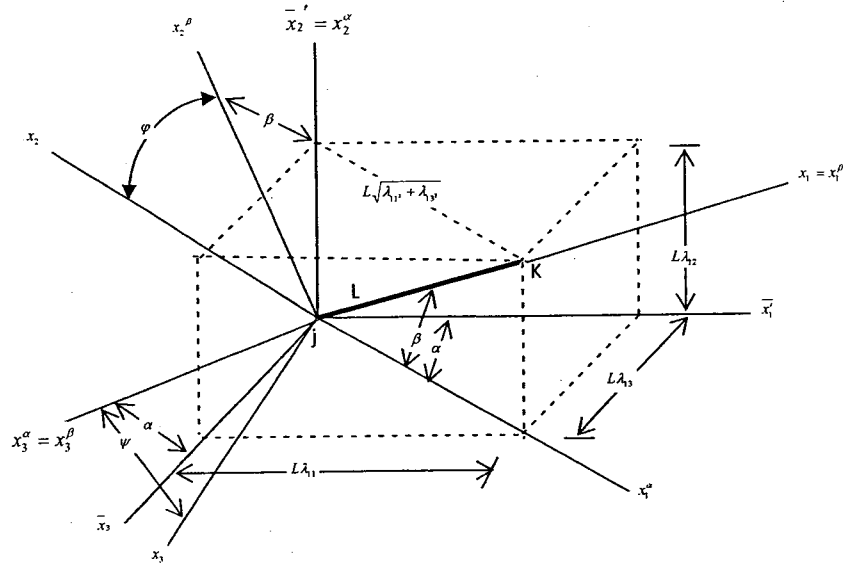

Figure B.6: Rotation of the axes.

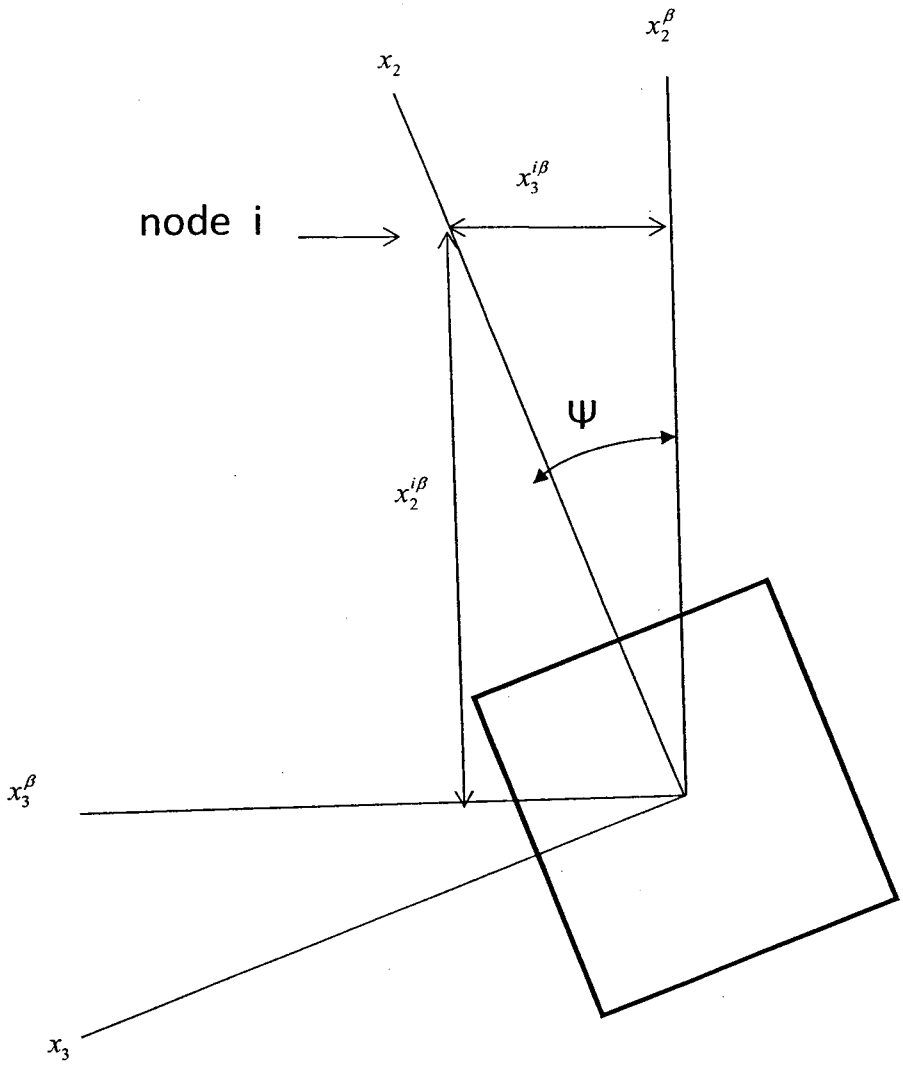

Figure B.7: The angle of the roll ψ of the local axes of an element.

Appendix C

Reproduced Earthquake Record

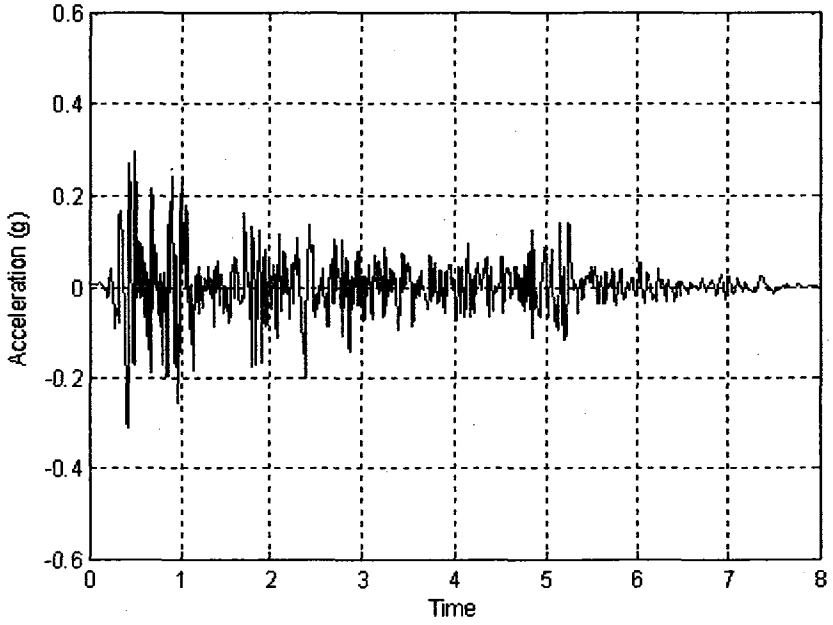

Figure C1: Reproduced acceleration Time-History Record of El-Centro (IMPVALL/I-ELC180) 1940/05/19

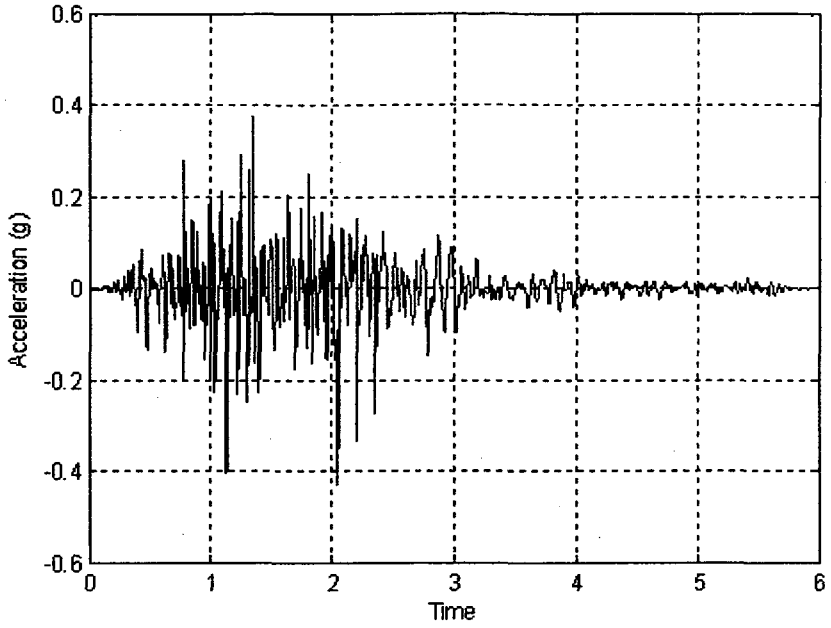

Figure C2: Reproduced acceleration Time-History Record of Mammoth lakes (MAMMOTH/I-LUL000) 1980/05/25

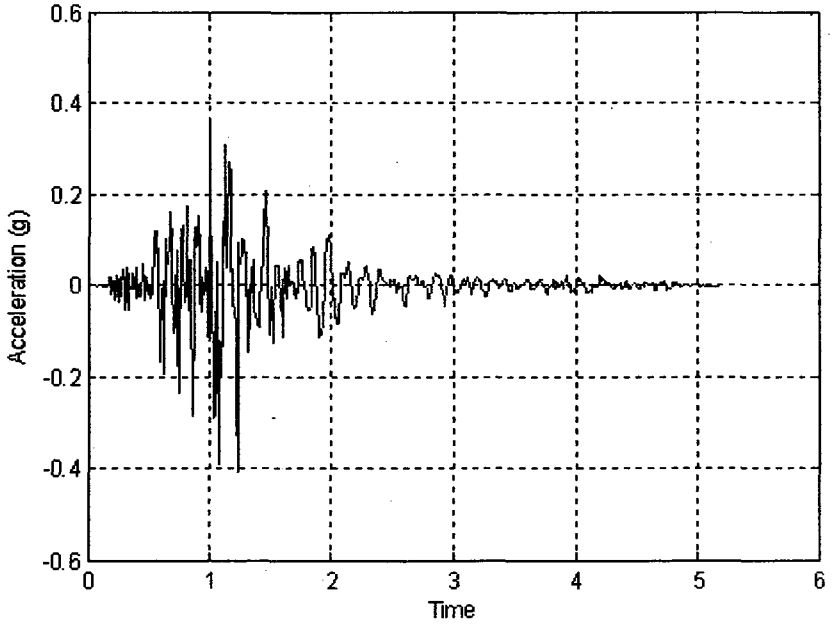

Figure C3: Reproduced acceleration Time-History Record of Mammoth lakes (MAMMOTH/L-LUL090) 1980/05/27.

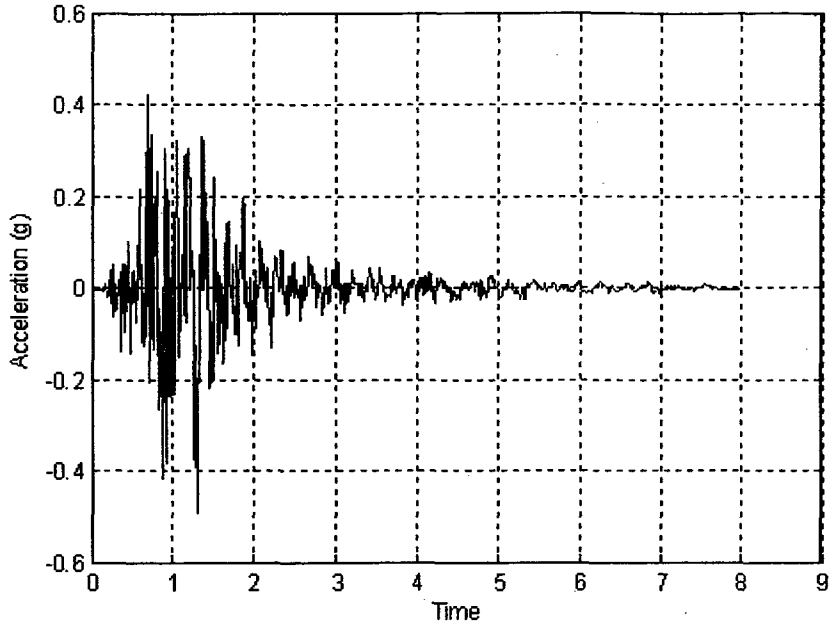

Figure C4: Reproduced acceleration Time-History Record of Northridge (NORTHR/SCE288) 1994/04/17.

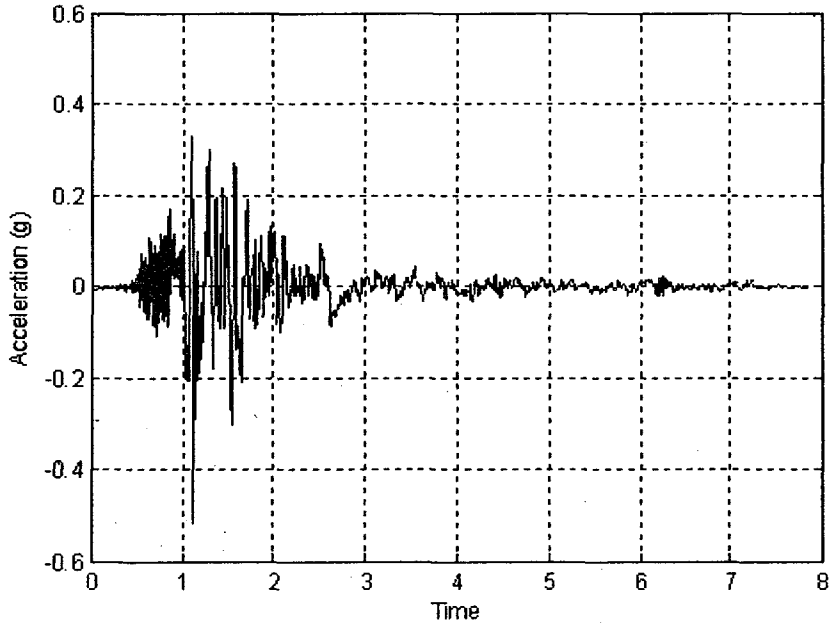

Figure C5: Reproduced acceleration Time-History Record of Imperial Valley (IMPVALL/H-E05140) 1979/10/15.